Advanced Nonlinear Control
Final Project Reports
Fall 1995

Dawn Tilbury, Assistant Professor

Technical Report UM-MEAM-96-01

January 12, 1996

Advanced Nonlinear Control
Final Project Reports
ME 662 / EECS 662 / Aero 672
Fall 1995

This technical memo contains the final project reports of the students taking Advanced Nonlinear Control at the University of Michigan in the fall semester of 1995. The course was taught by Prof. Dawn Tilbury and covered the modern geometric and algebraic approaches to the analysis and design of nonlinear control systems. More information on the course is available on the WWW at http://www-personal.engin.umich.edu/~tilbury/me662.html.

Each student in the course did a term project, gave an oral presentation, and submitted a written report. This collection of papers is a record of the final projects. There was considerable flexibility in the choice of the project, which is reflected in the diversity of the final reports. Most students did simulation studies, implementing one or more controllers on a specific example. A few students studied adaptive control, which was not covered in the course. There were also some observer designs, one literature survey, and new theoretical results. Most students did an individual project; there was one joint project.

Overall, the projects were excellent. I have reproduced here the project reports as they were turned in. In the interests of space, I have eliminated most of the appendices, many of which contained Mathematica, Maple, or Matlab code, long derivations, or supplemental plots. Anyone interested in more information on a given project may send email to tilbury@umich.edu.

Table of Contents

Aircraft Control in Emergency Situations

Ella M. Atkins

December 6, 1995

Objectives

- Aircraft dynamics
  - Develop the 3-D equations of motion for the aircraft based on forces and moments
  - Evaluate ability of nonlinear control techniques (i.e. I/O and exact linearization) to handle the aircraft state equations
- Aircraft control
  - Implement a "working" control system to fly an F-16 simulated aircraft
  - System must control the aircraft during takeoff, cruise, turning to new heading, and approach to landing during an emergency
- Emergency situation handling
  - Simulate an emergency situation in the simulator
  - Create code to detect the emergency and exhibit the correct pre-determined control response

Outline

- **Aircraft dynamics -- Force computation**
- **Aircraft dynamics -- Moment computation**
- **Aircraft control system development**
- **Emergency detection and handling procedure**
- **Emergency test situation -- "Engine Out"**
- **Test results of controller and emergency handling**

Aircraft Force Diagram

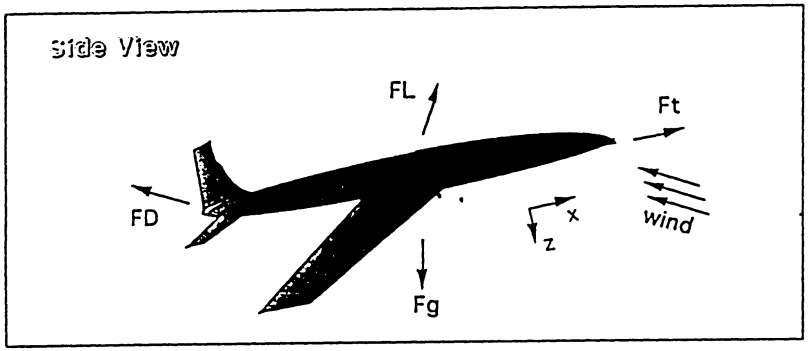

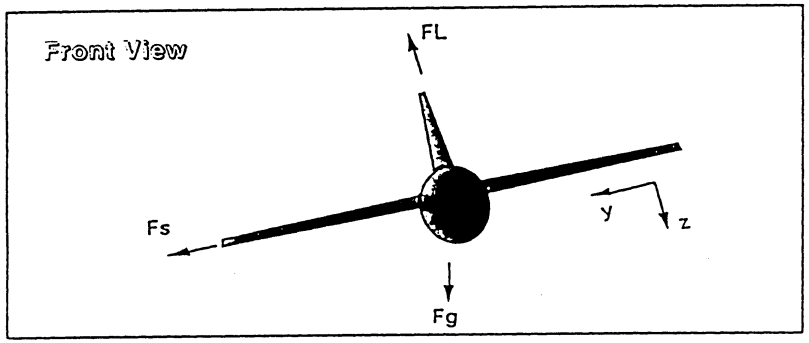

Fg = Force due to gravity

Ft = Aircraft engine thrust

FL = Aerodynamic lift force

FD = Aerodynamic drag force

Fs = Aerodynamic sideslip force

Forces: Thrust

$$F_t = t_{max} * f(v) * (rpm)^2$$

t_{max} = maximum possible thrust

rpm = engine rotations per minute

f(v) = thrust coefficient (v = velocity)

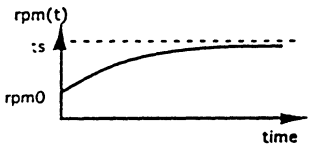

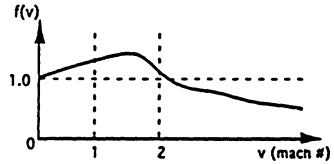

- RPM matches throttle setting (ts) after "spool-up" delay
  - Create "rpm" state to model this delay
- Thrust coefficient f(v) approximately linear in operating region (v< Mach 1).
- After substituting numbers:

$$rpm_{new} = 0.9592 * rpm_{old} + 0.0408 * ts$$

$$F_t = [3.186 * \dot{x}_{local} + 14080] * (rpm_{new})^2$$

Forces: Gravity

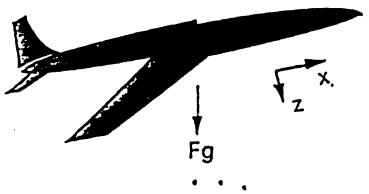

$$F_g = \text{(empty weight)} + \text{(fuel weight)}$$

$$F_g = 24326 \text{ lbs.}$$

- Gravity always acts in the global +z direction
- Force magnitude assumed constant throughout short flight

Aerodynamic Forces: Lift

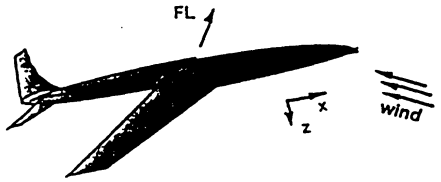

$$F_L = \frac{1}{2}\rho A v^2 C_L$$

ρ = air density; A = wing surface area;

v = wind velocity $\approx$ aircraft x-velocity;

C_L = lift coefficient ($\approx$ linear function of α)

α = aircraft angle of attack $\approx \tan^{-1}\left(\frac{\dot{z}}{\dot{x}}\right)$

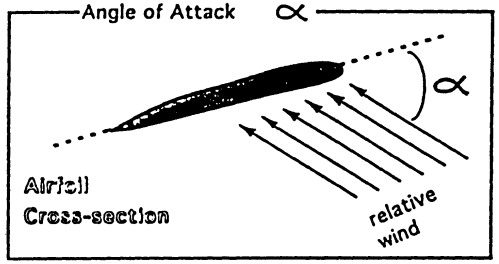

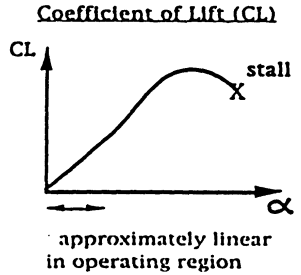

- After numerical substitutions:

$$F_L = 1.496 * \dot{x}^2 * \alpha$$

Aircraft Moment Diagram

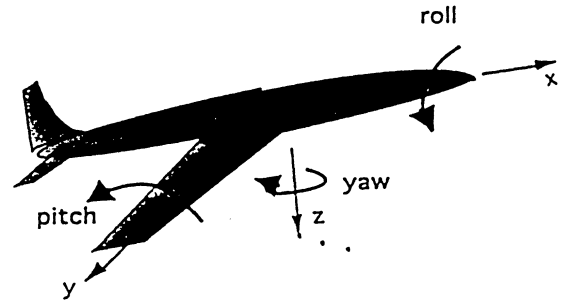

- Roll, pitch, and yaw rotations computed about the local x, y, and z axes, respectively

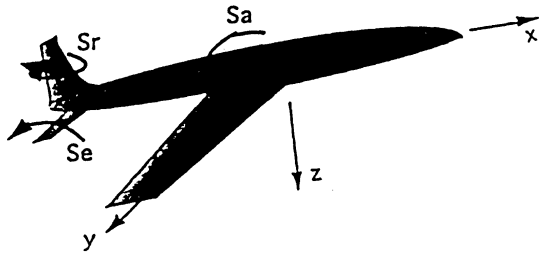

- Elevator (Se) actuator force affects pitch
- Aileron (Sa) actuator force affects roll
- Rudder (Sr) actuator force affects yaw and roll

Moments -- Roll Angle

- Both aileron and rudder inputs affect roll
- Sideslip angle also induces roll angle changes
- Roll rate is a function of velocity since it is aerodynamically induced
- Roll rate change is represented as follows:

$$\Delta\text{roll} = \frac{-\text{xd} * \text{xb}}{\text{xa} * e^{-\text{xa}/\text{xb}*\Delta t}} - \frac{\Delta t * \text{xc}}{\text{xa} - \text{r0}}$$

where

$$\text{xa} = (\text{Clp}) * \rho \text{Av} \left(\frac{1}{2}\text{span}\right)^2$$

$$\text{xb} = -I_{xx}$$

$$\text{xc} = \rho \text{Av}^2 \left(\frac{1}{2}\text{span}\right) * [(\text{Clda}) * \text{Sa}_{max} * \text{Sa} + (\text{Clbeta}) * \beta + (\text{Cldr}) * \text{Sr}_{max} * \text{Sr}]$$

$$\text{xd} = (\text{old\_roll\_rate}) + \frac{\text{xc}}{\text{xa}}$$

- After numerical substitution, this "simplifies" to:

$$\Delta\text{roll} = \frac{7240 * (\text{old\_roll\_rate}) - 1676 * \text{v} * (0.096 * \text{Sa} + 0.08 * \text{Sr} - 0.0125 * \beta)}{-49.29 * \text{v} * e^{-0.054\text{v}}} - \frac{1.426 * \text{v}^2 * (0.096 * \text{Sa} + 0.08 * \text{Sr} - 0.0125 * \beta)}{49.29 * \text{v} + \frac{146.9}{\text{v}} (-(\text{old\_roll\_rate}) + 0.231)}$$

Aerodynamic Forces: Sideslip

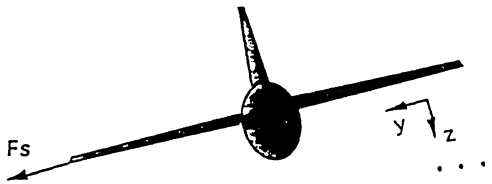

$$F_S = \frac{1}{2}\rho A v^2 C_Y$$

- For the F-16 aircraft, the sideslip coefficient Cy is given by:

$$C_Y = -0.85 * \beta$$

where β is the sideslip angle (as shown below) and will be assumed to have a very small value.

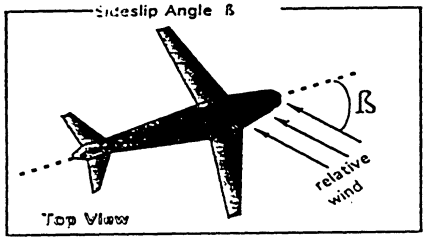

- After numerical substitution, sideslip is given by:

$$F_S = 0.3031 * \dot{x}^2 * \beta$$

Aerodynamic Forces: Drag

$$F_D = \frac{1}{2}\rho A v^2 C_D$$

- Drag Coefficient (C_D) includes components from Body / wave, induced, and sideslip drag
- Body drag coefficient (CDb) depends on α:

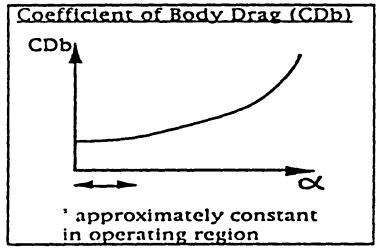

- Total drag coefficient given by: (AR=aspect ratio)

$$C_D = \sqrt{\left(C_{D_0} + \frac{C_L^2}{\pi * AR}\right)^2 + (0.5 * \sin(\beta))^2}$$

- Total drag force after numerical substitutions:

$$F_D = 0.3566 * \dot{x}^2 * \sqrt{\left(0.02 + 1.869 * (\tan^{-1}\alpha)^2\right)^2 + (0.5 * \sin(\beta))^2}$$

Aircraft Dynamics...

- Roll equation illustrates the complexity of aircraft moment equations
- Pitch and yaw equations are even more complex
- Forces as shown were not all aligned with local or global coordinate systems
  - Force coordinate transformations necessary, adding additional sin and cos terms.
- Due to time limitations, I took a very different approach to aircraft control:
  - New Approach:

Most pilots do not understand the nonlinear aircraft equations of motion. Instead they rely on several basic "linear" rules involving sensor-actuator relationships when flying.

The control system used for this project was based on sensor-actuator relationships used by pilots.

Aircraft Control System - 1

- 3-D x,y,z and roll, pitch, yaw still must be controlled
- Aircraft is inherently stable rotationally so long as "normal" flight configuration maintained
  - Keep upright attitude and high airspeed, and a few basic rules will allow control of state
- Input vector:

$$\bar{u} = \begin{Bmatrix} ts \\ es \\ as \\ rs \end{Bmatrix}$$

  - ts = throttle setting
  - es = elevator setting
  - as = aileron setting
  - rs = rudder setting
- State vector (transposed):

$$\{x, \dot{x}, y, \dot{y}, z, \dot{z}, \phi, \dot{\phi}, \theta, \dot{\theta}, \Psi, \dot{\Psi}\}$$

  - x,y,z = global position coordinates with z "down" and x = North
  - ϕ, θ, ψ = roll, pitch, and yaw angles about local aircraft axes

Aircraft Control System - 2

- Linear control equations are shown below:

  - Heading (Ψ) and roll (Φ) controlled by ailerons (Sa) and rudder (Sr)

$$Sa = K_1 * (\Psi_d - \Psi) - \dot{K}_2 * \Phi$$

$$Sr = K_3 * (\Psi_d - \Psi) - K_4 * \Phi$$

  - Since velocity is nearly all in local x-direction, heading also controls global x and y.

  - Altitude (z) and pitch (θ) are controlled by throttle and elevator (Se).

  (These also control airspeed, but airspeed always just kept "sufficiently high" here)

$$throttle = K_5 * (z_d - z) + (throttle)_0$$

$$Se = K_6 * (z_d - z) + K_7 * (\theta_d - \theta)$$

- Control gains (K1-K7) calculated via quick estimation and iterated to their final value during tests

- Different gain values used during emergency reactions than during normal flight

Emergency Situation Handling Procedure

- Must have working control law set for handling each possible emergency situation

  - For simple controller, the basic control laws always remain the same, but the gains change

- Emergency detection procedure:

  - Check expected vs. commanded inputs and state.

  - If large discrepancy, identify the emergency.

- Emergency handling procedure:

  - Select the appropriate pre-programmed reaction sequence based on the nature of the emergency and current state

    - Reactions range from doing nothing to emergency off-field landings

    - Problem with this approach: Many potential emergencies possible. "Catalog" of responses with associated control laws indexed by problem and state may be prohibitively large

Emergency Handling Tests

- Simulated the "engine out" emergency for testing
- Three different reactions exist for different conditions:

Case 1:
- Problem: Engine Power Limited (e.g. 45% max)
- State: (Any)
- Reaction: Turn left to enter normal landing pattern
- Result: Plane can land safely with minimal disruption to air traffic.

Case 2:
- Problem: Complete engine failure
- State: z > 3000 ft and < 10 miles from airport
- Reaction: Turn 180° and land at the airport
- Result: Plane lands safely, but air traffic disrupted because plane lands in wrong direction

Case 3:
- Problem: Complete engine failure
- State: z < 3000 ft or >10 miles from airport
- Reaction: Descend "gracefully" to land off-field
- Result: Plane may not land safely if the terrain is unfriendly, but plane will have a decent chance because it's in "landing configuration "

- All three cases successfully tested using an F-16 simulator with the simple control law with different gains for normal flight and each emergency reaction

Partial engine failure:

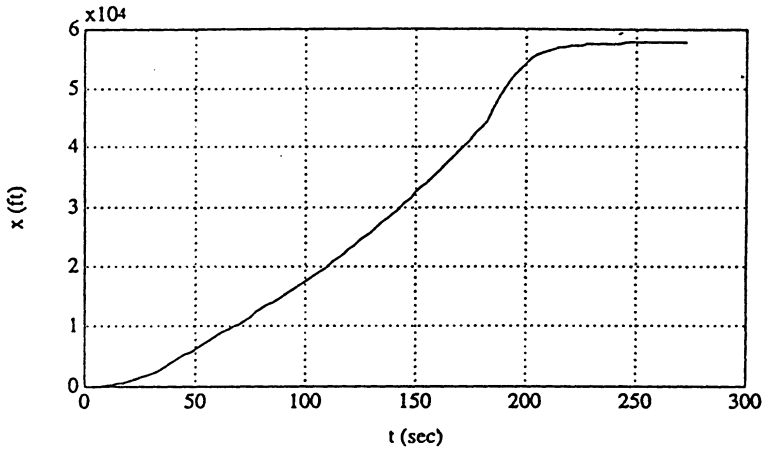

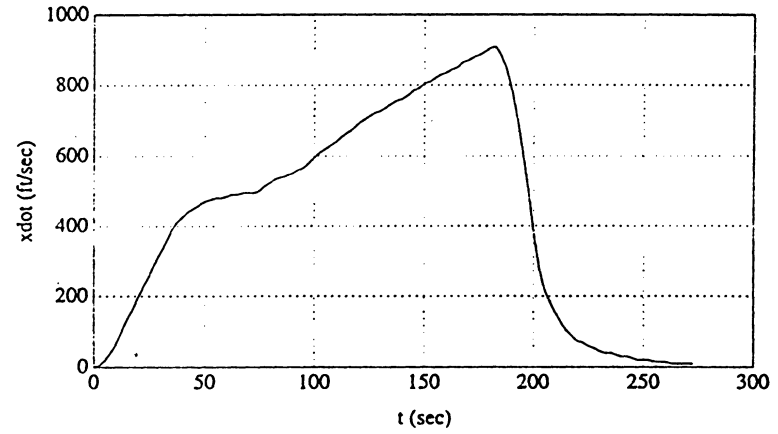

Partial engine failure:

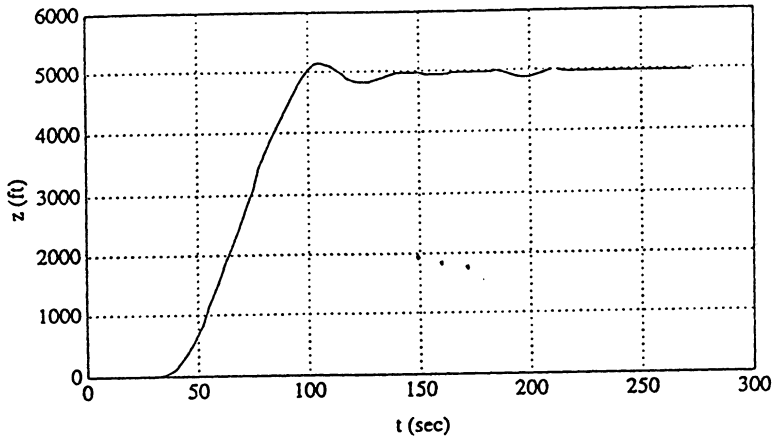

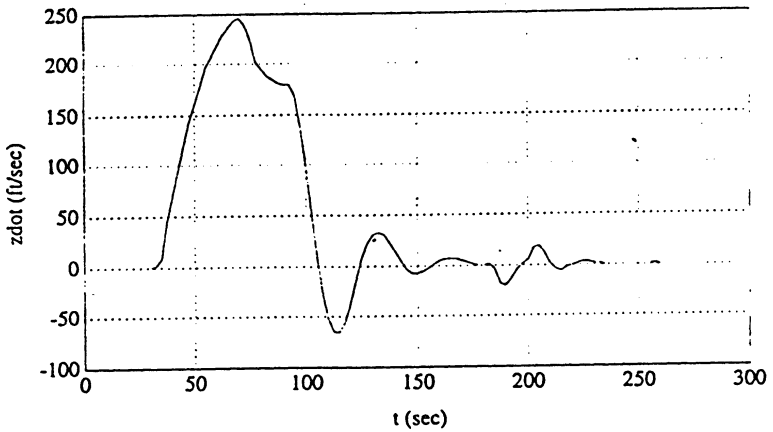

Partial engine failure:

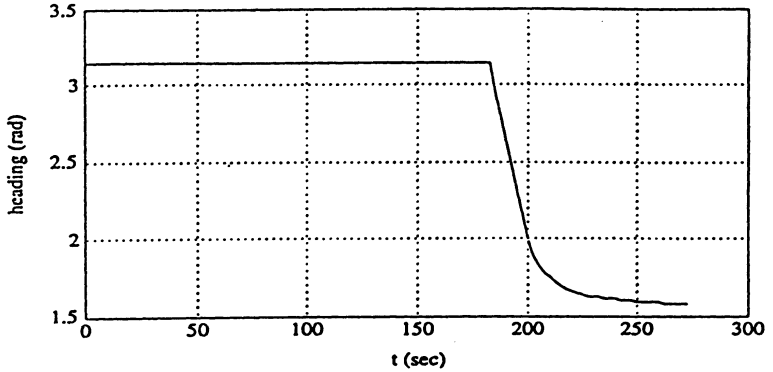

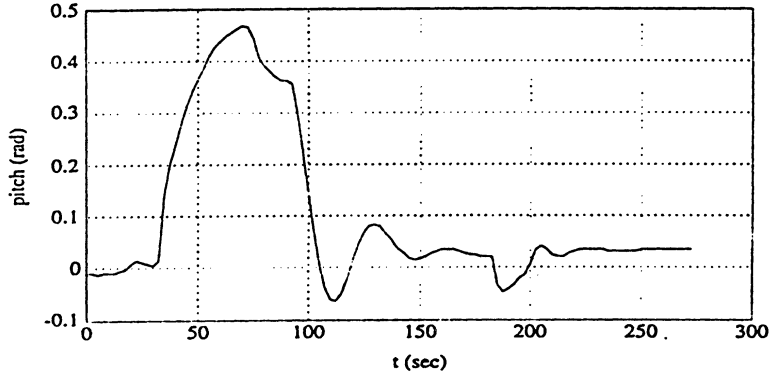

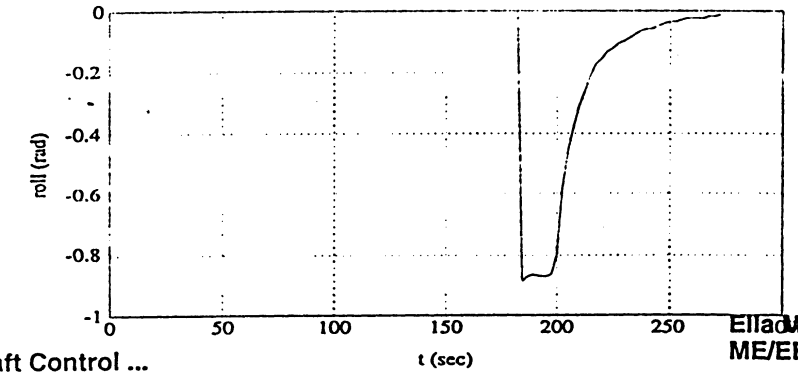

Partial engine failure:

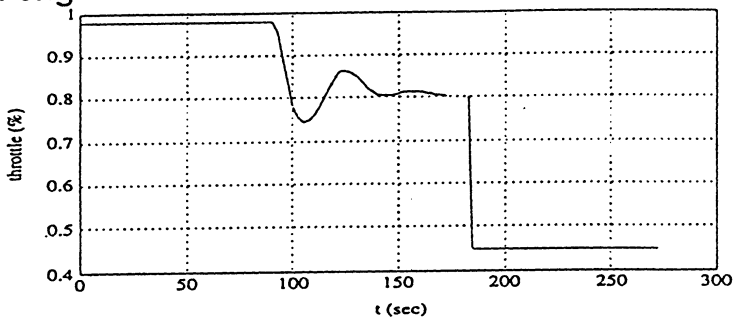

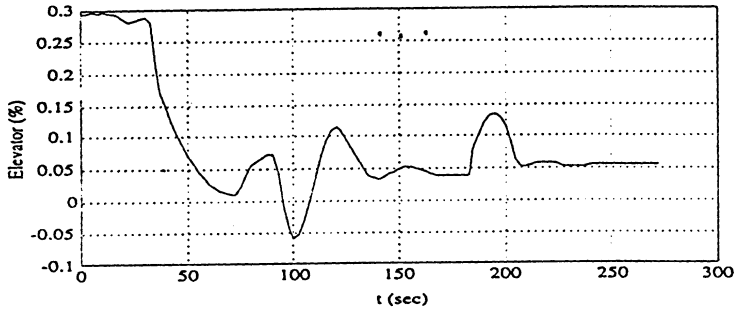

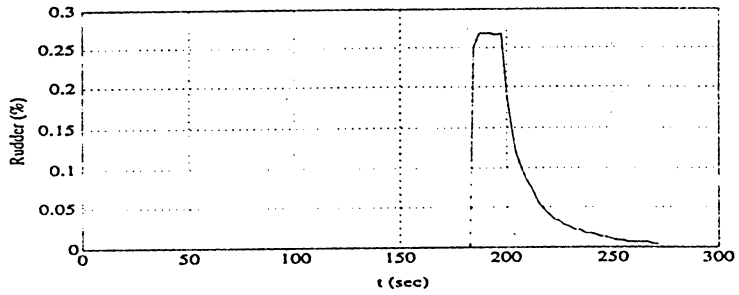

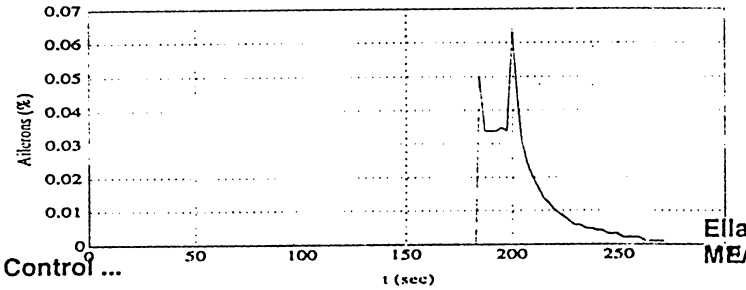

Engine out; turn back to airport

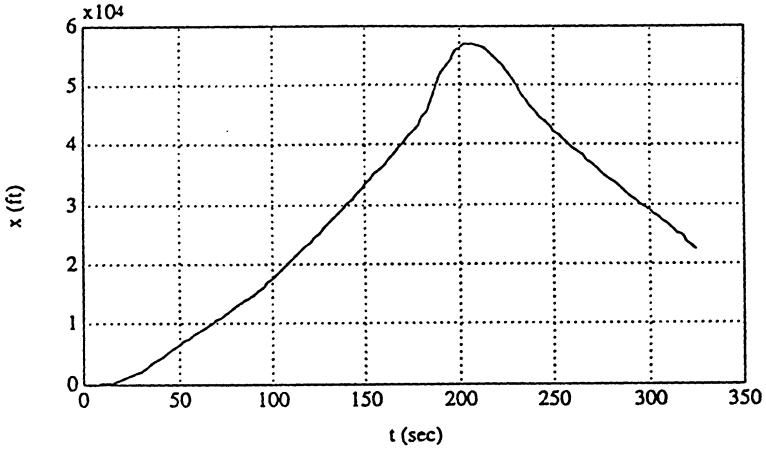

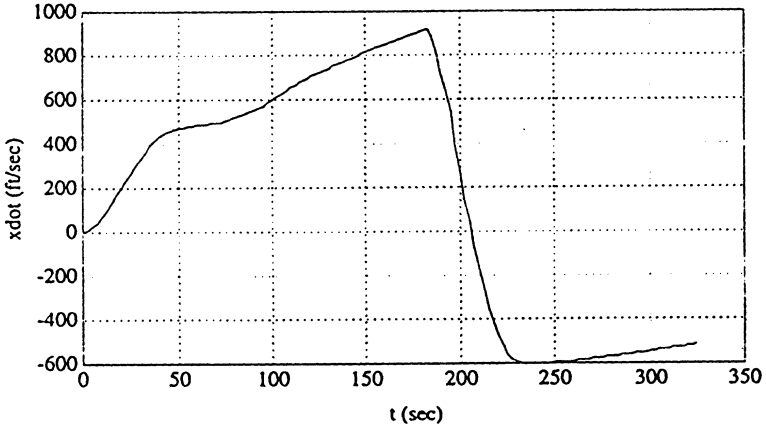

Engine out; turn back to airport

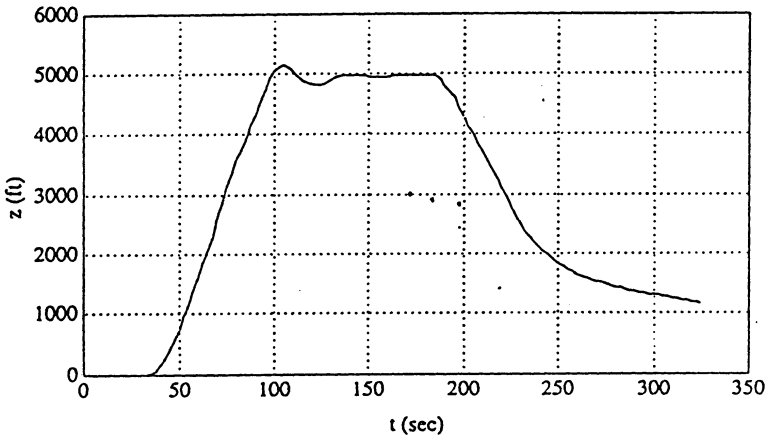

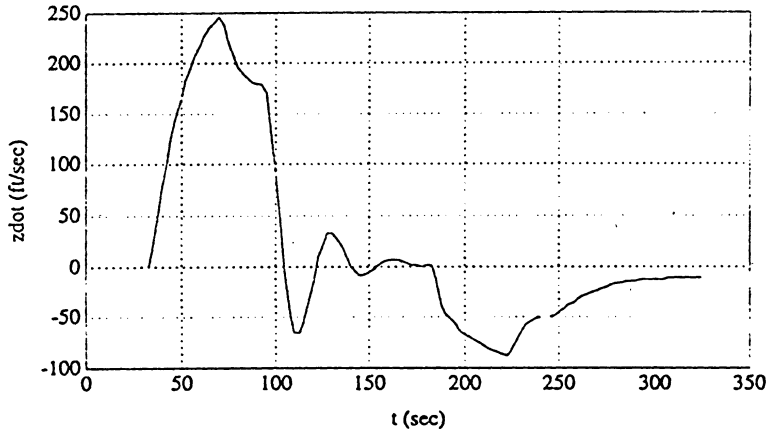

Engine out; turn back to airport

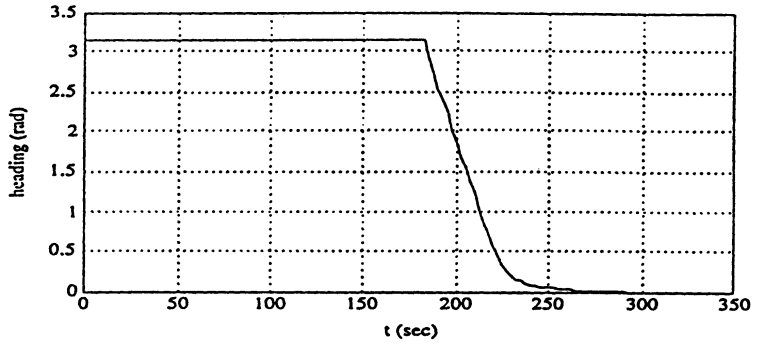

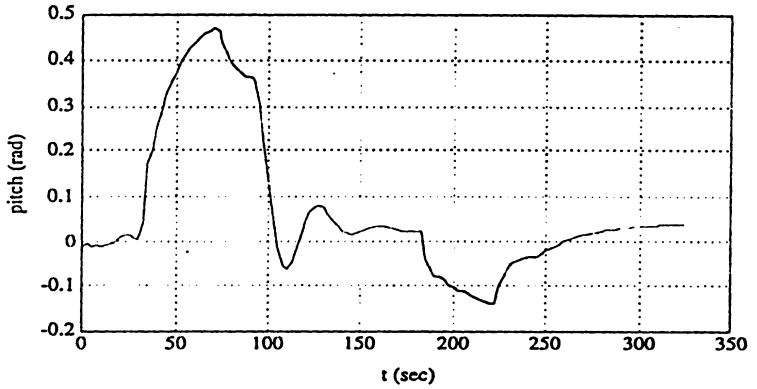

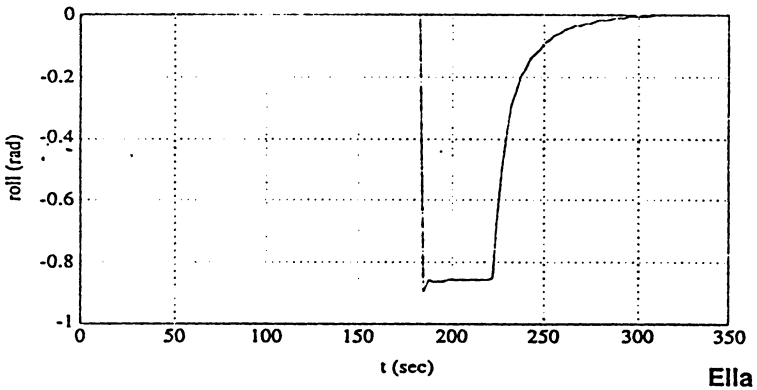

Engine out; turn back to airport

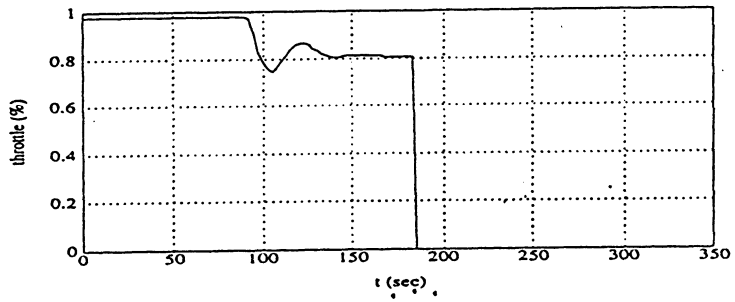

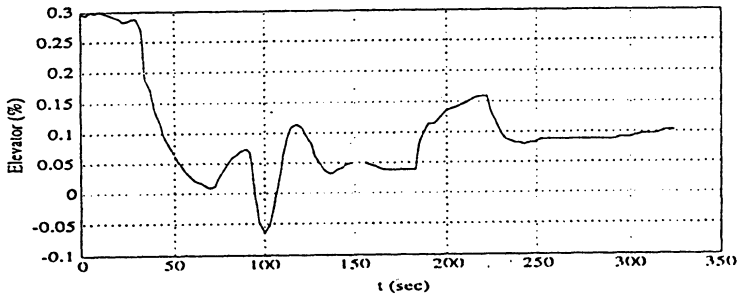

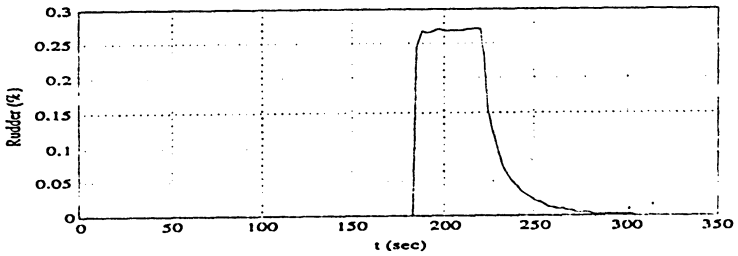

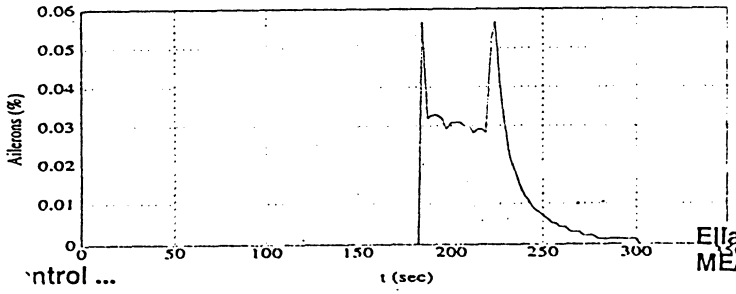

Engine Out Land Straight Ahead

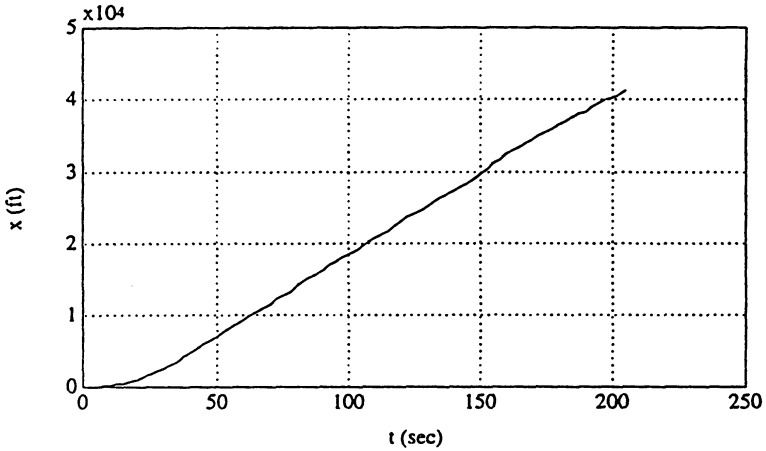

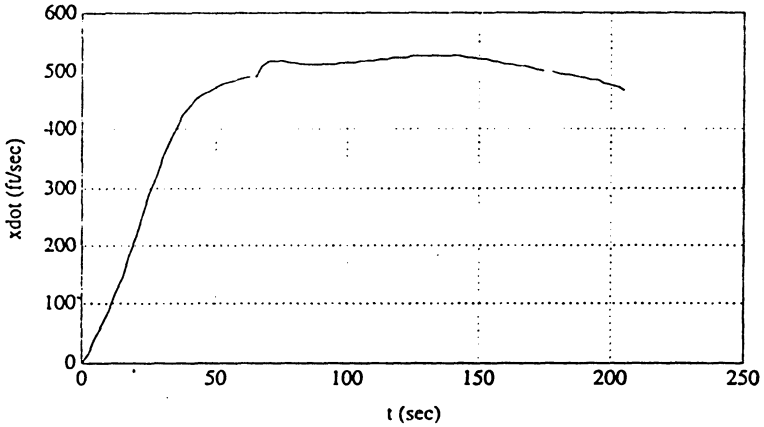

Engine Out Land Straight Ahead

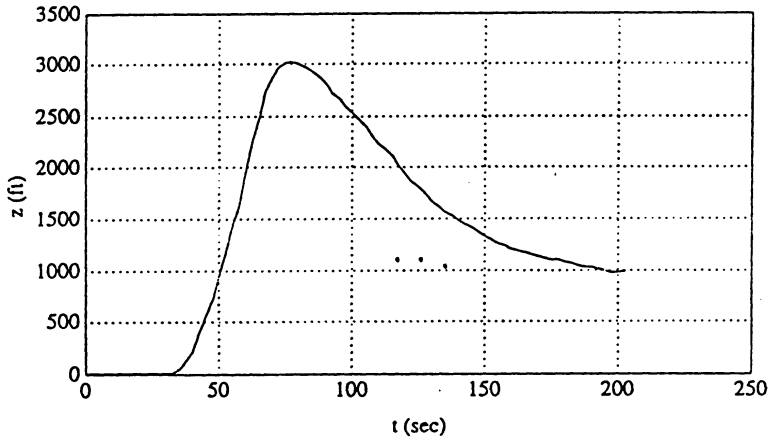

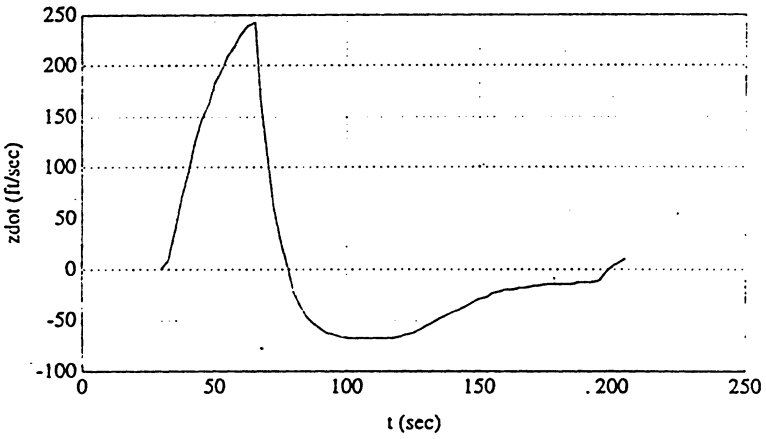

Engine Out Land Straight Ahead

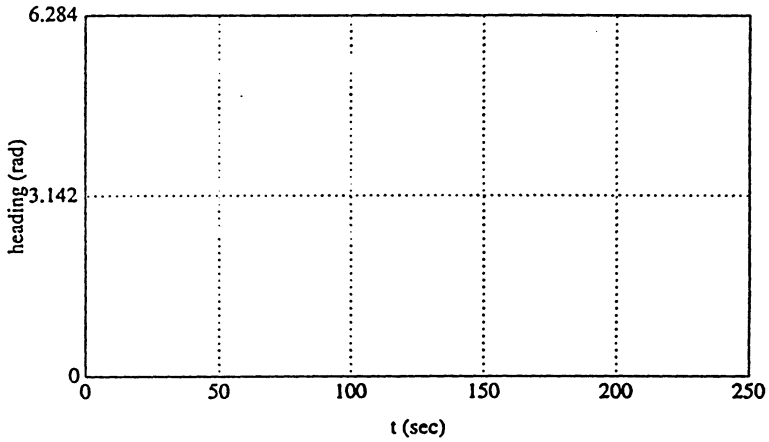

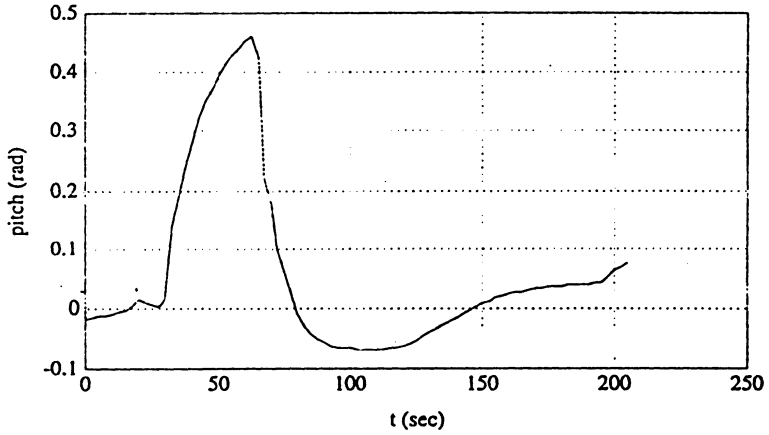

Engine Out Land Straight Ahead

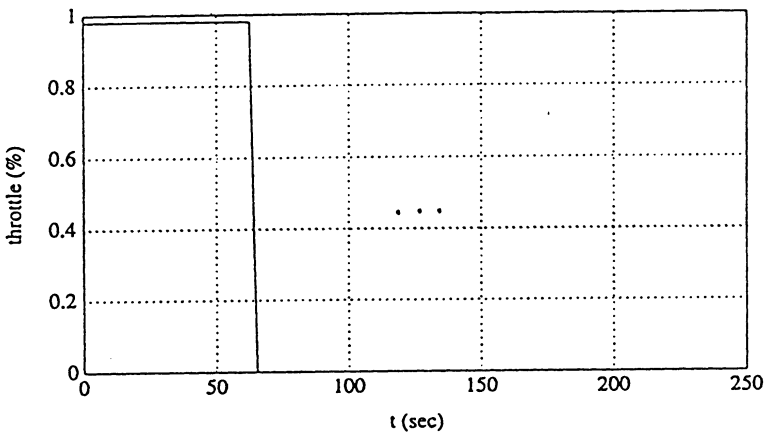

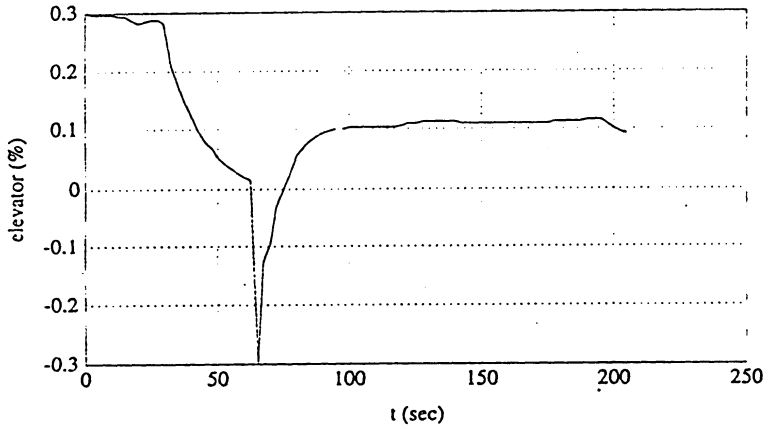

Summary

- **Aircraft dynamics are complicated**
  - Full 3-D motion present
  - Aerodyamics and engine "spool up" introduce nonlinear delays between input actuation and system response
  - Cannot assume small state changes for most normal aircraft maneuvers, thus a controller must be valid for large portion of state-space
- **Linear aircraft control system for this project based on pilot's standard use of sensor-actuator relations**
  - Control gains computed by "back of envelope" calculations and iteration during simulator runs
  - Interesting that such a non-mathematically-based controller could produce decent results...
- **Simple mathematical logic routine used to detect "engine out" emergency and select appropriate action based on state and failure severity**
- **Results show adequate performance, but would certainly need a more mathematically based controller before system could be called "robust"**

Discussion

- **Current commercial aircraft autopilots use linearized dynamical models for control**
  - These models make substantial approximations when state does not fall within "expected" parameters
  - Result: Pilot must currently fly manually when significant external disturbances or system failures occur
- **Most control design theory relies on linearized equations or luck in finding "ideal functions" to solve the control problem**
  - Finding an exhaustive set of such solutions that handle all possible aircraft situations seems unlikely in the near future
- **How should aircraft of the future be controlled?**

  a) Assume that the linearized models are "good enough" and that pilots should handle the other situations. (?)

  b) Nonlinear controls technology is ready to tackle the problem. (?) [suggestions of how?]

  c) ????

Assumptions

- **No unmodelled external disturbances (e.g. wind)**
  - Easy to achieve in a simulated environment
- **Full-state feedback possible**
  - Feasible with today's technology including GPS
- **Mach 1 (speed of sound) is constant**
  - Varies by <1% in test region
- **Air density is constant**
  - Varies by 14% for test region altitudes (0-5000 ft)
- **Aircraft weight, including fuel, is constant**
  - Test flights very short
- **Mach number does not affect Cd**
  - True for low Mach numbers
- **Aircraft local x-velocity much greater than y or z velocity**
  - Allows substituting $\dot{x}_{local}$ for velocity magnitude

December 1995

Finding the Feedback in Open-Loop Control

AE672 Project Report

by

Sanjay P. Bhat

Contents

1 Introduction

Consider the single-input control system on $\mathbb{R}^n$ given by

$$\begin{aligned} \dot{z}(t) &= f(z(t), v(t)), \\ z(0) &= x,\ z(t), x \in \mathbb{R}^n, v(t) \in \mathbb{R}. \end{aligned} \tag{1.1}$$

An *open-loop control* for this system is a choice of a control function for every initial condition x. In other words, the initial value of the state decides the control values at all subsequent instants of time, i.e.,

$$v(t) = u(x, t).$$

As opposed to this, *feedback control* is where the control value at any instant is decided by the value of the state variables at that same instant. Thus a feedback law is given by

$$v(t) = \phi(z(t)),$$

where ϕ is a function on the state space.

Open-loop controls suffer from poor disturbance rejection. This is because the state is measured only at the initial instant and any disturbance that comes into play after the initial instant cannot be accounted for. For instance, the control

$$u(x,t) = -B^{\mathrm{T}} e^{A^{\mathrm{T}} t} \left[\int_0^{t_1} e^{A\tau} B B^{\mathrm{T}} e^{A^{\mathrm{T}} \tau} d\tau \right]^{-1} x$$

drives the state of the controllable linear system (A, B) from the initial condition x to the origin in time t_1. But an impulsive disturbance acting at some instant in the interval $[0, t_1]$ causes the state at the final instant t_1 to be different from 0. Feedback strategies have better disturbance rejection properties. In the case where the disturbances act only over a finite time interval, eventually complete rejection maybe achieved.

It would be useful if open-loop strategies could be implemented through feedback. This would enhance disturbance rejection properties of the controller while retaining the original performance. Hence it is natural to ask the question:

(Q) *Which open-loop controls can be represented as feedback controls?*

This is a feasible question to ask, because the class of open-loop controls that can be written as feedbacks is non empty. This follows from the fact that every feedback can be written as an open-loop control by evaluating the feedback law along the closed-loop trajectories and then storing the result as a function of the initial conditions. In the notation of our example,

$$u(x,t) = \phi(\psi_t(x)), \tag{1.2}$$

where ψ_t is the flow of the closed-loop vector field, $f(x, \phi(x))$.

The main thrust of this project is towards finding some answers to the question (Q) posed above. In particular, given an open-loop control $u(x,t)$, we attempt to find out when there exists a feedback law ϕ such that (1.2) is satisfied.

One way of obtaining a feedback from an open-loop control is to treat the current state as the initial condition and the current time as the initial time. This has the effect of replacing $u(x,t)$ by $u(x(t),0)$. In this project we will also examine when this "resetting" is appropriate and in what sense. We will show that if an open-loop control arises from a feedback, then the feedback is recovered by resetting the open-loop control in the above fashion.

In section 2, we introduce the key concept of the terminal-subarc property and show how this concept can be used to answer the question (Q) in the time-invariant case.

In section 3, we indicate how the results of section 2 can be extended to time-varying systems.

In section 4, we show how the ideas of section 2 can be used to answer the following realization-type question:

> *When can a function $y(x,t)$ be written as a output function evaluated along the flow of a dynamical system?*

Section 5 shows how these same ideas can be used to show that solving a system of n ODEs is equivalent to finding n solutions of a linear PDE.

Finally, in section 6, we point out some interesting connections to geometric optics and optimal control theory that are worth exploring.

2 Open-Loop Control as Feedback: Time Invariant Case

Throughout this report, we assume that all required partial derivatives exist everywhere and are continuous, all vector fields have uniquely defined flows and are complete. Finally, it should be noted that depending on the problem data, some results may hold only locally, but this will be ignored to keep the discussion simple.

2.1 Compatibility and the Terminal-Subarc Property

Given a complete vector field f on $\mathbb{R}^n$ with the flow ψ_t^f and a function $y : \mathbb{R}^n \times \mathbb{R}^{\geq 0} \to \mathbb{R}$, we say that y is *compatible* with f if there exists a function $\phi : \mathbb{R}^n \to \mathbb{R}$ such that

$$y(x,t) = \phi \circ \psi_t^f(x), \tag{2.1}$$

for all $t \geq 0$ and $x \in \mathbb{R}^n$. In this subsection, we shall attempt to find a simple test for compatibility.

We say that y has the *terminal-subarc property* with respect to f if

$$y(x,t) = y(\psi_h^f(x), t-h), \tag{2.2}$$

for all $h \in [0,t]$, $t > 0$ and $x \in \mathbb{R}^n$.

To understand this property better, we rewrite (2.2) as

$$y(x, T+s) = y(\psi_T^f(x), s), \; T > 0, \; s \geq 0. \tag{2.3}$$

To every trajectory of f, we can assign the time-function $y(x,t)$, where x is the initial point of the trajectory. Note that the trajectory of the point ψ_T^f forms the terminal subarc of the trajectory of x. Thus (2.3) can be interpreted roughly as saying the following:

> *The time-function corresponding to every terminal subarc of a given trajectory forms the terminal part of the time-function corresponding to the given trajectory.*

Hence the name terminal-subarc property.

The following proposition gives a simple and useful characterization of this property.

Proposition 2.1. The function y has the terminal-subarc property with respect to f if and only if the partial differential equation

$$\frac{\partial y}{\partial x}(x,t) f(x) - \frac{\partial y}{\partial t}(x,t) = 0. \tag{2.4}$$

holds on $\mathbb{R}^n \times \mathbb{R}^{\geq 0}$.

Proof. Denote $\bar{x} = \begin{bmatrix} x \\ t \end{bmatrix}$. Consider the vector field $\bar{f}(\bar{x}) = \begin{bmatrix} f(x) \\ -1 \end{bmatrix}$ on $\mathbb{R}^{n+1}$ and let $\psi_t^{\bar{f}}$ be the corresponding flow. Then $\psi_h^{\bar{f}}(\bar{x}) = \begin{bmatrix} \psi_h^f(x) \\ t-h \end{bmatrix}$. Equation (2.2) can be rewritten as

$$y(\bar{x}) = y(\psi_h^{\bar{f}}(\bar{x})),$$

for $h \in [0,t]$, $t > 0$. In other words, y is constant along the trajectories of $\bar{f}$. This can happen if and only if

$$L_{\bar{f}} y = 0. \tag{2.5}$$

Rewriting (2.5) in terms of the coordinates (x,t) yields (2.4). □

The following proposition reveals the relationship between compatibility and the terminal-subarc property, and is a key result of this project.

Proposition 2.2. The function y is compatible with f if and only if y has the terminal-subarc property with respect to f. If y is compatible with f, then the function ϕ satisfying (2.1) is uniquely given by

$$\phi(x) = y(x, 0). \tag{2.6}$$

Proof. If y is compatible with f, then (2.1) holds for some $\phi : \mathbb{R}^n \to \mathbb{R}$. Now, for $t > 0$ and $h \in [0, t]$,

$$\begin{aligned} y(x,t) &= \phi \circ \psi_t^f(x) \\ &= \phi \circ \psi_{t-h}^f(\psi_h^f(x)) \\ &= y(\psi_h^f(x), t-h). \end{aligned}$$

Thus y satisfies the terminal-subarc property.

On the other hand, if (2.2) holds, then for $h = t$,

$$y(x,t) = y(\psi_t^f(x), 0).$$

Therefore, (2.1) holds with $\phi(x) = y(x,0)$.

Finally, if (2.1) holds, then taking $t = 0$ yields (2.6). □

The following theorem follows from the previous two propositions.

Theorem 2.1. The function y is compatible with f if and only if (2.4) holds on $\mathbb{R}^n \times \mathbb{R}^{\geq 0}$.

2.2 Open-Loop Control and Feedback

Consider the single-input control system

$$\dot{x} = f(x,u) \tag{2.7}$$

on $\mathbb{R}^n$. By an *open-loop control*, we mean a function $u : \mathbb{R}^n \times \mathbb{R}^{\geq 0} \to \mathbb{R}$ such that for every x, the solution to the initial value problem

$$\dot{z} = f(z, u(x,t)),\ z(0) = x,$$

is uniquely defined on $[0, \infty)$. We say that the open-loop control u is *equivalent to a feedback* for (2.7) if u is compatible with the vector field $f(x, u(x,0))$. The following proposition brings out the motivation behind this definition. Essentially, if u is equivalent to a feedback for (2.7), then resetting the open-loop control leaves the solutions of the controlled system unchanged.

Proposition 2.3. If u is equivalent to a feedback for (2.7), then, for any given initial condition x, the two initial value problems

$$\dot{z}(t) = f(z(t), u(x,t)),\ z(0) = x, \tag{2.8}$$

$$\dot{z}(t) = f(z(t), u(z(t),0)),\ z(0) = x, \tag{2.9}$$

have the same solution.

Proof. Let ψ_t denote the flow of the vector field $f(x, u(x,0))$. Then the unique solution to (2.9) is $z(t) = \psi_t(x)$. If u is equivalent to a feedback for (2.7), then it satisfies the terminal-subarc property with

respect to $f(x, u(x,0))$. Therefore, $u(x,t) = u(\psi_t(x), 0) = u(z(t), 0)$. Thus, for a given initial condition, the right-hand sides of (2.8) and (2.9) are equal. By uniqueness, the two initial value problems have the same solution. □

The following corollary provides the answer to our original question (Q) and follows directly from Proposition 2.2.

Corollary 2.1. The open-loop control u is equivalent to a feedback for (2.7) if and only if the partial differential equation

$$\frac{\partial u}{\partial x}(x,t) f(x, u(x,0)) - \frac{\partial u}{\partial t}(x,t) = 0. \tag{2.10}$$

holds on $\mathbb{R}^n \times \mathbb{R}^{\geq 0}$.

3 Time-Varying Systems

Given a time-varying vector field $f(x,t)$ on $\mathbb{R}^n$ with the time-varying flow $\psi^f_{t_0,t}$ and a function $y : \mathbb{R}^n \times \mathbb{R}^{\geq 0} \times \mathbb{R}^{\geq 0} \to \mathbb{R}$, we say that y is compatible with f if there exists a function $\phi : \mathbb{R}^n \times \mathbb{R}^{\geq 0} \to \mathbb{R}$ such that

$$y(x, t_0, h) = \phi(\psi^f_{t_0, t_0+h}(x), t_0 + h), \tag{3.1}$$

for $(x, t_0, h) \in \mathbb{R}^n \times \mathbb{R}^{\geq 0} \times \mathbb{R}^{\geq 0}$.

Given a single-input time-varying control system

$$\dot{z} = f(z, u, t) \tag{3.2}$$

on $\mathbb{R}^n$ and a time-varying open-loop control $u(x, t_0, h)$, we say that u is equivalent to a feedback for (3.2) if u is compatible with the time-varying vector field $f(z, u(z, t, 0), t)$.

Using arguments similar to those used in Section 2, it can be shown that

1. y is compatible with f if and only if it satisfies the *time-varying terminal-subarc property*,

$$y(x, t_0, h) = y(\psi^f_{t_0, t_0+\tau}(x), t_0 + \tau, h - \tau), \tag{3.3}$$

for all $\tau \in [0, h]$ and $(x, t_0, h) \in \mathbb{R}^n \times \mathbb{R}^{\geq 0} \times \mathbb{R}^{\geq 0}$.

2. y satisfies the terminal-subarc property with respect to f if and only if the partial differential equation

$$\frac{\partial y}{\partial x}(x, t_0, h) f(x, t_0 + h) + \frac{\partial y}{\partial t_0}(x, t_0, h) - \frac{\partial y}{\partial h}(x, t_0, h) = 0 \tag{3.4}$$

holds on $\mathbb{R}^n \times \mathbb{R}^{\geq 0} \times \mathbb{R}^{\geq 0}$.

3. If u is equivalent to a feedback for (3.2), then, for any given initial condition x and initial time t_0, the two initial value problems

$$\dot{z}(t) = f(z(t), u(x, t_0, t-t_0), t),\ z(t_0) = x, \tag{3.5}$$

$$\dot{z}(t) = f(z(t), u(z(t), t, 0)),\ z(t_0) = x, \tag{3.6}$$

have the same solutions for $t \geq t_0$.

4. The open-loop control u is equivalent to a feedback for (3.2) if and only if the partial differential equation

$$\frac{\partial u}{\partial x}(x, t_0, h) f(x, u(x, t_0+h, 0), t_0+h) + \frac{\partial u}{\partial t_0}(x, t_0, h) - \frac{\partial u}{\partial h}(x, t_0, h) = 0 \tag{3.7}$$

holds on $\mathbb{R}^n \times \mathbb{R}^{\geq 0} \times \mathbb{R}^{\geq 0}$.

4 A Question on Realization

Given a function $y : \mathbb{R}^n \times \mathbb{R}^{\geq 0} \to \mathbb{R}$, we say that y is *time-invariantly dynamically generated* if there exists a vector field f on $\mathbb{R}^n$ such that y is compatible with f. It follows from Proposition 2.2 that y is time-invariantly dynamically generated if and only if there exists a vector field $\bar{f}$ on $\mathbb{R}^n \times \mathbb{R}^{\geq 0}$ such that

$$L_{\bar{f}} y = 0,\ (compatibility), \tag{4.1}$$

$$[\bar{f}, \tfrac{\partial}{\partial t}] = 0,\ (time-invariance), \tag{4.2}$$

$$dt(\bar{f}) = -1. \tag{4.3}$$

For convenience, define the following codistributions on $\mathbb{R}^{n+1}$:

$$\Omega_r = \left\{dy, dL_{\frac{\partial}{\partial t}} y, \ldots, dL^r_{\frac{\partial}{\partial t}} y\right\}, \tag{4.4}$$

$$\hat{\Omega}_r = \left\{dy, dL_{\frac{\partial}{\partial t}} y, \ldots, dL^r_{\frac{\partial}{\partial t}} y, dt\right\},\ r = 1, 2, 3, \ldots. \tag{4.5}$$

Remark 4.1. Let $r^* = \max_r \operatorname{rank} \Omega_r$. Then $\operatorname{rank} \Omega_{r^*} = r^*$. This is because if $dL^k_{\frac{\partial}{\partial t}} y \in \Omega_r$ for some $k > r$, then $dL^l_{\frac{\partial}{\partial t}} y \in \Omega_r$ for $l = k, k+1, \ldots$.

Remark 4.2. If $\bar{f}$ satisfies (4.1) and (4.2), then $L_{\bar{f}} L_{\frac{\partial}{\partial t}} y = L_{[\bar{f}, \frac{\partial}{\partial t}]} y + L_{\frac{\partial}{\partial t}} L_{\bar{f}} y = 0$. Similarly, it can be shown that $L_{\bar{f}} L^r_{\frac{\partial}{\partial t}} y = 0$ for $r = 2, 3, \ldots$. Thus $\bar{f} \in \ker \Omega_{r^*}$. On the other hand, if $\bar{f} \in \ker \Omega_{r^*}$, then $\bar{f}$ satisfies (4.1).

Remark 4.3. The codistributions Ω_{r^*} and $\hat{\Omega}_{r^*}$ are invariant w.r.t. the vector field $\frac{\partial}{\partial t}$. This simply follows from our definition of r^*.

These remarks lead to the following proposition.

Proposition 4.1. The function y is time-invariantly dynamically generated if and only if rank $\hat{\Omega}_{r^\bullet} = r^*+1$.

Proof. The necessity follows by noting that if there exists a vector field $\bar{f}$ isatisfying (4.1) and (4.3), then $\bar{f} \in \ker \Omega_{r^\bullet}$ and $dt(\bar{f}) \neq 0$. Therefore, $dt \notin \Omega_{r^\bullet}$ and rank $\hat{\Omega}_{r^\bullet} = r^* + 1$.

The sufficiency will not be worked out in detail, but can be established by proving the following statements:

1. There exist vector fields $\bar{f}_i$, $i = r^* + 1, \ldots, n+1$, such that $\ker \hat{\Omega}_{r^\bullet} = \{\bar{f}_{r^\bullet+1}, \ldots, \bar{f}_n\}$ and $\ker \Omega_{r^\bullet} = \ker \hat{\Omega}_{r^\bullet} + \{\bar{f}_{n+1}\}$.

2. The vector field $\bar{f}_{n+1}$ can be chosen to satisfy (4.2) and (4.3).

□

5 An Application to Differential Equations

Given a vector field f on $\mathbb{R}^n$, define the vector field $\bar{f}$ on $\mathbb{R}^{n+1}$ as before. The codistribution, $\Omega = \{\bar{f}\}^\perp$ is integrable. Therefore, there exist n functions $y_i(x,t)$ such that the differentials dy_i are independent on $\mathbb{R}^{n+1}$ and $dy_i(\bar{f}) = 0$. Furthermore, the vectors $\frac{\partial y_i}{\partial x}(x,0)$ are linearly independent over $\mathbb{R}$ at every x. Consequently, if we form the vector $Y(x,t) = [y_1(x,t), \cdots, y_n(x,t)]^{\mathrm{T}}$, then $\Phi(x) = Y(x,0)$ is a diffeomorphism on $\mathbb{R}^n$. Each of the functions y_i is compatible with the vector field f, so that $Y(x,t) = \Phi(\psi_t^f(x))$. Hence, we can obtain the flow of f as

$$\psi_t^f(x) = \Phi^{-1}(Y(x,t)).$$

Thus solving the system of ODEs

$$\dot{z} = f(z),$$

is equivalent to finding n independent solutions of the PDE

$$\frac{\partial y}{\partial x}(x,t)f(x) - \frac{\partial y}{\partial t}(x,t) = 0.$$

This is also equivalent to finding a basis of exact forms for the codistribution Ω.

6 Ideas to Explore

This section, which is somewhat speculative in nature, documents some of the ideas that suggested themselves during the course of this project.

6.1 Geometric Optics and Compatibility

We briefly review the fundamental notions of geometric optics. Concise treatments of these ideas can be found in [1] and [2].

Consider a medium that fills out $\mathbb{R}^n$ and in which a disturbance propagates according to the principles of geometric optics. Assume that the medium is inhomogeneous and anisotropic, so that the velocity of propagation of the disturbance depends both on the position and the direction of propagation. Let $f(x,v)$ denote the reciprocal of this velocity at the point $x \in \mathbb{R}^n$ in the direction $v \in T\mathbb{R}^n_x$. If $\gamma : [s_0, s_1] \to \mathbb{R}^n$ is a differentiable curve in $\mathbb{R}^n$ joining $x_0 = \gamma(s_0)$ to $x_1 = \gamma(s_0)$, then the time taken by the disturbance to traverse this curve is

$$\int_{s_0}^{s_1} f(\gamma(s), \gamma'(s))ds. \tag{6.1}$$

According to *Fermat's Principle*, the actual path taken by the disturbance in going from x_0 to x_1 is the one that takes the least time, i.e., the one that minimises (6.1). Curves that minimise (6.1) are the *rays* of the disturbance. A *wavefront* at any instant is the set of points that the disturbance has reached at that instant. Rays take a wavefront at any given instant to wavefronts at subsequent instants. *Huygen's principle* relates wavefronts corresponding to different time instants. If the wavefront at time t is given by $\mathcal{W}_t = \{x : S(x,t) = 0\}$, then S satisfies the Hamilton-Jacobi equation,

$$\tfrac{\partial S}{\partial t} + H(x, \tfrac{\partial S}{\partial x}) = 0, \tag{6.2}$$

for a certain Hamiltonian H. Furthermore, the rays satisfy a Hamiltonian system of equations with Hamiltonian H.

Now, given a function $y(x,t)$ as before and a vector field f, define wavefronts as $\mathcal{W}_t = \{x : y(x,t) = 0\}$ and the Hamiltonian $H(p,x) = -p^{\mathrm{T}} f(x)$. Then, it can be shown that y is compatible with f if and only if the flow of the vector field $-f$ carries wavefronts to wavefronts, i.e.,

$$\psi_h^{-f}(\mathcal{W}_t) = \mathcal{W}_{t+h}.$$

Moreover, equation (2.4) can be rewritten as the Hamilton-Jacobi equation

$$\tfrac{\partial y}{\partial t} + H(\tfrac{\partial y}{\partial x}, x) = 0.$$

The function y is thus analogous to the function S in (6.2) while the trajectories of the flow ψ_t^{-f} are analogous to the rays of a disturbance. It would be interesting to see if the analogy can be completed. In other words:

> *Given a dynamical system, can we ascribe the state space with inhomogeneous and anisotropic disturbance-carrying properties characterized by some function $f(x,v)$, such that the trajectories of the dynamical systems satisfy Fermat's principle? If so, then what does Huygen's principle tell us about dynamical systems?*

These ideas are summarized in the following table.

Optics	Dynamical Systems
Medium of propagation	State space
Rays	Trajectories
Wavefronts	Level sets of an output function
$f(x, v)$	??
Fermat's Principle	??
Huygen's Principle	??

6.2 Connections to Optimal Control Theory

The *Principle of Optimality* [3] states that the solutions to certain types of optimal control problems, which are typically in the form of open-loop controls, have the property that they are also optimal on every terminal subarc of the optimal trajectory. Stated differently, *an optimal control satisfies the terminal-subarc property on the optimal trajectory.* One is, therefore, led to ask if an optimal control satisfies a condition similar to (2.10). It is also of interest to see if (2.10) is related to the maximum principle or to Hamilton-Jacobi-Bellman theory.

7 Conclusion

Useful and satisfying answers were found to the original questions posed at the beginning of the project. These answers further suggested other interesting questions which were also answered. In the process, a few novel ideas were thrown up that deserve closer inspection.

An attempt was made to come up with examples to illustrate the utility of some of the results to control problems. However, no interesting example has yet been found.

References

[1] V. I. Arnold, *Mathematical Methods of Classical Mechanics*, IInd edition, Springer Verlag, New York (1989), pp. 248-258.

[2] I. M. Gelfand and S. V. Fomin, *Calculus of Variations*, Prentice-Hall, Englewood Cliffs, NJ (1963), pp. 208-217.

[3] G. Leitmann, *The Calculus of Variations and Optimal Control: An Introduction*, Plenum Press, New York (1981), pp. 85-87.

December 8, 1995

Virtual Resetting Absorbers: New Ways to Get Energy Out Of a System

Robert T. Bupp
Term Project
Advanced Nonlinear Control
Prof. Dawn Tilbury
Fall 1995

Contents

1 Scope of Project

This term project represents the current state of the author's research progress in the area of virtual resetting absorbers for control. This project began only a few weeks prior to the beginning of the Fall '95 term, and thus represents approximately one semester's work.

The overall goals for this project include developing or modifying a theory to describe systems with virtual resetting absorbers, and developing control stategies utilizing the virtual resetting absorbers that outperform linear time-invariant controllers in terms of energy dissipation and disturbance rejection.

Due to the goal-oriented nature of this early stage of the research, Section 3, which is devoted to theoretical developments, is neither detailed nor complete. Instead this development will be pursued during the course of the next semester.

A description of the synthesis approaches for designing virtual resetting absorbers for control is divided between Section 3.2, Section 4, and Section 5 of this report. Section 3.2 introduces and develops a virtual resetting absorber design that we will refer to as a one-way absorber, since it has the property that energy can flow from the primary system to the absorber, but not from the absorber back to the primary system. The one-way energy flow property can be interpreted as follows: the plant can do positive work on the absorbr subsystem ,but the absorber can never do positive work on the plant. Consequently, the one-way absorber controller can never increase the energy of the plant.

Section 4 deals with finite-time stabilization problems. Since this section contains the strongest results, it is given the most detailed description. These results, however, are restricted to finite-time stabilization of the double integrator and the undamped oscillator, which are feedback equivalent, second-order systems. The extension of these results to plants of order greater than two is incomplete. Such an extension would potentially provide some very strong results, and as such, this extension is currently receiving the "lion's share" of the author's research efforts.

Section 5 deals with the application of virtual resetting absorbers to disturbance rejection problems. The results here are fairly weak, in the sense that it is not clear what, if any, advantage the virtual resetting absorbers can provide compared to certain linear time-invariant controllers. However, the advantage of virtual resetting absorber for disturbance rejection could be greatly increased if results could be obtained for finite-time stabilization of, say, fourth-order systems. This issue will be investigated within Section 5, in the context of a conjecture. Furthermore, the linear time-invariant controllers used as comparisons for the virtual resetting absorbers, represent linear absorber designs that may as yet unexplored in the literature.

Clearly, there is much work to be done in the area of virtual resetting absorbers for control. Section 6 describes what the author sees as some of the important directions to pursue in this research area. Some conclusions are given in Section 7.

2 Introduction

Stabilization of undamped motion is a fundamental problem in control engineering. Consider the case of the double integrator $M\ddot{q} = u$. While exponential stability can be obtained by simply setting $u = -a\dot{q} - bq$, where a and b are positive constants, it is often of interest in practice to stabilize the motion in finite time. For this objective the classical optimal control literature provides two approaches, namely, the minimal-time controller and the minimal-energy controller [1, 2]. The purpose of this paper is to develop an alternative control approach to yield a third controller that stabilizes the double integrator in finite time, and, in addition, eliminates the need for full-state feedback.

The controllers we develop in this paper are based upon physical principles rather than optimality criteria. Inspired by the extensive literature on mechanical absorbers [3], these new controllers are designed to emulate the action of mechanical proof-mass absorbers by applying forces to the plant that a physical proof-mass absorber would apply. Since the proof-mass absorbers are emulated rather than implemented, these controllers can be viewed as *virtual* absorbers.

The controller design involves choosing the values of the virtual proof mass and spring elements so that, at some instant in time, all of the energy associated with the double integrator is transferred to the absorber subsystem. Ordinarily the absorber subsystem would possess all of the energy only instantaneously, after which time energy would begin to return to the plant. However, since the time at which the total energy transfer occurs is known, the controller can be turned off at that instant, and the energy will appear to be instaneously removed, as if it had exited through a trap door. The double integrator will then remain at rest at the origin. For this reason, this controller is called a *virtual trap-door absorber.*

Since the virtual trap-door absorber is only active on a finite time interval, it is useful to consider an extension of this controller that can be turned off, or *reset*, and then restarted. This class of controllers is called *virtual resetting absorber* controllers, and it contains the virtual trap-door absorber as a subclass.

Another subclass of virtual resetting absorber controllers, called *one-way absorber* controllers is developed in this report. This class of controllers is characterized by allowing energy to be transferred from the plant to the controller, while prohibiting energy from being transferred from the controller back to the plant. The one-way absorber controllers can be shown to be passive[1], and thus they have desirable stability robustness properties.

The structure of the report is as follows: in Section 3 some theoretical foundation is given for the description of systems with virtual resetting absorber subsystems, and in Section 3.2 the one-way absorber controller is developed.

In Section 4 finite-time stablization control problems are solved for the double integrator and the undamped oscillator, using virtual resetting absorbers; in particular, virtual trap-door absorbers are used. The virtual trap-door absorber controllers used to finite-time stabilize the double integrator are compared to the minimal-time and minimal-energy solutions for this problem.

[1]Technically, this is only a conjecture at this point. Arguments to support this statement are given in Section 3.2 to support this conjecture, in lieu of a proof.

In Section 5, virtual resetting absorber controllers are applied to the disturbance rejection problem. Examples, weaknesses, and keys to further development are discussed. A discussion of directions for futher research in the area of virtual resetting absorber controllers is given in Section 6, and some final conclusions are given in Section 7.

3 Theoretical Framework

The virtual resetting controllers developed in this paper can be described by "jump" or "impulsive" differential equations. The (readily) available literature on systems described by impulsive differential equations, for example [4], is not well suited to describe the systems of interest in this paper. Consequently, the following development will not borrow much in the way of notation from the literature, but instead will feature notation especially well suited to virtual resetting controllers.

3.1 Virtual Resetting Controllers

The virtual resetting absorber controllers considered in this paper can be described by the following resetting differential system.

$$\begin{aligned} \dot{x}_c(t) &= f_c(x_c(t)) + G_c(x_c(t))y(t), \qquad t \neq t_k, && (1)\\ x_c(t_k) &= f_{ck}(x_c(t_k^-), y(t_k^-)), && (2)\\ u(t) &= h_c(x_c(t)) + J_c(x_c(t))y(t), && (3) \end{aligned}$$

where $x_c \in \mathbb{R}_c^n$, $y \in \mathbb{R}^p$, $u \in \mathbb{R}^m$, $f_c : \mathbb{R}_c^n \to \mathbb{R}$, $G_c : \mathbb{R}_c^n \to \mathbb{R}^{n_c \times p}$, $h_c : \mathbb{R}_c^n \to \mathbb{R}^m$, $J_c : \mathbb{R}_c^n \to \mathbb{R}^{m \times p}$, $f_{ck} : \mathbb{R}_c^n \times \mathbb{R}^p \to \mathbb{R}_c^n$, $k = 0, 1, 2, \ldots$; $\{t_k\}$ is a sequence of time instants, not necessarily equally spaced, such that $0 = t_0 < t_1 < \cdots < t_k$ and $t_k \to \infty$ as $k \to \infty$ and

$$x_c(t_k^-) \triangleq \lim_{\varepsilon > 0, \varepsilon \to 0} x_c(t_k - \varepsilon). \qquad (4)$$

In words, the resetting controller (1) - (3) is described by a well-behaved ordinary differential equation, with the exception that the states x_c of the controller are reset at possibly irregularly spaced times. Notice that the mechanism for determination of the time t_k at which the states of the system are reset is not made explicit.

3.2 Virtual One-Way Absorbers

A novel application of resetting differential equations for control is the virtual one-way absorber controller. This controller is useful for enhancing the energy dissipation of a lossless or lightly damped plant. For example, consider the single-input, single-output plant

$$\begin{aligned} \dot{x} &= Ax + Bu, && (5)\\ y &= Cx, && (6) \end{aligned}$$

where

$$x \triangleq \begin{bmatrix} q \\ \dot{q} \end{bmatrix}, \quad A \triangleq \begin{bmatrix} 0 & 1 \\ -1 & 0 \end{bmatrix}, \quad B \triangleq \begin{bmatrix} 0 \\ 1 \end{bmatrix}, \quad C \triangleq \begin{bmatrix} 1 \\ 0 \end{bmatrix}^{\mathrm{T}}, \qquad (7)$$

which describes a controlled undamped oscillator with position output. This sum of the kinetic and potential energies of this plant provide a suitable Lyapunov function, given by

$$V(x) = \frac{1}{2} x^{\mathrm{T}} x. \qquad (8)$$

It follows that for the uncontrolled oscillator $V \triangleq V'(x)x = 0$.

The classical Den Hartog absorber consisting of a mass m on a spring k, can be used as a starting point for the design of the one-way absorber. The effect of the absorber on the plant is given by the dynamic compensator

$$\begin{aligned} \dot{x}_c &= A_c x_c + B_c y, \qquad (9) \\ u &= C_c x_c + D_c y, \qquad (10) \end{aligned}$$

where

$$x_c \triangleq \begin{bmatrix} q_c \\ \dot{q}_c \end{bmatrix}, \quad A_c \triangleq \begin{bmatrix} 0 & 1 \\ -k/m & 0 \end{bmatrix}, \quad B_c \triangleq \begin{bmatrix} 0 \\ 1/m \end{bmatrix}, \quad C_c \triangleq \begin{bmatrix} k \\ 0 \end{bmatrix}^{\mathrm{T}}, \quad D_c = -k. \qquad (11)$$

The total (virtual) energy of the absorber subsystem is given by the sum of its kinetic and potential energies, as

$$V_c(x_c, y) = \frac{1}{2} m \dot{q}_c^2 + \frac{1}{2} k (q_c - y)^2. \qquad (12)$$

A Lyapunov function for the closed-loop system is given by

$$V_{cl}(x, x_c) = V(x) + V_c(x_c, y). \qquad (13)$$

It is readily seen that $\dot{V}_{cl} = 0$, and the closed-loop system is lossless.

The next stage of the design of the one-way absorber controller, is accomplished by defining the resetting law

$$x_c(t_k) = \begin{bmatrix} y(t_k^-) \\ 0 \end{bmatrix}, \quad k = 0, 1, 2, \ldots, \qquad (14)$$

where $t_0 = 0$. It follows from this resetting scheme that $V_c(x_c(t_k)) = 0$.

Lemma 1. The feedback interconnection of the plant (5)-(6) with the resetting compensator (9)-(10), (14) is Lyapunov stable.

Proof: The closed-loop Lyapunov function satisfies

$$\dot{V}_{cl}(x(t), x_c(t)) = V_{cl}(x(t_k), x_c(t_k)), \quad t \in [t_k, t_{k+1}), \quad k = 0, 1, 2, \ldots, \qquad (15)$$

and

$$V_{cl}(x(t_k), x_c(t_k)) = V(x(t_{k-1})) - V_c(x_c(t_k^-), y(t_k^-)) \leq V_{cl}(x(t_{k-1}), x_c(t_{k-1})), \qquad (16)$$

and thus $V_{cl}(x(t), x_c(t))$ is nonincreasing. □

To complete the design of the virtual one-way absorber controller, let the times t_k correspond to the times at which the (virtual) energy in the absorber (compensator) stops increasing. It is possible to determine the resetting times by computing $\dot{V}_c$ online, and resetting the states whenever $\dot{V}_c = 0$. Note that

$$\dot{V}_c(x_c, y) = \frac{\partial V_c}{\partial q_c} \dot{q}_c + \frac{\partial V_c}{\partial \dot{q}_c} (y - q_c) + \frac{\partial V_c}{\partial y} \dot{y}, \qquad (17)$$

and thus an accurate computation of V_c requires the ability to compute $\dot{y}$. If the plant dynamics are well know, then this approach for determining the resetting times may work well. However, the virtual one-way absorber controller is passive, and as such, it would be desirable to make the resetting scheme be independent of the plant model.

In practice, the resetting times can be determined by monitoring the value of the compensator energy $V_c(x_c, y)$, and resetting the states when $V_c(x_c, y)$ stops increasing. While technically, this may only approximate a one-way absorber, the associated error is very small (see Conjecture 2), and this technique is effective and easy to implement.

Conjecture 1. The virtual one-way absorber controller is passive.

By definition of the virtual one-way absorber, either the energy of the absorber subsystem is increasing, or the states of the absorber are reset – in which case the energy in the absorber is set to zero. If the energy of the absorber is increasing, then the plant is necessarily doing positive work on the absorber. Equivalently, the absorber is doing negative work on the plant. Consequently, this one-way algorithm has no mechanism for doing positive work on the plant, and this observation is the basis for Conjecture 1.

Conjecture 2. While small delays in determining the resetting times may allow the virtual one-way absorber to do positive work on the plant, this effect should be very small.

The control signal generated by the virtual one-way absorber must always have the opposite sign of the velocity of the point on the plant where it is attached; otherwise, the absorber would be doing positive work on the plant. It follows, then, that the resetting times are associated with times at which either the velocity or the control force generated by the virtual absorber subsystem changes sign[2]. Since both the velocity and the control signal are continuous functions in time, it follows that a short time after one of these signals passes through zero, it is still close to zero, and therefore the product of force and velocity – the rate at which work is done on the plant – is also small. Conjecture 2 is based on this observation.

Results of numerical simulations of this example system consisting of an undamped oscillator with a virtual one-way absorber controller are illustrated by the following figures. The parameters for the one-way absorber in this example are $m = 1$, and $k = 1$. Figure 1 and Figure 2 illustrate the response of the system to an initial velocity of the plant mass, while Figure 1 and Figure 2 illustrate the response of the system to an initial displacement of the plant mass. It is apparent in the figures that asymptotic stability is achieved, although the proof of asymptotic stabilization by resetting control is not easy, even for this rather simple control system.

Conjecture 3. A virtual one-way absorber controller is (asymptotically) stabilizing if and only if the system that results from replacing the one-way absorber with a linear damped absorber is asymptotically stable.

Generally speaking, one-way absorber controllers provide a mechanism for energy dissipation. While they are nonlinear time-varying controllers, there are also linear controllers which can also provide energy dissipation, for example, dashpot elements or damped absorbers. Furthermore, even

[2]Resetting times are always times at which either the velocity of the attachement point or the control signal changes sign. However, it is possible, and it has been observed in simulations, that the control signal and velocity may both pass through zero at the same time, in which case the states are not reset.

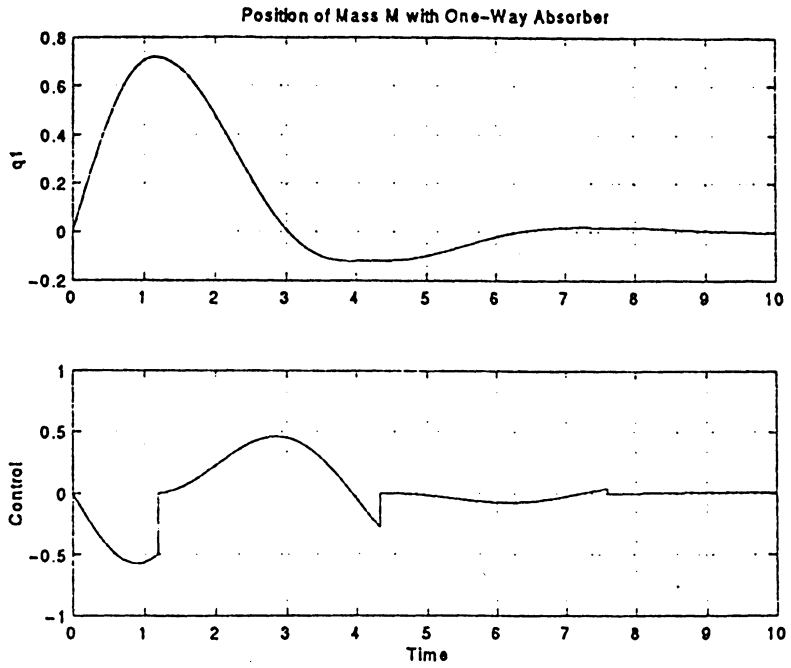

Figure 1: Time history of the position of the oscillator mass controlled by a one-way absorber controller (top), and control history (bottom) for an initial velocity of the oscillator mass

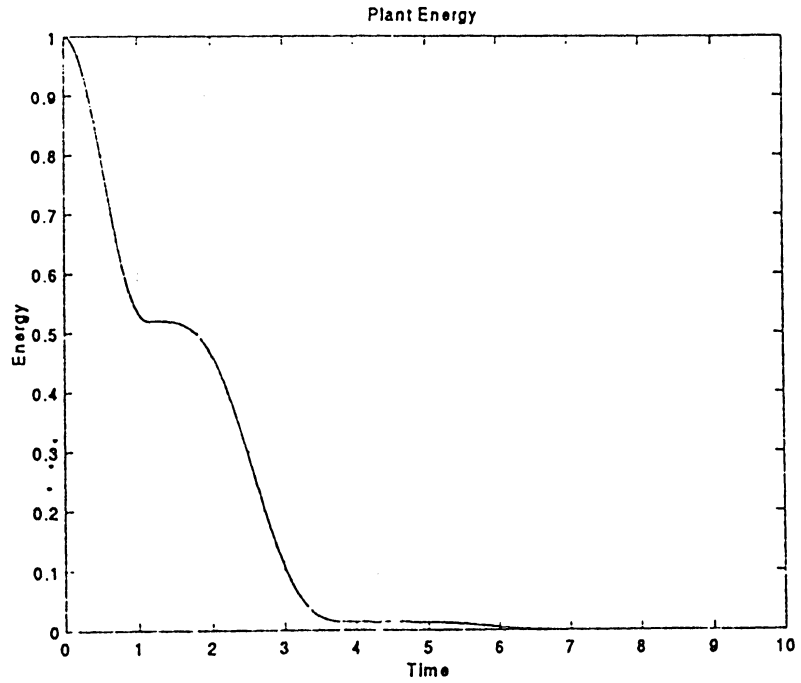

Figure 2: Time history of the plant energy for the oscillator controlled by a one-way absorber controller with a nonzero initial velocity

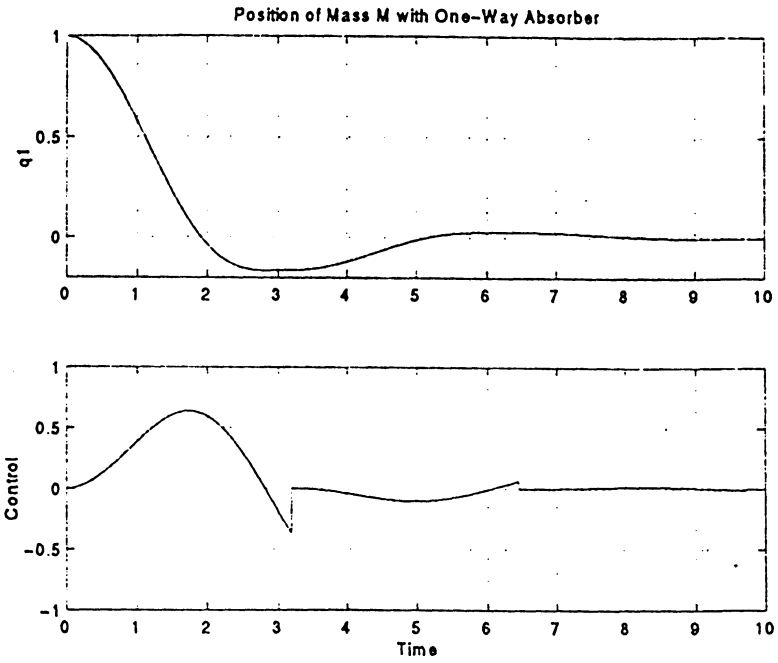

Figure 3: Time history of the position of the oscillator mass controlled by a one-way absorber controller (top), and control history (bottom) for an initial displacement of the oscillator mass

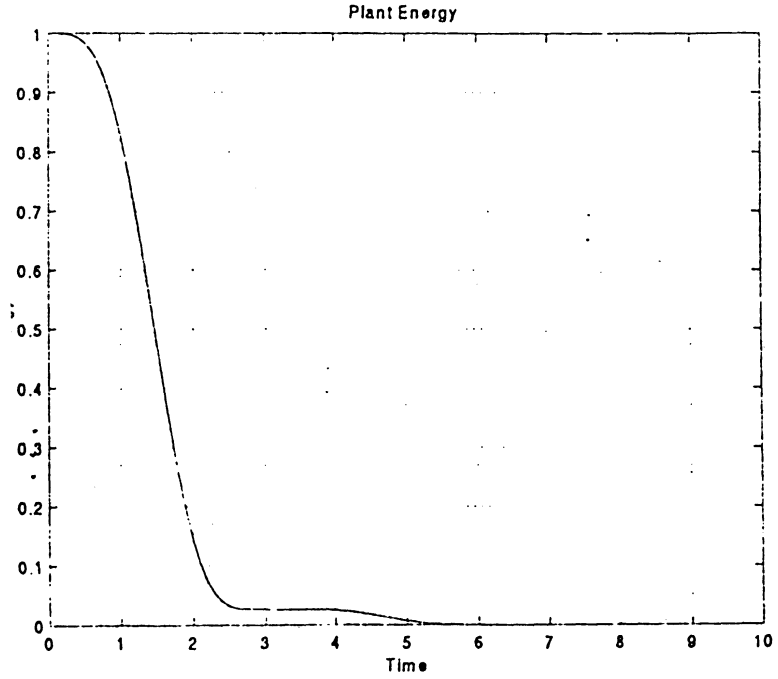

Figure 4: Time history of the plant energy for the oscillator controlled by a one-way absorber controller with a nonzero initial velocity

if the one-way absorber controllers are indeed passive, there are linear, output-feedback positive-real controller synthesis techniques, for example [5, 6].

Perhaps the one-way absorber controllers can offer some advantages over linear designs in terms of efficiency of energy dissipation. Possibly by tuning the lossless absorber portion of the controller to some desired frequency the energy dissipation is enhanced. However, the existence of an advantage of the one-way absorber controller over a linear design at this point is unclear, and therefore no further investigation of the one-way absorber controller for energy dissipation is considered here.

4 Finite-Time Stabilization of the Double Integrator Using a Virtual Trap-Door Absorber

In this section, a particular type of resetting lossless absorber controller – called a virtual trap-door absorber – is developed. This controller is used to achieve finite-time stabilization of the double integrator and, by extension, finite-time stabilization of the undamped oscillator is also achieved. The resulting controller is compared to the minimal-time and minimal-energy optimal controllers.

4.1 System Description

Consider the double integrator described by

$$M\ddot{q}_1 = u, \tag{18}$$

with initial conditions $q_1(0) = q_{10}$, $\dot{q}_1(0) = \dot{q}_{10}$. Our goal is to bring the position $q_1(t)$ and velocity $\dot{q}_1(t)$ of the double integrator to zero in finite time. The controller we consider emulates the lossless system shown in Figure 5, where the springs K and k as well as the mass m are virtual elements

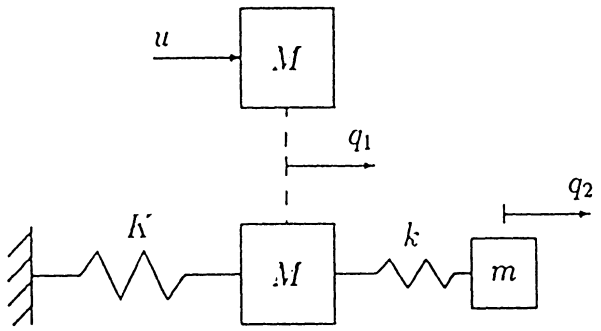

Figure 5: The double integrator without (above) and with (below) the virtual absorber subsystem.

whose effect on the mass M is implemented by means of a dynamic compensator and a force actuator. The dynamics of the closed-loop system are given by

$$\begin{aligned} M\ddot{q}_1 &= u, & (19)\\ m\ddot{q}_2 + kq_2 - kq_1 &= 0, & (20)\\ u &= kq_2 - (K + k)q_1, & (21) \end{aligned}$$

where q_2 represents the position of the virtual mass m. As shown in Figure 6, the system (19) - (21) can be represented as the single-input, single-output feedback interconnection of the double integrator plant with a second-order, proper dynamic compensator whose input is the position of the mass M.

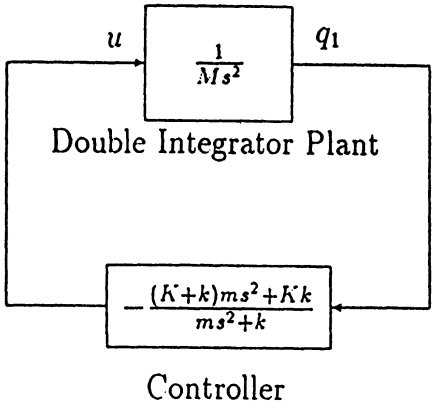

Figure 6: Feedback control of the double integrator

For notational convenience, we define the quantities

$$x_1 \triangleq Kq_1, \qquad x_2 \triangleq Kq_2, \qquad x_r \triangleq x_2 - x_1,$$
$$\kappa \triangleq k/K, \qquad \tau \triangleq \sqrt{\frac{K}{M}}t, \qquad \omega_a \triangleq \sqrt{\frac{k/m}{K/M}}.$$

With this notation, (19) - (21) become

$$\ddot{x}_1 = u, \tag{22}$$
$$\ddot{x}_2 + \omega_a^2 x_r = 0, \tag{23}$$
$$u = \kappa x_r - x_1, \tag{24}$$

where ($\dot{}$) now represents differentiation with respect to normalized time τ. The closed-loop system (22) - (24) has the form

$$\dot{x} = \mathcal{A}x, \qquad x = \begin{bmatrix} x_1 \\ \dot{x}_1 \\ x_r \\ \dot{x}_2 \end{bmatrix}, \qquad \mathcal{A} = \begin{bmatrix} 0 & 1 & 0 & 0 \\ -1 & 0 & \kappa & 0 \\ 0 & -1 & 0 & 1 \\ 0 & 0 & -\omega_a^2 & 0 \end{bmatrix}. \tag{25}$$

The characteristic equation of $\mathcal{A}$ is given by

$$s^4 + (1 + \kappa + \omega_a^2)s^2 + \omega_a^2 = 0, \tag{26}$$

which can be factored as

$$(s^2 + \omega^2)(s^2 + \Omega^2) = 0, \tag{27}$$

where

$$\omega = \sqrt{\frac{1}{2}(1 + \kappa + \omega_a^2) - \frac{1}{2}\sqrt{(1 + \kappa + \omega_a^2)^2 - 4\omega_a^2}}\ , \tag{28}$$

$$\Omega = \sqrt{\frac{1}{2}(1 + \kappa + \omega_a^2) + \frac{1}{2}\sqrt{(1 + \kappa + \omega_a^2)^2 - 4\omega_a^2}}\ . \tag{29}$$

and the eigenvalues of $\mathcal{A}$ are $\lambda_{1,2} = \pm j\omega$, $\lambda_{3,4} = \pm j\Omega$. The closed-loop system (25) is thus Lyapunov stable. By noting

$$(1+\kappa+\omega_a^2)^2 - 4\omega_a^2 = (1+\kappa-\omega_a^2)^2 + 4\kappa\omega_a^2 > 0, \tag{30}$$

it is clear that the expressions (28) and (29) are well defined. It follows from (26), (27) that

$$\omega\Omega = \omega_a, \quad \omega^2 + \Omega^2 = 1 + \kappa + \omega_a^2. \tag{31}$$

Next, we derive an expression for the time history of the state x_1 due to an initial condition of the form

$$x_0 = [\ x_{10} \quad \dot{x}_{10} \quad 0 \quad 0\ ]^{\mathrm{T}}, \tag{32}$$

or, equivalently,

$$q_1(0) = q_{10}, \quad \dot{q}_1(0) = \dot{q}_{10}, \quad q_2(0) = q_{10}, \quad \dot{q}_2(0) = 0, \tag{33}$$

which corresponds to an arbitrary initial position $q_{10} = \frac{1}{K}x_{10}$ and an arbitrary initial velocity $\dot{q}_{10} = \frac{1}{\sqrt{KM}}\dot{x}_{10}$ of the mass M, with zero initial elongation of the spring k and zero initial velocity of the virtual mass m.

Taking the Laplace transform of (25) gives

$$X_1(s) = \frac{s(s^2+\omega_a^2+\kappa)}{s^4+(1+\kappa+\omega_a^2)s^2+\omega_a^2}x_{10} + \frac{s^2+\omega_a^2}{s^4+(1+\kappa+\omega_a^2)s^2+\omega_a^2}\dot{x}_{10}, \tag{34}$$

which yields

$$x_1(\tau) = x_{10}\left[\frac{1}{2}(1+c_1)\cos\omega\tau + \frac{1}{2}(1-c_1)\cos\Omega\tau\right] + \dot{x}_{10}\left[\frac{1}{2\omega}(1+c_2)\sin\omega\tau + \frac{1}{2\Omega}(1-c_2)\sin\Omega\tau\right], \tag{35}$$

where

$$c_1 \triangleq \frac{\omega_a^2 - 1 + \kappa}{\sqrt{(1+\kappa+\omega_a^2)^2 - 4\omega_a^2}}, \qquad c_2 \triangleq \frac{\omega_a^2 - 1 - \kappa}{\sqrt{(1+\kappa+\omega_a^2)^2 - 4\omega_a^2}}. \tag{36}$$

4.2 Finite Settling Time Controller Synthesis

The following theorem provides a method for selecting the controller parameters K, k, and m for the virtual trap-door absorber controller.

Theorem 4.1. Consider the double integrator (19) with the virtual absorber subsystem (20), (21), and initial conditions (33). Let n and p be nonnegative integers, and choose positive numbers K, k, and m such that

$$\frac{k}{K} = \frac{m}{M} = \frac{4(2(p-n)+1)^2}{(4n+1)(4p+3)}. \tag{37}$$

Then

$$q_1(t_s) = 0, \quad \dot{q}_1(t_s) = 0, \tag{38}$$

where

$$t_s = \frac{\pi}{2}\sqrt{\frac{(4n+1)(4p+3)M}{K}}. \tag{39}$$

Furthermore, the control force $u(t)$ given by (24) is bounded by

$$|u(t)| \leq \sqrt{(K+k)(Kq_{10}^2 + M\dot{q}_{10}^2)}, \quad t \geq 0. \tag{40}$$

The proof of this theorem is given in the Appendix.

Remark 4.1. If K, k, and m satisfy (37), then $q_1(t)$ is given by

$$q_1(t) = \frac{1}{\omega+\Omega}\left\{q_{10}\left[\Omega\cos\sqrt{\frac{K}{M}}\omega t + \omega\cos\sqrt{\frac{K}{M}}\Omega t\right] + \dot{q}_{10}\sqrt{\frac{M}{K}}\left[\sin\sqrt{\frac{K}{M}}\omega t + \sin\sqrt{\frac{K}{M}}\Omega t\right]\right\}, t \geq 0, \tag{41}$$

where

$$\omega = 1/\Omega = \sqrt{\frac{4n+1}{4p+3}}\ . \tag{42}$$

Remark 4.2. Note that the time t_s is independent of the initial states q_{10} and q_{10}. Furthermore, the smallest value of t_s for which $q_1(t_s) = 0$ and $\dot{q}_1(t_s) = 0$ is obtained by choosing $n = p = 0$ in (39), which yields

$$t_s = \frac{\pi}{2}\sqrt{\frac{3M}{K}}. \tag{43}$$

This value is achieved by setting $k = 4K/3$ and $m = 4M/3$. Furthermore, note that t_s can be made arbitrarily small by choosing K to be sufficiently large, although large K tends to increase the control amplitude as suggested by the bound in (40).

The trap-door absorber design is based on Theorem 4.1. Specifically, the controller shown in Figure 6 is implemented for $0 \leq t \leq t_s$. At time $t = t_s$, the controller is shut off, so that the mass M remains at rest at the origin. For the double-integrator plant written in state-space form as

$$\dot{q} = Aq + Bu, \tag{44}$$

$$y = Cq, \tag{45}$$

where

$$q = \begin{bmatrix} q_1 \\ \dot{q}_1 \end{bmatrix}, \quad A = \begin{bmatrix} 0 & 1 \\ 0 & 0 \end{bmatrix}, \quad B = \begin{bmatrix} 0 \\ 1/M \end{bmatrix}, \quad C = \begin{bmatrix} 1 & 0 \end{bmatrix}, \tag{46}$$

the resulting linear time-varying controller has the form

$$\dot{x}_c(t) = A_c x_c(t) + B_c y(t), \tag{47}$$
$$u(t) = C_c(t) x_c(t) + D_c(t) y(t), \tag{48}$$

where

$$A_c = \begin{bmatrix} 0 & 1 \\ -k/m & 0 \end{bmatrix}, \qquad B_c = \begin{bmatrix} 0 \\ k/m \end{bmatrix},$$

$$C_c(t) = \begin{cases} \begin{bmatrix} k & 0 \end{bmatrix}, & t \in [0, t_s), \\ \begin{bmatrix} 0 & 0 \end{bmatrix}, & t \geq t_s, \end{cases} \qquad D_c(t) = \begin{cases} -K - k, & t \in [0, t_s), \\ 0, & t \geq t_s. \end{cases} \tag{49}$$

It now follows from Theorem 4.1 that the compensator (47), (48) is a finite-settling-time controller with settling time t_s. Furthermore, it follows from Remark 4.2 that t_s can be made arbitrarily small by choosing K sufficiently large.

4.3 Performance Analysis

In this section, we compare the trap-door absorber controller with the minimal-time and minimal-energy controllers.

4.3.1 Controller Designs

We first consider the classical minimal-time controller given by [1, 2]

$$u(q) = \begin{cases} -u_{\max} \text{sign}\left(\dot{q}_1 + \text{sign}(q_1)\sqrt{2|q_1|\frac{u_{\max}}{M}}\right), & \dot{q}_1 + \text{sign}(q_1)\sqrt{2|q_1|\frac{u_{\max}}{M}} \neq 0, \\ -u_{\max}\text{sign}(q_1), & \dot{q}_1 + \text{sign}(q_1)\sqrt{2|q_1|\frac{u_{\max}}{M}} = 0. \end{cases} \tag{50}$$

This controller is characterized by a discontinuous control force $u(t)$ that switches between $\pm u_{\max}$ on the switching curve $\dot{q}_1 + \text{sign}(q_1)\sqrt{2|q_1|\frac{u_{\max}}{M}} = 0$.

Next we consider the minimal-energy controller given in open-loop form by [1, 2],

$$u(t) = B^{\mathrm{T}} e^{A^{\mathrm{T}}(t_s - t)} \left(\int_0^{t_s} e^{As} B B^{\mathrm{T}} e^{A^{\mathrm{T}} s} \mathrm{d}s \right)^{-1} e^{At_s} q_0, \quad t \in [0, t_s], \tag{51}$$

and in linear time-varying feedback form by

$$u(t) = -B^{\mathrm{T}} e^{A^{\mathrm{T}}(t_s - t)} \left(\int_t^{t_s} e^{As} B B^{\mathrm{T}} e^{A^{\mathrm{T}} s} \mathrm{d}s \right)^{-1} e^{A(t_s - t)} q(t), \quad t \in [0, t_s], \tag{52}$$

where $q(0) = q_0$, $q(t_s) = 0$, and the cost functional

$$J = \int_0^{t_s} u^2(t) \mathrm{d}t, \tag{53}$$

is minimized. For the double integrator (18) the control laws (51), (52) become, respectively,

$$u(t) = M\left(\frac{12q_{10}}{t_s^3} + \frac{6\dot{q}_{10}}{t_s^2}\right)t - M\left(\frac{6q_{10}}{t_s^2} + \frac{4\dot{q}_{10}}{t_s}\right), \quad t \in [0, t_s], \tag{54}$$

$$u(t) = -\frac{6(t_s - 3t)}{(t_s - t)^3}Mq_1(t) - \frac{4(t_s^2 - 5t_s t + 7t^2)}{(t_s - t)^3}M\dot{q}_1(t), \quad t \in [0, t_s]. \tag{55}$$

It can be shown that if the initial condition q_0 satisfies

$$q_{10}^2 + \dot{q}_{10}^2 = 1, \tag{56}$$

then the control amplitude satisfies the bound

$$|u(t)| \leq \frac{2M\sqrt{9 + 4t_s^2}}{t_s^2}, \quad t \in [0, t_s]. \tag{57}$$

To design the virtual trap-door absorber controller, we choose $k = 4K/3$ and $m = 4M/3$, corresponding to $n = p = 0$ in (37). The value of the parameter K will be chosen later to satisfy a control amplitude constraint.

To compare these three controllers, we let $M = 1$ and impose the control amplitude constraint

$$|u(t)| \leq 1, \quad t > 0. \tag{58}$$

To satisfy (58) for the minimal-time controller, we set $u_{\max} = 1$ in (50). In order to ensure for the minimal-energy controller that (58) is satisfied for initial conditions (56), we set $t_s = 3\sqrt{2} \approx 4.24$. For this value of t_s, (57) is equivalent to (58). For the virtual trap-door absorber, we choose $K = 3/7$, so that $k = 4/7$ and $m = 4/3$. With these values, the control bound in (40) is equivalent to (58), while the settling time given by (39) is $t_s = \sqrt{7}\pi/2 \approx 4.16$.

Remark 4.3. Finite-time stabilization of an undamped oscillator can be achieved by designing a controller based on Theorem 4.1 where the parameter K represents either the stiffness of the oscillator's actual spring element or the sum, or parallel connection, of the actual spring and a virtual spring. The control bound (40) will require modification in this case, however.

4.3.2 Performance Comparison

In Figure 7 and Figure 8 we choose initial conditions of the form $q_{10} = \cos\theta$, $\dot{q}_{10} = \sin\theta$ for $\theta = \{0, 6, 12, \ldots, 360\}$ degrees. A comparison of the phase portraits for the optimal controllers and the trap-door absorber controller is given in Figure 7, while a comparison of the settling times of the three controllers is given in Figure 8. Notice in Figure 8 that the settling times of the minimal-time controller depend on the initial condition, while the settling times of the minimal-energy and virtual trap-door absorber controllers, as mentioned in Remark 4.2, do not. Also notice that the settling times of the minimal-time controller are all substantially smaller than those of the virtual trap-door absorber controller, while the virtual trap-door absorber is marginally faster than the minimal-energy controller.

In Figure 9 and Figure 10, we choose two initial conditions, specifically, $q_{10} = \cos\theta$, $\dot{q}_{10} = \sin\theta$, for $\theta = 45°$ and $\theta = 135°$ degrees. The time history of the double integrator plotted as velocity versus position is given in Figure 9, while the control history is plotted in Figure 10. It can be seen in Figure 10 that the minimal-time controller is piecewise constant with three discontinuities in control: switching on at $t = 0$, switching sign, and switching off when the mass M is at the origin. The minimal-energy and virtual trap-door absorber controllers each have two discontinuities in control: switching on at $t = 0$, and swiching off when M has reached the origin.

As a final performance comparison, Figure 11 illustrates the tradeoff of control magnitude versus settling time, while Figure 12 illustrates the tradeoff of the control energy (53) versus settling time. The tradeoff analysis is performed for the single initial condition $q_{10} = \cos 45°$ and $\dot{q}_{10} = \sin 45°$. To generate the data for the minimal-time controller, values of $u_{\max}$ were chosen and the corresponding settling times and energy integrals were computed. For the minimal-energy controller, values of the final time t_s were chosen and the resulting values of $u_{\max}$ and the energy integral J were computed. Similarly, for the virtual trap-door absorber controller, values of t_s were chosen, and the parameter K was chosen according to (43). The values of $u_{\max}$ and the energy integral J were determined after numerical simulation. The simulations indicate that the virtual trap-door absorber has a better tradeoff of maximum control magnitude versus settling time than the minimal-energy controller, and a better tradeoff of control energy versus settling time than the minimal-time controller.

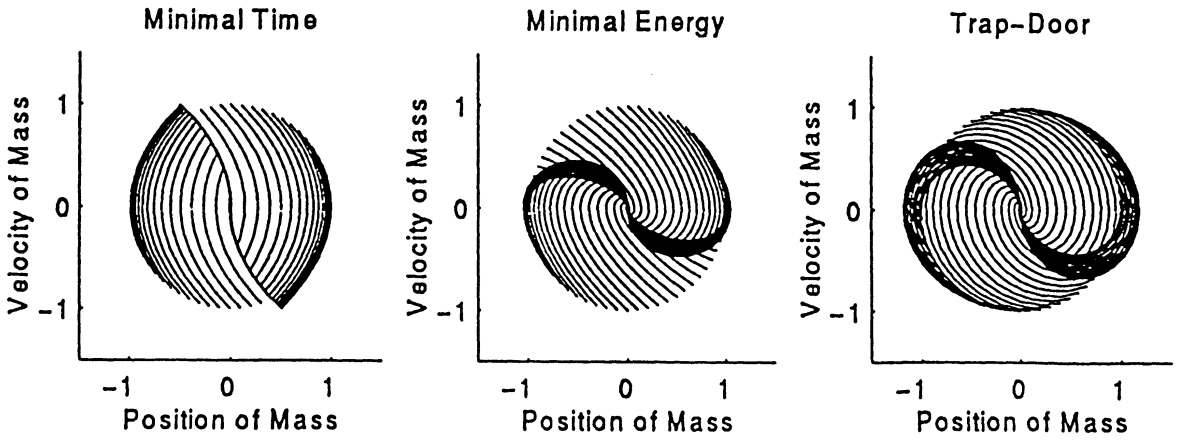

Figure 7: A comparison of the phase trajectories for various initial conditions on the unit circle.

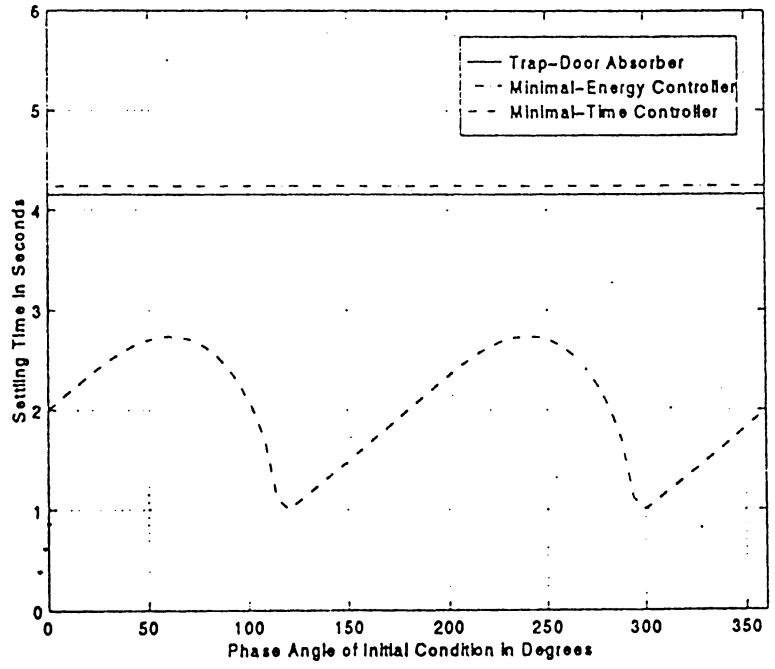

Figure 8: A comparison of settling times versus θ in degrees for initial conditions $q_{10} = \cos\theta$, $\dot{q}_{10} = \sin\theta$.

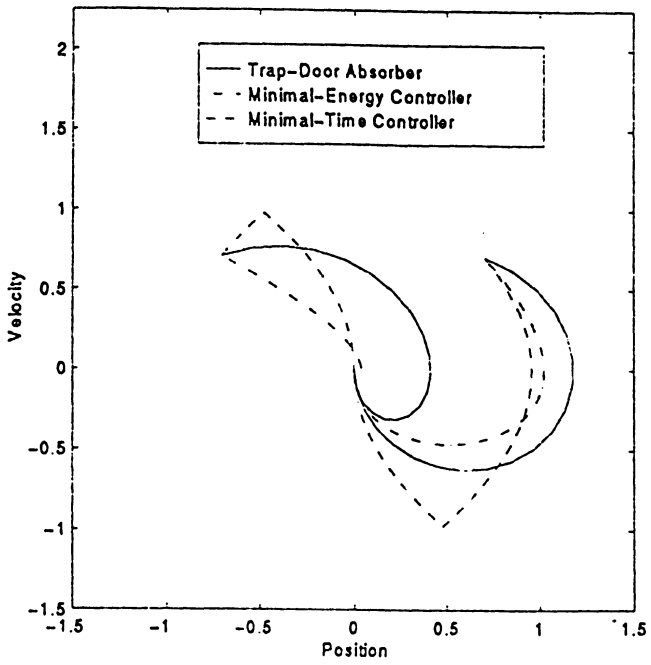

Figure 9: Trajectories for two initial conditions plotted in phase space.

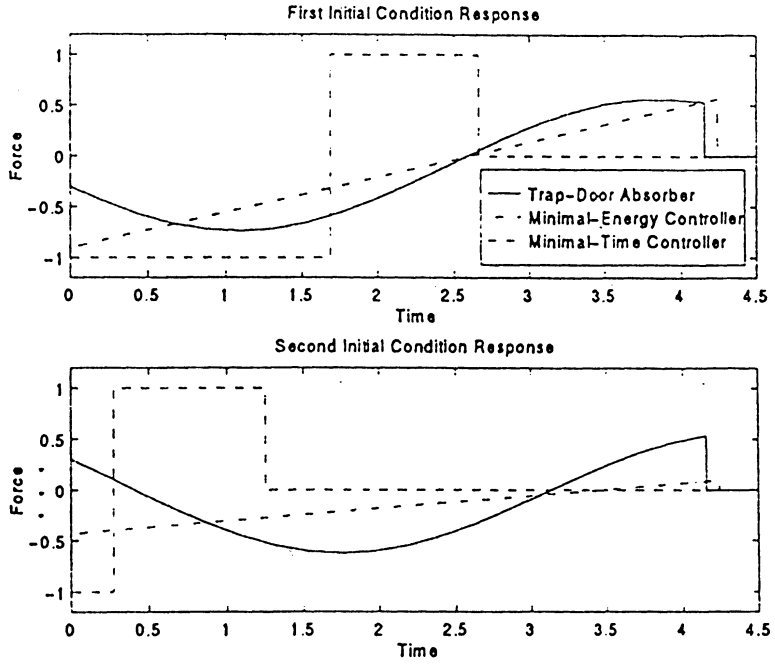

Figure 10: Comparison of control histories: initial condition is $q_{10} = \cos\theta$, $\dot{q}_{10} = \sin\theta$ for $\theta = 45°$ (top) and $\theta = 135°$ (bottom).

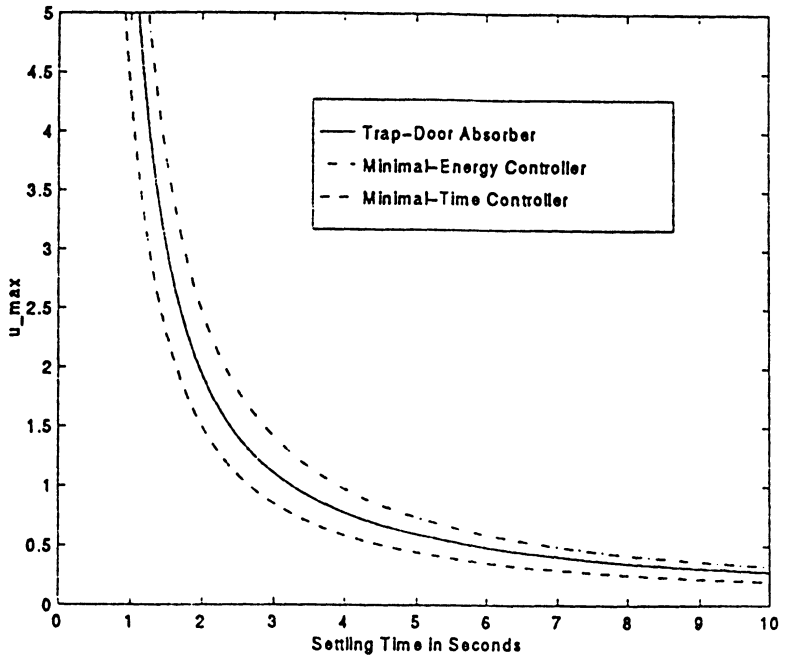

Figure 11: Maximum control magnitude versus settling time for the initial condition $q_{10} = \cos 45°$, $\dot{q}_{10} = \sin 45°$.

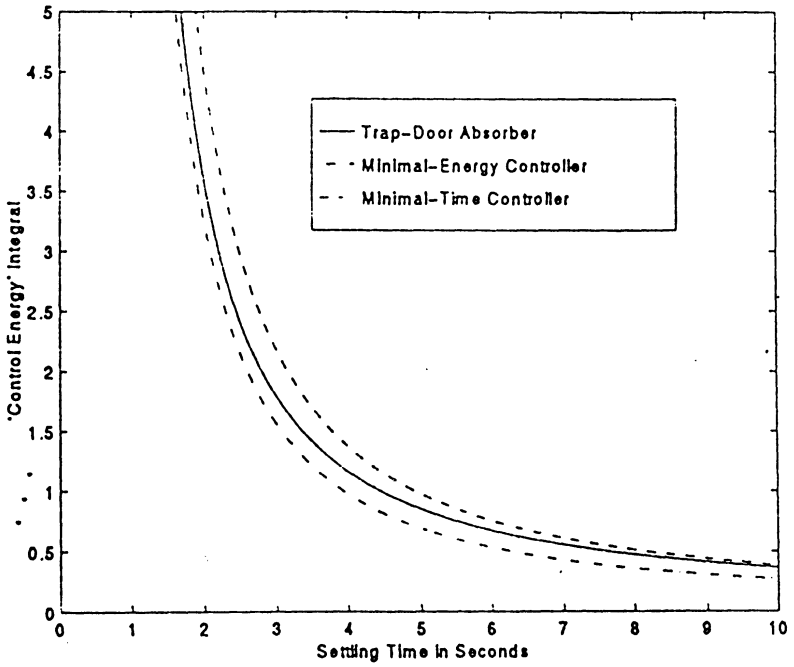

Figure 12: $\int_0^{t_s} u^2(t)dt$ versus settling time for the initial condition $q_{10} = \cos 45°$, $\dot{q}_{10} = \sin 45°$.

5 Virtual Resetting Absorbers for Disturbance Rejection

Virtual resetting absorbers, by the nature of their energy dissipation mechanism, are well suited for removing energy from a system; for example, dissipating finite-energy disturbances such as a single impulse or a displaced initial condition response. To embellish this description, consider the following analogy.

Suppose you are floating in the middle of an ocean, in a rowboat that has some water in the bottom. Here the rowboat is the plant, and the finite-energy disturbance is represented by the finite amount of water in the bottom of the boat. The analog for the virtual resetting absorber is a bucket, which can be filled with water from the bottom of the boat, and emptied into the ocean, thereby resetting the state of the bucket. The process of baling the water represents the closed-loop control used to bring the plant to the desired (dry) state.

Although the virtual resetting absorber is well suited for the finite-energy dissipation problem, now consider the infinite-energy disturbance rejection problem. Returning to the rowboat analogy, the disturbance rejection problem might correspond to a hole in the bottom of the rowboat. Now using the bucket to bale the water may not be a particularly effective approach for bringing the rowboat to the desired state. A better use of the bucket/control would be to place the bucket over the hole, so that no more water can come into the boat. While the virtual resetting absorber does not "place the bucket over the hole," there is a linear control system that does.

Consider the classical problem of disturbance rejection for an undamped oscillator, or isolator [7]. It can be shown that disturbances at the resonant frequency of the isolator can be completely rejected by mounting a second undamped oscillator, or absorber, onto the isolator, where the absorber resonance frequency is tuned to the isolator resonance frequency. The addition of the absorber subsystem effectively "places the bucket over the hole," so that the disturbance source is completely blocked from disturbing the isolator.

There are two basic problems with this aborber design. The first is that the resulting system now has two resonance frequencies, one below and one above the original isolator resonance frequency. This problem is considered by Snowdon [8] who proposed adding damping to the absorber subsystem for a solution. This approach indeed is effective at removing the resonant peaks; however, it also destroys the desired effect of complete disturbance rejection at the isolator natural frequency.

The second problem with the Den Hartog absorber design relates to the claim that in steady state the isolator is motionless. The problem is that the isolator is motionless only after the transient motion is dissipated; however, because there is no damping in the system, the transient motion is *never* dissipated, and thus the isolator is never brought to rest as predicted. Returning to the rowboat analogy, the bucket is placed over the hole so that no more water leaks into the boat, however, there is still water in the boat that doesn't get removed, and the boat therefore never achieves the desired "dry" condition.

It is desirable to design a controller for the undamped isolator that provides perfect disturbance rejection at a given frequency *and* stabilizes the closed-loop system - one that plugs the hole in the bottom of the boat and gets rid of any water left in the bottom. A hybrid controller consisting of a parallel connection of an undamped absorber subsystem and a virtual resetting aborber - a one-way absorber in particular - will solve the control problem.

Consider the undamped oscillator plant with hybrid absorber + virtual resetting absorber shown in Figure 13. Without loss of generality, let $M_1 = 1$, and $K_1 = 1$ with appropriate units.

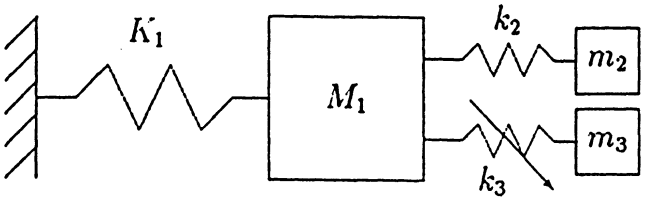

Figure 13: Undamped Oscillator with Hybrid Absorber

One particular hybrid controller that puts a zero at the isolator resonance frequency while avoiding resonant peaks is obtained by choosing $k_2 = a$, and $m_2 = a$, for some positive number a, and implementing a one-way absorber with k_3, and m_3.

The particular design that is considered in a numerical example uses $a = 0.5$, $k_3 = 0.5$, and $m_3 = 0.5$. The closed loop is given in state-space form by

$$\dot{x} = Ax, \quad A = \begin{bmatrix} 0 & 1 & 0 & 0 & 0 & 0 \\ -\frac{K_1+k_2+k_3}{M_1} & 0 & \frac{k_2}{M_1} & 0 & \frac{k_3}{M_1} & 0 \\ 0 & 0 & 0 & 1 & 0 & 0 \\ \frac{k_2}{m_2} & 0 & -\frac{k_2}{m_2} & 0 & 0 & 0 \\ 0 & 0 & 0 & 0 & 0 & 1 \\ \frac{k_3}{m_3} & 0 & 0 & 0 & -\frac{k_3}{m_3} & 0 \end{bmatrix}, \quad x = \begin{bmatrix} q_1 \\ \dot{q}_1 \\ q_2 \\ \dot{q}_2 \\ q_3 \\ \dot{q}_3 \end{bmatrix}, \tag{59}$$

where q_1, q_2, and q_3 represent the positions of the masses M_1, m_2, and m_3 respectively. The one-way absorber is implemented by monitoring the energy of the (m_3, k_3) subsytem, given by $E = \frac{1}{2}m_3\dot{q}_3^2 + \frac{1}{2}k_3(q_3 - q_1)^2$. When this energy stops increasing, the state q_3 is set to q_1, and the state $\dot{q}_3$ is set to zero.

By running a number of simulations, a type of magnitude Bode plot is developed. It is seen from Figure 14 that the resulting hybrid controller asymptotically rejects sinusoidal disturbances at the isolator resonant frequency, and avoids introducing resonances at neighboring frequencies. Figure 15 shows the disturbance rejection in the time domain.

That asymptotic disturbance rejection is achieved with a hybrid Den Hartog/one-way absorber subsystem is not particularly remarkable since this problem can be readily solved with a linear time-invariant controller. This is evident from the following lemma.

Lemma 2. Consider the scalar real-rational transfer function $G(s) = \frac{n(s)}{d(s)}$, where $n(s)$ and $d(s)$ have no common roots, and let $\omega_z \in \mathbb{R}$ satisfy $n(\pm j\omega_z) = 0$. Let $G_c(s) = \frac{n_c(s)}{d_c(s)}$ be an asymptotically stable, stabilizing, real-rational transfer function description of a dynamic compensator. Then the closed-loop transfer function $G_{cl}(s) = \frac{G(s)}{1+G(s)G_c(s)}$ satisfies $G_{cl}(j\omega_z) = 0$.

Proof: The closed-loop transfer function is

$$G_{cl}(s) = \frac{G(s)}{1 + G(s)G_c(s)} = \frac{\frac{n(s)}{d(s)}}{1 + \frac{n(s)n_c(s)}{d(s)d_c(s)}} = \frac{n(s)}{d(s) + \frac{n(s)n_c(s)}{d_c(s)}}. \tag{60}$$

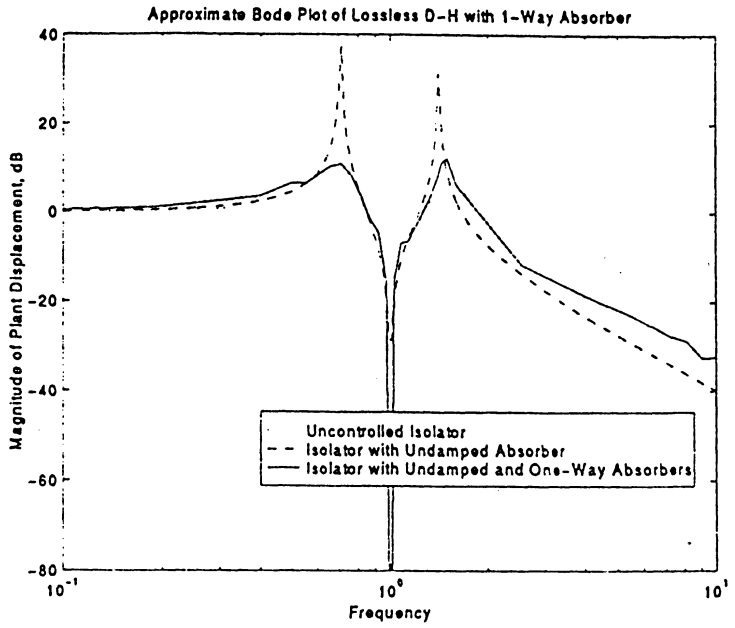

Figure 14: Magnitude Bode-type plot for the virtual resetting absorber

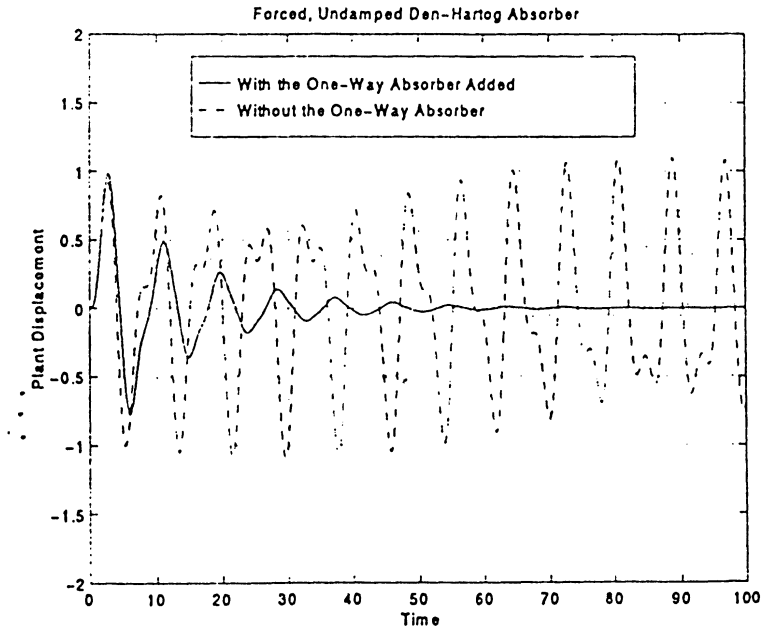

Figure 15: Asymptotic disturbance rejection: Position of the mass M_1 subject to sinusoidal forcing

Since G_c is asymptotically stable, $G_c(j\omega_z)$ is finite, and

$$\frac{n(j\omega_z)n_c(j\omega_z)}{d_c(j\omega_z)} = 0,$$

and thus

$$G_{cl}(j\omega_z) = \frac{n(j\omega_z)}{d(j\omega_z)} = 0.$$

□

Lemma 2 shows that, for example, we can use a Positive-Real LQG controller to stabilize the closed loop, and still maintain the desired transfer function zero.

A potential contribution to the disturbance rejection problem that the virtual resetting absorber algorithm may be able to provide is suggested by the following conjectures.

Conjecture 4. The virtual trap-door absorber results can be extended to systems of order greater than two.

Conjecture 5. It may be possible to design a hybrid Den Hartog/trap-door absorber that will reject disturbances at a fixed frequency and have finite-settling-time transient response.

6 Future Work

The following items are noted as important research directions for further research in the area of virtual resetting absorbers for control.

1. Further develop the theoretical foundations for systems with virtual resetting absorber controllers. Specifically, develop or adapt notation and stability results for resetting control systems described by impulsive differential equations.

2. Use a one-way absorber controller to asymptotically stabilize a lossless plant, and *prove* asymptotic stability – this may involve some sort of application of the invariant set theorem or pervasive damping-type arguments.

3. Extend the results of Section 4 to systems of order greater than two.

4. Extend the results of Section 4 to plants with damping.

5. Investigate the degree to which the implementation of a virtual resetting absorber (one-way absorber) as a dissipation mechanism gives improved transient performance compared to a linear dissipation mechanism within the context of the enhanced Den Hartog problem of Section 5.

6. The modified Den Hartog absorber designs of Section 5 that give perfect rejection at one frequency as well as providing stabilization, ought to be related to disturbance accomodation results, for example [9, 10]. The relationship should be investigated.

7. Investigate the use of a *tunable* virtual Den Hartog absorber plus a *tunable* virtual resetting absorber for adaptive disturbance cancellation, and investigate the degree to which this approach may be preferable to using tunable linear absorber subsystems.

8. Investigate the performance robustness of the one-way absorber controller when the resetting subsystem is poorly tuned.

9. Investigate the stability and performance robustness of the virtual trap-door absorber controller under parameteric uncertainties in the mass of the double integrator. Compare the robustness of the virtual trap-door absorber design to the robustness of classical optimal control results.

7 Conclusions

The work done this semester for this project has yielded the following results:

1. A new nonlinear control design technique has been introduced.

2. This control design technique has been shown to have two important variations, the virtual one-way absorber and the virtual trap-door absorber.

3. The virtual one-way absorber is (more or less) shown to be a passive controller design, and thus represents a novel nonlinear passive controller design algorithm.

4. The virtual trap-door absorber has been shown to finite-time stabilize the double integrator and undamped oscillator.

5. The virtual trap-door absorber has been shown to finite-time stabilize the double integrator and undamped oscillator *using only position measurements*: I know of no other controller that will do this.

6. Numerous directions for future research are given.

While only linear plants are explicitly considered in this report, the results are in no way limited to linear systems. For example, the one-way absorber can be used as an energy dissipation mechanism in a nonlinear system, although the benefits of a one-way absorber compared to a linear damped absorber have not yet been determined. Furthermore, many nonlinear systems can be effectively linearized. For such systems, it may be possible to use the trap-door absorber approach to finite-time stabilize the dynamics. In order to use the trap-door absorber results developed this semester, the linearized system would have to be of order two. Clearly, the extension of the trap-door absorber results to systems of order four or more would greatly increase the power of the approach.

8 Acknowledgements

The concept of resetting a lossless compensator for the purpose of dissipating energy was born during collaboration of the author and Professor Dennis Bernstein with Vijaya Chellaboina and Professor Wassim Haddad, both of Georgia Tech, during August, 1995. Research support for the author under Professor Bernstein was provided by AFOSR grants F49620-95-1-0019 and F49620-93-1-0502, and the support of Professor Haddad and Vijaya Chellaboina was in part provided by NFS grant ECS-9496249. The analytical and numerical results concerning finite-time stabilization of the double integrator and the undamped oscillator using a virtual trap-door absorber were obtained by the author, and a journal paper has been written and submitted to the IEEE Transactions on Automatic Control [11]. Consequently, the material of Section 4, as well as some of Section 2, which is borrowed in large part from the text of [11], while primarily written by the author, has been influenced and edited by the coauthors of [11].

The rowboat analogy of Section 5 was suggested by Professor Bernstein. The author acknowleges the assistance of Tobin van Pelt, a graduate student in Aerospace Engineering also working for Professor Bernstein, in clarifying some of the Frahm/Den Hartog/Snowdon results discussed in Section 5.

References

[1] M. Athans and P. L. Falb. *Optimal Control: An Introduction to the Theory and Its Applications.* McGraw-Hill, New York, 1966.

[2] A. E. Bryson, Jr. and Y.-C. Ho. *Applied Optimal Control.* Hemisphere Publishing, 1975.

[3] B. G. Korenov and L. M. Reznikov. *Dynamic Vibration Absorbers: Theory and Technical Applications.* Wiley, 1993.

[4] V. Lakshmikantham, D. D. Bainov, and P. S. Simeonov. *Theory of impulsive differential equations*, volume 6 of *Series in Modern Applied Mathematics.* World Scientific, Singapore, 1989.

[5] R. Lozano-Leal and S. M. Joshi, "On the Design of Dissipative LQG-Type Controllers," *Proc. IEEE Conf. Dec. Contr.*, pp. 1645–1646, Austin, TX, December 1988.

[6] W. M. Haddad, D. S. Bernstein, and Y. W. Wang, "Dissipative H_2/H_∞ Controller Synthesis," *IEEE Trans. Autom. Contr.*, Vol. 39, pp. 827–831, 1994.

[7] J. P. Den Hartog. *Mechanical Vibrations.* McGraw Hill, 4th edition, 1956.

[8] J. C. Snowdon. *Vibration and Shock in Damped Mechanical Systems.* John Wiley and Sons, 1968.

[9] A. G. Sparks and D. S. Bernstein, "Asymptotic Regulation with H_2 Disturbance Rejection," *Proc. IEEE Conf. Dec. Contr.*, pp. 3614–3615, December 1994.

[10] J. Abedor, K. Nagpal, and K. Poolla, "Does Robust Regulation Compromise $\mathcal{H}_2$ Performance," *Proc. IEEE Conf. Dec. Contr.*, pp. 2002–3615, December 1992.

[11] R. T. Bupp, D. S. Bernstein, V. S. Chellaboina, and W. M. Haddad. Finite-time stabilization of the double integrator using a virtual trap-door absorber. To be submitted to IEEE Transactions on Automatic Control, 1995.

STUDY OF STABILIZATION OF DRIFTLESS SYSTEMS

ME662-Final project

Krishanraju Datla

646-12-4967

Date:20th Dec' 95

1. Introduction

I have started this project with the goal of studying stabilization problems with driftless systems namely stabilization of trajectories, stabilization to a point etc. This was motivated by the many practical applications of systems which fall into the category of driftless systems. Trajectory generation and therefore trajectory tracking are important aspects in the motion planning of these systems as some of their applications involve autonomous motion, docking/parking etc. When conditions like rolling without slipping(nonholonomic constraints) are imposed these system would also fall under the class od Nonholonomic systems. The kinematic model of a car fits in this category and is the subject of the study here. The kinematic equations of the mid-point of the rear axle of the car is given by

$$\begin{aligned} \dot{x} &= \cos\theta \cos\phi \, u_1 \\ \dot{y} &= \sin\theta \cos\phi \, u_1 \\ \dot{\phi} &= u_2 \\ \dot{\theta} &= \frac{1}{L} \sin\phi . u_1 \end{aligned} \tag{1}$$

Using the yaw velocity of the car as an input instead of the steering velocity, the ϕ equation drops and we have the (see [1]).

$$\begin{aligned} \dot{x} &= u_1 \cos\theta \\ \dot{y} &= u_1 \sin\theta \\ \dot{\theta} &= \omega \end{aligned} \tag{2}$$

This also results in a bound on the controls as shown in Fig. 12[1]. The constrained controls have to remain in either of the two triangles in the figure. The fact that yaw motion-w is not possible at 0 forward velocity-v can also be observed from the plot. The corresponding equations for a point ϵ distance forward from the midpoint of the rear axle are[1]

$$\begin{aligned} \dot{x}_\epsilon &= u_1 \cos\theta - \epsilon\omega \sin\theta \\ \dot{y}_\epsilon &= u_1 \sin\theta + \epsilon\omega \cos\theta \\ \dot{\theta} &= \omega \end{aligned} \tag{3}$$

By using the transformation R(Θ):(x,y)--->(z1,z3), the set of equations (2) become

$$\begin{aligned} \dot{z}_1 &= u_1 - z_3 u_2 \\ \dot{z}_2 &= \dot{\theta} = u_2 \\ \dot{z}_3 &= z_1 u_2 \end{aligned} \tag{4}$$

where ω = u2 and v = u1. Without the second term in the right hand side of the 1st equation of (4) the system would be in the so called chained form[2]. This will be discussed later. (3) and (4) are used in this study. What follows is the study of stabilizers given by [1],[2] & [3] for these equations. R(Θ) is

$$\begin{bmatrix} \cos\theta_0 & \sin\theta_0 \\ \sin\theta_0 & -\cos\theta_0 \end{bmatrix}$$

and $R(\theta) : (z_1, z_3) \longrightarrow (x, y)$ too.

2. Study of the Controllers of [2] and [3]

2.1 Introduction to the controllers

In [2], the authors propose an exponential controller(stabilizer) which stabilizes the car in (4) to a point. The control law uses a homogeneous norm ρ(z) and is given as follows

$$
\begin{aligned}
u_1 &= -c_{11}z_1 + c_{12}\frac{z_3}{\rho(z)}\cos\frac{t}{2} \\
u_2 &= -c_{21}z_2 + c_{22}\frac{z_3^2}{\rho^3(z)}\sin\frac{t}{2} \\
\rho(z) &= (z_1^4 + z_2^4 + z_3^2)^{1/4} \qquad c_{ij}\text{'s} > 0
\end{aligned}
\tag{5}
$$

The above law stabilizes the system exponentially with respect to the homogeneous norm ρ and hence is called *homogeneous* controller(H). Note that the controls are smooth except at the origin but continuous everywhere.

As [3] works with the same system and with a similar control structure, it is appropriate to study that controller alongwith. It offers a globally asymptotically stabilizing(GAS) control law using saturation functions and is given by

$$
\begin{aligned}
u_1 &= -c_{11}z_1 - c_{12}\sigma^2(z_3)(\sin t - \cos t) \\
u_2 &= -c_{21}z_2 - c_{22}z_3\cos\left(\frac{t}{2}\right) \\
& c_{ij}\text{'s} > 0 \\
\text{and} \quad & \sigma(z_3) = z_3 \text{ for } |z_3| \le .3 \\
& \qquad = .3\,\mathrm{sgn}(z_3) \text{ for } |z_3| > .3
\end{aligned}
\tag{6}
$$

This controller is smooth everywhere and is henceforth also referred to as *smooth* controller(S). Both the controllers in concept derive from [4]

2.2 Simulation with the Controllers (5) & (6)

The two controllers were simulated on the system given by (4) using MATLAB. Figures 1-10 correspond to these simulations. They are done to verify/study convergence and to study the qualitative nature of the control laws. The system did not converge with C22>0 as specified by (5) ([2]), hence in all simulations using (5), C22 is chosen <0 (as -3). Similarly the parameters given in (5) for the (S) did not give satisfactory results either (see fig. 2a) . The chosen structure(sign) of the parameters for (S) is however in accordance with the one given in [3]. Figures 3 and 7 give the system trajectories in R^2 for (H) and (S) respectively. The 6 different initial conditions studied are (x0, y0, θ0) = (-.1,-.2, 0) , (.3, .2, 0), (-.2, 0, -pi/2), (-.11, .15, pi/2), (0 -.2,-pi/2) and (.2,-.1,-pi/2) respectively. These real coordinates are transformed into Z coordinates and the systems simulated and the obtained trajectories transformed back to (x,y,θ) co-ordinates. In all simulations the goal wa to stabilize the system to Xr = (0,0,0).

The following observations can be made:

* Both controllers tend to first pull the system into a sector like region and then slowly approch the origin through movements similar to the 2nd lie brackett movements(call these Ly) - resulting in a net y directional convergence. Also the system is first stabilized w.r.t x in the beginning in both the cases.
* (H) stabilizes exponentially (*w.r.t* ρ) where as (S) does a poor job relatively though it is not fair to use the homogeneous norm ρ as the benchmark for (S). But it can be seen that Ly movements of (S) tend to be circular around the origin giving very small net movements.
* The inputs, states etc., with (H) exhibit the same exponential behaviour (Fig. 5,9 and Figs 6,10)
* As the system uses sinusoids of low amplitude to converge, one might wonder in a real vehicle will the plant dynamics (approximated to kinematics in these models) act as a filter and produce no movement at all when the system is close to Xr.

3. Other Controllers

[1] proposes a very interesting controller which can do point to point stabilzation. It uses a two stage controller and is the most convincing controller intuitively. However, the author feels that stage1 will not take the system to an invariant manifolds as required for sage2 controller to work. Because the system reaches the region where Vdot = d(V)/dt = 0(V(.) is the lyapunov potential) only exponentially and not in finite time.(see fig. 11) Also Vdot = 0 results in many invariant points and regions.

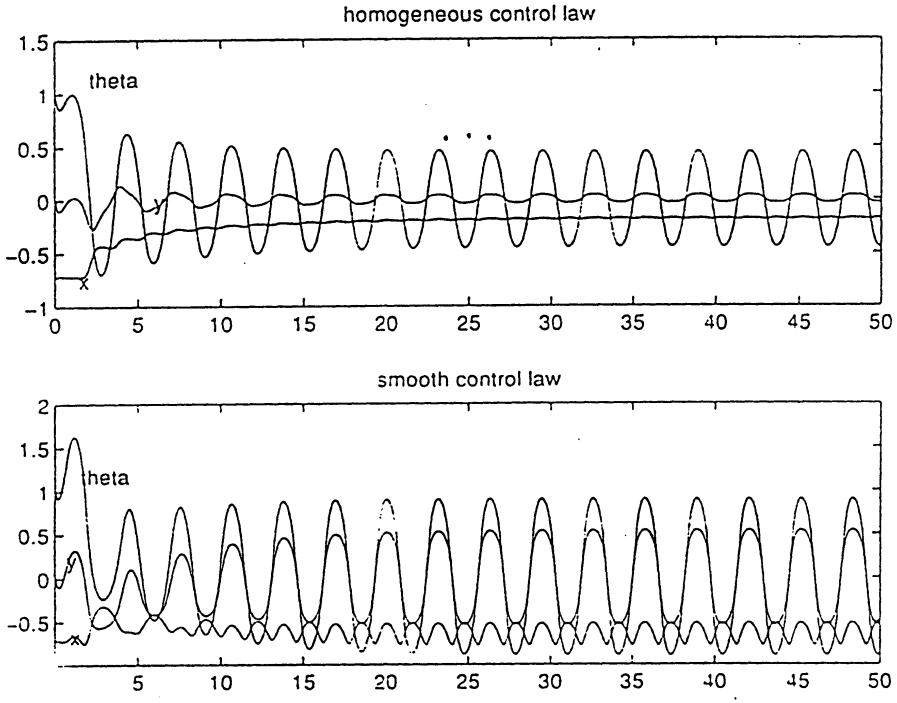
homogeneous control law
theta
smooth control law
theta

fig.1

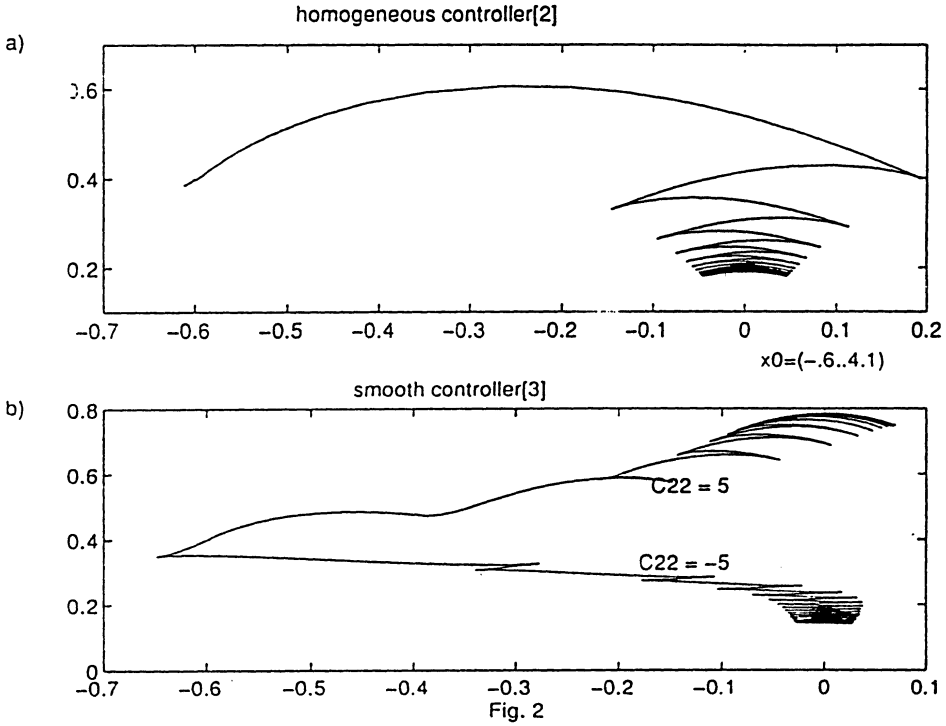
a)
homogeneous controller[2]
x0=(-.6..4.1)
b)
smooth controller[3]
C22 = 5
C22 = -5

Fig. 2

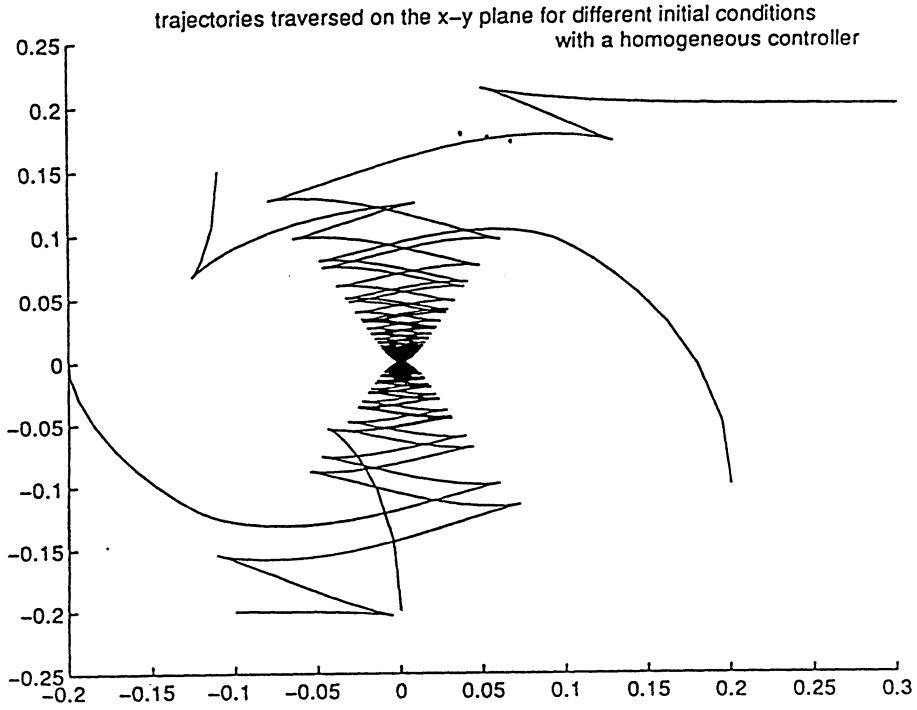
trajectories traversed on the x–y plane for different initial conditions
with a homogeneous controller
0.25
0.2
0.15
0.1
0.05
0
−0.05
−0.1
−0.15
−0.2
−0.25
−0.2
−0.15
−0.1
−0.05
0
0.05
0.1
0.15
0.2
0.25
0.3

Fig. 3

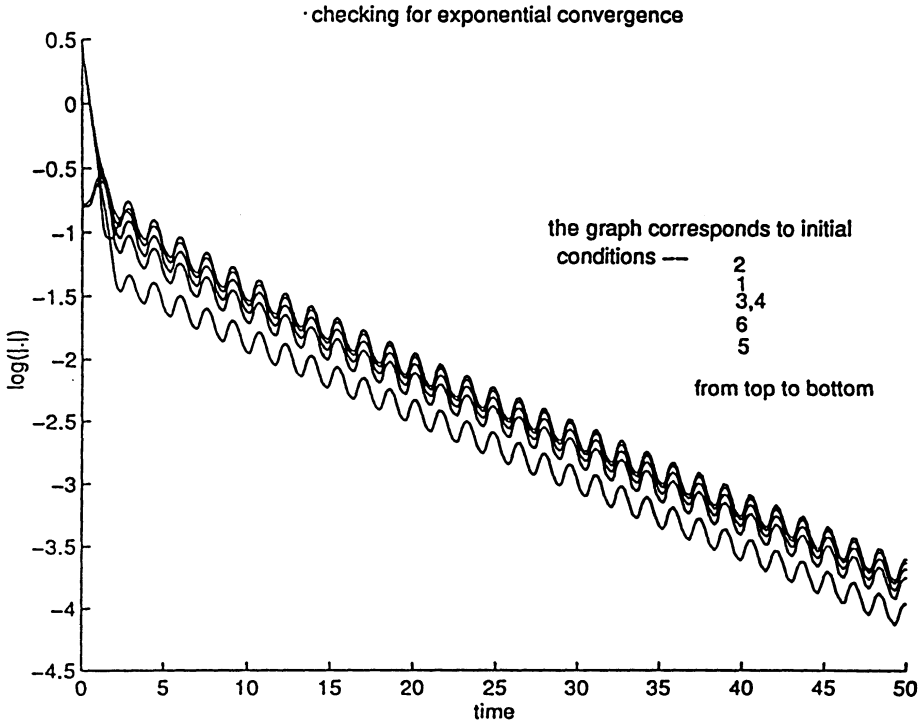
checking for exponential convergence
log(|.|)
time
the graph corresponds to initial conditions —
2
1
3,4
6
5
from top to bottom
0.5
0
−0.5
−1
−1.5
−2
−2.5
−3
−3.5
−4
−4.5
0
5
10
15
20
25
30
35
40
45
50

Fig. 4

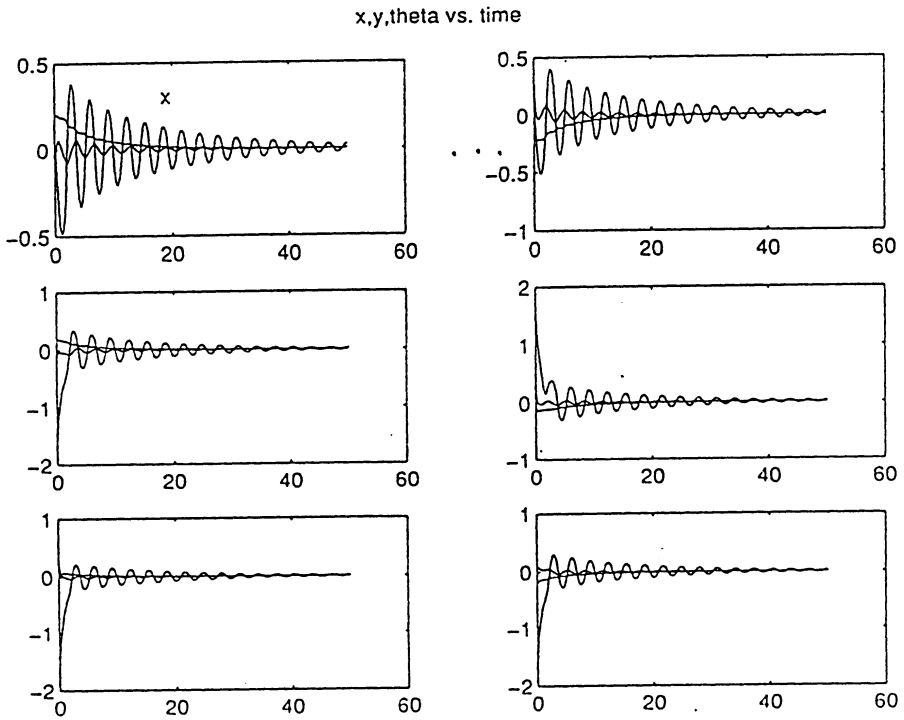

Fig. 5

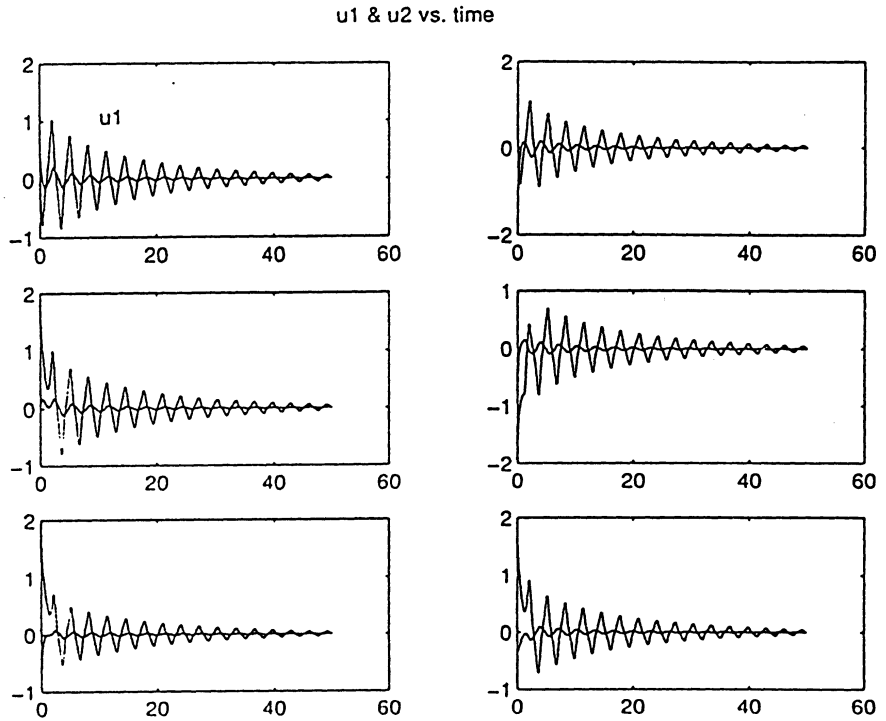

Fig. 6

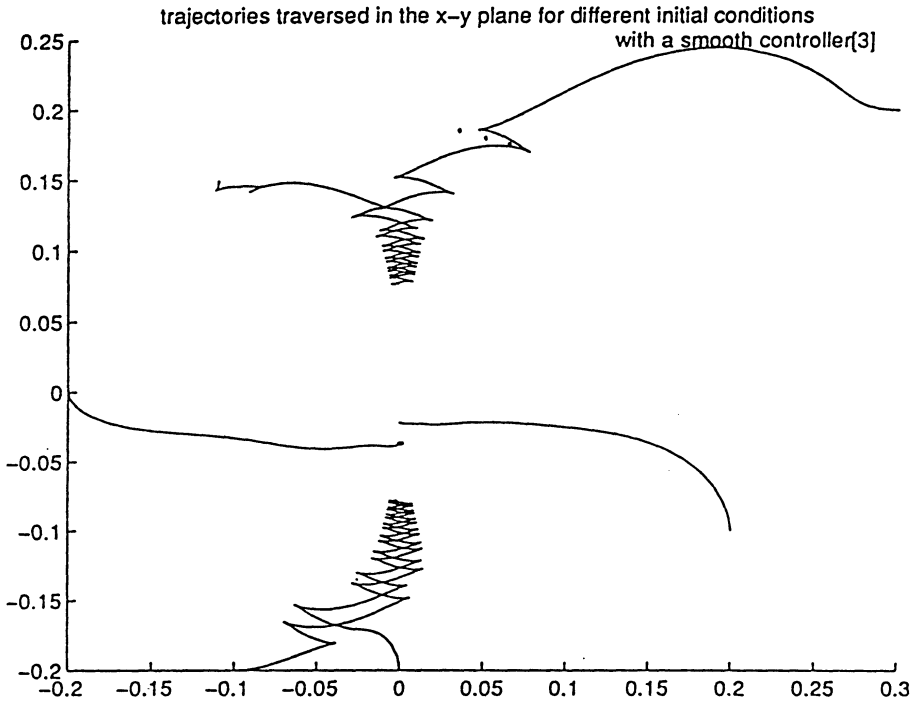
trajectories traversed in the x–y plane for different initial conditions
with a smooth controller[3]
0.25
0.2
0.15
0.1
0.05
0
−0.05
−0.1
−0.15
−0.2
−0.2
−0.15
−0.1
−0.05
0
0.05
0.1
0.15
0.2
0.25
0.3

Fig. 7

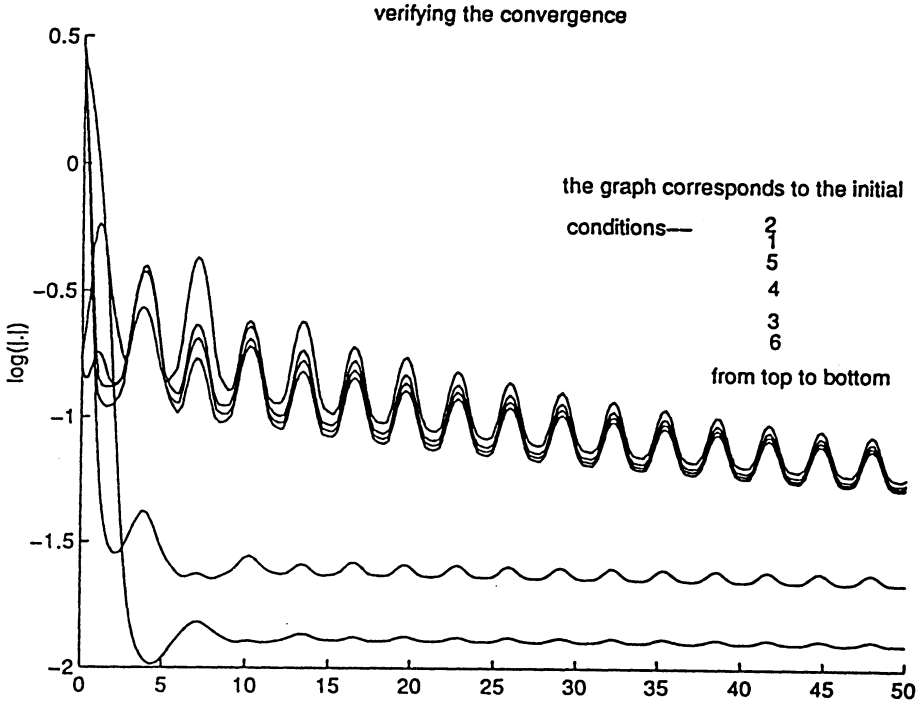
verifying the convergence
log(|.|)
0.5
0
−0.5
−1
−1.5
−2
0
5
10
15
20
25
30
35
40
45
50
the graph corresponds to the initial
conditions—
2
1
5
4
3
6
from top to bottom

Fig. 8

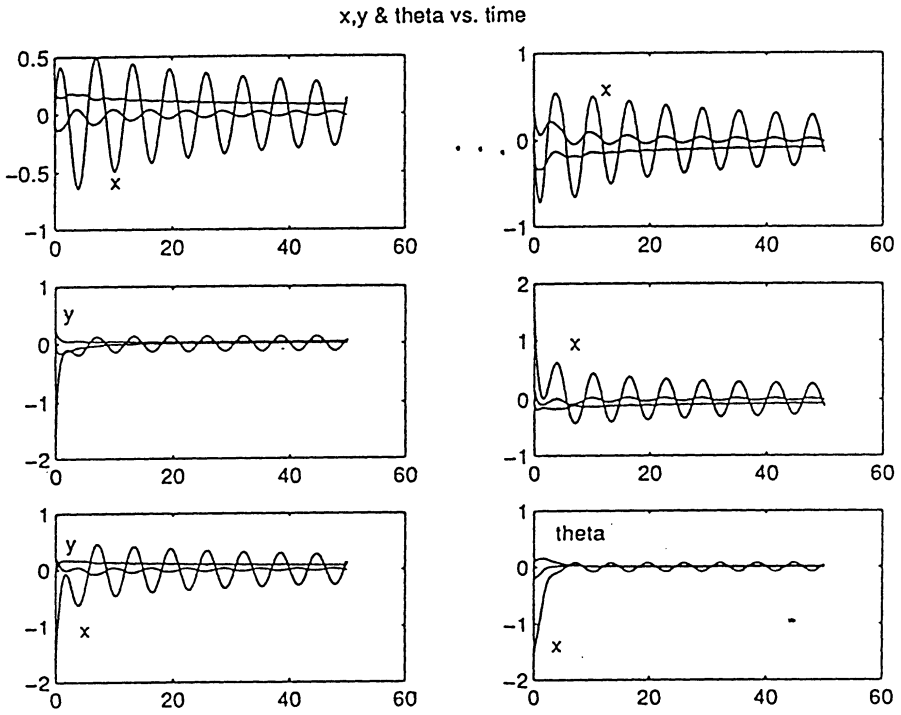

Fig. 9

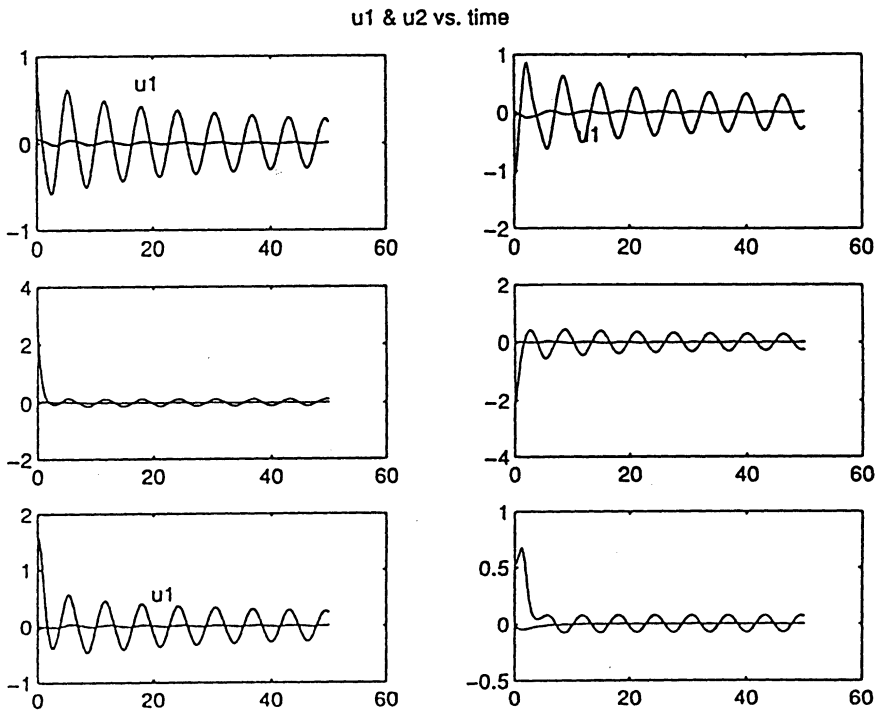

Fig. 10.

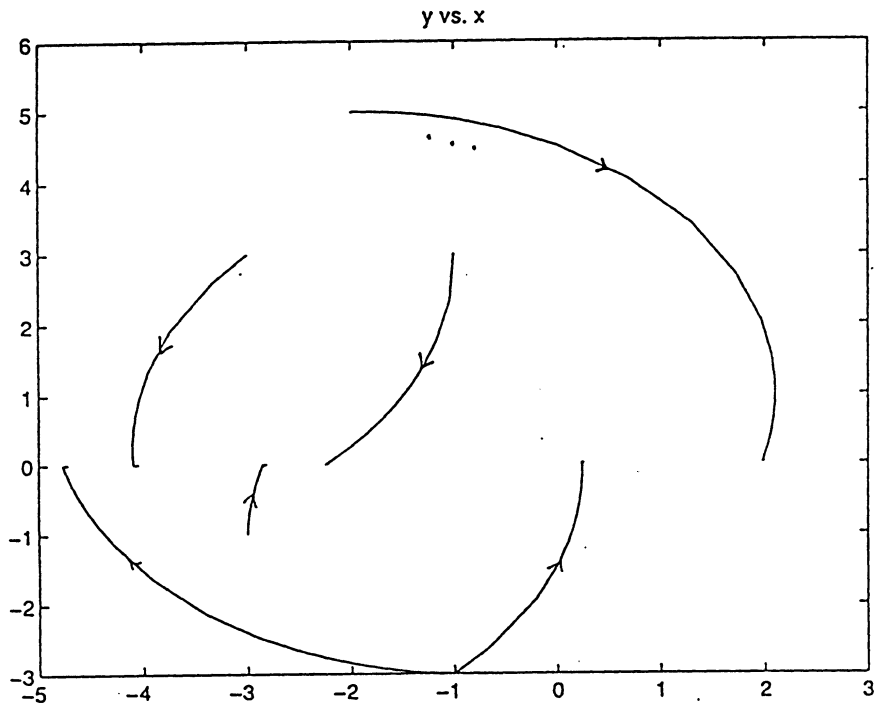
y vs. x
6
5
4
3
2
1
0
-1
-2
-3
-5
-4
-3
-2
-1
0
1
2
3

Fig. 11

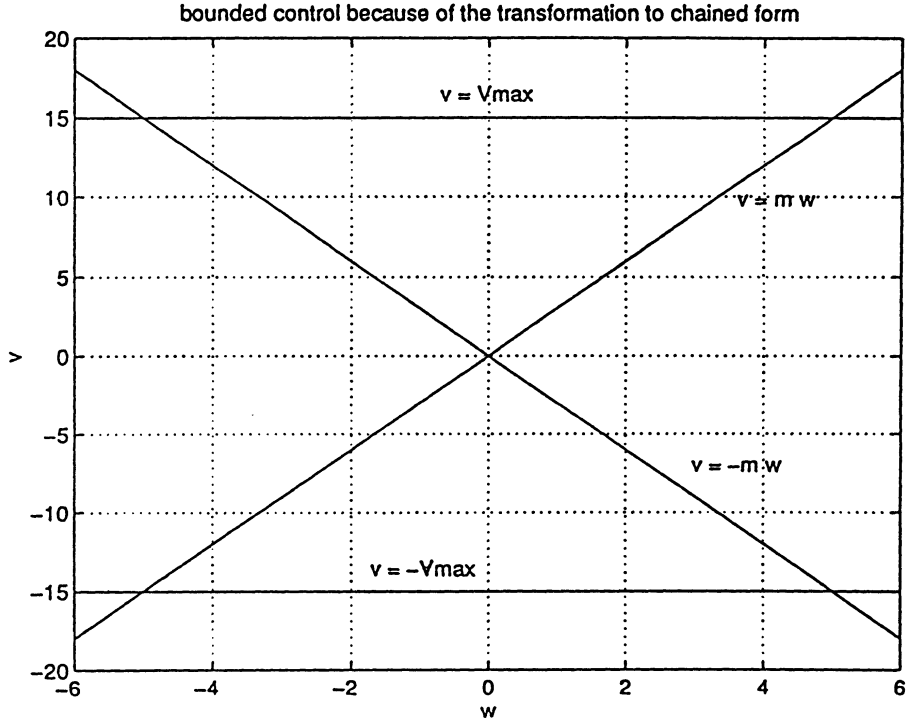
bounded control because of the transformation to chained form
v = Vmax
v = m w
v = -m w
v = -Vmax
v
w
20
15
10
5
0
-5
-10
-15
-20
-6
-4
-2
0
2
4
6

Fig. 12

References

[1] G. J. Pappas and K. J. Kyriakopoulos. Stabilization of non-holonomic vehicles under kinematic constraints. In *International Journal Of Control*, pages 933-947, 1995.

[2] R. T. M'closky and R. M. Murray. Experiments in exponential stabilization of a mobile robot towing a trailer. In *ACC*, pages 988-993, 1994.

[3] A. R. Teel, R. M. Murray and G. Walsh. Nonholonomic Control Systems: From steering to stasbilization with Sinusoids. In *CDC*, pages 1603-1609, 1992.

[4] R. Murray and S. Sastry. Steering nonholonomic systems using sinusoids, In *CDC*, pages 2097-2101, 1990.

[5] G. Walsh, D. Tilbury, S. Sastry, R. Murray and J. P. Laumond. Stabilisation of trajectories for systems with Nonholomic Constraints. In *IEEE T. A. C* 39, 1994.

[6] D. Tilbury, R. Murray and S. Sastry. Trajectory generation for the N-trailer problem using Goursat normal form. *UC-Berkeley ERL memorandum*, 1994.

[7] M. Fleiss, J. Levine, Ph. Martin and P. Rouchon. Nonlinear Control and Lie-Backlund Transformations: Towards a new differential geometric standpoint. In *CDC*, pages 339-344, 1994.

[8] M. Fleiss, J. Levine, Ph. Martin and P. Rouchon. Flatness and defect of Non-linear systems: Introductory theory and examples. *In International Journal Of Control*, pages 1327-1361, 1995.

Nonlinear Control Final Project

Craig Garvin - EECS 662

Abstract

A real time ion flux estimator was designed and implemented as a computer simulation. A reduced order model of plasma dynamics was developed in order to serve as a nonlinear estimator. Because of the multiple time scales in the system, the method of singular perturbation was employed to decouple the fast and slow dynamics of the system. Two different estimator strategies were evaluated. A linear technique based on Jacobean linearization about an operating point was compared to a non linear constant coefficient extended Kalman filter. The linear observe gave poor performance, while the non linear observer was capable of estimating ion flux with less than 25% error over a 50% variation in power and a 50% variation in pressure from the nominal setpoint.

Introduction

Dynamic state estimation is a valuable tool for estimating quantities that are difficult to measure directly. The reactive ion etching (RIE) process used extensively in semiconductor manufacturing is an excellent testbed for estimator design. As in all manufacturing processes, optimal performance is achieved when processing parameters are maintained at ideal levels. This goal is difficult to achieve in RIE because many of the important processing parameters are either difficult or impossible to measure. State estimation offers us a way to improve these measurements. By creating a simple model of the RIE process, the accuracy of available measurements can be improved by comparing these measurements to model predictions. Probabilistic methods are used to weight estimate and measurement in order to arrive at an optimal estimate of the actual quantities. The goal of this project is to develop an ion flux estimator that gives a better estimate of this quantity than is currently available.

Application Background

In this section, sufficient background in the physics of Reactive Ion Etching is given in order to place the model and estimator development in a relevant context. RIE is one of the most used processing steps in the manufacture of semiconductor devices. To date, the process control has lacked robustness and technical sophistication. The University of Michigan is involved in a major research initiative to improve the control of the etching process. Hopefully this project can provide some of the groundwork for parameter estimation and control.

Reactive Ion Etching is the main way by which material is selectively removed from semiconductor wafers, thus allowing the generation of small scale features. RIE can be simplified to two components: chemical etching, which is highly selective, and physical etching, which is highly directional. A schematic of the RIE system is shown in figure 1. The process involves placing the wafer to be etched on the positive electrode of an evacuated chamber. A plasma of specific gasses is formed by electrical excitation, resulting in reactive, energetic ions. As a byproduct of the ionization effect, an electric potential develops at the edge of the plasma near the electrode surface. This region is referred to as the sheath.

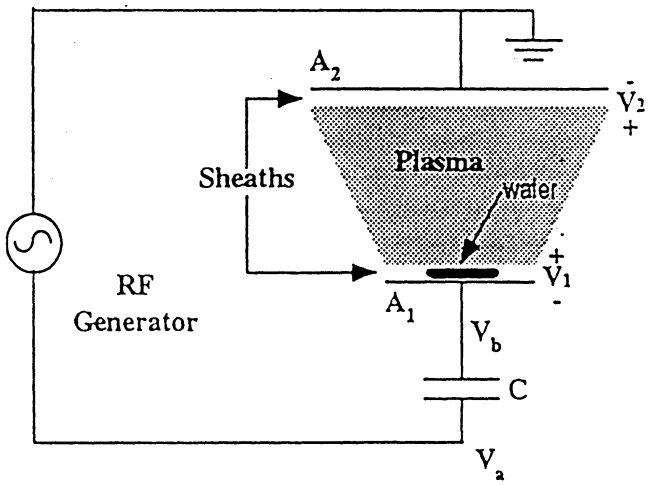

fig. 1: Plasma Chamber Schematic

The combination of ionization and sheath potential result in the chemical and physical etching mechanisms. By proper choice of plasma gasses, species are formed in the plasma that react with exposed silicon, but not

with the mask material. This results in etching selectivity: the ability to etch the desired material without affecting the masked areas. The combination of sheath electrical potential and presence of positive ions results in the acceleration of these ions towards the surface of the wafer. The ion concentration is multiplied by ion velocity to result in the ion flux, the main quantity that we are interested in estimating. Depending on the surface material and the energy of the ions, the ion collision causes the surface molecule to be ejected, referred to as 'sputtered'. The advantage of physical etching is the enhanced anisotropy achieved, as shown in figure 2. Because the ion velocity is perpendicular to the surface, vertical etches with straight sidewalls are possible. The result is smaller feature sizes and more dense component layouts.

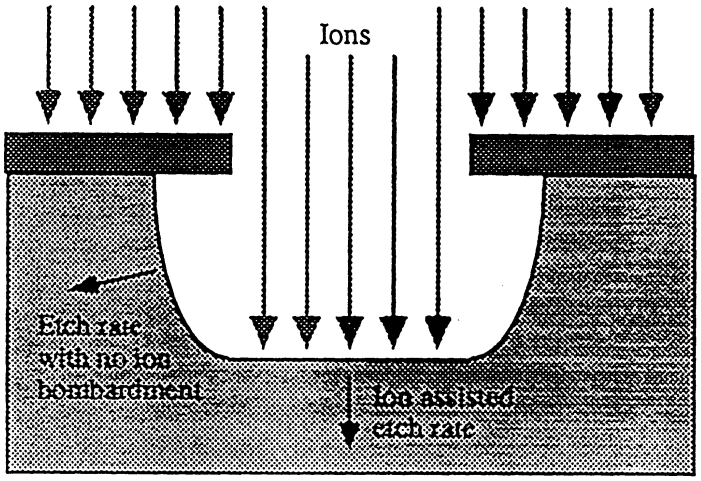

fig. 2: Anisotropic Etching

It is clear from the above discussion that control over the chemical and physical aspects of the etch is desirable. At present information on concentration of reactive species is difficult to obtain, and information on ion flux almost impossible to obtain. The goal of this project is to use a simple nonlinear dynamic model of plasma generation in combination with a static equation relating ion flux to easily measured quantities. A weighted average of these two is used to obtain an optimal estimate of ion flux.

Modeling Background

The chemical and physical processes that occur in a plasma are extremely complex and rather poorly understood. Additionally, little work has been done to date on understanding and modeling these processes for the purpose of real time control. A complete quantification of the RIE process requires close to one hundred chemical states, and simulations of this level o complexity can take days to run on an engineering workstation. Fortunately, work has been done to simplify the models in order to reduce the system to a tractable set of equations. A major first step in simplification is the division of the RIE process into two subsystems, as shown in figure 3. Plasma generation is viewed as one subsystem, wafer etching as another. The inputs to the plasma generation subsystem are gas flow rate into the plasma chamber, RF power, and throttle position. These inputs combine to produce reactive chemical species, or radicals, ion flux, polymer precursors, bias voltage and pressure. These states then act as inputs to the wafer etch process, whose outputs are etch rate of the substrate (Rate #1) and mask (Rate #2), and etch direction.

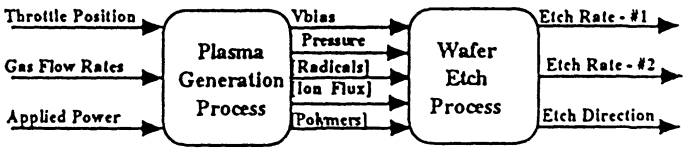

figure 3

The current thrust of the University of Michigan controls research is to improve the observability and controllability of the plasma generation process. It is believed that an improved plasma generation process will result in improved wafer etching, by simple cascading. Observing the Plasma Generation Process is a major challenge. The bracketed terms in figure 3: radicals, ion flux, and polymer precursers, are quantities for which no reliable, industry compatible measurement technique has been developed. Detection and measurement of radicals is achieved in research laboratories with the use of delicate and expensive instruments and time consuming measurements. Progress is currently being made at the University of Michigan in measuring important radicals using faster and less expensive techniques.

To date, no proven technique exists to measure ion flux. We will tackle this problem by simplifying an existing plasma model to form a dynamic model of ion formation and ion velocity. We will use existing simple plasma models to convert easily measurable quantities to a static estimate of ion flux. We then use relative confidence estimates to blend these two estimates into a final estimate. We then test the estimator against the predictions of the more complete plasma model in order to evaluate the performance of the estimation algorithm.

The Plasma Factory Model

Researchers at the University of Michigan have developed a greatly simplified plasma model that has shown reasonable correlation with experimental measurements. This model will be referred to as the real time simplified plasma factory or PF model. The PF model uses CF_4 as its input or 'feed gas', and calculates the concentration of the main radicals dynamically. This model is used as a starting point for development of a simplified ion flux model.

A qualitative description of the plasma generation process is useful. When low pressure gas is subject to an electric field, free electrons are accelerated in the direction of the electric field. At higher pressures, these electrons immediately encounter other molecules and are reabsorbed before they can do anything interesting. As pressure drops, the distance between molecules is sufficient that the electrons can gain enough energy that when they collide with molecules in the gas, they cause the molecules to dissociate, producing new radicals and more electrons . The product of these reactions alter the pressure in the chamber and the conductivity of the gas. Additionally, a potential is developed in the edges of the plasma which accelerates positively charged particles towards the surface of the electrodes. Typically, the potential is much larger in the positive electrode sheath than the ground electrode sheath. As a result, the bias between the two electrodes, Vbias, is an accurate measure of sheath potential.

Analysis of the plasma dynamics is made difficult by the enormous variation in time and magnitude scale of important processes. It is obvious from the above discussion that the electron concentration is an essential variable affecting plasma generation. Electrons are very sparse, comprising less than 1 % of the species in the plasma. Likewise, the ions that result in a major part of the etch process comprise less than 0.1 % of the species in the plasma. Additionally, electron, ion, and bias voltage dynamics are almost instantaneous, whereas generation of major plasma radicals such as CF_3 and F has time scales in the seconds.

The existing PF model calculates the 'fast' quantities such as electron density, electron energy, and bias voltage using a large look-up table indexed by power and pressure. One of the main assumptions of this project is that RF power into the plasma chamber and pressure inside the chamber are the dominant factors affecting plasma parameters. It should be noted that the 'fast' quantities do change slowly with time, but only as a function of pressure changes resulting from slower reactions.

The model tracks 5 states with the equation set shown in **figure 4.** *Fin* is the flow rate of feed gas into the chamber, and acts as one of the inputs. *Fout* is the rate of gas flow out of the chamber and is a function of chamber pressure and throttle angle. The rate equations separate into two classes, those that are a function of particles collisions, usually an electron and a radical, and those which occure on the walls of the chamber. Much of the model complexity is not seen in the equation set because electron concentration, and rate constants *k1* .. *k7* and *kwall_1* .. *kwall_3* are complex function of power and pressure.

$$\frac{d[CF_4]}{dt} = F_{in} - k_1[e^-][CF_4] + k_2[F][CF_3] - F_{out}\cdot\chi_{CF_4}$$

$$\frac{d[F]}{dt} = k_3[e^-][CF_4] - k_4[F][CF_3] - k_{wall\_1}[CF_2] - F_{out}\cdot\chi_F$$

$$\frac{d[CF_3]}{dt} = k_5[e^-][CF_4] - k_6[F][CF_3] + k_{wall\_2}[CF_2] - F_{out}\cdot\chi_{CF_3}$$

$$\frac{d[CF_2]}{dt} = k_7[e^-][CF_4] - k_{wall\_3}[CF_2] - F_{out}\cdot\chi_{CF_2}$$

$$\frac{d[Ar]}{dt} = F_{inAr} - F_{out}\cdot\chi_{Ar}$$

Although not directly stated, these equations govern the pressure dynamics of the system, as the pressure is given by:

$$P = RT([CF_4]+[F]+[CF_3]+[CF_2]+[Ar]) \qquad (1)$$

Similarly, the flow of species out of the model is governed by the partial pressure of the species:

$$\chi_x = \frac{x}{([CF_4]+[F]+[CF_3]+[CF_2]+[Ar])} \qquad (2)$$

This division by the states can make for rapidly increasing complexity, and is one of the issues that must be addressed in model simplification.

Simplifying and Adapting the Model

Although the PF model is a great simplification from previous approaches, it requires substantial modification before it can be used for the purpose of ion flux estimation. The reaction set must be simplified, ions and ion flux dynamics must be included, measurement feedback must be added and the model must use continuous functions rather than table look up to express reaction coefficients and other values.

A first step towards simplification is combining electron concentrations and rate constants. Since both are determined as static functions of power and pressure, there is no loss of accuracy in grouping k*[e] into a single term.

The next logical step is eliminating CF_2 and Ar from the reaction set. Eliminating argon is reasonable, as its only purpose is in fluorine estimation. Eliminating CF_2 is reasonable because its concentration is an order of magnitude below that of the CF_4, CF_3, and F concentrations.

The initial simplified model keeps track of three reactants, and calculates pressure using equation (1). A problem arises with this approach. Since the species are formed in the following reaction:

$$CF_4 \rightarrow CF_3 + F \qquad (3)$$

it is no surprise that the CF_3 and F states are unobservable when pressure is used as the only output. Since they are formed in equal quantity in equation (3), changes in pressure are equally attributable to CF_3 or F. An initial idea was to feed back a measurement of fluorine in order to improve observability. This is compatible with existing work on fluorine estimation, but a more logical solution is simplify the model even further.

Our main goal is to estimate ion flux. Since ions are formed almost exclusively from CF_4, and formation rate and ion velocity are functions of power and pressure, then the only three states needed in order to estimate ion concentration are CF_4, pressure and power. Accordingly, we can group all the plasma species together into a single pressure state whose dynamics are a function of the number of additional gas molecules formed when CF_4 disassociates. In addition to reducing the model by one state, the rate constant equations are greatly simplified, as these are now functions of pressure directly, rather than substituting the quantity ($[CF_4] + [CF_3] + [F]$) for pressure.

The model so far:

$$\frac{d[CF_4]}{dt} = F_{in} - K_{CF_4}(pres, pow)\cdot[CF_4] + \frac{[CF_4]}{pres} F_{out}(pres)$$

$$\frac{d\,pres}{dt} = F_{in} + K_{CF_4}(pres, pow)\cdot pres - F_{out}(pres)$$

Several reasons motivate the inclusion of power as a model state. Since non linear systems which are afine in the control are more easily analyzed, expressing the power delivered to the plasma as a state greatly simplifies the formulation. Additionally, although the power supply voltage is unquestionably an input, the power delivered is a dynamic function of the plasma condition. As the plasma's chemical composition changes, so does its resistance. An additional component in the system is the matching network that matches the plasma load to the generator, allowing maximum power transfer. The matching network functions by moving variable capacitors, whose time constant is on the order of 1 second. As a result, power delivered to the plasma is a dynamic function of the plasma states. At present, an accurate model of power dynamics is not available, so a first order lag is used.

$$\frac{d\,pow}{dt} = T(-pow + P_{in})$$

The model may need additional coefficients to account recombination dynamics. It is well documented that as pressure rises, recombination reactions are favored, and these cause the dynamics to stabilize. In order to obtain proper equilibrium values for the states, a linear recombination coefficient was included in the pressure dynamics and CF_4 dynamics and tuned to give results that agreed with the larger simulation. It is not clear whether these coefficients represent corrections of inaccurate coefficients or a physically different recombination reactions.

Modeling the ion concentration and ion flux dynamics is essential to developing an accurate estimator, but the ion dynamics are difficult to represent and require careful handling. The ion flux equation is given by:

$$\Gamma_i = V_b \cdot n_s \qquad (4)$$

The ion flux (Γ_i) is equal to the ion density at the edge of the sheath (n_s) multiplied by the ion velocity at the edge of the sheath (V_s). V_s can be approximated by the Bohm velocity V_b:

$$V_b = \sqrt{\frac{k\,T_e}{m}}$$

where T_e is the electron temperature, k is the boltzmann constant and m is the ion mass.

A reasonable course of action is to determine the ion concentration from the dynamic equations of ion concentration, then multiply by V_b. The differential equation can be approximated as

$$\frac{d[n_s]}{dt} = K_{iz}(pres, pow)\cdot[CF_4] - V_b \cdot n_s \qquad (5)$$

This equation is of little value for designing an estimator because of the numbers involved. Ion concentration is much lower than CF_4 concentration because the Bohm velocity is 100,000 times higher than the ionization constant. As a result equation (5) is effectively decoupled from the rest of the system. Our goal of estimating ion concentration by making accurate estimates of the other states cannot be met.

Again, the solution to this problem is found by returning to the goal of the project: ion flux estimation. If we take the derivative of equation (4), we obtain an expression for change in ion flux with time:

$$\frac{d\Gamma_i}{dt} = \frac{dV_b}{dt}\cdot n_s + V_b \cdot \frac{dn_s}{dt} \qquad (6)$$

Since V_b changes with power and pressure, it is effectively constant compared to the rate of change of ion concentration. Accordingly, equations (5) and (6) can be combined to give

$$\frac{d\Gamma_i}{dt} = V_b \cdot \left(K_{iz}\cdot[CF_4] - V_b \cdot n_s\right) \qquad (7)$$

Vb ns is ion flux, and now we have an equation for ion flux dynamics explicitly:

$$\frac{d\Gamma_i}{dt} = V_b \cdot \left(K_{iz}\cdot[CF_4] - \Gamma_i\right) \qquad (8)$$

This equation still presents a problem. Although ion flux is now strongly dependent on other states, the time scale is orders of magnitude faster that other states. This is a textbook example of a singularly perturbed system, and because of the way the equations are formed it is extremely easy to separate the fast and slow systems (we just did). As long as the fast dynamics are stable (which they are), we can solve for ion flux by assuming that (8) is a static equation and setting the right hand side equal to zero. Furthermore, since the method of singular perturbations allows us to separate the dynamics, the fast system (ion flux dynamics) can be expressed as a three input, single state system. The other states of the system are so slow that they can effectively considered constant inputs to the ion flux system.

The final step in modeling the plasma dynamics is determining analytic functions for the rate constants and electron temperature. As can be seen in figure 4, three dimensional plots of these parameters show them to be smooth functions of power and pressure.

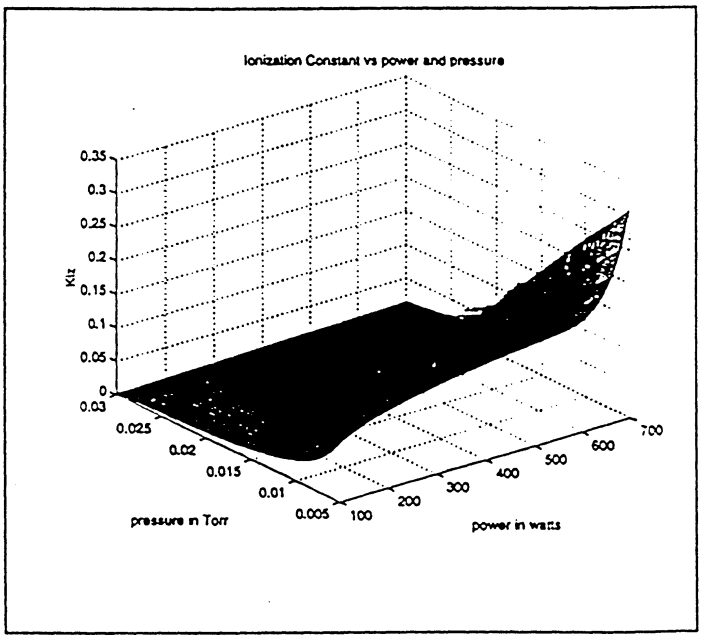

fig 4: Ionization Coefficient vs. Power and Pressure

A least squares algorithm is used to fit a second order proportional and inverse polynomial function to the data. In order to properly interpret the polynomial coefficients, power, pressure and output variables are all normalized. Since inverse functions are used, variables are normalized to 0.5 to 2.5 in order to avoid division by zero. To maintain simplicity, only the four largest coefficients were kept for each parameter. Further simplification is achieved by fitting a polynomial function to the square root of electron

temperature rather than fitting to electron temperature, then taking the square root. All data fits with less than 5% error, and the following equations are obtained:

$$K_{CF_3} = -0.4549 + 0.6245 \cdot pow + \frac{1.285}{pres} - \frac{0.3803}{pres \cdot pow}$$

$$K_{IZ} = -0.6775 + \frac{1.143}{pres} + \frac{0.5503}{pow} - \frac{0.7803}{pres \cdot pow}$$

$$\sqrt{T_e} = 1.177 - 0.5846 \cdot pres + \cdot \frac{1.032}{pres}$$

Since normalized power and pressure are already used to calculate coefficients, it is an added simplification to express the pressure dynamics, CF_4 dynamics, and flux dynamics in terms of normalized pressure. The conversion from concentration to partial pressure is simple and flux can be expressed as a rate of partial pressure per second.

Measurement Feedback

The model can now be used for estimator design. However, a suitable feedback must be determined in order to implement the design. The most common estimation problem involves noisy signals: The actual parameter of interest, corrupted by noise is available to the outside world. In the case of ion flux estimation, no measurement however noisy is available. What we can do is create a static estimate of ion flux based on a different theory and use the combination of static and dynamic estimate in proportion to their relative certainty. The Child Langmuir law can be used to derive an equation for ion flux:

$$\Gamma_i = k \frac{I^2}{\sqrt{Vbias}} \qquad (9)$$

where I is the total current into the plasma and k is an empirically derived fitting constant. This 'measurement' is useful because it is constructed from readily available measurements of electrical parameters. Two other readily available measurements are also used: power into the cell and pressure. A measurement of CF_4 is not used because measuring chemical species accurately is difficult and costly. It is hoped that the simple dynamic model is sufficiently accurate to estimate CF_4 concentration power and pressure.

Estimator Design

Two separate estimator designs are used. An estimator based on a Jacobean linearization of the dynamics is designed. Simulation shows this approach to be inadequate, so a non linear estimator is developed.

In order to design a linear estimator, an operating point must be chosen about which to linearize the dynamics. A typical processing point of 400 watts input power, 25 sccm (standard cubic centimeters per minute) CF_4 flow, and 12.5% throttle position is chosen. This results in a pressure of 18.75 mTorr (approximately 2% of atmospheric) a CF_4 concentration of 1.0 E14 cm-3 (particles per centimeter cubed) and ion flux of 1.25 E14 s-1 cm-2 (particles per second per square centimeter). These values are obtained from the PF simulation and are input into the Jacobean of the nonlinear equations. The result is:

$$A = \begin{bmatrix} -0.19 & 0.024 & -0.049 \\ 0.099 & -0.046 & 0.049 \\ 0 & 0 & -1 \end{bmatrix} \quad B = \begin{bmatrix} 0 & 1 & -1.8 \\ 0 & 1 & -7.5 \\ 1 & 0 & 0 \end{bmatrix}$$

$$C = \begin{bmatrix} 0 & 1 & 0 \\ 0 & 0 & 1 \end{bmatrix}$$

A linear quadratic estimator is designed using this linear model. Since the measurements used for the dynamic model are relatively noise free and the dynamic model of the system is in question, this is reflected in the choice state and measurement noise matrices. Consideration is also given to limiting the measurement feedback gains in order to limit the risk of instability. The following state and measurement covariance matrices were used, resulting in the following estimator gain matrix:

$$Q_{xx} = \begin{bmatrix} 0.001 & 0 & 0 \\ 0 & 0.001 & 0 \\ 0 & 0 & 0.001 \end{bmatrix} \quad Q_{yy} = \begin{bmatrix} 0.05 & 0 \\ 0 & 0.3 \end{bmatrix}$$

$$L = \begin{bmatrix} 0.0616 & -0.001 \\ 0.417 & 0.0005 \\ 0.003 & 0.016 \end{bmatrix}$$

Since a non linear estimator will be implemented, special consideration must be given to its stability. The stability of the LQG based linear estimator is well established. The extended kalman filter stability has been proved for both continuous and discrete case, but stability with constant coefficients is not completely certain. A simple solution at this early stage is to limit the magnitude of the feedback gains. As we shall see, even with moderate gains, the estimator quickly converges the measured values. The relationship between actual and estimated CF_4 concentration is mostly of function of model accuracy and and only be slightly influenced by state feedback.

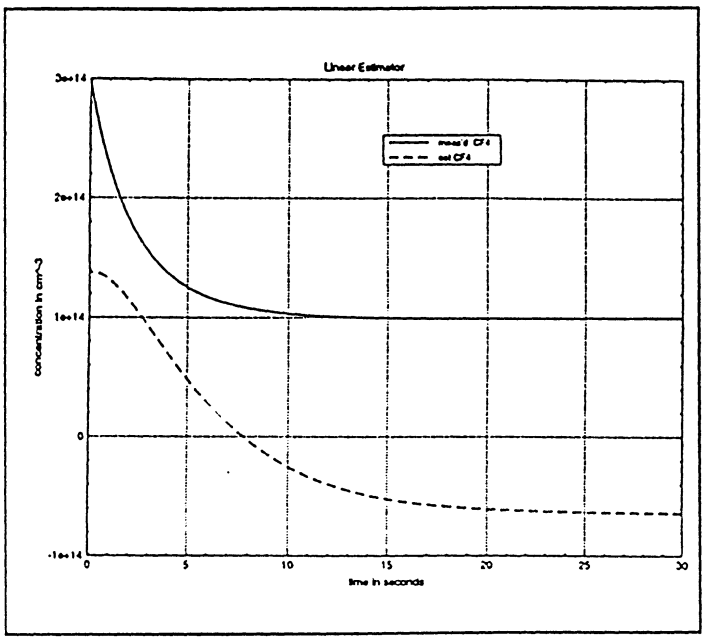

figure 5: Linear Estimator CF_4 Calculation

Estimation methodology for the ion flux dynamics (8) is in some ways simpler, yet in some ways it is more unclear how to proceed. Since there is only a single state in the perturbed system, we write the estimator equations as :

$$\frac{d\Gamma_i}{dt} = V_b \cdot \left(K_{iz} \cdot [CF_4] - \dot{V}_b \cdot n_s\right) + L(y - \hat{y}) \qquad (10)$$

This equation is solved statically by setting the time derivative to zero. The question of an estimator gain must be addressed. The most well documented approach is a probabalistic one, where we estimate the relative uncertainty of the state and measurement. The way our system is formulated, the measurement is imprecise but not uncertain. Because of the nature of the errors in the system, it is unlikely that a more sophisticated way of handling stochastic variation will be advantageous. Accordingly, it makes sense to use a simple constant gain feedback that reflects the relative accuracy of the static and dynamic ion flux estimates.

Linear Estimator Performance

Despite the fact that the system dynamics are stable and relatively simple, the linear estimator performs poorly. The states are observable given power and pressure feedback, but the linearized dynamics fail to capture the relationship between CF_4 concentration and the measured states. As seen in **figure 5**, the linear estimator does a very poor job of estimating CF_4. Since the power and pressure are accurately determined, changing the estimator gains will no effect on the CF_4 estimate. The only way to improve the linear prediction is by changing the linear model from the values obtained by Jacobean linearization.

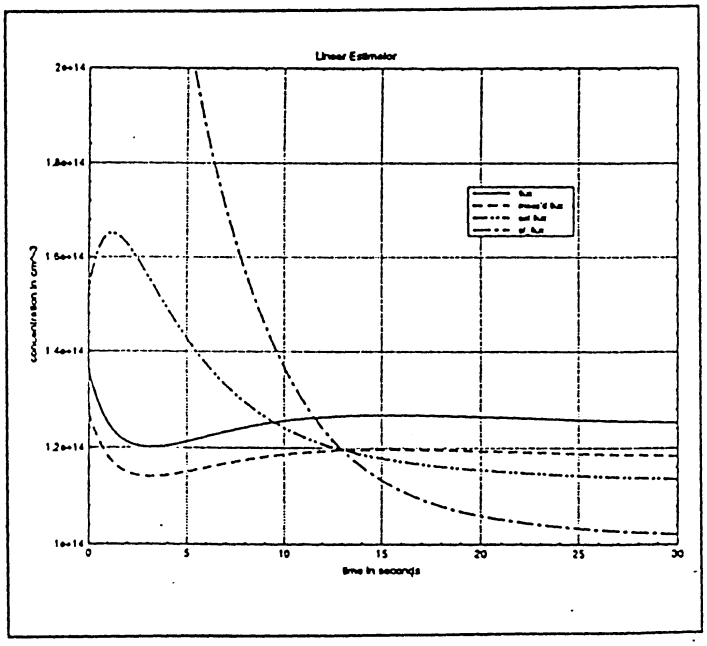

figure 6: Linear Flux Estimate

Given that the CF_4 estimate is so far off, we can expect the flux estimate to be equally bad. As can be seen in **figure 6**, the flux error is tempered by the static estimator which is quite accurate. Four values are given in graphs of flux. "flux" is the actual ion flux, which is not available to the estimator. "meas'd flux" is the flux calculated by the static model, eqn (9). "ol_flux" is the dynamic flux estimate, eqn (8). "est_flux" is the weighted average of equations (8) and (9).

Clearly, in order to arrive at a better ion flux estimate, a better model of the relationship between the quantities we can measure: power and pressure, and the quantities we estimate: CF_4 and ion flux, is needed. This can be achieved through the use of a non linear model of the dynamic and static relationships.

Non Linear Estimator

Before developing a non linear observer, we must address the observability of the non linear system. First let us consider the ion flux dynamics. As discussed previously, these can be separated from the slower dynamics by the method of singular perturbation. Although from a physical standpoint, we cannot measure ion flux, the system is observable from a control systems standpoint, since the model produces and output which we compare to the static estimate. Accordingly, the ion flux dynamics form a three input, single state, single output system that is trivially observable.

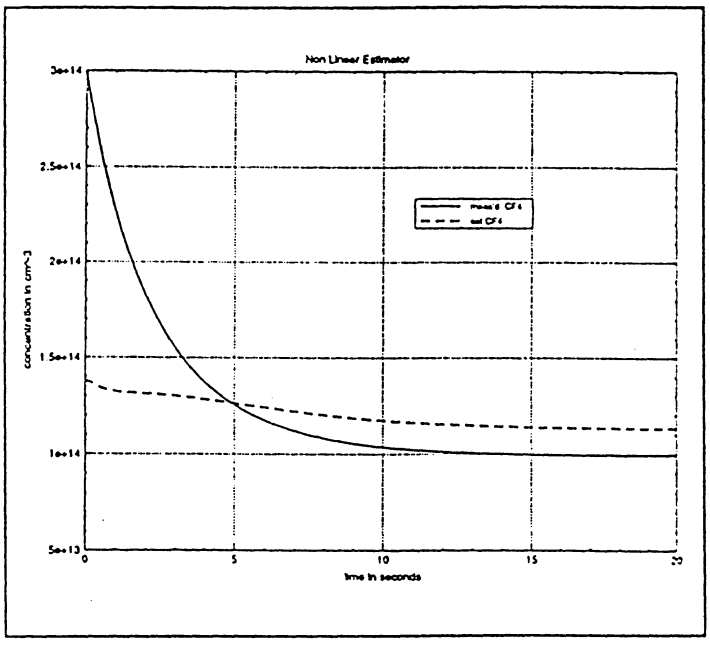

fig 7: Non Linear CF_4 Estimate at Nominal Operating Point

We can evaluate the nonlinear obsevability by taking successive Lie derivatives of the output and determining the null space of the resulting distribution. This calculation is performed in appendix 2, and the resulting empty null space indicates the system is mathematically observable. We can take singular value decompositions of the linearized equations at representative operating points to get an idea of the relative impact of states on the output. This gives an indication of the relative magnitude of the effect of the states on the output. The singular value decomposition at the chosen operating point is representative:

$$SVD(\vartheta) = \begin{bmatrix} 1.73 \\ 1.12 \\ 0.10 \end{bmatrix}$$

The ratio between largest and smallest value is about an order of magnitude. This is not ideal, but is certainly in the range where we can expect the state to be detectable above the noise background. As the system is observable, it is reasonable to proceed with a non linear estimator based that uses the non linear dynamic model and constant feedback gains. As discussed earlier, since this is not a stochastic problem, there is not likely to be much gained from the use of dynamic feedback gains and a definite computational price to be paid

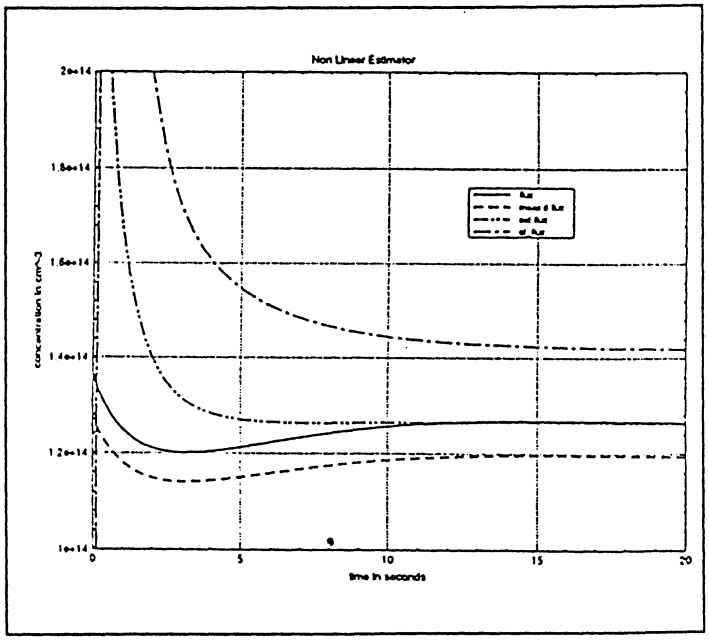

fig 8: Non Linear Ion Flux Estimate at Nominal Operating Point

The performance of our estimator is evaluated at the nominal operating point: 400 watts input power, 25 sccm flow, and 12.5% throttle opening. As can be seen from figure 7, the CF_4 estimate is much better than in the non linear case. This is not surprising, with a more accurate model to relate power and pressure to CF_4 concentration, more accurate results are expected. Given a more accurate calculation of CF_4, figure 8 is no surprise either. As can be seen, the flux estimate closely matches actual values.

Appendix 3 gives CF_4 and flux estimates at different power levels and different input flow rates. The accuracy of the estimate is a function of relationship between static flux estimate, dynamic flux estimate and actual flux values. If, for example, the static estimate over calculates flux, and the dynamic estimate under calculates flux, both by a constant percentage regardless of operating point, then the total estimate will be accurate. If, as can be seen in appendix 3, both estimates predict the same erroneous value, then there is nothing that the estimator as designed can do to remedy the situation. Even when the estimate is inaccurate, the magnitude of error is comparatively small. Considering that almost nothing is available to date to measure ion flux, if these estimates hold up under actual operation, this system will be a significant improvement.

Conclusion

At least in simulation, the estimator shows promise. The main area requiring improvement is in the modeling of the system and of the feedback paths. As it stands, the ion flux estimator has no feedback to 'reality'. Since we cannot measure ion flux, we can track the static flux estimate very closely, and track power and pressure exactly, and still have an erroneous estimate with no indication that anything is wrong. The likely approach is to include a feedback of etch rate, currently being developed in our group, along with some probabilistic causal models. This estimator can be included in a larger scale etch rate estimator. In this way a feedback path is available. If the etch rate deviates from predicted values, a model can be used to determine which of the etching inputs is likely to be incorrectly estimated. This feedback can then be used to modify the flux rate estimate.

ME 662 / EECS 662 / AERO 672

ADVANCED NONLINEAR CONTROL

FINAL PROJECT

Stabilization of a Tightrope Walker

by

Cevat GOKCEK

1. Introduction

In this project the stabilization problem for a simplified planar model of a tightrope walker is studied. The goals of this work are to model and analyze the problem, specify some performance criteria, design several controllers that achieve these criteria and evaluate the performances of proposed controller.

First, a simple model is considered and the equations of motion are derived. Then, the resulting system is analyzed and several control techniques are applied to stabilize the system.

Later, the model is revised to obtain a more accurate model and the equations of motion is derived. Then, these equations are normalized and by using preliminary feedback transformation the relationship between this problem and the nonlinear benchmark problem is established. Using this relationship, a controller is designed and its performance is evaluated.

Finally, the conclusions of this work and suggestions for future work are presented.

2. The Tightrope Walker System Model

The planar model for the tightrope walker is shown in Fig. 1. This model involves a body of mass M and length L whose lower end is hinged to a fixed surface. A balancing bar of mass m and length l is hinged at its midpoint to the upper part of the body. The moment of inertia of the body and the balancing bar about their respective center of mass are I and i, respectively.

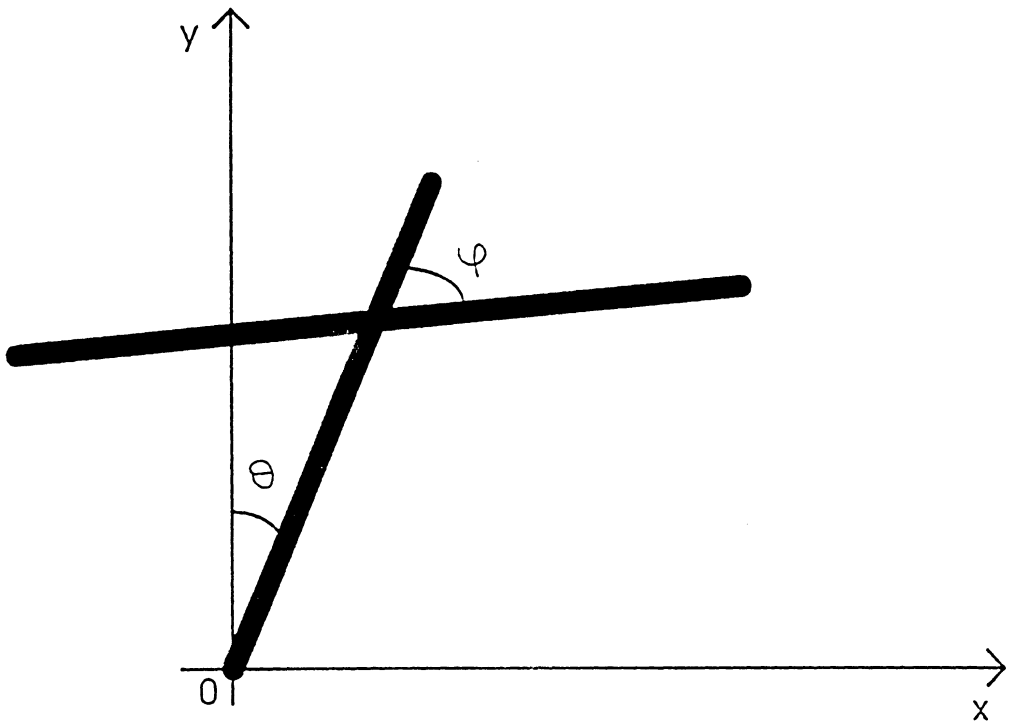

Fig. 1. The tightrope walker model.

Denoting the torque applied to the bar by τ, the equations of motion are given by

$$\begin{aligned} &(\frac{ML^2}{4}+md^2+I+i)\ddot{\theta}+i\ddot{\varphi}-(\frac{ML}{2}+md)g\sin\theta=0 \\ &i\ddot{\varphi}+I\ddot{\theta}=\tau \end{aligned} \tag{1}$$

Let $B=\frac{ML^2}{4}+md^2+I$ and $N=(\frac{ML}{2}+md)g$ so that

$$
\begin{aligned}
&(B+i)\ddot{\theta}+i\ddot{\varphi}-Ng\sin\theta=0\\
&i\ddot{\varphi}+I\ddot{\theta}=\tau
\end{aligned}
\tag{2}
$$

Defining the states of the system as $x_1=\theta,\ x_2=\dot{\theta},\ x_3=\varphi,\ x_4=\dot{\varphi}$, the equations (2) can be written in state space form as

$$
\begin{bmatrix}\dot{x}_1\\ \dot{x}_2\\ \dot{x}_3\\ \dot{x}_4\end{bmatrix}=\begin{bmatrix}x_2\\ \frac{N}{B}\sin x_1\\ x_4\\ \frac{-N}{B}\sin x_1\end{bmatrix}+\begin{bmatrix}0\\ \frac{-1}{B}\\ 0\\ \frac{1}{i}+\frac{1}{B}\end{bmatrix}u \tag{3}
$$

The equilibrium points of the system are in the form $x_e=[0\ \ 0\ \ x_{3e}\ \ 0]^T$ or $x_e=[\pi\ \ 0\ \ x_{3e}\ \ 0]^T$, where x_{3e} is an arbitrary constant. This implies that the origin is not an isolated equilibrium point. Furthermore, the Jacobian linearization at origin

$$
\begin{bmatrix}\dot{z}_1\\ \dot{z}_2\\ \dot{z}_3\\ \dot{z}_4\end{bmatrix}=\begin{bmatrix}0 & 1 & 0 & 0\\ \frac{N}{B} & 0 & 0 & 0\\ 0 & 0 & 0 & 1\\ \frac{-N}{B} & 0 & 0 & 0\end{bmatrix}\begin{bmatrix}z_1\\ z_2\\ z_3\\ z_4\end{bmatrix}+\begin{bmatrix}0\\ \frac{-1}{B}\\ 0\\ \frac{1}{i}+\frac{1}{B}\end{bmatrix}u \tag{4}
$$

has eigenvalues $\lambda_1=0,\ \lambda_2=0,\ \lambda_3=-\sqrt{N/B},\ \lambda_4=+\sqrt{N/B}$. Thus, the origin is a critical point of this system. Fortunately, it is controllable, so that the eigenvalues of (4) can be located arbitrarily.

Let the output be $y=\theta$ then

$$y=x_1$$

$$y=x_2$$

$$y=\frac{N}{B}\sin x_1-\frac{1}{B}u$$

which implies that the relative degree r of this system is 2 and the zero dynamics is governed by

$$\dot{\varphi} = 0 \tag{5}$$

This equation implies that (3) is a non-minimum phase system.

3. Controller Specifications

Having derived the state space equation for the tightrope walker, we want to design a controller that satisfies the following criteria:

i. The closed loop system is at least partially stable in $x_1 = \theta$ and $x_2 = \theta$.

ii. The closed loop system exhibits good disturbance rejection.

iii. The control effort is reasonable.

iv. The settling time behavior of the closed loop system is acceptable.

v. The closed loop system is robust with respect to parameter variations.

4. Controller Design

Our first controller is based on the Jacobian linearization of (3) at $x_{op} = [0 \quad 0 \quad \pi/2 \quad 0]$ and $u_{op} = 0$. First, we design an LQR controller for (4) as

$$u = -Kz \tag{6}$$

and using and close the feedback loop of the nonlinear system by

$$u = -k_{j1}x_1 - k_{j2}x_2 - k_{j3}(x_3 - \pi/2) - k_{j4}x_4 \qquad \text{(C1) (7)}$$

where the controller gain $K = [k_{j1} \quad k_{j2} \quad k_{j3} \quad k_{j4}]$ is then optimized to achieve the design goals.

This control law achieves the design specifications. However, the main drawback to this control law is that it distinguishes the physically equivalent states $\theta_0 \mod 2\pi$, $\varphi_0 \mod 2\pi$ and thus suffers from unwinding which increases the settling time and the control effort unnecessarily. These difficulties can be overcome by the introduction of the control law

$$u = -k_{j1}\sin x_1 - k_{j2}x_2 + k_{j3}\cos x_3 - k_{j4}x_4 \qquad \text{(C2) (8).}$$

Note that (C1) is the linearized form of (C2). Then, using the total energy of the system as a Lyapunov function the local stability of the closed loop system can be shown easily.

Our, next controller is based on input-output feedback linearization. In (3) let

$$u = N\sin x_1 + Bk_{1f}x_1 + Bk_{2f}x_2 \qquad \text{(C3) (9)}$$

where k_{f1} and k_{f2} are the controller gains. This feedback transforms (3) into

$$\begin{bmatrix} \dot{x}_1 \\ \dot{x}_2 \\ \dot{x}_3 \\ \dot{x}_4 \end{bmatrix} = \begin{bmatrix} x_2 \\ -k_{f1}x_1 - k_{f2}x_2 \\ x_4 \\ \frac{N}{i}\sin x_1 + (\frac{1}{i} + \frac{1}{B})Bk_{f1}x_1 + (\frac{1}{i} + \frac{1}{B})Bk_{f2}x_2 \end{bmatrix} \tag{10}$$

which implies that the subsystem involving x_1 and x_2 is globally asymptotically exponentially stable for any positive k_{f1} and k_{f2}. This will make x_3 and x_4 approach to $\alpha t + \beta$ and α, respectively, where α and β are some constant. That is, while the angular position and velocity of the main body approach to zero, the motion of the balancing bar approaches to uniform circular motion with angular velocity α. Obviously, this control law satisfies the first design criterion stated above and k_{f1}, k_{f2} can be used to optimize the system response in such a way that it meets the other design specifications.

Next, the control law C3 is modified to prevent unwinding as

$$u = (N + Bk_{f1})\sin x_1 + Bk_{f2}x_2 \tag{11}$$

Defining the controller gains as $l_{f1} = N + Bk_{f1}$ and $l_{f2} = Bk_{f2}$ (11) becomes

$$u = l_{f1}\sin x_1 + l_{f2}x_2 \tag{C4) (12}$$

Note that, this modification preserves the stability in the subsystem involving x_1 and x_2.

5. Simulation Results

All controller designed are animated and simulated by using Matlab. Both closed loop and open loop system are simulated for the following three cases: without disturbance, small disturbance and large disturbance. The following parameter values

$M = 70.0\ kg$
$m = 2.5\ kg$
$L = 1.8\ m$
$l = 3.0\ m$
$d = 1.3\ m$
$I = 18.9\ kgm^2$
$i = 1.875\ kgm^2$
$g = 9.81\ m/s^2$

and the optimized controller gains

$k_{j1} = -3.1879 \times 10^3$
$k_{2j} = -1.1250 \times 10^3$
$k_{j3} = +7.0711 \times 10^3$
$k_{j4} = -1.0225 \times 10^3$

$l_{f1} = +7.2974 \times 10^2$
$l_{f2} = +1.3826 \times 10^2$

are used for simulations. The initial condition is set to $x_0 = [\pi/4 \quad 1/2 \quad \pi/4 \quad 0]$. The state trajectories and control input of the system are plotted in Fig. 2 and Fig. 3, when the system is controlled by the controller C2 and C4, respectively. The simulation results with C1 are very similar to those of C2 and the same is true for C3 and C4, as expected. In these simulations, the disturbance is taken as a sinusoid of amplitude 100 Ntm at 4 Hz.

Some quantitative performance measures for C1 and C2 are given in Table. 1.

	maximum torque	input power	settling time
C2	2822	743020	3
C4	587	511110	6

Table 1. Some performance values for C1 and C2

Furthermore, it is observed that the robustness and disturbance rejection of the system is very good. The system can tolerate at least 100% change in parameter values and can compensate a sinusoidal disturbance torque of amplitude 500 Ntm at 4 Hz. If friction is included in the model, the performances of proposed controllers even become better.

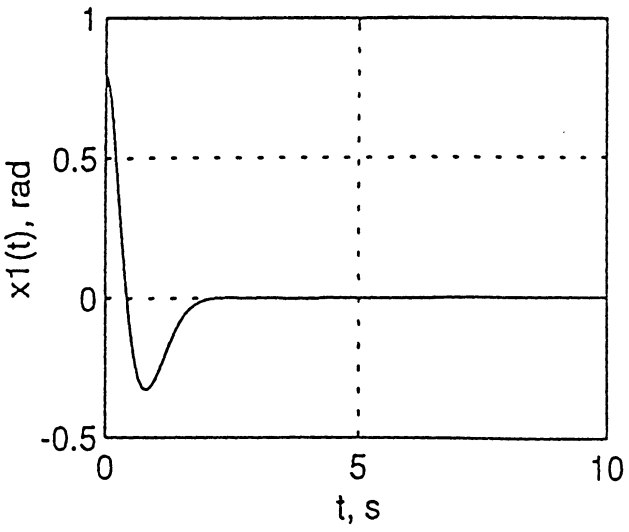
x1(t), rad
1
0.5
0
-0.5
0
5
10
t, s

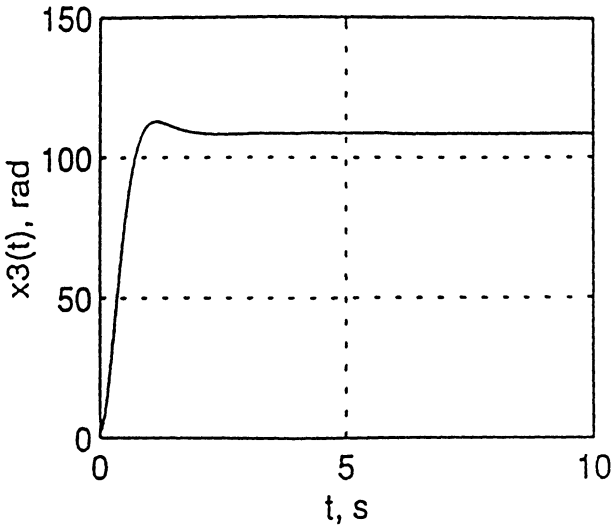
x3(t), rad
150
100
50
0
0
5
10
t, s

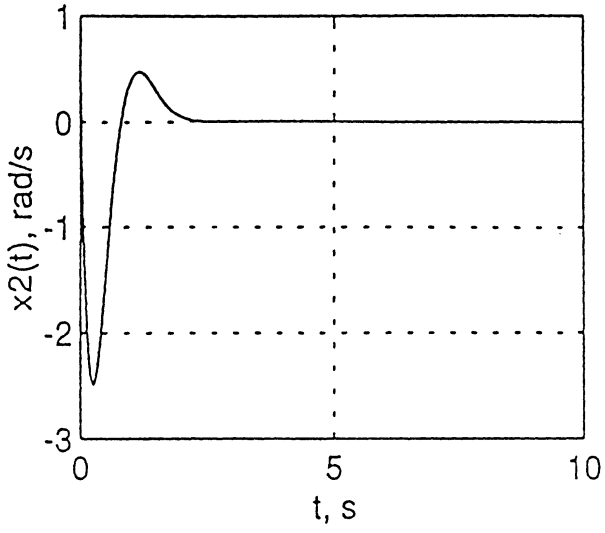
x2(t), rad/s
1
0
-1
-2
-3
0
5
10
t, s

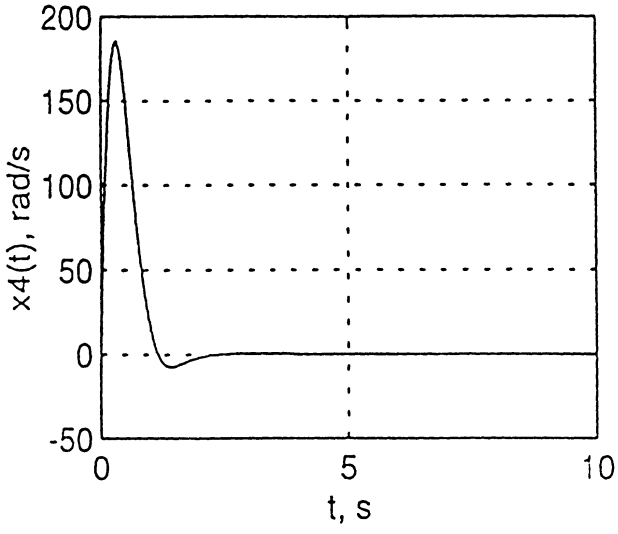
x4(t), rad/s
200
150
100
50
0
-50
0
5
10
t, s

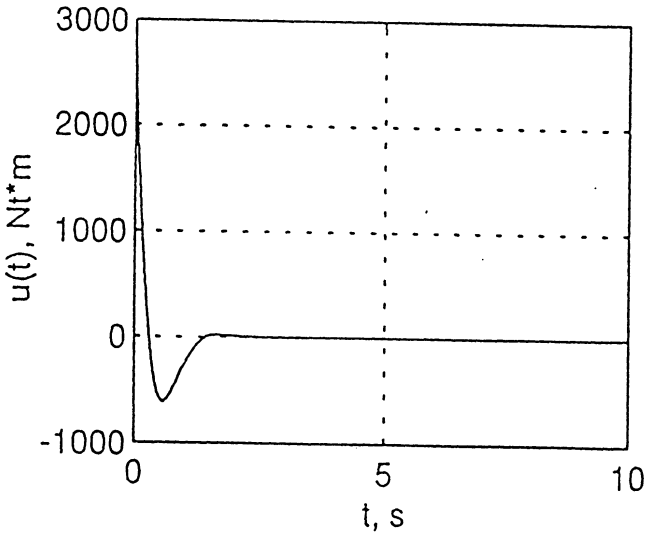
u(t), Nt*m
3000
2000
1000
0
-1000
0
5
10
t, s

(a)

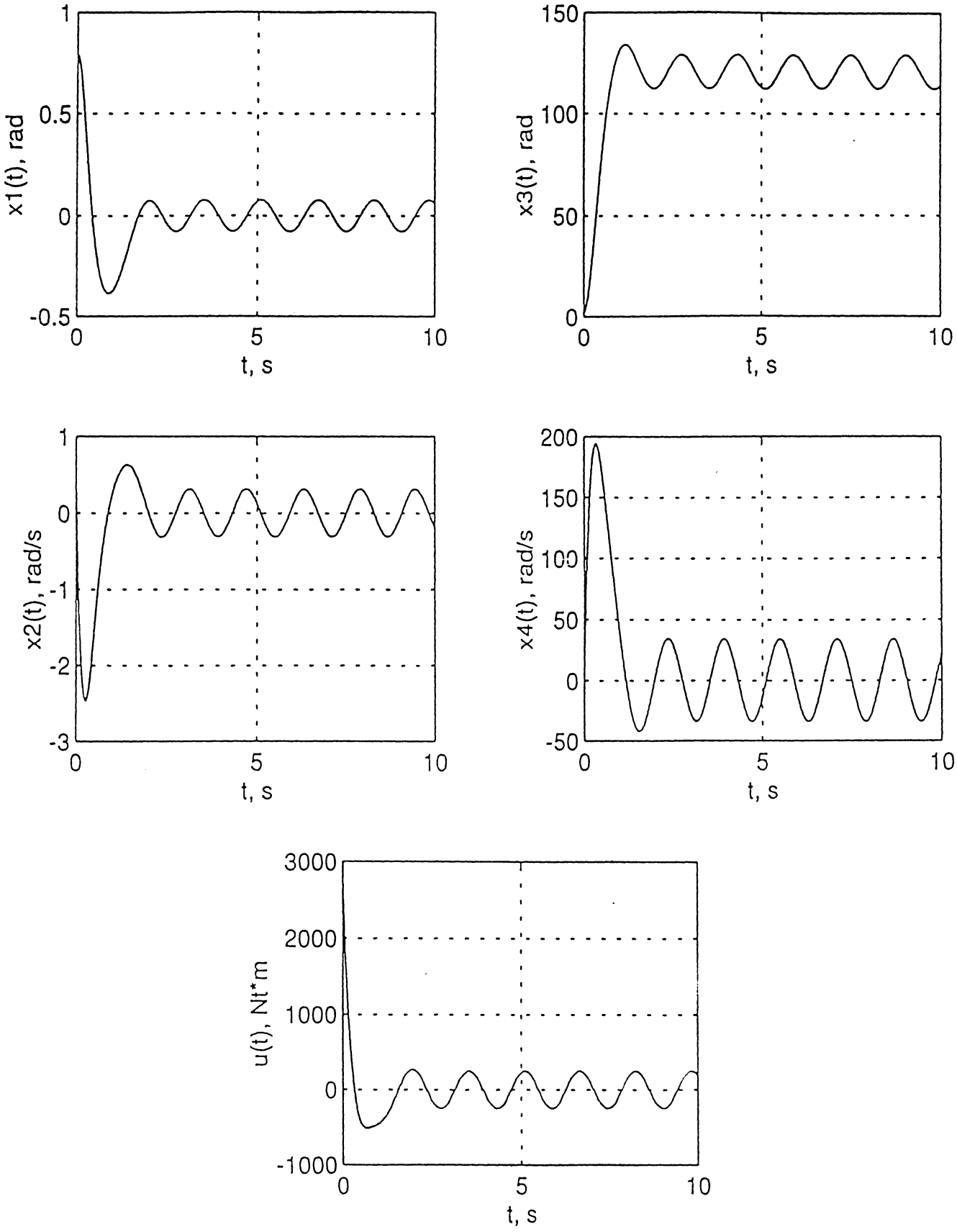

Fig. 2 Response with C2 controller: (a) without disturbance, (b) with disturbance.

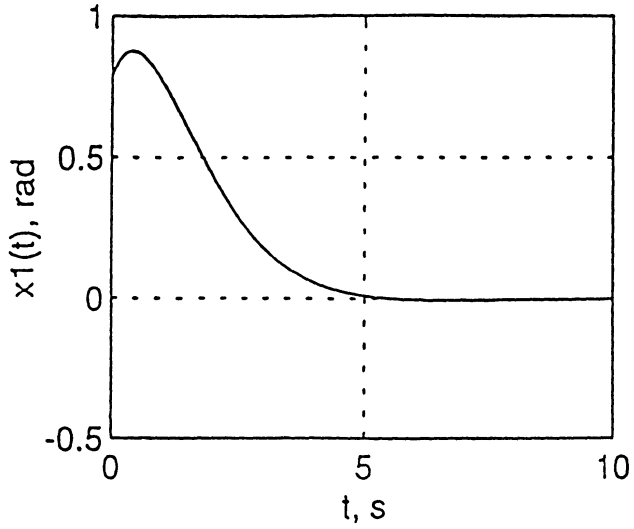
1
0.5
0
-0.5
x1(t), rad
0
5
10
t, s

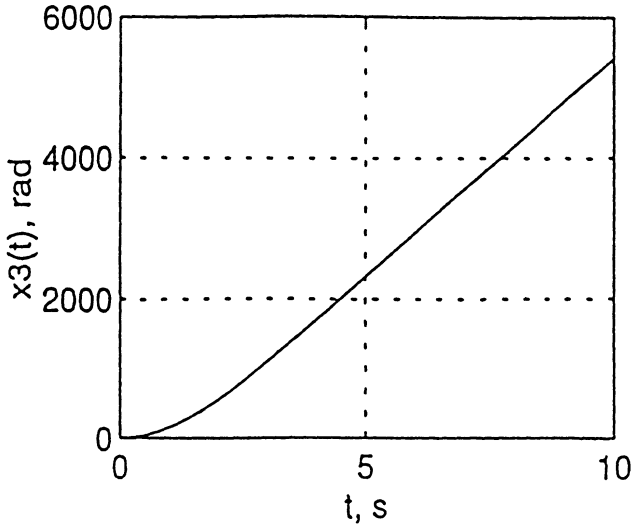
6000
4000
2000
0
x3(t), rad
0
5
10
t, s

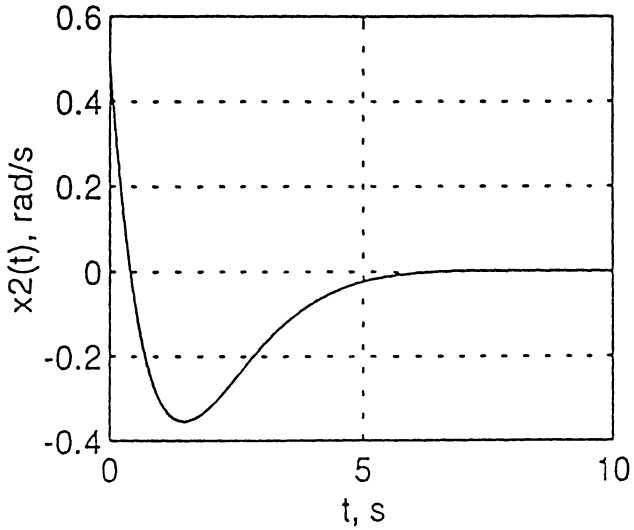
0.6
0.4
0.2
0
-0.2
-0.4
x2(t), rad/s
0
5
10
t, s

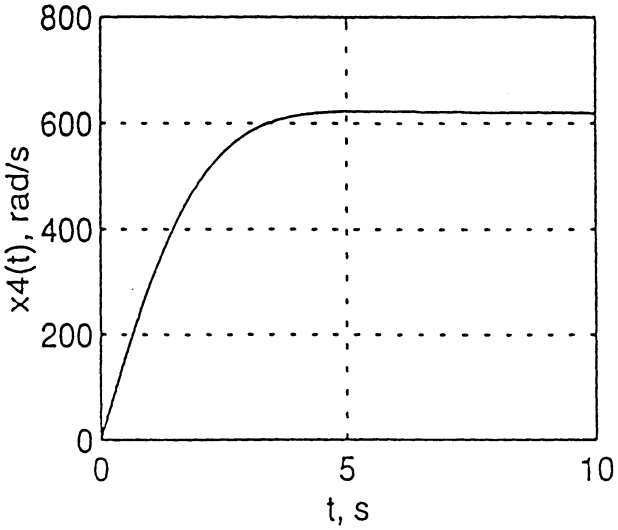
800
600
400
200
0
x4(t), rad/s
0
5
10
t, s

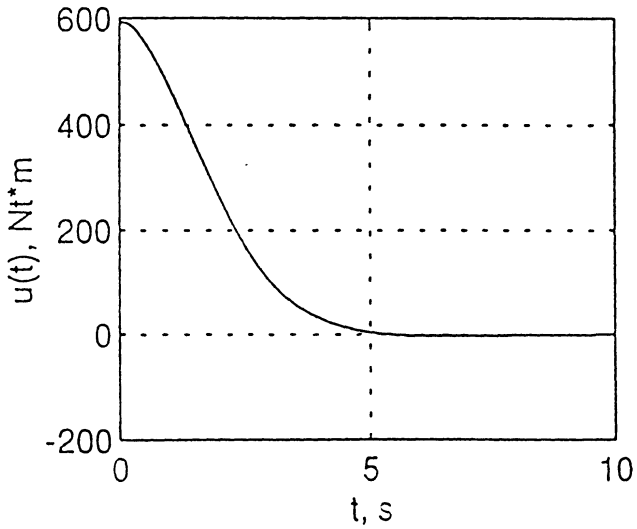
600
400
200
0
-200
u(t), Nt*m
0
5
10
t, s

(a)

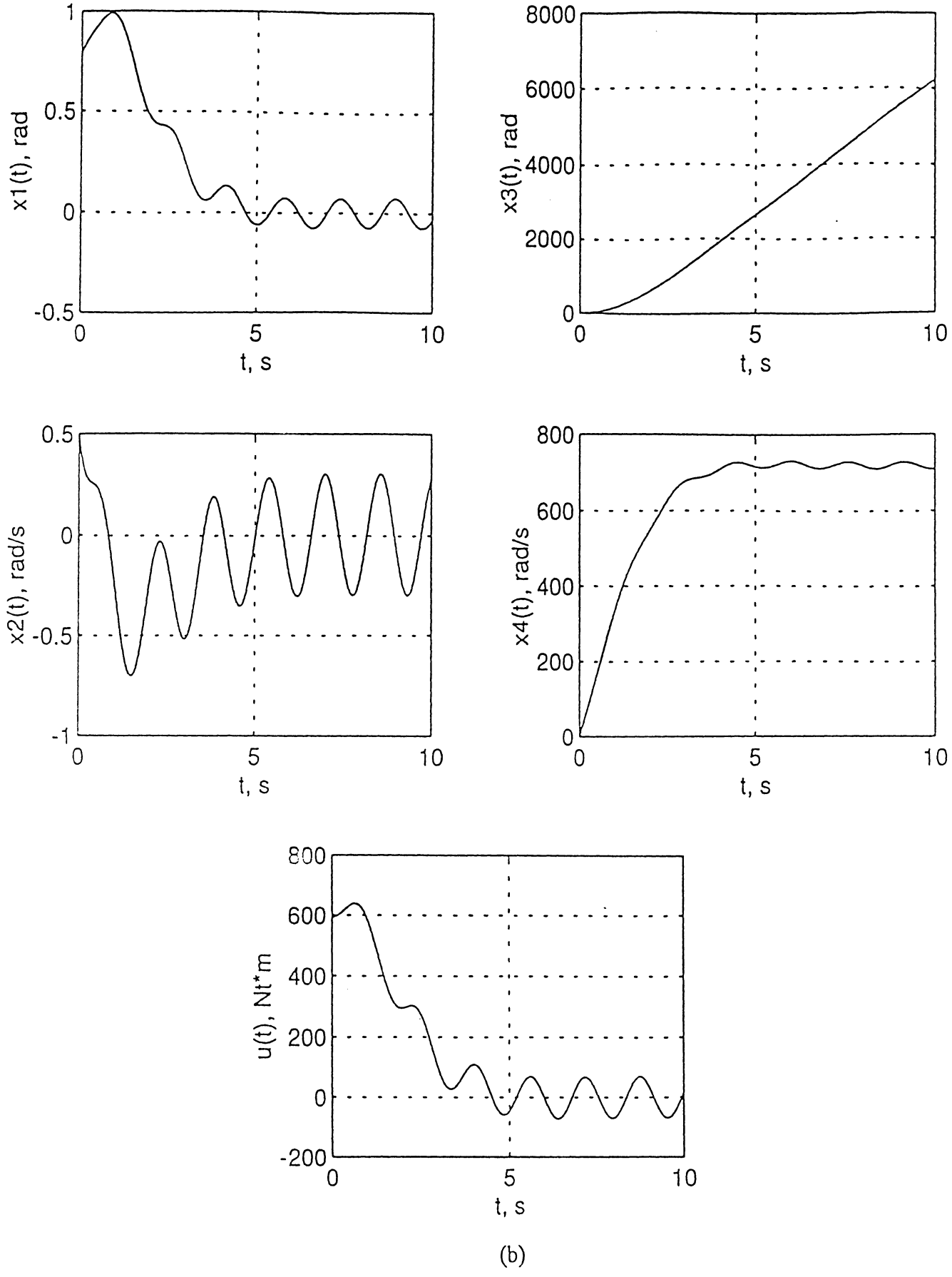

(b)

Fig. 3 Response with C4 controller: (a) without disturbance, (b) with disturbance.

6. Model Improvement

A more accurate model for the tightrope walker is shown in Fig 4, where a spring of spring constant k is added into the previous model to take into account the elasticity of the rope.

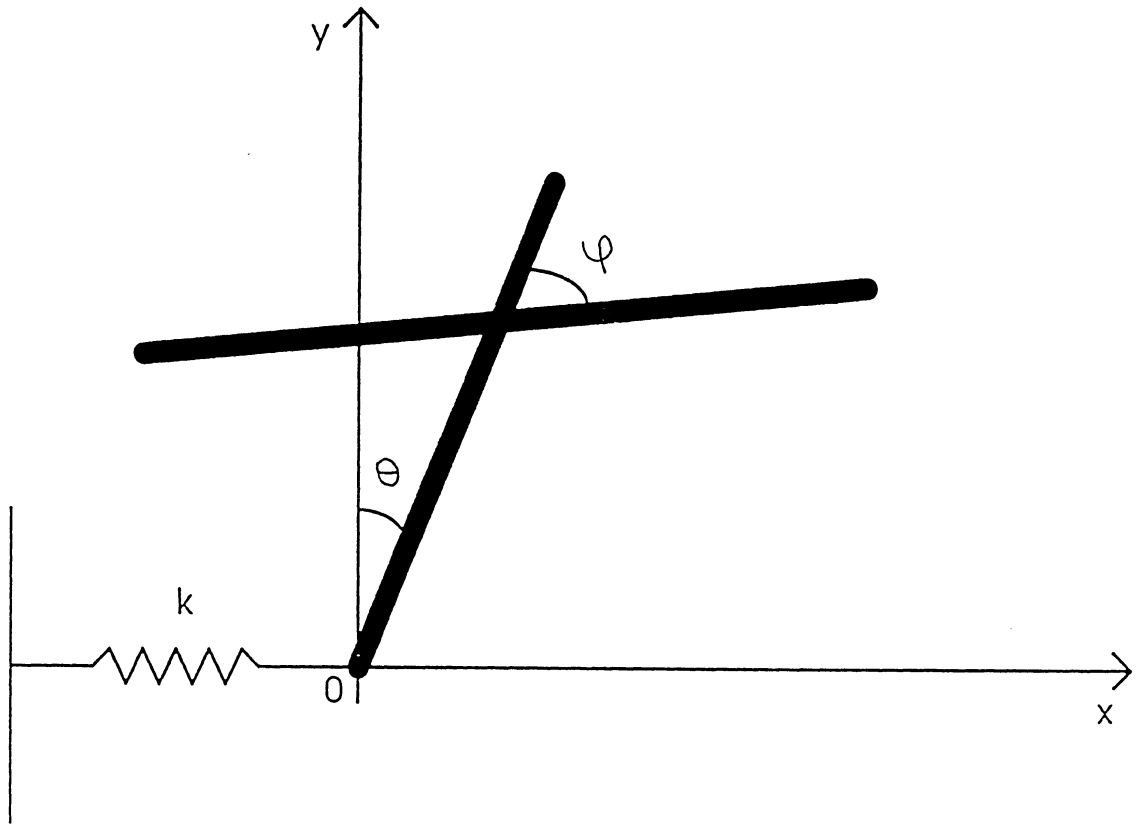

Fig. 4. The tightrope walker improved model.

Using Lagrangian method, the equations of motion are obtained as

$$\begin{aligned}
&(M+m)\ddot{X}+kX+E\ddot{\theta}\cos\theta-E\dot{\theta}^2\sin\theta=0\\
&(B+i)\ddot{\theta}+i\ddot{\varphi}+E\ddot{X}\cos\theta-N\sin\theta=0\\
&i\ddot{\varphi}+i\ddot{\theta}=\tau
\end{aligned} \tag{13}$$

where $B=ML/2+md$. With the normalization substitutions

$$X=\sqrt{\frac{ML^2/4+md^2+I}{M+m}}$$

$$e=\frac{D}{\sqrt{(M+m)B}}$$

$$w^2=\frac{k}{M+m}$$

$$\sigma=\frac{N}{Bw^2}$$

$$p=\frac{1}{Bw^2}$$

$$q=\frac{1}{\dot{t}w^2}$$

the equations in (13) can be written as

$$\begin{aligned}
&\ddot{x}+x+\varepsilon\ddot{\theta}\cos\theta-\varepsilon\dot{\theta}^2\sin\theta=0\\
&\ddot{\theta}+\varepsilon\ddot{x}\cos\theta-\sigma\sin\theta=-p\tau\\
&\ddot{\varphi}+\ddot{\theta}=q\tau
\end{aligned}\qquad(14)$$

Then, defining the states of the system as

$$\begin{aligned}
x_1&=x+\varepsilon\sin\theta\\
x_2&=\dot{x}+\varepsilon\dot{\theta}\cos\theta\\
x_3&=\theta\\
x_4&=\dot{\theta}\\
x_5&=\varphi\\
x_6&=\dot{\varphi}
\end{aligned}\qquad(15)$$

and applying the preliminary invertible feedback transformation

$$u=\frac{1}{1-\varepsilon^2\cos^2\theta}[\varepsilon x\cos\theta-\varepsilon^2\dot{\theta}^2\cos\theta\sin\theta-p\tau+\sigma\sin\theta]\qquad(16)$$

the state space model is obtained as

$$\begin{bmatrix} \dot{x}_1 \\ \dot{x}_2 \\ \dot{x}_3 \\ \dot{x}_4 \\ \dot{x}_5 \\ \dot{x}_6 \end{bmatrix} = \begin{bmatrix} x_2 \\ -x_1 + \varepsilon \sin x_3 \\ x_4 \\ u \\ x_6 \\ -[1+\gamma(1-\varepsilon^2 \cos^2 x_3)] + \gamma\varepsilon x_1 - \gamma\varepsilon^2 \sin x_3 \cos x_3 (1+x_4^2) + \gamma\sigma \sin x_3 \end{bmatrix} \tag{17}$$

where $\gamma = B/i$. Next, comparing (15) with the equations of the nonlinear benchmark problem we see that the subsystem involving x_1, x_2, x_3 and x_4 is exactly in the form of the nonlinear benchmark problem.

The nonlinear benchmark problem is extensively studied in literature [1]-[3] and several controllers are designed. Using the controller designed in [2] we can achieve global asymptotic stability in the benchmark problem block. Using a similar argument used above it can be shown that this controller will render the states of the system asymptotically to $[0 \quad 0 \quad 0 \quad 0 \quad \alpha t + \beta \quad \alpha]^T$, which is acceptable.

The control law designed in [2] is repeated below for convenience.

$$\begin{aligned} u = & -k_1(x_3 + \arctan(c_0 x_2)) - k_2 x_4 - \frac{k_2 c_0}{1 + c_0^2 x_2^2}(-x_1 + \varepsilon \sin x) \\ & + \frac{2c_0^3 x_2}{1 + c_0^2 x_2^2}(-x_1 + \varepsilon \sin x_3) - \frac{c_0}{1 + c_0^2 x_2^2}(-x_2 + \varepsilon x_4 \cos x_3) \end{aligned} \tag{C5) (18}$$

The simulation results are given in Fig. 5 for the controller parameters $c_0 = 2.3$, $k_1 = 0.56$, $k_2 = 1.2$ and the initial condition is set to $x_0 = [0.3 \quad 0.1 \quad \pi/4 \quad 0.5 \quad \pi/8 \quad 0]$. The disturbance is again a sinusoid of amplitude 100 Ntm at 4 Hz. The maximum torque, input power and settling time for this controller are given in Table 2.

	maximum torque	input power	settling time
C5	6487	14864325	10

Table 2. Some performance values for C5

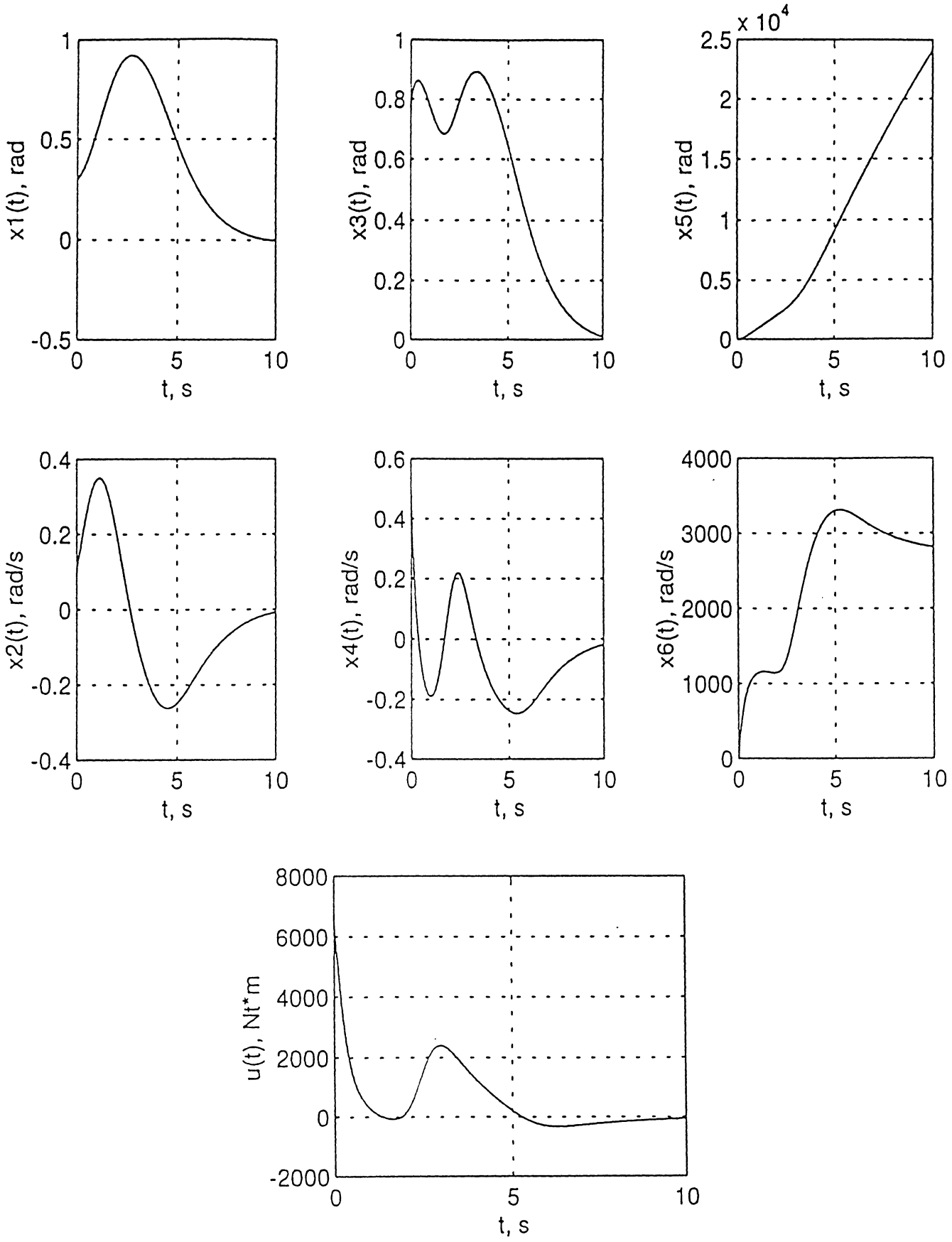
x1(t), rad
t, s
x3(t), rad
t, s
x 10^4
x5(t), rad
t, s
x2(t), rad/s
t, s
x4(t), rad/s
t, s
x6(t), rad/s
t, s
u(t), Nt*m
t, s

(a)

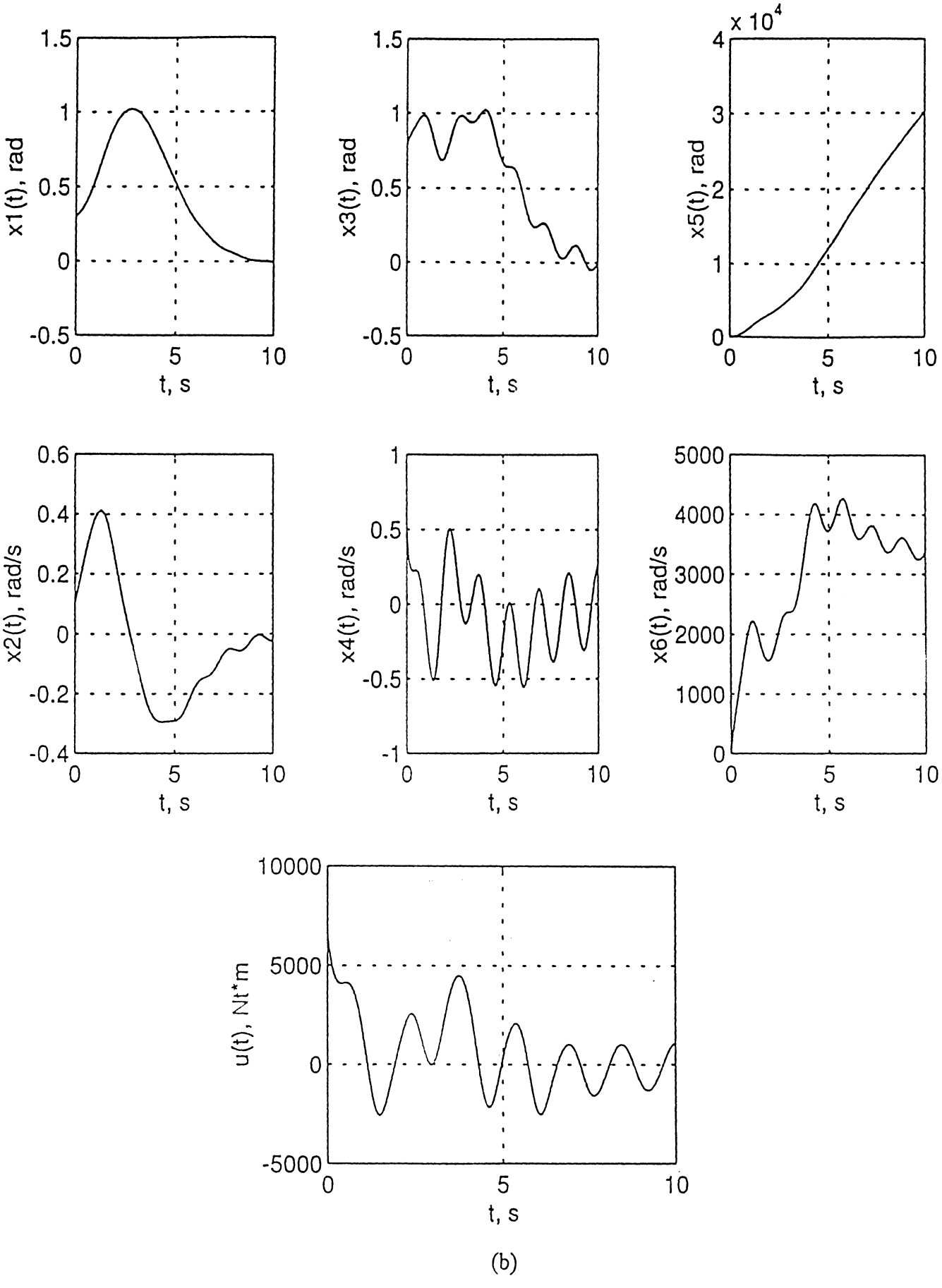

Fig. 5 Response with C5 controller: (a) without disturbance, (b) with disturbance.

7. Conclusions and Suggestions

In this project, two planar model for the tightrope walker is considered; the equations of motion are derived and analyzed. Some control goals are specified and several control laws are designed to stabilize the system about its natural equilibrium position. The performances of these controllers are evaluated by both animations and simulations. The effect of parameter uncertainty and disturbance are also considered. Furthermore, the relationship between the improved model and the nonlinear benchmark problem is established.

Based on above work, the following conclusions are inferred.

i. The performances of C1 and C2 are quite similar. The performances of C3 and C4 are quite similar.

ii. All controllers have reasonable settling times and control efforts. The settling times for C1 and C2 are smaller than those of C3 and C4 at he expense of increased control effort. The best one in terms of control effort is C3.

iii. C3 and C4 uses partial state feedback while C1 and C2 uses full state feedback.

iv. C1 and C2 guaranties semi-global asymptotic stability while C3 and C4 guaranties global asymptotic stability only in the subsystem involving x_1 and x_2. However, C3 and C4 always make x_3 and x_4 approach to $\alpha t + \beta$ and α, respectively.

v. The robustness of all controllers are excellent.

vi. The disturbance rejection of all controllers are very good.

vii. Unwinding problem can be eliminated.

Suggestions for future work:

i. Solve the following similar problem: Instead of balancing bar, the walker uses his arms for stabilization.

ii. Make a physical model for the system and compare this results with actual model.

iii. Make some generalizations for this kind of problems.

8. References

[1] R. T. Bupp, D. S. Bernstein, and V. T. Coppola, "Benchmark Problem for Nonlinear Control Design," Proc. American Control Conference, vol 6, pp. 4363-4367, 1995.

[2] M. Jankovic, D. Fontaine, and P.V. Kokotovic, "TORA Example: Cascade and Passivity Control Designs," Proc. American Control Conference, vol 6, pp. 4347-4351, 1995.

[3] I. Kanellakopoulos, and J. Zhao, "Tracking and Disturbance Rejection for the Benchmark Nonlinear Control Problem," Proc. American Control Conference, vol 6, pp. 4360-4362, 1995.

Linear-Fractional Representations and Linear Matrix Inequalities. Application to Duffing's equation.

ME 662-Final Project
Jérôme Guillen

Contents

1 Introduction

Our prime subject of interest is the study of blades assemblies in turbo-machineries. The blades are subject to hard conditions of work and the design goal is to reduce their wear.

It has been proven that the motion of the N blades can be deduced from the motion of one blade. Modal analysis enables to decouple the modes and limit the study of the blade response to the study of only one mode response. Finally, condensation techniques allow to reduce the model of a blade to a one degree of freedom system.

In order to prevent the blade from fluttering, when it vibrates dangerously with increasing amplitudes, some dry-friction dampers are placed in between the blades and/or between the blades and their rotor. Because of these dampers, the equation of motion of the single degree of freedom system is non analytical but piecewise continuous.

In order to study the forced response, we elaborated a multi incremental harmonic balance method (MIHB) with use of Toeplitz jacobian matrices and fast Fourier transforms (TJM/FFT), based on alternating time/frequency techniques (AFT). These methods are extremely efficient and powerful to predict forced responses but, so far, nothing has been published with respect to the free response, that is the stability problem of these systems. A few numerical integrations have been performed but the extremely low time step required in order to avoid bifurcations from critical points prevents the method from being technically efficient.

This project wanted to explore new ways of studying the stability of these systems. The systems we mentioned aboved are rational (each of the different ways they can be expressed in is rational), and the theories presented here were developped for rational systems only.

It was beyond the scope of that project to implement these techniques to our research systems. Instead, we applied them to the system that is traditionally used as their first non-linear approximation, the cubic spring, which is represented by the Duffing's equation.

In conclusion, this project introduces the Linear Matrices Inequalities (LMI) used to study the Linear Fractional Representations (LFR) of the rational systems. It presents some of the properties of these representations and, in particular, how to determine domains of attraction and how to design state-feedback controllers. Finally, we applied these techniques to the Duffing's equation.

2 Notation

For a real matrix P, $P > 0$ means that P is symmetric and positive-definite. $\mathcal{E}_P$ denotes the ellipsoid $\{x|\ x^T P x \leq 1\}$. For $\sigma > 0$, $\mathcal{B}_\sigma$ denotes the set $\{x|\ |x_i| \leq \sigma^{-1},\ i = 1, \cdots, n\}$. I_r is the identity matrix of $\mathrm{R}^{r \times r}$. e_k stands for the k-th column of I_n. For a given integer vector $r \in \mathrm{N}_+^n$, we associate the sets

$$\begin{aligned}
\mathcal{I}(r) &= \{i \in \{1, \cdots, n\}|\ \ r_i \neq 0\}, \\
\mathcal{D}(r) &= \{\Delta = \mathrm{diag}(\delta_1 I_{r_1}, \cdots, \delta_n I_{r_n})|\ \ \delta_i \in \mathrm{R}, i \in \mathcal{I}(r)\}, \\
\mathcal{B}(r) &= \{B = \mathrm{diag}(B_1, \cdots, B_n),|\ \ B_i \in \mathrm{R}^{r_i \times r_i}, i \in \mathcal{I}(r)\}, \\
\mathcal{S}(r) &= \{S \in \mathcal{B}(r),|\ \ S = S^T, S > 0\}, \\
\mathcal{G}(r) &= \{G \in \mathcal{B}(r),|\ \ G = G^T\}.
\end{aligned}$$

3 Numerical Techniques

We consider a nonlinear, time-invariant, continuous-time system

$$\begin{aligned}
\dot{x} &= \mathrm{A}(x) + \mathrm{B}_u(x)u \\
y &= \mathrm{C}_y(x) + \mathrm{D}_{yu}(x)u,
\end{aligned} \tag{1}$$

where $x \in \mathrm{R}^n$ is the state vector, $u \in \mathrm{R}^{n_u}$ is the input, and $y \in \mathrm{R}^{n_y}$ is the output. We furthermore assume that:

- A, B_u, C_y and D_{yu} are multi variable rational functions of x.
- $\mathrm{A}(0) = 0$, 0 is an equilibrium point of the unforced system.
- $\mathrm{C}_y(0) = 0$ and $\mathrm{B}_u, \mathrm{D}_{yu}$ have no singularities at the origin.

The systems satisfying (1) and verifying the three previous assumptions are called *rational systems.*

This project shows how to compute quadratic Lyapunov functions for the analysis of system (1): stability region estimates, decay rate bounds, L_2 gain bounds, etc. The results of this analysis are extended to the synthesis of static, state-feedback control laws. The results can also be applied to a restricted class of rational systems, those for which only the non-linear part is measured in order to design output-feedback controllers. The linear-fractional representation (LFR) that can be established for system (1) is suitable for the use of Linear Matrix Inequalities (LMI) techniques.

3.1 Linear Matrices Inequalities

Each of the previously mentioned problems is a convex optimization problem over Linear Matrix Inequalities (LMIs). A LMI is a matrix inequality of the form

$$F(\xi) = F_0 + \sum_{i=1}^{m} \xi_i F_i > 0, \tag{2}$$

where $\xi \in \mathrm{R}^m$ is the variable, and $F_i = F_i^T \in \mathrm{R}^{n\times n}$, $i = 0, \cdots, m$ are given. A typical problem is the feasibility problem: "find ξ such that $F(\xi) > 0$". Another optimization one is the generalized eigenvalue minimization problem

$$\begin{array}{ll} \text{minimize} & \lambda \\ \text{subject to} & \lambda B(\xi) - A(\xi) > 0, \\ & B(\xi) > 0, \quad C(\xi) > 0 \end{array} \tag{3}$$

where A, B and C are symmetric matrices that are affine functions of ξ. The LMIs being convex, these problems can be solved very efficiently.

3.2 Methods and software

LMI problems such as (2) and (3) are solved using dual problems. The duality results are weaker for semidefinite programs than for linear programming, and there is no straightforward or practical simplex method for semidefinite programs. If we write our problem as

$$\begin{array}{ll} \text{minimize} & C^T x \\ \text{subject to} & F(x) \geq 0 \end{array} \tag{4}$$

where F has the same expression as in (2) and the problem data are the vector $c \in \mathrm{R}^m$ and $m + 1$ symmetric matrices $F_0, \cdots, F_m \in \mathrm{R}^{n\times n}$. The dual problem associated with (4) is

$$\begin{array}{ll} \text{maximize} & -\mathrm{Tr} F_0 Z \\ \text{subject to} & \mathrm{Tr} F_i Z = c_i, \quad i = 1, \cdots, m \\ & Z \geq 0. \end{array} \tag{5}$$

The variable is here the matrix $Z = Z^T \in \mathrm{R}^{n\times n}$ which is subject to m equality constraints and the matrix non negativity condition.

It is not within the scope of this project to look at the algorithms used to solve these problems. A comprehensive paper by Vandenberghe details the whole procedure [2].

The software to solve these problems is available by anonymous ftp at *ftp.ensta.fr* in */pub/elghaoui/lmitool* for *LMITOOL* and at *isl.stanford.edu* in */pub/boyd/semidef_prog* for the *SP* package. *SP* solves problems of the form of (2) and (3). *LMITOOL* is a user-friendly package that makes the interface with *SP* for LMI optimization problems. More information can be obtained by ftp at those sites.

4 Representation of Rational Systems

4.1 Existence of a LFR

In order to establish the Linear-Fractional Representation (LFR) of system (1), let us first consider such a representation for a rational matrix.

For any rational matrix function $\mathrm{M} : \mathrm{R}^n \to \mathrm{R}^{p\times q}$, *with no singularities at the origin, there exists nonnegative integers* $r_1, \cdots, r_n$, *and matrices* $A \in \mathrm{R}^{p\times q}, B \in \mathrm{R}^{p\times N}, C \in \mathrm{R}^{N\times q}, D \in \mathrm{R}^{N\times n}$, *with* $N = r_1 + \cdots r_n$, *such that* M *has the following Linear-Fractional Representation (LFR): For all* x *where* M *is defined,*

$$\mathrm{M}(x) = A + B\Delta(x)(I - D\Delta(x))^{-1}C, \tag{6}$$

where

$$\Delta(x) = \mathrm{diag}(x_1 I_{r1}, \cdots, x_n I_{rn}). \tag{7}$$

If M does not depend on, say, the variable x_1, *the LFR can be constructed such that* $r_1 = 0$.

The algorithm to construct a LFR turns out to be relatively easy in the special case when the rational matrix can be written as $\mathrm{M}(x) = \mathrm{N}(x)/d(x)$, where N is a polynomial matrix function and $d(x)$ is a scalar polynomial, such that $d(0) \neq 0$.

It is important to notice that, when $n = 1$ (that is, for a *mono variable* rational matrix function), the matrices A, B, C, D are simply a state-space realization of the transfer matrix $A + B(sI - D)^{-1}C$, where $s = 1/x$. Thus, the LFR generalizes the state-space representation known for (mono variable) transfer matrices, to the multi variable case. The previous theorem can be extended to any rational vector field.

Any rational vector field $f : \mathrm{R}^n \to \mathrm{R}^n$ *such that* $f(0) = 0$ *can be written as follows: For every* x *such that* $f(x)$ *is well-defined,*

$$f(x) = (A + B\Delta(x)(I - D\Delta(x))^{-1}C)x$$

with $\Delta(x) = \mathrm{diag}(x_1 I_{r_1}, \cdots, x_n I_{r_n})$, *for appropriate nonnegative integers* $r_1, \cdots, r_n$, *and appropriate matrices* A, B, C, D. *If* f *is linear in, say, the variable* x_1, *we can choose* $r_1 = 0$.

Using that last property and assuming that we are dealing with a system (1) satisfying the assumptions of section (3), we can write, for every x such that $\mathrm{A}(x), \mathrm{B}_u(x), \mathrm{C}_y(x), \mathrm{D}_{yu}(x)$ are well-defined,

$$\begin{bmatrix} \mathrm{A}(x) & \mathrm{B}_u(x) \\ \mathrm{C}_y(x) & \mathrm{D}_{yu}(x) \end{bmatrix} = \begin{bmatrix} A & B_u \\ C_y & D_{yu} \end{bmatrix} + \begin{bmatrix} B_p \\ D_{yp} \end{bmatrix} \Delta(x)(I - D_{qp}\Delta(x))^{-1} \begin{bmatrix} C_q & D_{qu} \end{bmatrix}$$

for appropriate integers $r_1, \cdots, r_n$ and matrices $A, B_u, B_p, C_q, D_{qu}, D_{qp}, C_y, D_{yu}$ and D_{yp}. System (1) thus admits the following LFR

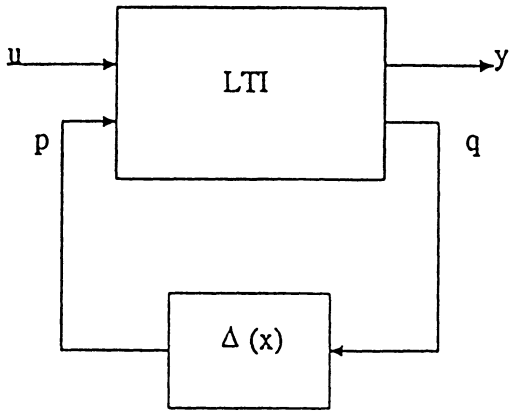

Figure 1: Linear-Fractional Representation of the rational system (1).

$$\begin{aligned} \dot{x} &= Ax + B_u u + B_p p, \\ q &= C_q x + D_{qu} u + D_{qp} p, \\ y &= C_y x + D_{yu} u + D_{yp} p, \\ p &= \Delta(x) q, \\ \Delta(x) &= \mathrm{Diag}(x_1 I_{r_1}, \cdots, x_n I_{r_n}). \end{aligned} \tag{8}$$

The LFR can be interpreted as follows: the rational system can be viewed as an LTI system, with a feedback connection between some fictitious inputs p and fictitious outputs q (Fig. 4.1). The feedback matrix Δ is linear in the state x, and its structure (the integers $r_1, \cdots, r_n$) reflects the "degree of nonlinearity".

We furthermore assume that there is no direct feedthrough term from u to y ($D_{yu} = 0$) and that the matrix C_y in (1) is a constant matrix ($D_{yp} = 0$).

4.2 Construction of a LFR

The construction is an iterative process. The following rules show how to construct such a representation in the case where $\mathrm{M}(x) = \mathrm{N}(x)/d(x)$, where N is a polynomial matrix function, $d(x)$ is a scalar polynomial, such that $d(0) = 0$.

First, we construct a LFR for polynomial matrices. The function of the scalar variable x, $\mathrm{M}(x) = x$ has the following LFR: $A = B = C = 1$, $D = 0$. To construct an LFR for an arbitrary polynomial matrix function of several variables, all we need to know is how to get the LFR (A, B, C, D, r) from a "combination" of two LFR's $(A_1, B_1, C_1, D_1, r_1)$ and $(A_2, B_2, C_2, D_2, r_2)$. Let us denote $\tilde{\Delta}(x) = \mathrm{diag}(\Delta_1(x), \Delta_2(x))$, and

$$\mathrm{M}_i(x) = A_i + B_i \Delta_i(x)(I - D_i \Delta_i(x))^{-1} C_i, \quad i = 1, 2,$$

The following rules apply:

Addition The sum of $\mathrm{M}_1(x)$ and $\mathrm{M}_2(x)$ equals

$$\begin{aligned} \mathrm{M}(x) &= \mathrm{M}_1(x) + \mathrm{M}_2(x) \\ &= A + B\tilde{\Delta}(x)(I - D\tilde{\Delta}(x))^{-1}C, \end{aligned} \tag{9}$$

with

$$A = A_1 + A_2, \quad B = \begin{bmatrix} B_1 & B_2 \end{bmatrix}, \tag{10}$$

$$C = \begin{bmatrix} C_1 \\ C_2 \end{bmatrix}, \quad D = \mathrm{diag}(D_1, D_2). \tag{11}$$

Multiplication The product of $\mathrm{M}_1(x)$ and $\mathrm{M}_2(x)$ is given by:

$$\begin{aligned} \mathrm{M}(x) &= \mathrm{M}_1(x)\mathrm{M}_2(x) \\ &= A + B\tilde{\Delta}(x)(I - D\tilde{\Delta}(x))^{-1}C, \end{aligned}$$

where

$$A = A_1A_2, \quad B = \begin{bmatrix} B_1 & A_1B_2 \end{bmatrix} \tag{12}$$

$$C = \begin{bmatrix} C_1A_2 \\ C_2 \end{bmatrix}, \quad D = \begin{bmatrix} D_1 & C_1B_2 \\ 0 & D_2 \end{bmatrix}. \tag{13}$$

Stacking The combination of $\mathrm{M}_1(x)$ and $\mathrm{M}_2(x)$ is

$$\begin{aligned} \mathrm{M}(x) &= \begin{bmatrix} \mathrm{M}_1(x) & \mathrm{M}_2(x) \end{bmatrix} \\ &= A + B\tilde{\Delta}(x)(I - D\tilde{\Delta}(x))^{-1}C, \end{aligned}$$

with

$$A = \begin{bmatrix} A_1 & A_2 \end{bmatrix}, \quad B = \begin{bmatrix} B_1 & B_2 \end{bmatrix} \tag{14}$$

$$C = \mathrm{diag}(C_1, C_2), \quad D + \mathrm{diag}(D_1, D_2). \tag{15}$$

More rules apply (in order to compute the LFR of a shuffled matrix, or the LFR of the inverse of a matrix for example) but we will not need them here.

4.3 LFR of the equation of Duffing

We write the equation of Duffing under the form:

$$\ddot{y} - k\dot{y} + \omega^2(y + \epsilon y^3) = u. \tag{16}$$

We choose as a state vector $x = \begin{bmatrix} y & \dot{y} \end{bmatrix}^T$. This system has an LFR, determined according to the previous rules:

$$\begin{gathered} A = \begin{bmatrix} 0 & 1 \\ -\omega^2 & -k \end{bmatrix}, \quad B_u = \begin{bmatrix} 0 \\ 1 \end{bmatrix}, \quad C_y = \begin{bmatrix} 1 & 0 \end{bmatrix}, \\ B_p = \begin{bmatrix} 0 & 0 \\ -\omega^2\epsilon & 0 \end{bmatrix}, \quad C_q = \begin{bmatrix} 0 & 0 \\ 1 & 0 \end{bmatrix}, \quad D_{qp} = \begin{bmatrix} 0 & 1 \\ 0 & 0 \end{bmatrix}, \end{gathered} \tag{17}$$

For a given scalar $\sigma > 0$, we associate to the system a "Linear Differential Inclusion" (LDI).

$$\begin{aligned} \dot{x} &= Ax + B_u u + B_p p, \\ q &= C_q x + D_{qu} + D_{qp} p \\ y &= C_y x \\ p &= \Delta(t) q, \ \|\Delta(t)\| \leq \sigma^{-1}, \ \Delta(t) \in \mathcal{D}(r), \ t > 0. \end{aligned} \tag{18}$$

5 Analysis of Rational Systems

In this section, we look at the properties of systems as (1), using their LFR.

5.1 Well-posedness

Let $\mathcal{R}$ be a region containing 0. The LFR (8) is *well-posed* in the region $\mathcal{R}$ if for every $x \in \mathcal{R}$, $\det(I - D_{qp}\Delta(x)) \neq 0$. If the LFR (8) is well-posed over $\mathcal{R}$, then it is an accurate representation of (1) over $\mathcal{R}$.

We seek a condition which ensures that over a given ball $\mathcal{B}_\sigma$, the LFR is well-posed. A conservative condition is that over the unit-ball $\mathcal{B}$, $||D_{qp}|| < 1$. this does not take into account the structure (diagonal, with repeated elements) of the matrix function $\Delta(x)$.

If the structure of $\Delta(x)$ is taken into account, a less conservative condition for the system to be well-posed in the ball $\mathcal{B}_\sigma$ is that the LMI

$$D_{qp}^T S D_{qp} + D_{qp}^T G - G D_{qp} - \sigma^2 S < 0 \tag{19}$$

holds for some $S \in \mathcal{D}(r)$ and $G \in \mathcal{G}(r)$. This sufficient condition for well-posedness can be checked by solving an LMI problem. Moreover, finding the smallest $\sigma > 0$ such that the system is well-posed over $\mathcal{B}_\sigma$ is also an LMI problem (use as an objective function a decreasing function of σ).

5.2 Stability

We consider the input-free version of the system of (1). That is $\dot{x} = \mathrm{A}(x), y = \mathrm{C}_y(x)$. For this system, we construct a LFR

$$\begin{aligned} \dot{x} &= Ax + B_p p, \\ q &= C_q x + D_{qp} p, \\ y &= C_y x \\ p &= \Delta(x) q, \\ \Delta(x) &= \mathrm{Diag}(x_1 I_{r_1}, \cdots, x_n I_{r_n}). \end{aligned} \tag{20}$$

In (20), the matrix A can be viewed as the "linearized model" around the equilibrium point 0. Local stability can thus be inferred from the stability of the constant matrix A. Here, we look at a more "global" stability analysis of the system: we look for a region $\mathcal{R}$ which is a domain of attraction, that is,

$$x(0) \in \mathcal{R} \Rightarrow \lim_{t \to \infty} x(t) = 0.$$

Since system (20) is time-invariant, any domain of attraction $\mathcal{R}$ is also *invariant*, that is,

$$x(0) \in \mathcal{R} \Rightarrow t \geq 0, x(t) \in \mathcal{R}.$$

$\mathcal{R}$ is called a *stable* region.

We look for a condition ensuring that the LDI associated to (20) for a given scalar $\sigma > 0$ is quadratically stable. That is, we want to prove the existence of a quadratic, positive-definite function V which decreases along every trajectory of (18) with zero input.

For a given $\sigma > 0$, the LDI system (18) is quadratically stable if there exist $P = P^T \in \mathrm{R}^{n\times n}, S \in \mathcal{S}(r)$ and $G \in \mathcal{G}(r)$ such that the LMI in variables P, S, G

$$\begin{gathered} P > 0, \\ \left[\begin{array}{cc} A^TP + PA + C_q^TSC_q & PB_p + C_q^TG + C_q^TSD_{qp} \\ (PB_p + C_q^TG + C_q^TSD_{qp})' & D_{qp}^TSD_{qp} - \sigma^2 S + D_{qp}^TG - GD_{qp} \end{array}\right] < 0, \end{gathered} \tag{21}$$

holds. Then, for every $\Delta \in \mathcal{B}(r)$, such that $||\Delta|| \leq \sigma^{-1}$, we have

$$\det(I - D_{qp}\Delta) \neq 0$$

and

$$(A + B_p\Delta(I - D_{qp}\Delta)^{-1}C_q)^TP + P(A + B_p\Delta(I - D_{qp}\Delta)^{-1}C_q) < 0.$$

That is, the ellipsoid $\mathcal{E}_P$ is an invariant domain of attraction for (18).

Performing this analysis for different values of σ, we can find the domain of attraction of (18). In order to find the domain of attraction of largest volume, we have to use $\log\det P^{-1}$ as objective function (in the previous analysis, the absence of objective function converted the problem into an existence problem).

To obtain lower bounds on the decay rate of the trajectories over an ellipsoidal domain of attraction, we have to solve the following problem:

If there exist matrices $P = P^T \in \mathrm{R}^{n\times n}, S \in \mathcal{S}(r), G \in \mathcal{G}(r)$ and scalars $\alpha > 0, \sigma > 0$ such that

$$\begin{gathered} P > 0, \quad \left[\begin{array}{cc} \sigma^{-2} & e_k^T \\ e_k & P \end{array}\right] > 0, \quad k \in \mathcal{I}(r), \\ \left[\begin{array}{cc} 2\alpha P + A^TP + PA + C_q^TSC_q & PB_p + C_q^TG + C_qSD_{qp} \\ (PB_p + C_q^TG + C_qSD_{qp})^T & D_{qp}^TSD_{qp} - \sigma^2 S + D_{qp}G - GD_{qp} \end{array}\right] < 0 \end{gathered} \tag{22}$$

Then, system (1) is well-posed over the ellipsoid $\mathcal{E}_P$, and for every trajectory initiating in $\mathcal{E}_P$, we have

$$\lim_{t\to\infty} e^{\alpha t}||x(t)|| = 0$$

In order to check the stability of a polytope P defined by its vertices $v_1, \cdots, v_p$, that is in order to ensure that every trajectory initiating in P converges to 0, we just have to add the condition the P is contained in a sufficient large ellipsoid $\mathcal{E}_P$ satisfying the conditions of (22). This condition can be written as:

$$v_j^TPv_j \leq 1, \quad j = 1, \cdots, p$$

We can also impose an upper bound on output peak, which is defined as $\max_{t\geq 0} ||y(t)||$. To do so, we only have to add the extra condition

$$\begin{bmatrix} y_{max}^2 I & C_y \\ C_y^T & P \end{bmatrix} \geq 0$$

where y_{max} is the desired upper bound on the output peak for every trajectory initiating in $\mathcal{E}_P$.

Finally, we can impose conditions on the gain of the system. We consider the rational system (8) with a non-zero input, and zero initial condition. We assume moreover that the system is locally stable. The L_2 gain of the system is said to be less or equal to γ if, for every $T \geq 0$, and for every piecewise continuous input $u \in L_2(0,T)$ such that

$$\int_0^T u(t)^T u(t) dt \leq 1,$$

the corresponding output y exists and satisfies

$$\int_0^T y(t)^T y(t) dt \leq \gamma^2.$$

To implement that condition, we write the following LMI.

If there exist matrices $P = P^T \in \mathrm{R}^{n\times n}, S \in \mathcal{S}(r), G \in \mathcal{G}(r)$ and a scalar $\sigma > 0$ such that

$$\begin{bmatrix} \gamma^{-2}\sigma^{-2} & e_k^T \\ e_k & P \end{bmatrix} > 0, \quad k \in \mathcal{I}(r),$$

$$\begin{bmatrix} A^T P + PA + C_q^T S C_q + C_y^T C_y & PB_p + C_q^T S D_{qp} + C_q^T G & PB_u \\ (PB_p + C_q^T S D_{qp} + C_q^T G)^T & \begin{pmatrix} D_{qp}^T S D_{qp} - \sigma^2 S \\ + D_{qp}^T G - G D_{qp} \end{pmatrix} & 0 \\ B_u^T P & 0 & -\gamma^2 I \end{bmatrix} < 0, \tag{23}$$

then, we have:

1. *System (1) is well-posed over $\mathcal{B}_\sigma$ (and thus on the ellipsoid $\gamma\mathcal{E}_P$).*
2. *Every trajectory of system (1) with zero initial condition, and input $u \in L_2$ such that $||u||_2 \leq 1$, is entirely contained in $\gamma\mathcal{E}_P$.*
3. *For every trajectory, and $T \geq 0$,*

$$\int_0^T y(t)^T y(t) dt \leq \gamma^2.$$

That is the L_2 gain of the system is less than γ.

6 Controller Synthesis

6.1 State-feedback controller synthesis

In this section, we look for a control law of the form $u = Kx$, with K a constant matrix, which achieves stability properties for the closed-loop system. The latter has the LFR

$$\begin{array}{rcl} \dot{x} & = & (A + B_u K)x + B_p P, \\ q & = & (C_q + D_{qu} K)x + D_{qp} P, \\ p & = & \Delta(x) q, \\ \Delta(x) & = & \mathrm{diag}(x_1 I_{r_1}, \cdots, x_n I_{r_n}). \end{array} \tag{24}$$

We have the stability theorem: *If there exist matrices* $Q = Q^T \in \mathrm{R}^{n \times n}, Y \in \mathrm{R}^{n_u \times n}, T \in \mathcal{S}(r), H \in \mathcal{G}(r)$ *and a scalar* $\sigma > 0$ *such that*

$$\begin{array}{c} Q > 0, \quad e_k^T Q e_k < \sigma^{-2}, \quad k \in \mathcal{I}(r), \\ \left[\begin{array}{cc} \left(\begin{array}{c} AQ + QA^T + B_p T B_p^T \\ + B_u Y + Y^T B_u^T \end{array} \right) & \left(\begin{array}{c} QC_q^T + Y^T D_{qu}^T \\ + B_p T D_{qp}^T + B_p H \end{array} \right) \\ \left(\begin{array}{c} C_q Q + D_{qu} Y \\ + D_{qp} T B_p^T - H B_p^T \end{array} \right) & D_{qp} T D_{qp}^T - \sigma^2 T + D_{qp} H - H D_{qp}^T \end{array} \right] < 0, \end{array} \tag{25}$$

then, the static, state-feedback law $u = YQ^{-1}x$ *is such that:*

1. *The closed-loop system (24) is well-posed over* $\mathcal{B}_\sigma$ *and thus, over the ellipsoid* $\mathcal{E}_P$.
2. *The ellipsoid* $\mathcal{E}_{Q^{-1}}$ *is an invariant domain of attraction for the closed-loop system (24).*
3. *The function* $V(x) = x^T Q^{-1} x$ *is a Lyapunov function that proves it.*

As for the study of the stability of the open-loop system (1), we may impose additional conditions on the previous system in order to meet some requirements. For example, we may desire to compute K that maximizes the volume of an ellipsoidal domain of attraction for the closed-loop system (in that case, the objective function should be $trace(Q)$). We may also want to impose a given decay rate α on the trajectories of the closed-loop system initiating in the ellipsoid $\mathcal{E}_{Q^{-1}}$ (change A by $A + \alpha I$ in (25)). As we did for the open-loop system (1), we may be interested by the stability of a given polytope (*ie* its inclusion inside a domain of attraction). If the vertices of the polytope $\mathcal{P}$ are denoted $(v_1, \cdots, v_n)$, the extra condition would be

$$\left[\begin{array}{cc} 1 & v_j^T \\ v_j & Q \end{array} \right] \geq 0, \quad j = 1, \cdots, p.$$

To impose saturation constraints on the command input, the additional condition to add to (25) is

$$\left[\begin{array}{cc} u_{max}^2 I & Y \\ Y^T & Q \end{array} \right] \geq 0$$

and then, with the control law $u = YQ^{-1}x$, any trajectory of the closed-loop system initiating in $\mathcal{E}_{Q^{-1}}$ will converge to zero, while the corresponding command input satisfies: $\forall t,\ ||u(t)||_2 \leq u_{max}$. If one wants to impose an upper bound y_{max} on the output peak, the following LMI has to be added

$$C_y Q C_y^T \leq y_{max}^2 I.$$

6.2 Dynamic Output-feedback Controller Synthesis

The method allows us to construct dynamic output feedback controller for some special systems. The condition is that the system should be linear in the non-measured states. The conditions on the controller design are much more complex and there was no time to apply them to the Duffing equation (that verifies by the way all the necessary conditions).

7 Application to the Duffing's equation

Notice: all the Maple and Matlab files are available on request.

We consider the following Duffing's equation [1, 7, 6]

$$\ddot{y} + k\dot{y} + \omega^2(y + \epsilon y^3) = u \tag{26}$$

In the first part of this section, we look at the stability of this equation. In the second part, we focus on the control (state-feedback controller synthesis). Unlike what is usually done, we do not consider harmonic forcing: as exposed in the introduction, we are mostly interested in the stability point of view. The forced motion is studied by *multi-harmonic balance method.* This method cannot, to our knowledge, predict the domain of stability of such an oscillator. That is why the LMI study that can be made of (26) is of uttermost importance.

7.1 Well-posedness

The Duffing equation admits the following LFR

$$\begin{gathered} A = \begin{bmatrix} 0 & 1 \\ -\omega^2 & -k \end{bmatrix}, \quad B_u = \begin{bmatrix} 0 \\ 1 \end{bmatrix}, \quad C_y = \begin{bmatrix} 1 & 0 \end{bmatrix}, \\ B_p = \begin{bmatrix} 0 & 0 \\ -\omega^2\epsilon & 0 \end{bmatrix}, \quad C_q = \begin{bmatrix} 0 & 0 \\ 1 & 0 \end{bmatrix}, \quad D_{qp} = \begin{bmatrix} 0 & 1 \\ 0 & 0 \end{bmatrix}, \end{gathered} \tag{27}$$

The matrix D_{qp} is strictly upper triangular. Hence, according to (19), the system is well-posed. Therefore, every trajectory of (26) is a trajectory for the LFR (27).

7.2 Stability

For this particular analysis, we chose $k = 1, \epsilon = 1, \omega = 1$. We minimize $\log\det P^{-1}$ subject to (21) for various values of σ. This has the effect of finding the ellipsoid satisfying these conditions with the largest sum of squared semi-axis lengths. The best estimate was found for $\sigma = 0.582$ and the corresponding ellipsoid is shown in (Fig.2). It is important to stress that the LMI problem of finding some matrices verifying (21) is associated with a line search over σ in order to find the domain of attraction with the largest volume.

It is worth stressing that this stability concept means that this ellipsoid $\mathcal{E}_P$ is an invariant domain of attraction for (26), that (27) is well-posed over $\mathcal{B}_\sigma$ and that $V(x) = x^T P x$ is a Lyapunov function that proves it.

The region is not the largest one that can be found with, say, backtracking but it is of the same order of magnitude [3] and the computation time to find it is extremely low (a few seconds). Hence, we can find easily a rather goods estimate.

We also performed the same study for different values of the parameters and we find a domain of the same kind but where the trajectories need a much larger time to reach the equilibrium point (Fig.3). The optimal value of σ for that case is $\sigma = 0.219$.

We also performed a L_2 gain stability analysis. In that case, we are looking for an optimal function over an R^2 space because we have two parameters: the L_2 gain γ and the

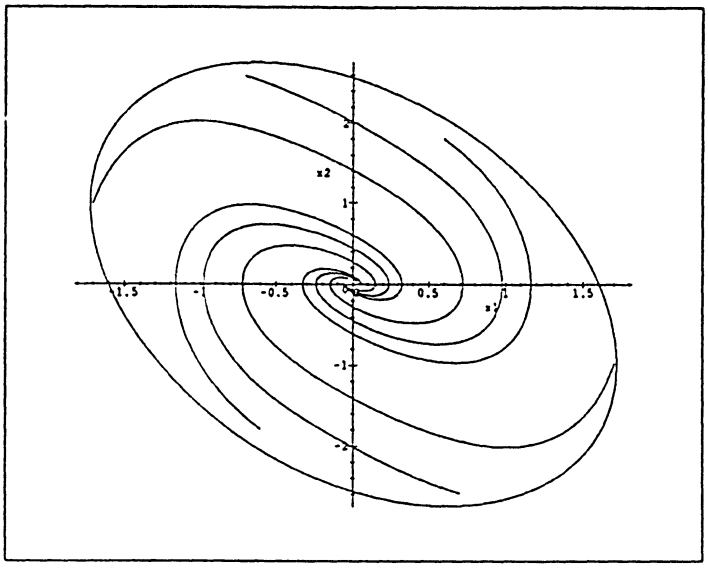

Figure 2: Invariant domain of attraction (plain stability) of Duffing equation for $k = 1, \omega = 1, \epsilon = 1$

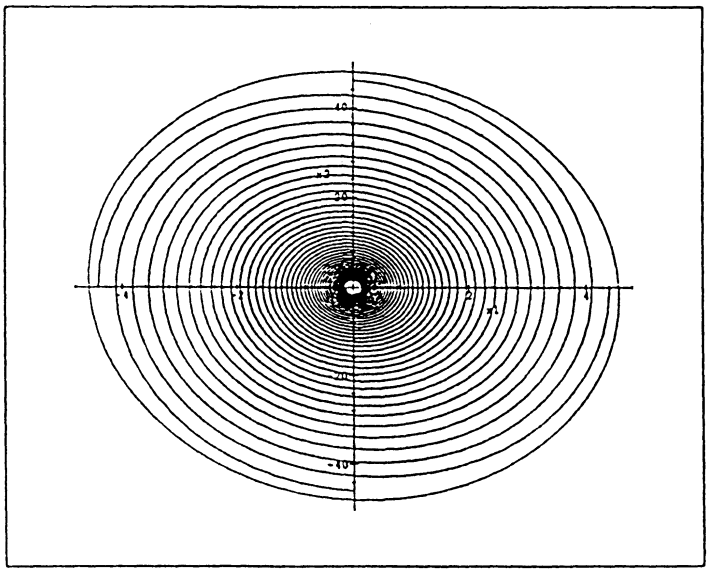

Figure 3: Invariant domain of attraction (plain stability) of Duffing equation for $k = 1, \omega = 10, \epsilon = .01$

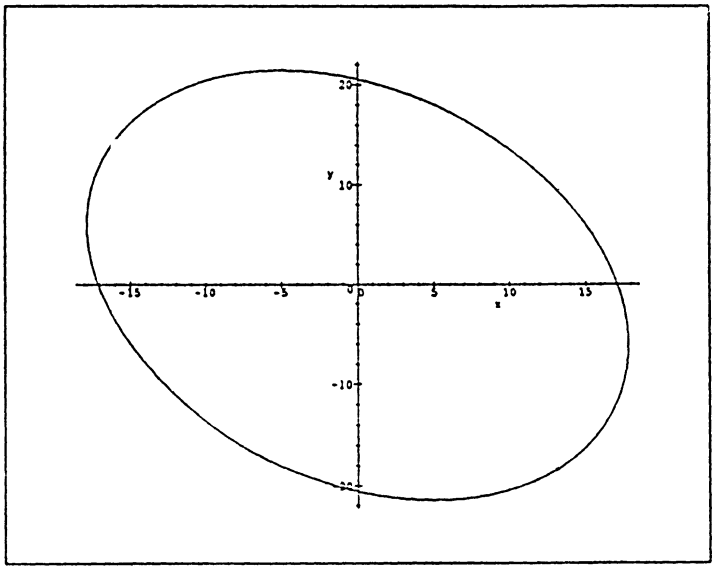

Figure 4: Invariant domain of attraction of Duffing equation , L_2 gain less than 100, for $k = 1, \omega = 1, \epsilon = 1$

well-posedness ball parameter σ. We have been unable to perform the line searches over the 2 parameters but, if we fix one parameter, say, the gain, we can perform the line search over the σ parameter. As an example, we fixed a L_2 gain of 100 and we searched over σ in order to get the largest domain of attraction possible. We found an optimal value of σ close to one. The corresponding ellipsoid is shown in (Fig.4).

In order to prove the stability of this domain, we simulated the time response of the system subject to "fancy" inputs that satisfy the required gain conditions. The results, shown in (Fig,5), shows that the ellipsoid we found is invariant (the trajectories never go out) and a domain of attraction: the trajectories eventually converge towards the equilibrium point after a relatively long time (due to the chosen inputs).

As an illustration, we included in (Fig.6) the phase plot of the first instants of the previous case.

7.3 State-feedback controller

We were interested to design a controller that would meet the following conditions

- Largest volume of the domain of attraction.
- Decay rate of the trajectories of $\alpha = 0.3$.
- Output peak less than 1000.

We performed the corresponding simulations and the results are presented in (Fig.7) and (Fig.8).

It is important to notice that the stability regions are increased with respect to the open loop case. The enlargement is greater in the linear direction (more or less one hundred times)

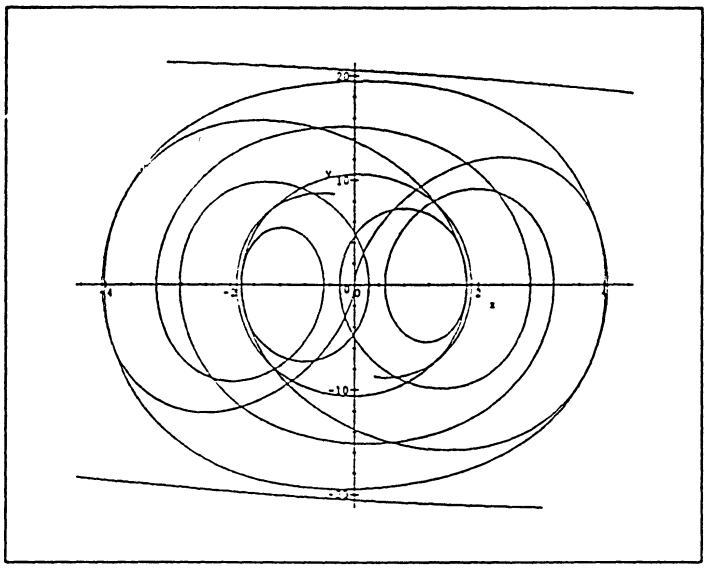

Figure 5: Invariant domain of attraction of Duffing equation , L_2 gain less than 100, stability for some inputs: the trajectories never escape and they converge towards the origin, $k = 1, \omega = 1, \epsilon = 1$

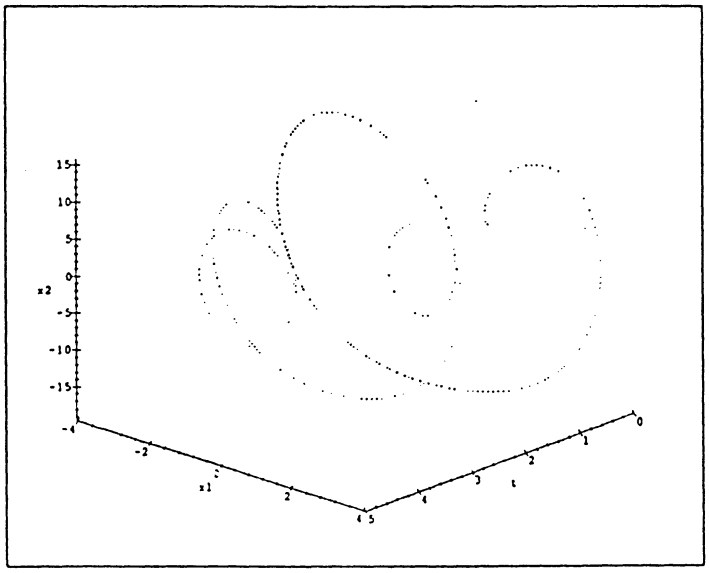

Figure 6: Invariant domain of attraction of Duffing equation , L_2 gain less than 100, phase plot for $k = 1, \omega = 1, \epsilon = 1$

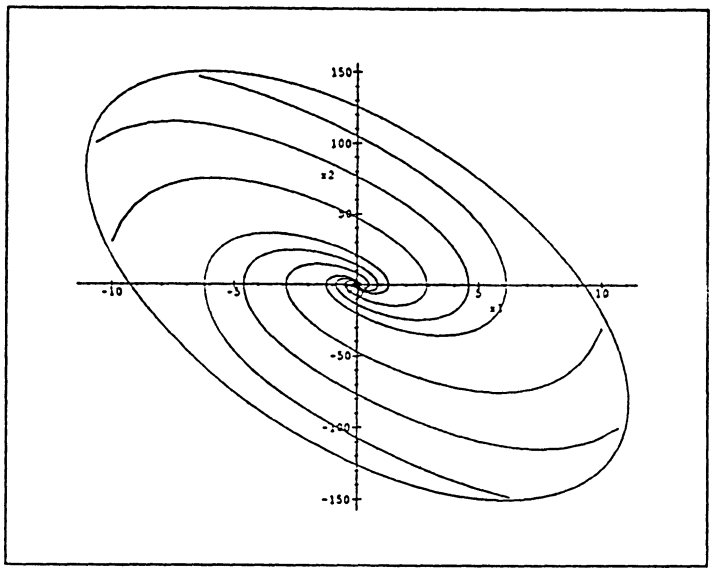

Figure 7: Invariant domain of attraction of Duffing equation , state-feedback controller, decay rate of $\alpha = 0.3$, output peak less than 1000, for $k = 1, \omega = 1, \epsilon = 1$

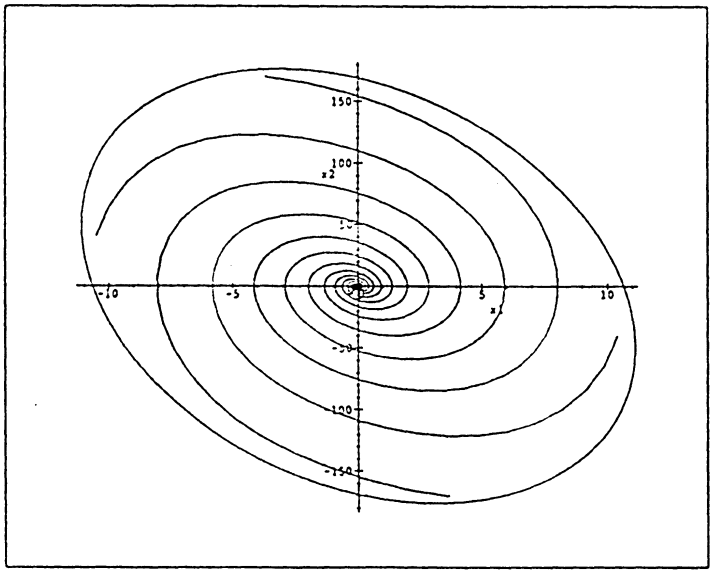

Figure 8: Invariant domain of attraction of Duffing equation , state-feedback controller, decay rate of $\alpha = 0.3$, output peak less than 1000, for $k = 1, \omega = 10, \epsilon = .01$

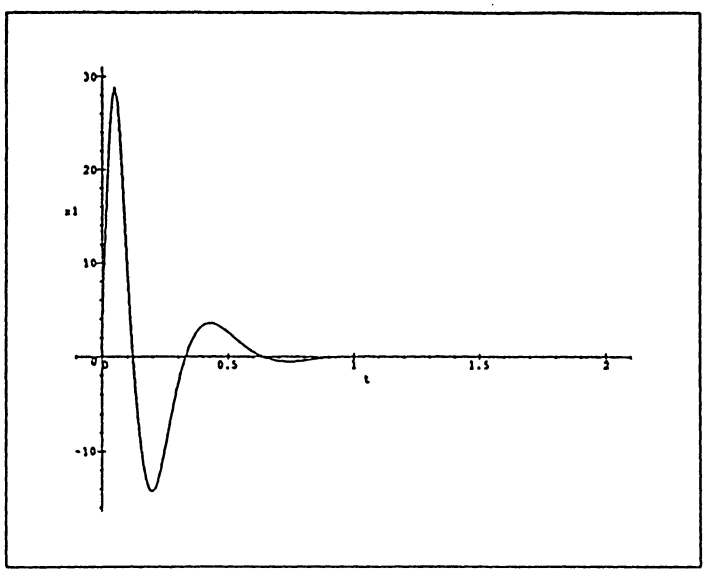

Figure 9: x time response , state-feedback controller, decay rate of $\alpha = 0.3$, output peak less than 1000, for $k = 1, \omega = 10, \epsilon = .01$

than in the non-linear direction (more or less ten times) because it is more difficult to control in the non-linear direction than in the linear one. It is also worth noting that the influence of the numerical parameters is greatly reduced by the feedback, the stability domains for the closed-loop system have almost the same size, whereas they were a lot more different in the open loop case. It is also interesting to see that the trajectories that were very slow to converge in the open loop case, are now constrained to converge with the imposed decay rate.

The vector K used in the control law, $K = YQ^{-1}$ is found to be equal to

$$K = \begin{bmatrix} -75.992 & -7.764 \end{bmatrix} \quad \text{for the first set of parameters}$$

$$K = \begin{bmatrix} -67.65 & -5.133 \end{bmatrix} \quad \text{for the second set of parameters}$$

We can see that the control laws are not excessive in size.

As a final illustration, we show in (Fig.9) and (Fig.10) the time response in the closed loop case of the two states.

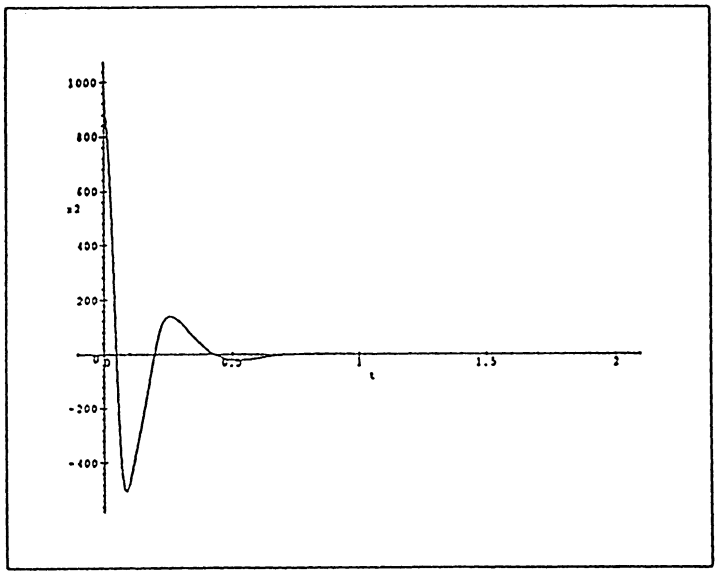

Figure 10: y time response , state-feedback controller, decay rate of $\alpha = 0.3$, output peak less than 1000, for $k = 1, \omega = 10, \epsilon = .01$

8 Conclusion

Linear Matrices Inequalities were presented. We showed what a Linear Fractional Representation of a system was and we focused on some on their properties.

We stated some existence theorems that can provide us with quadratic Lyapunov functions in order to prove the stability of such systems, along with some extra properties, like a fixed rate of decay, saturation constraints on inputs and outputs, fixed L_2 gain, etc. We showed how to design controllers with such conditions.

The techniques proved to be extremely amenable to Duffing's equation and we found stability domains, controllers that satisfy given requirements, etc.

In conclusion, from a class point of view, this project introduced another way to look at some special non-linear systems and showed how to control them. From a research point of view, we proved that the techniques were valuable in order to get stability domains of attraction of certain non-linear oscillators. The challenge is now to try to expand this formulation to non-analytical problems.

References

[1] F. Axisa, H. Bung, and J. Antunes. "Méthodes d'analyse en dynamique non linéaire des structures". Technical Report DMT/91.575, "Commissariat à l'énergie atomique, Direction des Réacteurs Nucéaires", 1991.

[2] S. Boyd, L. El Ghaoui, E. Feron, and V. Balakrishnan. *"Linear matrix inequalities in systems and control theory"*, volume 15 of *Studies in Applied Mathematics*. SIAM, 1994.

[3] L. El Ghaoui and G. Scorletti. "Control of Rational Systems using Linear-Fractional Representations and Linear Matrix Inequalities". Technical Report 279, Ecole Nat. Sup. Tech. Avancees, 32, Bd. Victor, 75739 Paris, France, November 1994. Also submitted to *Automatica.*

[4] L. El Ghaoui and M. Ait-Rami. "Robust state-feedback control of jump linear systems". Technical Report 283, Ecole Nat. Sup. Techniques Avancées, 32, Bvd. Victor, 75739 Paris, France, December 1994. Also submitted to *Int. Jour. Robust and Nonlinear Contr.*

[5] M.Ait-Rami and L. El Ghaoui. "LMI Optmization for Nonstandar Riccati Equations Arising in Stochastic Control". Technical Report 279, Ecole Nat. Sup. Tech. Avancees, 32, Bd. Victor, 75739 Paris, France, July 1995. Also submitted to *IEEE Trans. Aut. Control.*

[6] J. A. Murdock. *"Perturbations: Theory and Methods"*. John Wiley & Sons, 1988.

[7] A. H. Nayfeh and D. T. Mook. *"Nonlinear Oscillations"*. John Wiley & Sons, 1978.

[8] L. Vandenberghe and S. Boyd. "Semidefinite Programming". Technical report, Information Systems Laboratory, Stanford University, May 1995.

Hovercraft

< Aero 672 Final Project >

Jeongho Hong

Aerospace Engin.

CONTENTS

1. Introduction

Because of it's need of small space to take off and land, VTOL (vertical take off and land) aircraft is useful where landing fiel cannot be created. Ako, VTOL technology wil benefit society since it will need smaller space for it's airport and the noise from that airpor will be further localized.

Several ways of VTOL are developed so far, and one of them is used in military aircraft Harrier. Harrier is using fixed-wing - vector thrust method. One other way is to change wing configuration. (tilt-wing method). There is another way which is to take off like rocket and land like rocket but go forward or sideway by using differenti thrust or vector thrust.

Even though V-TOL technology benefits us in several way, it is not used widely because of several reasons like economical factor: and difficulty to control.

In this paper, we will concentrate on the thi method of VTOL and control issue. we will use fan engine for thrust and so the aircraft is called 'Hovercraft' which, in conventianal sense, is ground-effect transp tation.

2. Equations of motion

For the easiness of deriving equations of motion and controlling the hovercraft, we will use four engine configuration, which has symmetry (fig. 1) If we use rathe 3 engine or 2 engine then we will have trouble to configure controller design. We will assume each engine is heavy enough and all other heavy objects are centered in the haercraft so that we can choose principal axes which greatly simplifies the equation of motion. we will choose conventional aircr coordinate as set of axes and its corresps Euler angles as angular coordinates. That is, X indicates forward direction and $\hat{z}$ indicates the direction of gravitational field. Ψ, θ, ϕ indicate the angles yaw, pitch, and roll.

Lagrange's equation will be used to derive the equations of motion

2.1 Lagrange's Equation and the Generalised Equation's of Motion

The following nine pages after Figure. 1 contai the derivation of equations of motion from Lagrange's equation in general form under the assumption of using principal axes.

For the purpose of control, the equation of motion will be developed first. Then controllability issue will be studied. Finally, we will study several linearization method.

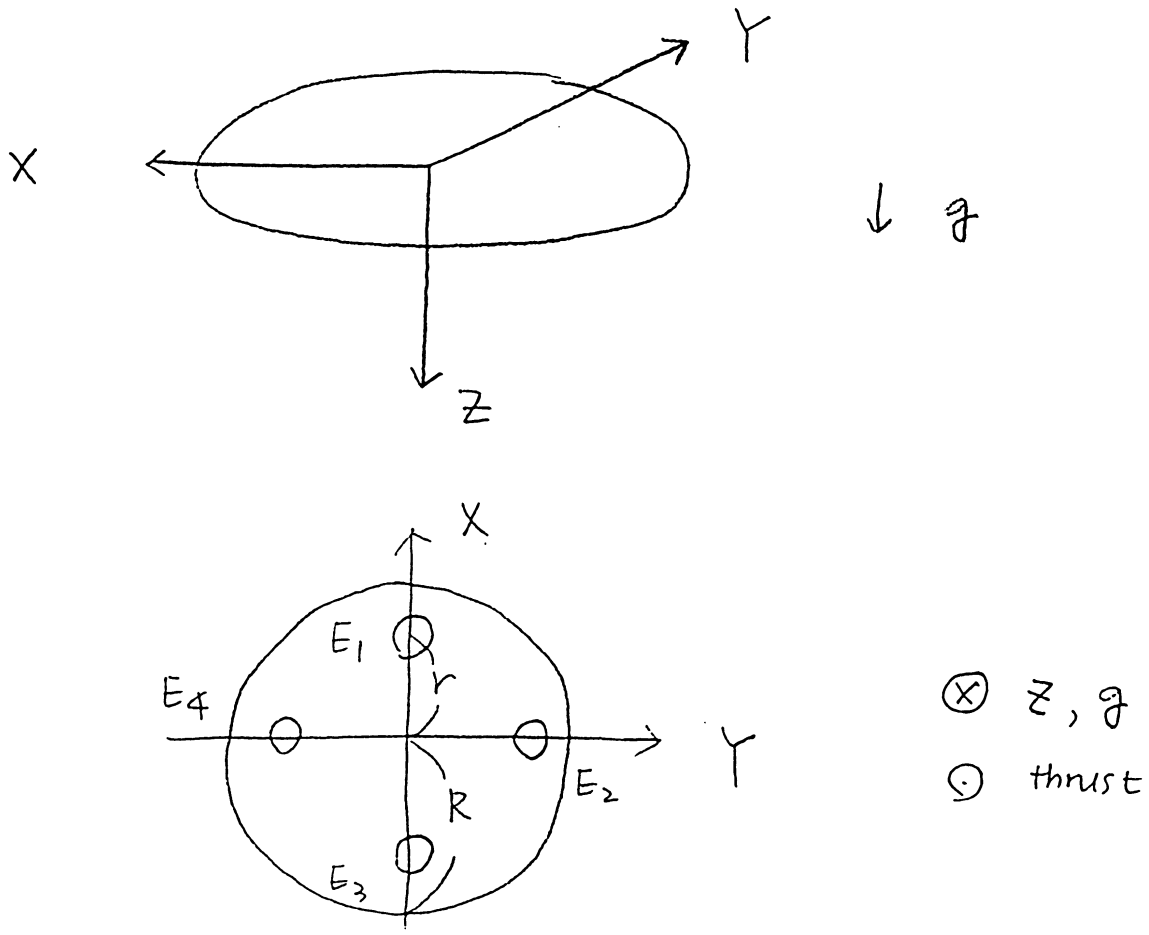

< Fig. 1 Hovercraft >

Lagrangian

$$L = T - V$$

$$T = T_{trans} + T_{rot}$$

$$T_{trans} = \frac{1}{2} M (\dot{X}^2 + \dot{Y}^2 + \dot{Z}^2)$$

$$T_{rot} = \frac{1}{2} I_{xx} (\dot{\phi} - \dot{\psi} \sin\theta)^2 + \frac{1}{2} I_{yy} (\dot{\theta} \cos\phi + \dot{\psi} \cos\theta \sin$$
$$+ \frac{1}{2} I_{33} (\dot{\psi} \cos\theta \cos\phi - \dot{\theta} \sin\phi)^2$$

$$V = -MgZ$$

$$L = \frac{1}{2} M (\dot{X}^2 + \dot{Y}^2 + \dot{Z}^2)$$
$$+ \frac{1}{2} I_{xx} (\dot{\phi} - \dot{\psi} \sin\theta)^2 + \frac{1}{2} I_{yy} (\dot{\theta} \cos\phi + \dot{\psi} \cos\theta \sin\phi)$$
$$+ \frac{1}{2} I_{33} (\dot{\psi} \cos\theta \cos\phi - \dot{\theta} \sin\phi)^2$$
$$+ MgZ$$

$$\frac{d}{dt} \frac{\partial L}{\partial \dot{q}_i} - \frac{\partial L}{\partial q_i} = Q_i$$

< Nonlinear Equations of Motion >

X
$$M\ddot{X} = F_x \cos\psi\cos\theta + F_y(-\sin\psi\cos\phi + \cos\psi\sin\theta\sin\phi) + F_z(\sin\psi\sin\phi + \cos\psi\sin\theta\cos\phi)$$

Y
$$M\ddot{Y} = F_x \sin\psi\cos\theta + F_y(\cos\psi\cos\phi + \sin\psi\sin\theta\sin\phi) + F_z(-\cos\psi\sin\phi + \sin\psi\sin\theta\cos\phi)$$

Z
$$M\ddot{Z} = -F_x\sin\theta + F_y\cos\theta\sin\phi + F_z\cos\theta\cos\phi + Mg$$

ψ
$$\ddot{\psi}\left[I_x\sin^2\theta + (I_y\sin^2\phi + I_z\cos^2\phi)\cos^2\theta\right] + \ddot{\theta}\,\tfrac{1}{2}I_{yz}\cos\theta\sin 2\phi - \ddot{\phi}\,I_x\sin\theta + \dot{\psi}\left[(I_x - I_y\sin^2\phi - I_z\cos^2\phi)\sin 2\theta\,\dot{\theta} + I_{yz}\sin 2\phi\cos^2\theta\,\dot{\phi}\right] - \dot{\theta}^2\tfrac{1}{2}I_{yz}\sin\theta\sin 2\phi + \dot{\theta}(I_{yz}\cos 2\phi - I_x)\cos\theta\,\dot{\phi} = -T_x\sin\theta + T_y\cos\theta\sin\phi + T_z\cos\theta\cos\phi$$

θ
$$\ddot{\psi}\,\tfrac{1}{2}I_{yz}\cos\theta\sin 2\phi + \ddot{\theta}(I_y\cos^2\phi + I_z\sin^2\phi) + \dot{\psi}(I_{yz}\cos 2\phi + I_x)\cos\theta\,\dot{\phi} - \dot{\psi}^2\tfrac{1}{2}(I_x - I_y\sin^2\phi - I_z\cos^2\phi)\sin 2\theta - \dot{\theta}\,I_{yz}\sin 2\phi\,\dot{\phi} = T_y\cos\phi - T_z\sin\phi$$

ϕ
$$-\ddot{\psi}\,I_x\sin\theta + \ddot{\phi}\,I_x - \dot{\psi}(I_x + I_{yz}\cos 2\phi)\cos\theta\,\dot{\theta} - \dot{\psi}^2\tfrac{1}{2}I_{yz}\cos^2\theta\sin 2\phi + \dot{\theta}^2\tfrac{1}{2}I_{yz}\sin 2\phi = T_x$$

2.2. Nonlinear Equations of Motion for Hovercraft

Define T_1, T_2, T_3 and T_4 as thrusts from engine 1, engine 2, engine 3 and engine 4 respectfully. Then applied force and applied torque has following components

$$\begin{aligned}\vec{F} &= -(T_1+T_2+T_3+T_4)\hat{3} \\ &= F_3\hat{3}\end{aligned}$$

$$\begin{aligned}\vec{T} &= \hat{x}\, r\,(T_4-T_2) + \hat{y}\, r\,(T_1-T_3) \\ &= \hat{x}\, T_x + \hat{y}\, T_y\end{aligned}$$

Thus, to obtain the nonlinear equations of motion for hovercraft, it is enough to plug the above applied force and torque componen in the equations of Nonlinear Equations of Motion in Section 2.1

2.3 2-dimensional equations of motion

In order simplify the complex nonlinear equations, we will deal with only 2-D problem in this poper that is X-Z plar Thus, the resulting equations of motion are

$$\ddot{X} = -U_1 \sin\theta$$
$$\ddot{Z} = -U_1 \cos\theta + 1$$
$$\ddot{\theta} = U_2$$

Where

$$M = g = 1, \quad U_1 = T_1 + T_3, \quad U_2 = T_1 - T_3.$$

3. Controllability

We have the nonlinear equations of motion

$$\begin{cases} \ddot{x} = -u_1 \sin\theta \\ \ddot{z} = u_1 \cos\theta + 1 \\ \ddot{\theta} = u_2. \end{cases} \qquad (3.1)$$

By using the accessibility rank condition, we can determine whether (3.1) is accessible or not. If accessibility distribution has full rank (in our case, 6) then the system is locally accessible, where accessibility distribution is the span of Liebrackets of f, g_1, g_2, where f, g_1, g_2 are defined as follows

$$\dot{x} = f(x) + g_1(x)\, u_1 + g_2(x)\, u_2 .$$

By calculating Liebrackets of f, g_1, g_2, we can find 6 independe columns, so the system (3.1) is locally accessible

However, currently there is no condition availa to check controllability for system with drift. Bu from the physical viewpoint of the system, it is controllable. You can make the hovercraft move in any direction in any angle.

4. Linearization

It would be wise to design nonlinear control for nonlinear systems. However, since there is no obvious way of designing nonlinear controller for nonlinear system and there are plenty ways of designing controller for linear systems, we will linearize the nonlinear equations. Cumently, there are several ways of getting nonlinear equations lineanzed. In this paper, we will consider two method, small magnitude approximation and state feedback linearization.

41 Small value approximation

Let's assume $\psi, \theta, \phi, \dot{\psi}, \dot{\theta}, \dot{\phi}$ are small in the equations which are derived in section Then we have the following "linearized" equat of motion

$$\ddot{X} = -u_1\theta$$
$$\ddot{z} = -u_1 + 1$$
$$\ddot{\theta} = u_2$$

we attempted to linearize the equations, however, the resulting equations have still nonlinearity in somewhat linear fashion. It is called bilinear system It makes sense in physical terms, since from the configuration of haver craft, in order to go forword you have to have nonzero pitch angle, otherwise there is no way you can achieve forward motion. Since bilinear problem is not easy to solve or to design a control law itself, we have not gain much advantage by assuming small magnitude of states of the equations. Next, we will discuss the state feedback linearization method.

4.2 State Feedback Linearization

As in section 3, by using geometric method, we can determine whether (3.1) is state feedback linearizable or not. Define D_i as

$$D_i = \text{span}\{ ad_f^r g_1(x), ad_f^r g_2(x) : r = 0, 1, \cdots, i-1 \}$$
$$i = 1, 2, \cdots$$

If the distributions D_i's are all involutive and constant dimensional around a neighborhood of x_0, then the system is static state feedback linearizable. However, as we can see from the calculations, D_i's are not involutive so the system (3.1) is not linearizable by the static state feedback. Thus the remaining choice is to use dynamic state feedback. This problem is dealt well in Sastry.
Let's denote (3.1) as

$$\begin{bmatrix} \ddot{x} \\ \ddot{z} \end{bmatrix} = \begin{bmatrix} 0 \\ 1 \end{bmatrix} + \begin{bmatrix} -\sin\theta & 0 \\ -\cos\theta & 0 \end{bmatrix} \begin{bmatrix} u_1 \\ u_2 \end{bmatrix}$$

then differentiate it twice

$$\begin{bmatrix} x^{(4)} \\ z^{(4)} \end{bmatrix} = \begin{bmatrix} \sin\theta\, \dot{\theta}^2 u_1 - 2\cos\theta\, \dot{\theta}\, \dot{u}_1 \\ \cos\theta\, \dot{\theta}^2 u_1 + 2\sin\theta\, \dot{\theta}\, \dot{u}_1 \end{bmatrix} + \begin{bmatrix} -\sin\theta & -\cos\theta\, u_1 \\ -\cos\theta & \sin\theta\, u_1 \end{bmatrix} \begin{bmatrix} \ddot{u}_1 \\ u_2 \end{bmatrix}$$

In this development, we allowed u_1 to be dynamic. By doing this and defining $\ddot{u}_1$ an-

equation from (3.1)

$$\begin{bmatrix} \ddot{u}_1 \\ \dot{u}_2 \end{bmatrix} = \begin{bmatrix} -\sin\theta & -\cos\theta \\ -\cos\theta/u_1 & \sin\theta/u_1 \end{bmatrix} \left(\begin{bmatrix} \sin\theta\,\dot{\theta}^2 u_1 - 2\cos\theta\,\dot{\theta}\dot{u}_1 \\ \cos\theta\,\dot{\theta}^2 u_1 + 2\sin\theta\,\dot{\theta}\dot{u}_1 \end{bmatrix} + \begin{bmatrix} v_1 \\ v_2 \end{bmatrix} \right)$$

$$= \begin{bmatrix} -\dot{\theta}^2 u_1 \\ 2\dot{\theta}\dot{u}_1/u_1 \end{bmatrix} + \begin{bmatrix} -\sin\theta & -\cos\theta \\ -\cos\theta/u_1 & \sin\theta/u_1 \end{bmatrix} \begin{bmatrix} v_1 \\ v_2 \end{bmatrix}$$

Then

$$\begin{bmatrix} x^{(4)} \\ z^{(4)} \end{bmatrix} = \begin{bmatrix} v_1 \\ v_2 \end{bmatrix} \qquad (4.1)$$

The system (4.1) is linear. So we can use powerful linear method to design controller. It will be discussed in next section.

5. Controller Design

We have two sets of equations

$$\begin{cases} \ddot{x} = -u_1 \sin\theta \\ \ddot{z} = u_1 \cos\theta + 1 \\ \ddot{\theta} = u_2 \end{cases} \tag{5.1}$$

$$\begin{cases} x^{(4)} = v_1 \\ z^{(4)} = v_2 . \end{cases} \tag{5.2}$$

(5.2) was obtained by using dynamic state feedback linearization method in (5.1). To look at the controller effect on (5.1) from the controller obtained in (5.2), we choosed simple control law

$$v_1 = \alpha_1 x + \alpha_2 \dot{x} + \alpha_3 \ddot{x} + \alpha_4 \dddot{x}$$
$$v_2 = \beta_1 z + \beta_2 \dot{z} + \beta_3 \ddot{z} + \beta_4 \dddot{z}$$

where

$$\alpha_i, \beta_i < 0$$

Then from Routh-Herwitz orgument, the closed loop is stable. So all the variables in (5.2) $x, \dot{x}, \ddot{x}, \dddot{x}, z, \dot{z}, \ddot{z}, \dddot{z}$ are going to zero as time increases. However, when we applied the same controller in (5.1), although $x, \dot{x}, z, \dot{z}$ went zero at steady state, we cannot predict the value of θ. At transient state, θ varies a lot from 0 degree to more than 100 degree, which is not acceptible to the havercraft. Because the main design specification is to make havercraft haver, and for that

we need δ as small as possible and we have to obtain 0 steady-state for hover. From this result, we find that the dynamic state feedback linearization done in section 4 is not good way for hovercraft

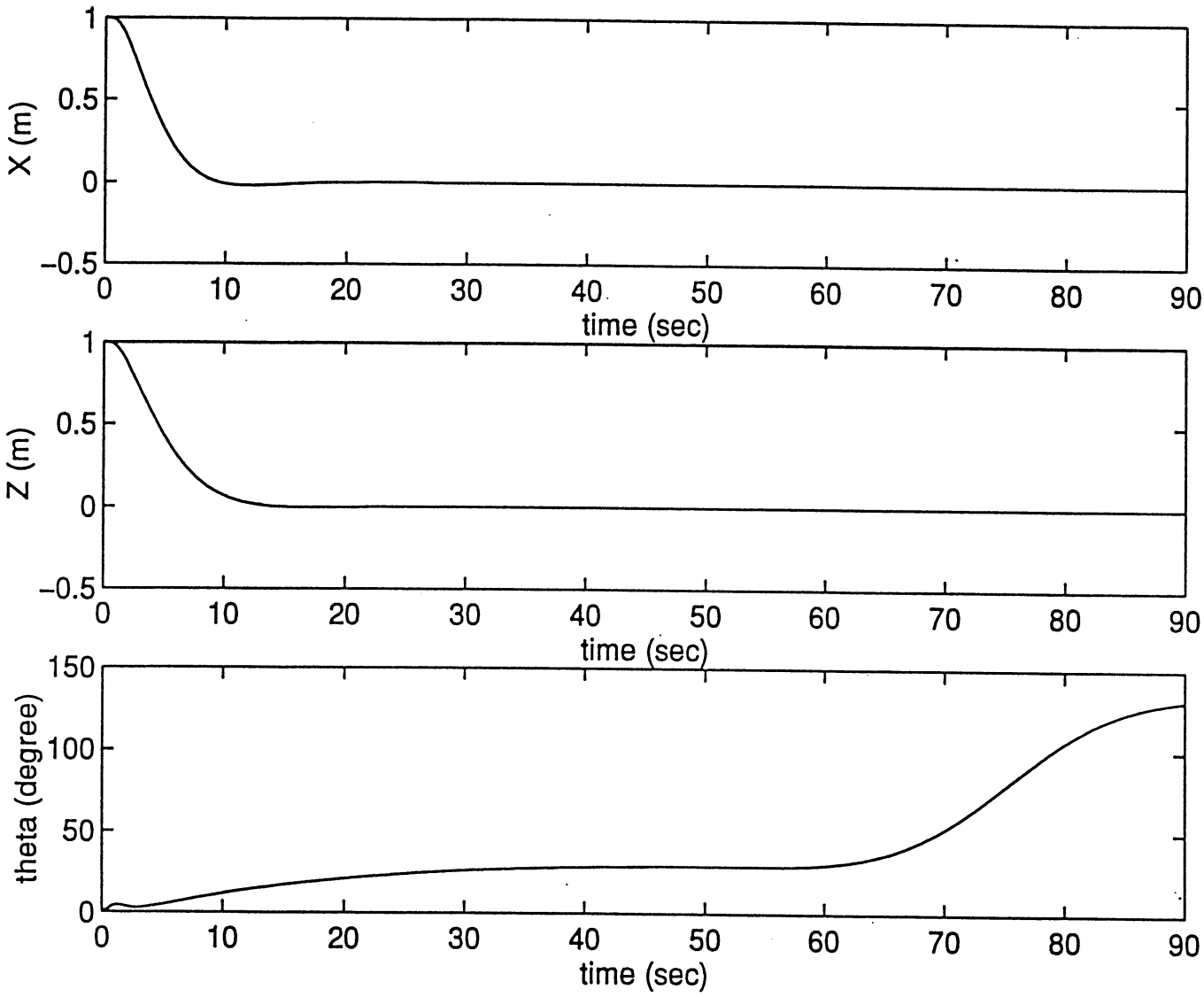

This plot shows that by the linear model obtained from dynamic state feedback linearization, we can obtain zero steady-state for X and Z coordinates. However, for θ, we don't have any control

6. Conclusion

In an attempt to design a controller for hovercraft, we derived the nolinear equations of motion by using Lagrange's equation. we used two method to lineanze the nonlinear equation. The small value approximation produ bilinear equations of motion which is not much easy to deal with. The dynamic state feedback linearization produced a linea equations of motion which is not suitable for hovercraft.

Thus, so far, we have the nonlinear equation motion and two failed attempt to linearize them. So future work will be another attempt to lineanze or to obtain a nonlin controller directly.

Tracking Control for a Telescopic Robot Arm

MEAM 662 Project

Chia-Shang Liu

Department of Mechanical Engineering and Applied Mechanics

Instructor

D. Tilbury : Professor of MEAM

Abstract

The objective of this project is to control the tip of the telescopic robot arm to follow a desired trajectory. Several existing tracking control methods are used, which include full state feedback linearization, robust control and adaptive control. A different approach for tracking control is proposed in this project, which is termed as disturbance estimation based tracking control. The proposed tracking control method need not knowing the dynamic structure of the system and the parameter value. Since it involves the disturbance estimation, not only the effect of system uncertainty but also the effect of external disturbance and unmodeled mechanism can be compensated. The results of simulation show that the proposed method can perform well in driving the telescopic robot arm to a desired trajectory with system uncertainty and external disturbance.

1. Introduction

Nonlinear systems actually appear in many engineering disciplines, e.g. chemical engineering, electrical circuits, robot manipulator etc. Since the powerful tools for linear systems have been developed successfully, it is quite intuitively and is a common practice to linearize the nonlinear system. State feedback linearization of nonlinear system has been extensively investigated and applied in literature [1-8]. There are several methods of the state feedback control to linearize the nonlinear system. One of them is the exact input output linearization which didn't have any approximation is used[9-10] . The other one is the full state linearization which uses a set of coordinates and a feedback law such that the input-to-state of the transformed is linear [10].

In this project we would like to control a nonlinear system (telescopic arm) to follow a desired trajectory which is referred to as tracking control. Tracking control can be quantitatively stated as the determination of the system input to keep the error of system output and desired output (varied with time) within prescribed values [11]. If the characteristics of the system is completely known and the system is feedback linearizable, a controller based on the feedback linearization can be designed. But in real life it is quite rare to exactly know the parameter value and in fact uncertainty is inevitable in system. Under this situation the controller design based on the feedback linearization will likely fail.

The system uncertainty is an important issue in many applications of robot manipulator control. Most of the proposed controllers thus far to compensate the system uncertainty are either adaptive control or robust control methods. The majority of the researches in

adaptive manipulator control assume that the structure of the manipulator dynamics is known and the system is linear to unknown parameters [12-21]. These schemes can be termed as model-based adaptive control [22], because they rely on the information of the system dynamic model. These controllers have been successfully applied in some computer simulations and experiments. However, there are some potential difficulties associated with these approaches. These designs require precise knowledge of the structure of the entire manipulator dynamic model, which rarely happens in real life. In practice, it is very likely that some unrealized mechanism wasn't included in the model and some unknown external disturbance will be present in system. Additionally, [23-24] have indicated that these model-based adaptive controllers can lack robustness to unmodeled dynamics, sensor noise, and other disturbance. Recently, there are many authors [22] [25-31] who are interested in developing adaptive controllers that require less model information than the model based adaptive controller. This kind of approach is referred to as performance-based adaptive control because the adaptive law adjust the controller gains based on the system performance rather than on system model. None of the adaptive schemes proposed in [22] [25-31] required the knowledge of system structure and parameter values, and the bound of the system signal are assured. In [25-28] the adaptive law is derived based on the variable structure control methods. In [22] [29-31] a more standard adaptive laws are used. In these project we will introduce a different approach to design the controller, which is termed as the disturbance estimation based tracking control. All the system dynamic structures and system uncertainty will be lumped with external disturbance and unmodeled mechanism, which is considered as the system disturbance. Then the controller can be designed by canceling the system disturbance with the application of a disturbance observer. Since the system dynamic structure and system uncertainty are considered to be the system disturbance, we don't need to know the dynamic structure and parameter values of the system. In fact the proposed method is robust to the unmodeled effects and external disturbance, because we don't rely on the model information and the external disturbance and unmodeled mechanism will be estimated.

This project is organized as follows. In section 2 the system model will be described. In section 3 the controller of feedback linearization, robust control and adaptive control will be investigated. The proposed control method (disturbance estimation based tracking control) will be introduced in section 4. The simulation results of the different controllers will be presented in section 5. And in section 6 we will summarize the project and make conclusions.

2. System Description

The system studied in this project is a telescopic robot arm in a vertical plane (Fig. 1), which is driven by two motors to control the angle ϕ and the arm length ℓ. It is assumed that the arm mass is negligible with respect to the mass M. The motion equations of the telescopic arm can be derived by the Lagarange method as

$$\ddot{\phi} + \alpha_1\dot{\phi} + \alpha_2\phi + \frac{g}{\ell}\sin(\phi) = \alpha_m \frac{u_1}{M\ell^2} \tag{2.1}$$

$$\ddot{\ell} + \alpha_3\dot{\ell} + \alpha_4\ell - g\cos(\phi) = k_m \frac{u_2}{M} \tag{2.2}$$

where $\alpha_1 = \frac{\alpha_f}{M\ell^2} + 2\frac{\dot{\ell}}{\ell}$, $\alpha_2 = \frac{\alpha_s}{M\ell^2}$, $\alpha_3 = \frac{k_f}{M}$, $\alpha_4 = \frac{k_s}{M} - \dot{\phi}^2$, M denotes the mass of the load, ℓ(t) is the variable length of the arm, ϕ(t) is the angle between the arm and the vertical axis, α_s and k_s are the stiffness coefficients, α_f and k_f are the viscous friction coefficients, u_1 and u_2 are the voltages applied to the electrical motors in the joint and the arm, respectively. The torque in the joint and the longitudinal force in the arm are $T_1 = \alpha_m u_1$ and $T_2 = k_m u_2$, respectively, where α_m and k_m are constants.

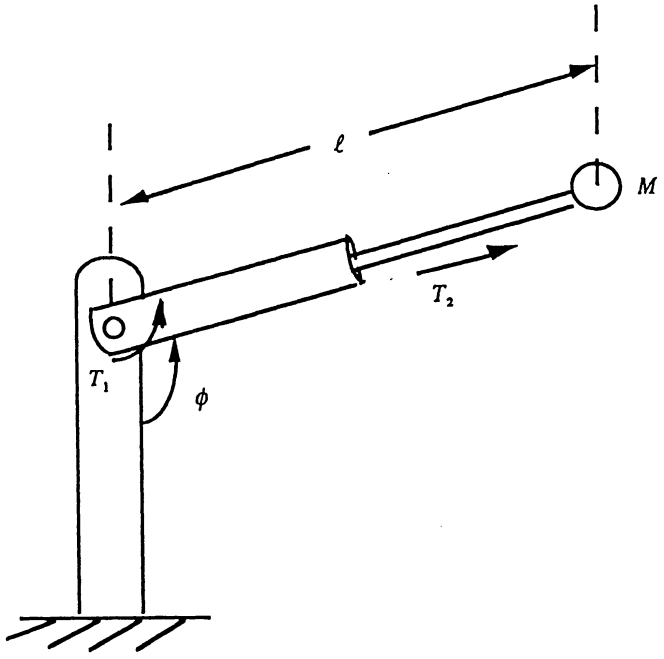

Fig. 1 Telescopic Robot Arm

3. Existing Control Method

In this section we would like to briefly introduce some existing controller for tracking control.

3.1 Full State Feedback Linearization

It is easily seen from equation. (2.1) , (2.2) that they are full state feedback linearizable [9-10]. The controller can be chosen as

$$u_1 = \frac{M\ell^2}{\alpha_m}(\ddot{\phi}_d + \alpha_1\dot{\phi} + \alpha_2\phi + \frac{g\sin(\phi)}{\ell} + k_1\dot{e}_\phi + k_2 e_\phi) \tag{3.1}$$

$$u_2 = \frac{M}{k_m}(\ddot{\ell}_d + \alpha_3\dot{\ell} + \alpha_4\ell - g\cos(\phi) + k_3\dot{e}_\ell + k_4 e_\ell) \tag{3.2}$$

where ϕ_d is the desired angle, ℓ_d is the desired arm length, k_i i= 1-4. which are feedback gains, $e_\phi = \phi - \phi_d$, $e_\ell = \ell - \ell_d$.

Substitute. (3.1) and. (3.2) into. (2.1), (2.2) we can get the error dynamics as

$$\begin{aligned} \ddot{e}_\phi - k_1\dot{e}_\phi - k_2 e_\phi = 0 \\ \ddot{e}_\ell - k_3\dot{e}_\ell - k_4 e_\ell = 0 \end{aligned} \tag{3.4}$$

The appropriate gains k_i i=1-4 can be chosen to let the error system (3.4) be asymptotically stable.

The application of feedback linearization needs that the parameter values are well known, or the system performance cannot be satisfied. It is a unrealizable situation in real life. To compensate the system uncertainty, the robust control and adaptive control can be applied.

3.2. Robust Control

Assume that the nominal system is described as

$$\ddot{\phi} + \bar{\alpha}_1\dot{\phi} + \bar{\alpha}_2\phi + \frac{g}{\ell}\sin(\phi) = \bar{\alpha}_m\frac{u_1}{M\ell^2} \tag{3.5}$$

$$\ddot{\ell} + \bar{\alpha}_3\dot{\ell} + \bar{\alpha}_4\ell - g\cos(\phi) = \bar{k}_m\frac{u_2}{M} \tag{3.6}$$

where $\bar{\alpha}_1 = \frac{\bar{\alpha}_f}{M\ell^2} + 2\frac{\dot{\ell}}{\ell}$, $\bar{\alpha}_2 = \frac{\bar{\alpha}_s}{M\ell^2}$, $\bar{\alpha}_3 = \frac{\bar{k}_f}{M}$, $\bar{\alpha}_3 = \frac{\bar{k}_f}{M}$, and - denotes the nominal value of the parameter.

The robust controller designed by Lyapunov method can be given as [9]

$$u_1 = \frac{M\ell^2}{\bar{\alpha}_m}(\ddot{\phi}_d + \bar{\alpha}_1\dot{\phi} + \bar{\alpha}_2\phi + \frac{g\sin(\phi)}{\ell} + k_1\dot{e}_\phi + k_2 e_\phi + v_1) \tag{3.7}$$

$$u_2 = \frac{M}{\bar{k}_m}(\ddot{\ell}_d + \bar{\alpha}_3\dot{\ell} + \bar{\alpha}_4\ell - g\cos(\phi) + k_3\dot{e}_\ell + k_4 e_\ell + v_2) \tag{3.8}$$

where $v_1 = -\frac{\eta_{\phi 0} + \eta_{\phi 1}}{1 - k_\phi}\frac{w_\phi}{\|w_\phi\|_2}$ $\quad \|w_\phi\|_2 \geq \varepsilon$

$= -\frac{\eta_{\phi 0} + \eta_{\phi 1}}{1 - k_\phi}\frac{w_\phi}{\varepsilon}$ $\quad \|w_\phi\|_2 < \varepsilon$

$v_2 = -\frac{\eta_{\ell 0} + \eta_{\ell 1}}{1 - k_\ell}\frac{w_\ell}{\|w_\ell\|_2}$ $\quad \|w_\ell\|_2 \geq \varepsilon$

$= -\frac{\eta_{\ell 0} + \eta_{\ell 1}}{1 - k_\ell}\frac{w_\ell}{\varepsilon}$ $\quad \|w_\ell\|_2 < \varepsilon$

Substitute (3.7), (3.8) into (2.1), (2.2), we get the error dynamics as

$$\ddot{e}_\phi = k_1\dot{e}_\phi + k_2 e_\phi + v_1 + \delta_\phi \tag{3.9}$$

$$\ddot{e}_\ell = k_3\dot{e}_\ell + k_4 e_\ell + v_2 + \delta_\ell \tag{3.10}$$

where

$$\begin{aligned}\delta_\phi = &[\frac{\alpha_m}{\bar{\alpha}_m}\bar{\alpha}_1 - \alpha_1 + (\frac{\alpha_m}{\bar{\alpha}_m} - 1)k_1]\dot{e}_\phi + [\frac{\alpha_m}{\bar{\alpha}_m}\bar{\alpha}_2 - \alpha_2 + (\frac{\alpha_m}{\bar{\alpha}_m} - 1)k_2]e_\phi \\ &+ (\frac{\alpha_m}{\bar{\alpha}_m} \div 1)[\ddot{\phi}_d + \frac{g}{\ell}\sin(\phi) + v_1] + (\frac{\alpha_m}{\bar{\alpha}_m}\bar{\alpha}_1 - \alpha_1)\dot{\phi}_d + (\frac{\alpha_m}{\bar{\alpha}_m}\bar{\alpha}_2 - \alpha_2)\phi_d \end{aligned} \tag{3.11}$$

$$\begin{aligned}\delta_\ell = &[\frac{k_m}{\bar{k}_m}\bar{\alpha}_3 - \alpha_3 + (\frac{k_m}{\bar{k}_m} - 1)k_3]\dot{e}_\ell + [\frac{k_m}{\bar{k}_m}\bar{\alpha}_4 - \alpha_4 + (\frac{k_m}{\bar{k}_m} - 1)k_4]e_\ell \\ &+ (\frac{k_m}{\bar{k}_m} - 1)[\ddot{\ell}_d + v_2] + (\frac{k_m}{\bar{k}_m}\bar{\alpha}_3 - \alpha_3)\dot{\ell}_d + (\frac{k_m}{\bar{k}_m}\bar{\alpha}_4 - \alpha_4)\ell_d \end{aligned} \tag{3.12}$$

$\eta_{\phi 0}$, $\eta_{\phi 1}$, k_ϕ, $\eta_{\ell 0}$, $\eta_{\ell 1}$ and k_ℓ are determined by the system uncertainty caused by parameter variation

Take the Euclidean norm of (3.11) and (3.12) gives

$$\|\delta_\phi\|_2 \le \rho_{\phi 0} + \rho_{\phi 1}\|\kappa_\phi(e_\phi)\|_2 + k_\phi\|v_1\|_2 \tag{3.13}$$

$$\|\delta_\ell\|_2 \le \rho_{\ell 0} + \rho_{\ell 1}\|\kappa_\ell(e_\ell)\|_2 + k_\ell\|v_2\|_2 \tag{3.14}$$

where $\eta_{\phi 0} \ge \rho_{\phi 0} \ge 0$, $\eta_{\phi 1} \ge \rho_{\phi 1} \ge 0$, $1 > k_\phi > 0$, $\eta_{\ell 0} \ge \rho_{\ell 0} \ge 0$, $\eta_{\ell 1} \ge \rho_{\ell 1} \ge 0$, $1 > k_\ell > 0$

w_ϕ, w_ℓ, κ_ϕ and κ_ℓ are determined by the Lyapunov function candidate

$$V(e_\phi) = E_\phi^t P_\phi E_\phi \tag{3.15}$$

$$V(e_\ell) = E_\ell^t P_\ell E_\ell \tag{3.16}$$

where $E_\phi^t = \begin{bmatrix} e_\phi & \dot{e}_\phi \end{bmatrix}$, $E_\ell^t = \begin{bmatrix} e_\ell & \dot{e}_\ell \end{bmatrix}$, P_ϕ and P_ℓ are positive definite matrix that satisfy $A_\phi^t P_\phi + P_\phi A_\phi = -Q_\phi$, $A_\ell^t P_\ell + P_\ell A_\ell = -Q_\ell$, if A_ϕ and A_ℓ are Hurwitz matrix, $Q_\phi > 0$ and $Q_\ell > 0$.

Then w_ϕ, w_ℓ, κ_ϕ and κ_ℓ are defined as

$$w_\phi = 2E_\phi^t P_\phi B_\phi \tag{3.17}$$

$$w_\ell = 2E_\ell^t P_\ell B_\ell \tag{3.18}$$

$$\kappa_\phi = \sqrt{E_\phi^t Q_\phi E_\phi} \tag{3.19}$$

$$\kappa_\ell = \sqrt{E_\ell^t Q_\ell E_\ell} \tag{3.20}$$

where $B_\phi = B_\ell = \begin{bmatrix} 0 \\ 1 \end{bmatrix}$.

If $\rho_{\phi 0} > 0$ and $\rho_{\ell 0} > 0$, then e_ϕ and e_ℓ are uniformly bounded in a neighborhood of the origin, whose size can be made arbitrarily small by choosing ε small enough.

3.3. Adaptive Control

The other way to compensate the uncertainty caused by the bias between nominal parameter value and true parameter value is to estimate the parameter. The well known adaptive observer [11] is applied to estimate the parameters α_m, α_f, α_s, k_m, k_f, k_s.

The adaptive observer is briefly introduced as follows

Assume that a nonlinear system can be described as

$$\dot{x} = Ax + B\theta^T f(y,u) + g(y,u) \tag{3.21}$$

$$\dot{\hat{x}} = A\hat{x} + B\hat{\theta}^T f(y,u) + g(y,u) + K(y - \hat{y}) \tag{3.22}$$

where $y = Cx$, u is the system input, θ is the unknown parameter, K is the feedback gain, ^ denotes estimation.

The adaptive law to estimate the parameter θ is given by

$$\dot{\hat{\theta}} = -f^t(y,u)B^tPe \tag{3.23}$$

where $e = \hat{x} - x$, P is a positive definite matrix that satisfies the relationship $A_k^tP + PA_k = -Q$, $Q > 0$, $A_k = A - KC$ which is a Hurwitz matrix. To assure the estimated parameters converge to true value, it needs that $f(y,u)$ is a persistent excited function.

The system described in (2.1) and (2.2) can be rewritten as

$$\begin{bmatrix}\dot{\phi}\\ \ddot{\phi}\end{bmatrix} = \begin{bmatrix}0 & 1\\ 0 & 0\end{bmatrix}\begin{bmatrix}\phi\\ \dot{\phi}\end{bmatrix} + \begin{bmatrix}0\\ 1\end{bmatrix}\begin{bmatrix}\alpha_s & \alpha_f & \alpha_m\end{bmatrix}\begin{bmatrix}-\phi\\ -\dot{\phi}\\ u_1\end{bmatrix}\frac{1}{M\ell^2} + \begin{bmatrix}0\\ -2\frac{\dot{\ell}}{\ell}\dot{\phi} - \frac{g}{\ell}\sin\phi\end{bmatrix} \tag{3.24}$$

$$\begin{bmatrix}\dot{\ell}\\ \ddot{\ell}\end{bmatrix} = \begin{bmatrix}0 & 1\\ 0 & 0\end{bmatrix}\begin{bmatrix}\ell\\ \dot{\ell}\end{bmatrix} + \begin{bmatrix}0\\ 1\end{bmatrix}\begin{bmatrix}k_s & k_f & k_m\end{bmatrix}\begin{bmatrix}-\ell\\ -\dot{\ell}\\ u_2\end{bmatrix}\frac{1}{M} + \begin{bmatrix}0\\ \dot{\phi}^2\ell + g\cos\phi\end{bmatrix} \tag{3.25}$$

We can see that (3.24) and (3.25) are in the form of (3.21). Then the adaptive observer is derived according to (3.22) and the adaptive law of estimating unknown parameters can be obtained according to (3.23).

The controller can be defined as

$$u_1 = \frac{M\ell^2}{\hat{\alpha}_m}(\ddot{\phi}_d + \hat{\alpha}_1\dot{\phi} + \hat{\alpha}_2\phi + \frac{g\sin(\phi)}{\ell} + k_1\dot{e}_\phi + k_2 e_\phi) \tag{3.26}$$

$$u_2 = \frac{M}{\hat{k}_m}(\ddot{\ell}_d + \hat{\alpha}_3\dot{\ell} + \hat{\alpha}_4\ell - g\cos(\phi) + k_3\dot{e}_\ell + k_4 e_\ell) \tag{3.27}$$

4. Proposed Tracking Control Method

We can see that the objective of adaptive or robust control shown in section 3 and in the literature [12-31] is to compensate the system uncertainty or disturbance. In fact we can say that it is somewhat in the sense of estimating the system uncertainty and disturbance. So why don't we estimate the uncertainty and disturbance directly instead of applying some robust controller or adaptive laws?

4.1 Disturbance Based Tracking Controller

First, I come out the following disturbance based tracking controller which needs the system dynamic structure.

We can rewritten the system shown in (2.1) and (2.2) as the nominal system plus the uncertainty and external disturbance as.

$$\ddot{\phi} + \bar{\alpha}_1\dot{\phi} + \bar{\alpha}_2\phi + \frac{g}{\ell}\sin(\phi) = \bar{\alpha}_m\frac{u_1}{M\ell^2} + \delta_{\phi d} \tag{4.1}$$

$$\ddot{\ell} + \bar{\alpha}_3\dot{\ell} + \bar{\alpha}_4\ell - g\cos(\phi) = \bar{k}_m\frac{u_2}{M} + \delta_{\ell d} \tag{4.2}$$

The controllers are chosen as

$$u_1 = \frac{M\ell^2}{\bar{\alpha}_m}(\ddot{\phi}_d + \bar{\alpha}_1\dot{\phi} + \bar{\alpha}_2\phi + \frac{g\sin(\phi)}{\ell} + k_1\dot{e}_\phi + k_2 e_\phi - \hat{\delta}_{\phi d}) \tag{4.3}$$

$$u_2 = \frac{M}{\bar{k}}(\ddot{\ell}_d + \bar{\alpha}_3\dot{\ell} + \bar{\alpha}_4\ell - g\cos(\phi) + k_3\dot{e}_\ell + k_4 e_\ell - \hat{\delta}_{\ell d}) \tag{4.4}$$

where $\hat{\delta}_{\phi d}$ and $\hat{\delta}_{\ell d}$ are the estimation of $\delta_{\phi d}$ and $\delta_{\ell d}$, respectively.

Substitute (4.3), (4.4) into (4.1) and (4.2), we have the error dynamics as

$$\ddot{e}_\phi - k_1\dot{e}_\phi - k_2 e_\phi = \delta_{\phi d} - \hat{\delta}_{\phi d} \tag{4.5}$$

$$\ddot{e}_\ell - k_3\dot{e}_\ell - k_4 e_\ell = \delta_{\ell d} - \hat{\delta}_{\ell d} \tag{4.6}$$

From (4.5) and (4.6), we can see that if we can have accurately estimation of $\delta_{\phi d}$ and $\delta_{\ell d}$ we can drive the system to follow the desired trajectory by choosing appropriate feedback gains. The method of disturbance observer will be shown later.

Then I thought that why don't we lump all the system dynamic structure with the uncertainty and external disturbance as the system disturbance? According to this idea, we can rewrite (2.1) and (2.2) as

$$\ddot{\phi} = u_1 + \delta_{\phi d} \tag{4.7}$$

$$\ddot{\ell} = u_2 + \delta_{\ell d} \tag{4.8}$$

The controller can be chosen as

$$u_1 = \ddot{\phi}_d + k_1\dot{e}_\phi + k_2 e_\phi - \hat{\delta}_{\phi d} \tag{4.9}$$

$$u_2 = \ddot{\ell}_d + k_3\dot{e}_\ell + k_4 e_\ell - \hat{\delta}_{\ell d} \tag{4.10}$$

The system error dynamics is the same of (4.5) and (4.6).

We can see that the controller described in (4.9) and (4.10) need not knowing the system dynamic structure and the parameter value. Since the external disturbance and the unmodeled mechanism are also estimated, it should be more robust than the existing tracking methods. The controller is more compact and easier to derived by comparing with the existing methods. The disturbance estimation is listed in the following.

4.2 Disturbance Observer

In the following we would like to introduce the disturbance observer in which the structure of the disturbance need not knowing. Assume that a system can be represented by

$$\begin{aligned} \dot{x} &= Ax + Bu + g(y) \\ y &= Cx \end{aligned} \tag{4.11}$$

where u is an unknown function, $g(y)$ is a known function, B is a full column rank matrix.

The disturbance observer is chosen as

$$\dot{\hat{x}} = A\hat{x} + B\hat{u} + g(y) + K(y - \hat{y}) \tag{4.12}$$

where K is the observer gain vector selected in a way such that the eigenvalues of the closed-loop state matrix $A-KC$ are located at desired locations. The error dynamics of this observer can be obtained by subtracting (4.11) from (4.12)

$$\dot{e} = A_k e + B e_u \tag{4.13}$$

where $e = \hat{x} - x$, $e_u = \hat{u}(t) - u(t)$ and $A_k = A - KC$. The adaptive law for the estimation of the unknown input is chosen to be

$$\dot{e}_{uo}(t) = -B^T P e \tag{4.14}$$

$$\hat{u}(t) = \hat{u}_o(t) - K_o e \tag{4.15}$$

$$A_k^T P + P A_k = -Q \tag{4.16}$$

$$K_o A_k + K_o B K_o + B^T P = 0 \tag{4.17}$$

where $e_{uo} = \hat{u}_o(t) - u(t)$, $\hat{u}_o(t)$ is the estimated input before correction, $\hat{u}(t)$ is the estimated input after correction, K_o is the linear correction gain, and P and Q are positive definite matrices. The detail derivation of the updating law can be referred to [32].

Here we will show a simple example to demonstrate the validation of the proposed disturbance observer. Assume that a system can be represented by

$$\dot{z} = -z + w \tag{4.18}$$

where $w = \sin(5t)$ is a unknown disturbance.
Following the procedures listed from (4.14) to (4.17), we have the following results

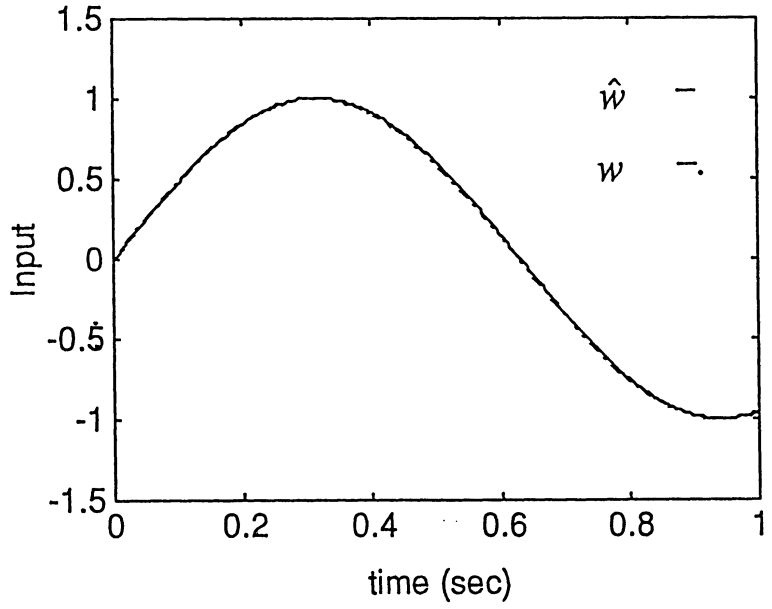

Fig. 2 Example of Input Estimation

We can see that the disturbance estimation is very accurate.

5. Simulation Results

In the following we will show the simulation results of different controllers. We will focus on the variation of the parameter α_m and k_m, since they will have much more significant effect on the system performance than the other parameters do. The nominal parameter values are assumed to be $\bar{\alpha}_m=\bar{k}_m=1.0$, $\bar{\alpha}_s=\bar{k}_s=0.65$, $\bar{\alpha}_f=\bar{k}_f=0.65$. The desired trajectories are $\phi_d=\frac{\pi}{2}\sin(2\pi t)+\pi$ and $\ell_d=0.2\sin(2\pi t)+1$.

5.1 Feedback Linearization

Here we will exam the controller designed by full-state feedback linearization. We will have three cases to study the performance of the controller based on the feedback linearization. First we assume that the parameter values of nominal system are the same of the true parameter values, i.e., $\alpha_m=\bar{\alpha}_m=k_m=\bar{k}_m=1.0$, $\alpha_s=\bar{\alpha}_s=k_s=\bar{k}_s=0.65$, $\alpha_f=\bar{\alpha}_f=k_f=\bar{k}_f=0.65$. The result is shown in Fig.3. We can see that the controller can drive the robot arm to follow a desired trajectory.

Since in real life we cannot exactly know the parameter values of the system. In Fig. 4, we assume that the true parameter values become $\alpha_m=k_m=0.54$, $\alpha_s=k_s=0.85$, $\alpha_f=k_f=0.45$. We can see that the system cannot follow the desired trajectory well. This case shows that feedback linearization controller will fail when the parameter is variant. In Fig.5, we assume that the true parameter values become $\alpha_m=k_m=0.35$, $\alpha_s=k_s=0.85$, $\alpha_f=k_f=0.45$. We can see that the performance even worse than case (2).

5.2 Robust Control

Here we will study two cases which are the same conditions of case (2) and (3) in section 5.1; one satisfies the controller criterion, and the other doesn't. We assume the maximum variation of α_m and k_m is 0.8, of α_s and k_s is 0.4, of α_f and k_f is o.4. The bound of the states is $5.5>\phi>0.5$, $20>\dot{\phi}>-20$, $2.0>\ell>0.5$, and $10>\dot{\ell}>-10$. ε is chosen as 0.01, $k_\phi=k_\ell=0.98$, $\eta_{\phi 0}=0.1$, $\eta_{\phi 1}=0.2$, $\eta_{\ell 0}=0.5$, $\eta_{\ell 1}=0.8$.

Fig. 6 is the case that $\alpha_m=k_m=0.54$, $\alpha_s=k_s=0.85$, $\alpha_f=k_f=0.45$. Comparing with Fig. 4 we can see it has much better performance than the feedback linearization controller does, but it has steady state error of the state ℓ.

When $\alpha_m=k_m=0.35$, the value of k_ϕ and k_t will greater than one, which contradict the requirement that k_ϕ, k_t <1. In Fig. 7 the true parameter values are assumed to be $\alpha_m=k_m=0.35$, $\alpha_s=k_s=0.85$, $\alpha_f=k_f=0.45$. We can see that for this case the robust controller doesn't work.

5..3 Adaptive Control

We can see that when $\alpha_m=k_m=0.35$, $\alpha_s=k_s=0.85$, $\alpha_f=k_f=0.45$, both methods of feedback linearization and robust control don't work. Right now we will try to use the adaptive control to control the system when $\alpha_m=k_m=0.35$, $\alpha_s=k_s=0.85$, $\alpha_f=k_f=0.45$. The result is shown in Fig. 8, we can see that it can follow the desired trajectory well.

In Fig. 9 we assumed that the system has unknown external disturbance which is assumed to be $50\sin(2\pi t)$. Under this situation, we can see from Fig. 9 that the adaptive observer fails to drive the system to the desired trajectory. It is because that when there is unknown external disturbance present, the estimated parameter value cannot converge to the true parameter value.

5..3 Disturbance Estimation Based Tracking Control

First we will apply the disturbance estimation based control (4.3), (4.4) which use the system dynamic structure. The true parameter values are $\alpha_m=k_m=0.35$, $\alpha_s=k_s=0.85$, $\alpha_f=k_f=0.45$. The result is shown in Fig. 10., we can see that it follows the desired trajectory well. Then the disturbance estimation based control (4.9) (4.10) without considering the system dynamic structure is applied in Fig. 11, which still shows a good tracking performance. The disturbance estimation based control without considering the system dynamic structure is also applied in Fig. 12 in which the system contained an unknown external disturbance assumed to be $50\sin(2\pi t)$. We can see that even there exists unknown external disturbance, it still works very well. It is expected, since the disturbance estimation can cancel the effect of the unknown external disturbance and unmodeled dynamics.

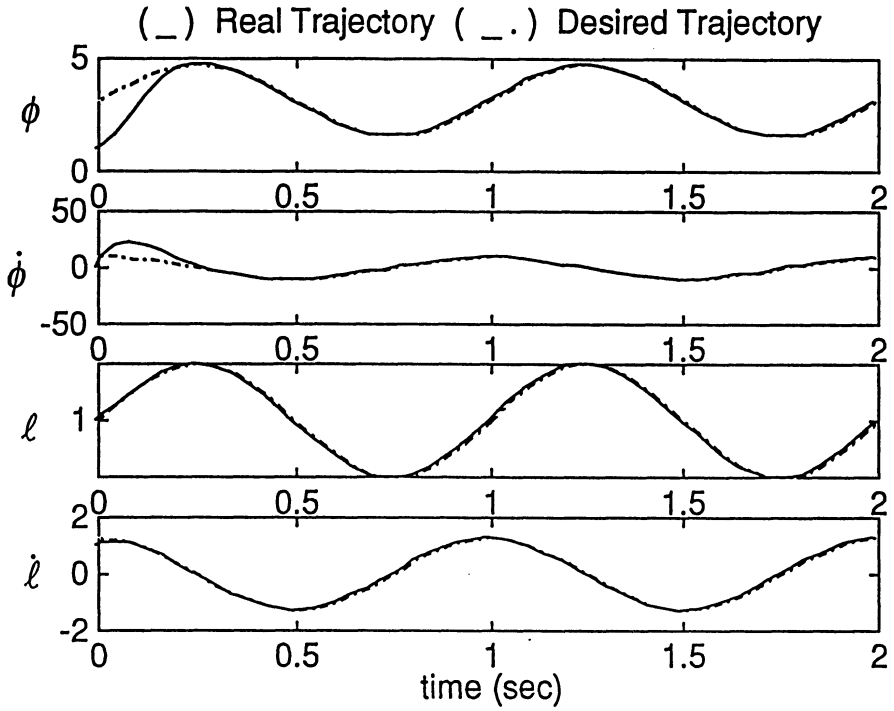

Fig.3 Feedback Linearization ($\alpha_m = k_m = 1.0$, $\alpha_s = k_s = 0.65$, $\alpha_f = k_f = 0.65$)

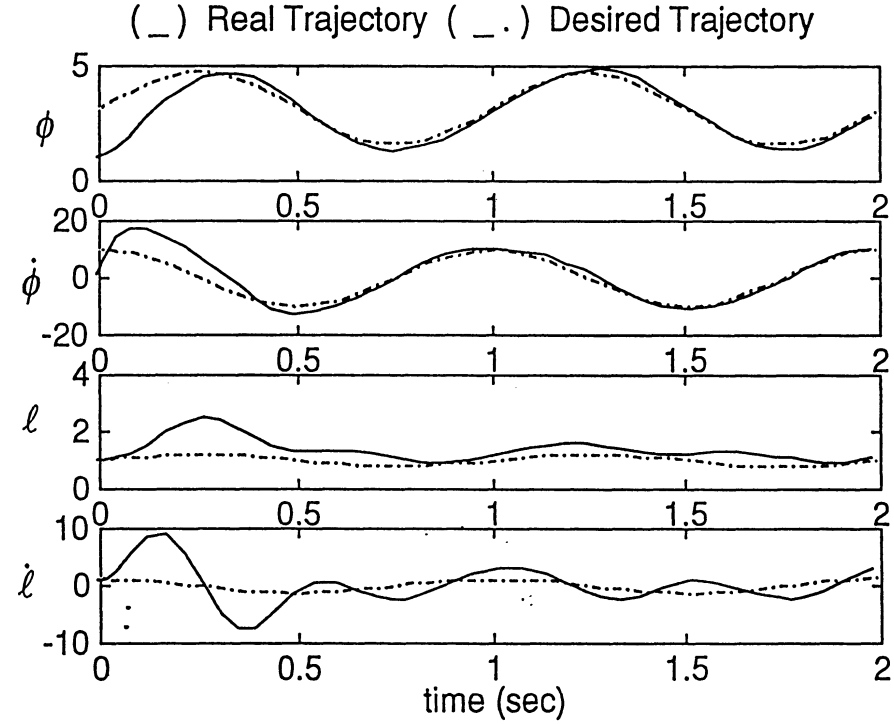

Fig. 4 Feedback Linearization ($\alpha_m = k_m = 0.54$, $\alpha_s = k_s = 0.85$, $\alpha_f = k_f = 0.45$)

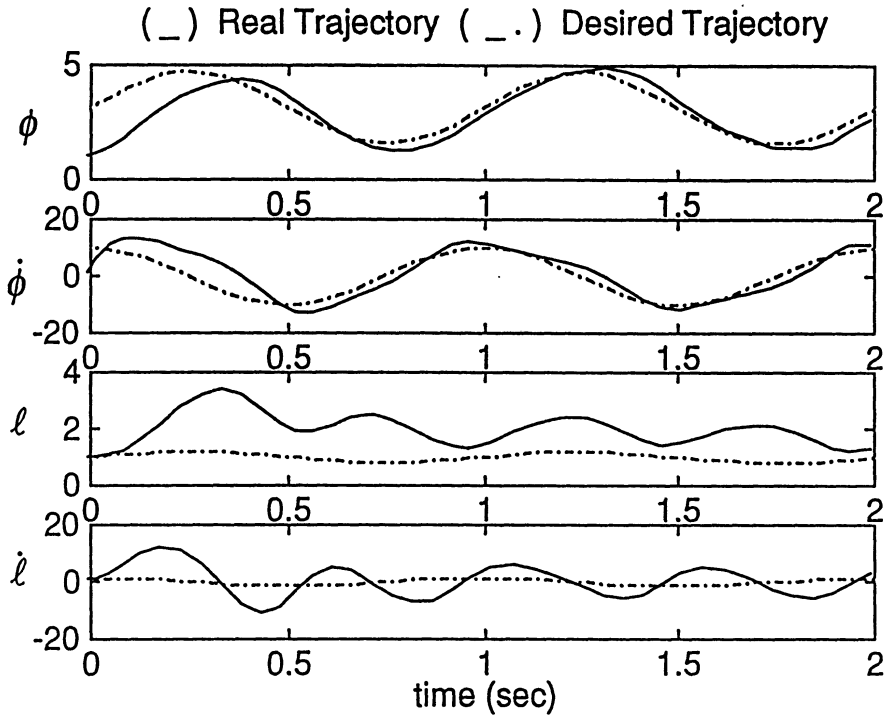

Fig. 5 Feedback Linearization ($\alpha_m = k_m = 0.35$, $\alpha_s = k_s = 0.85$, $\alpha_f = k_f = 0.45$)

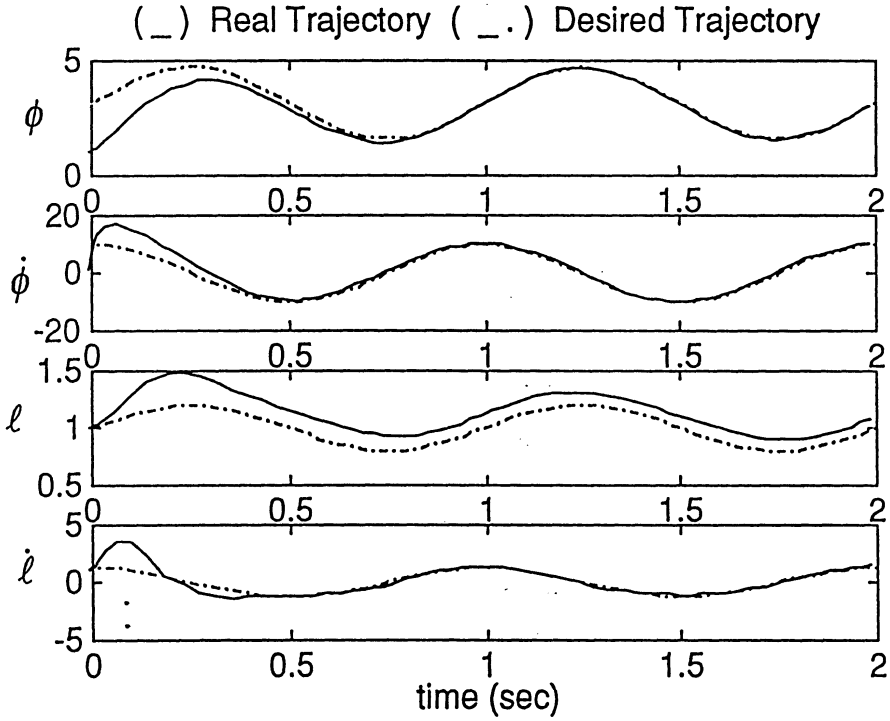

Fig. 6 Robust Control ($\alpha_m = k_m = 0.54$, $\alpha_s = k_s = 0.85$, $\alpha_f = k_f = 0.45$)

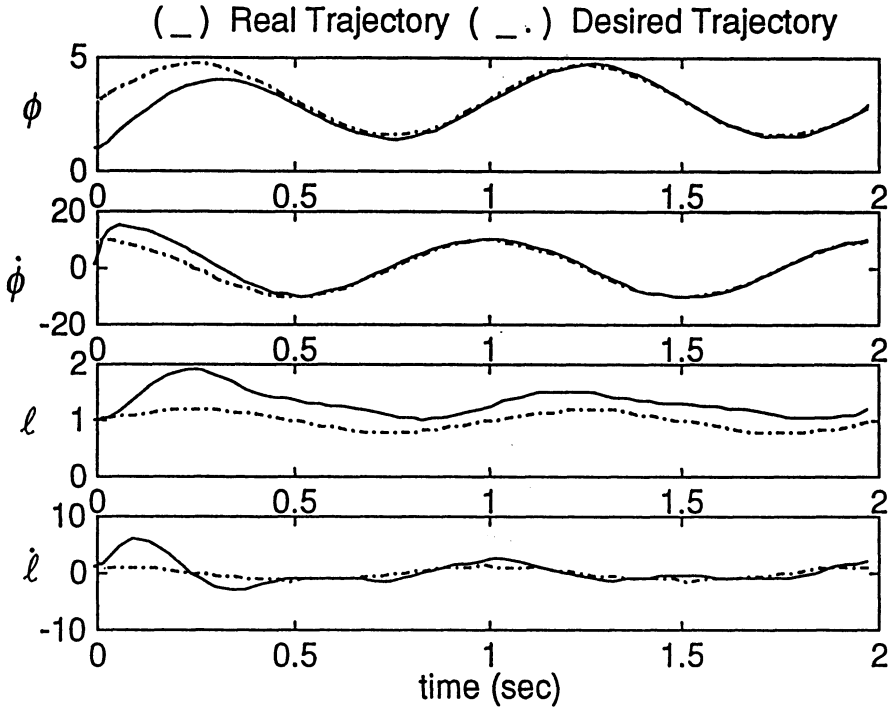

Fig. 7 Robust Control ($\alpha_m = k_m = 0.35$, $\alpha_s = k_s = 0.85$, $\alpha_f = k_f = 0.45$)

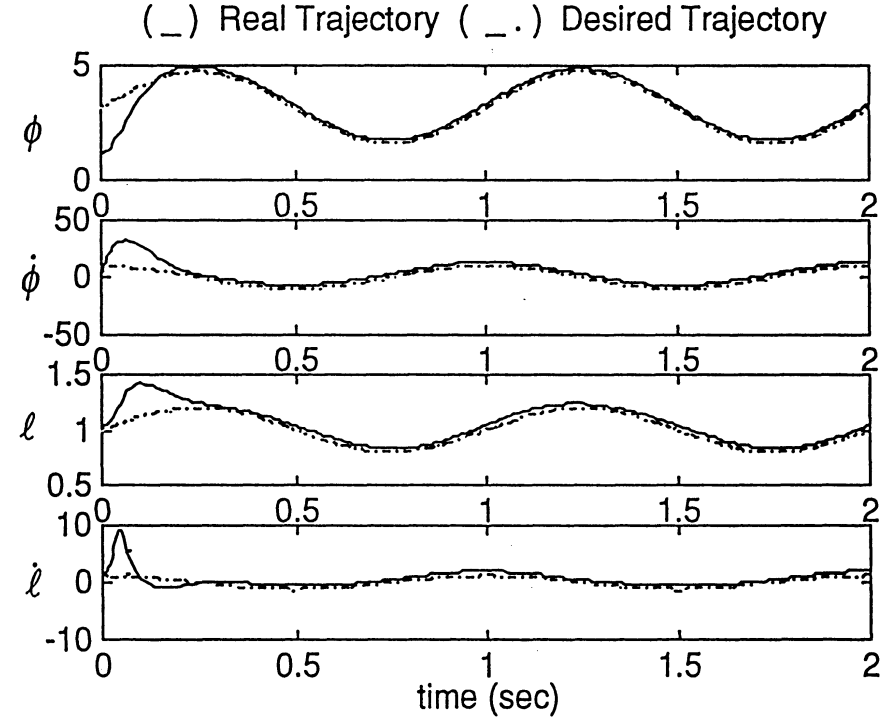

Fig. 8 Adaptive Control ($\alpha_m = k_m = 0.35$, $\alpha_s = k_s = 0.85$, $\alpha_f = k_f = 0.45$)

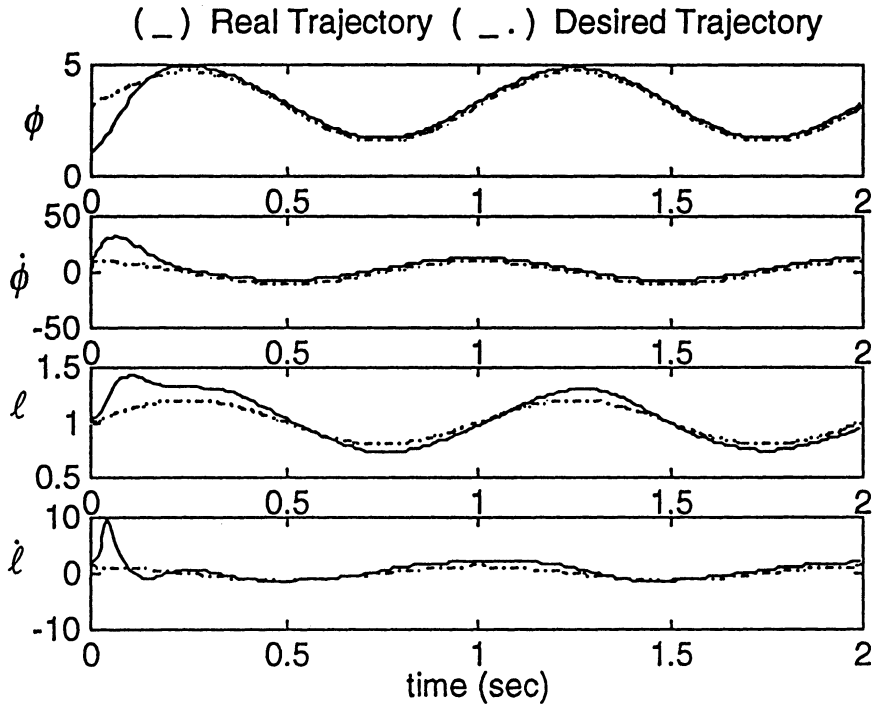

Fig. 9 Adaptive Control ($\alpha_m = k_m = 0.35$, $\alpha_s = k_s = 0.85$, $\alpha_f = k_f = 0.45$) with Unknown External Disturbance $50\sin(2\pi t)$

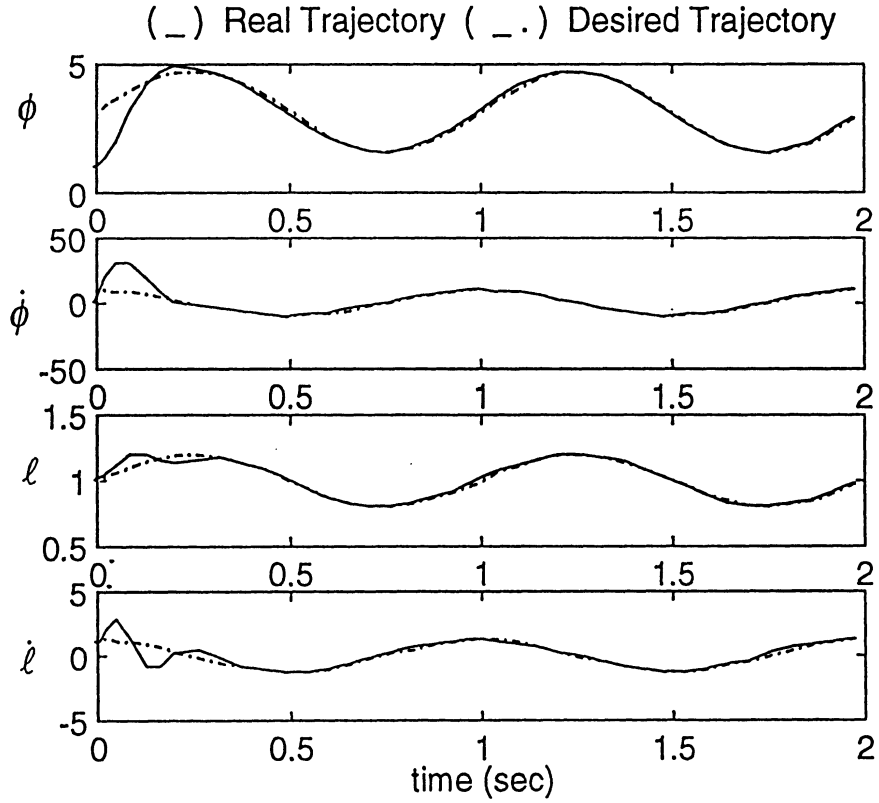

Fig. 10 Disturbance Estimation Based Tracking Control with Considering System Dynamic Structure ($\alpha_m = k_m = 0.35$, $\alpha_s = k_s = 0.85$, $\alpha_f = k_f = 0.45$)

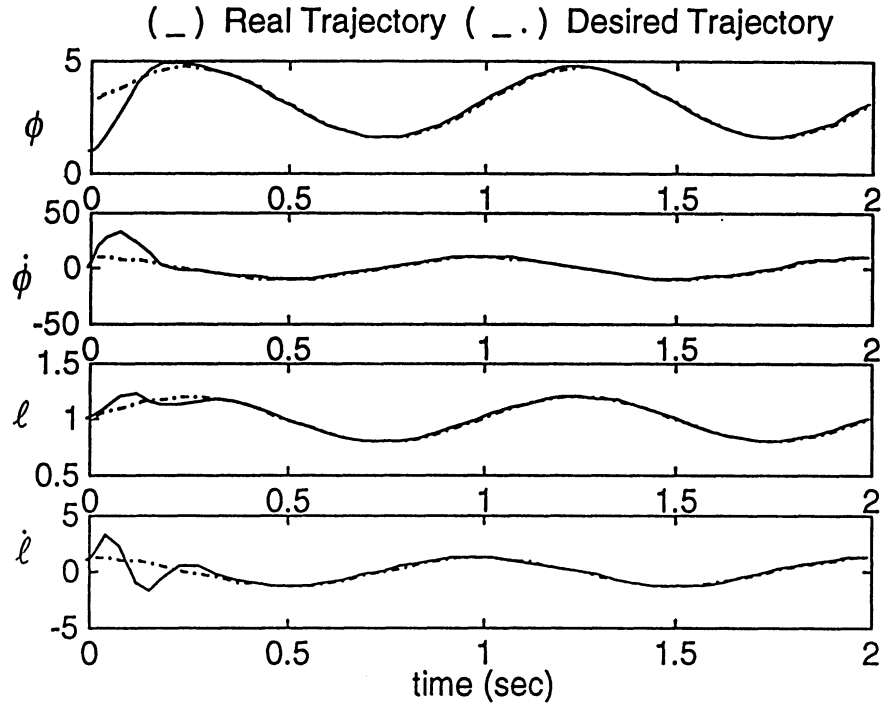

Fig. 11 Disturbance Estimation Based Tracking Control without Considering System Dynamic Structure ($\alpha_m = k_m = 0.35$, $\alpha_s = k_s = 0.85$, $\alpha_f = k_f = 0.45$)

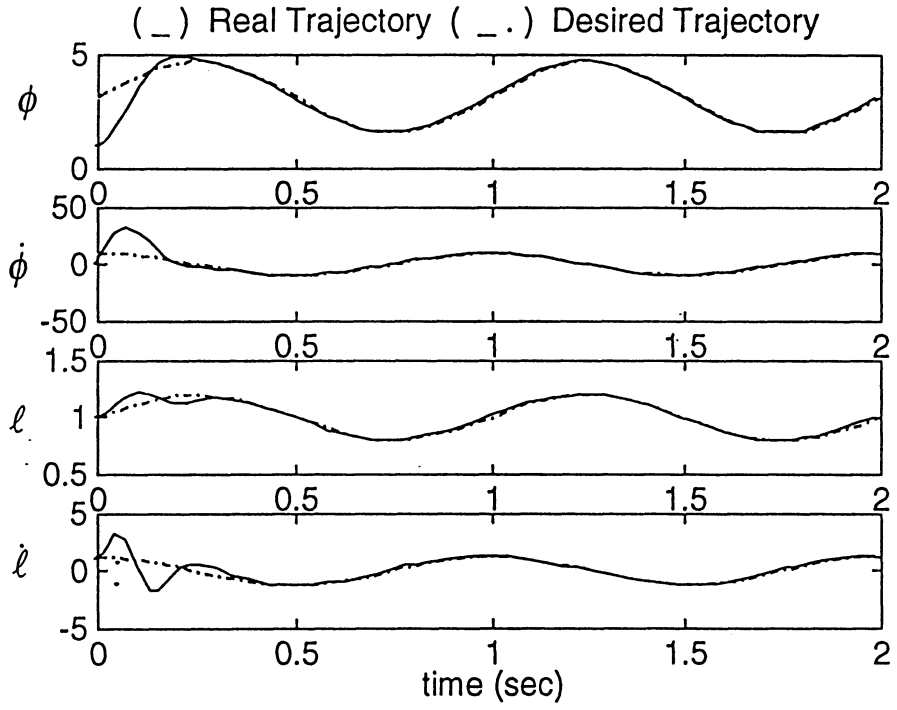

Fig. 12 Disturbance Estimation Based Tracking Control without Considering System Dynamic Structure ($\alpha_m = k_m = 0.35$, $\alpha_s = k_s = 0.85$, $\alpha_f = k_f = 0.45$). The System is Presented with the Unknown External Disturbance $50\sin(2\pi t)$

Conclusions

From the analysis and simulation results we can have the following conclusions.

1. For feedback linearization control, we need accurate system dynamic structure and parameter value or the controller will fail.

2. For robust control, we need accurate system dynamic model. The bound of parameter value and external disturbance should be known. The tracking accuracy will be sacrificed to maintain the robustness of system. If the system cannot satisfy the criterion of the controller, it will fail.

3. For adaptive control, we need accurate system dynamic model. The system input should be persistent excited to guarantee the convergence of the system parameter. If the system isn't persistent excited or some unmodeled mechanism and external disturbance present, it will fail.

4. The proposed tracking control method (disturbance estimation based tracking control) will overcome the aforementioned limitations. We don't need the system dynamic model and the parameter value. Since the controller don't need the information of system model, it will be a more robust method. And since the unknown external disturbance and unmodeled mechanism can be estimated, we don't have to sacrifice the tracking accuracy to assure the system robustness. The controller is compact and easy to formulate. From simulation results we can see that it can work well in trajectory tracking.

In this project we have applied several existing control methods to drive the telescopic robot arm to follow a desired trajectory. The situations that these methods will fail or succeed are investigated. And a different approach which overcomes the limitations of the investigated controller is successfully applied to do the tracking control.

Reference

1. Bedrossian, N. S., "Feedback Linearization of Robot Manipulator," J. Robotic System, vol. 12, pp. 517-530, 1995.

2. Xu, Z., and Hauser, J., "Higher Order Approximate Feedback Linearization about a manifold for Multi-Input Systems," IEEE Trans. Automatic Control, vol. 40, pp. 833-840, 1995.

3. Vandegrift, M. w., Lewis, F. L., and Zhu, S. q., " Flexible-Link robot Arm Control by a Feedback Linearization/Singular Pertubation Approach," J. Robotic System, vol. 11, pp. 591-603, 1994.

4. Chiasson, J., "Dynamic feedback Linearization of the Induction Motor," IEEE Trans. Automatic Control, vol. 38, pp. 1588-1594, 1993.

5. Charlet, B., Levine, J., and Marino, R., "Sufficient Conditions for Dynamic Feedback Linearization," SIAM J. Control Optimazitation, vol. 29, pp. 38-57, 1991.

6. Charlet, B., Levine, J., and Marino, R , "On Dynamic Feedback Linearization," System Control Letter, vol. 13, pp. 143-151, 1989.

7. Zribi, M., and Chiasson, J., "Position Control of a PM Stepper Motor by Exact Linearization," IEEE Trans. Automatic Control, vol. 36, pp. 620-625, 1991

8. Ilic-Spong, M, Marino, R., Peresada, and Taylor, D. G., "Feedback Linearizing Control of Switched Reluctance Motors," IEEE Trans. Automatic Control, vol. 32, pp. 620-625, 1987

9. Khalil, K., H., *Nonlinear Systems*, Macmillan Publishing Co., N. Y., 1992.

10. Sastry, S., *Nonlinear Systems: Analysis, Stability and Control*, MEAM 662 course pack.

11. Narendra, K. S., and Annaswamy, A. M., Stable Adaptive System, Prentice-Hall, Inc., N. J., 1989.

12. Craig, J. P., Hue, P., and Sastry. S.,"Adaptive Control of Mechanical Manipulators," Int. J. Rob. Res., vol. 6, no.2, pp. 16-28, 1987.

13. Slotine, J. and Li, W., "On the Adaptive Control of Robot Manipulators," Int. J. Rob. Res., vol 6., no 3., pp. 49-59, 1987.

14. Middleton R., and Goodwin, G., "Adaptive Computed Torque Control for Rigid Link Manipulators," System Control Letter, vol. 10, no. 1, pp. 9-16, 1988.

15. Bayard, D. and We, J., "New Class of Control Laws for Robotic Manipulators: Adaptive Case, " Int. J. Control, vol 47, no. 5, pp. 1387-1406, 1988.

16. Ortega, R., and Spong, M. W., "Adaptive Motion Control of Rigid Robots: A Tutorial," Automatic, vol. 25, pp. 877-888, 1989.

17. Spong, M. W., and Ortega, R., "On Adaptive Inverse Dynamics Control of Rigid Robots," IEEE Trans. Automatic Control, vol. 35, pp.92-95, 1990.

18.Sadegh, N., and Horowitz, R., " Stability and Robustness Analysis of a Class of Adaptive Controllers for Robot Manipulators," Int. J. Rob. Res., vol.9., no 3., pp. 74-92, 1990.

19.Johansson, R., "Adaptive Control of Robot Robot Manipulator Motion," IEEE Trans. Robotics and Automation, vol. 6, no. 4,, pp. 483-490 , 1990.

20.Kwon, D. S., and Book, W. J., "A Time-Domain Inverse Dynamic Tracking Control of a Single-Link Flexible Manipulator," ASME J. Dynamic Measurement Control, vol. 116, pp. 193-200, 1994.

21.Nicosia, S., and Tomei, P., "A Tracking Controller For Flexible Joint Robots Using Only Link Position Feedback," IEEE Trans. Automatic Control, vol. 40, pp.885-890, 1995.

22.Colbalugh, R., Glass, K., Seraji, H., "Performance-Based Adaptive Tracking Control of Robot Manipulators," J. Robotic System, vol. 12, pp. 517-530, 1995.

23.Reed, J., and Ioannou, P., "Instability Analysis and Robust Adaptive Control of Robotic Manipulator," IEEE Trans. Robotics and Automation, vol. 5, no. 3,, pp. 381-386 , 1989.

24.Schwartz, H., Warshaw, G and Janabi, T., "Issue in Robot Adaptive Control," Proc. American Control Conference, San Digeo., May., 1990.

25.Chen, Y., "Adaptive Robust Model-Following Control and Application to Robot Manipulators," ASME J. Dynamic Measurement Control, vol. 109, pp. 209-215, 1987.

26.Liao, T., Fu, L., and Hsu, C., "Adaptive Robust Tracking Control of Nonlinear Systems and with Application to a Robotic Manipulator," System Control Letter, vol. 15, pp. 339-348, 1990

27.Fu, L., "Robust Adaptive Decentralized Control of Robot Manipulators," IEEE Trans. Autom. control, vol. 37, pp. 106-110, 1992.

28.Guldner, J., and Utkin, V. I, "Sliding Mode Control for Gradient Tracking And Robot Navigation Using Artificial Potential Fields," IEEE Trans. Robotics and Automation, vol. 11, pp. 247-54 , 1995.

29.Stepaneko, Y., and Yuan., J., "Robust Adaptive Control of a Class of nonlinear Mechanical Systems with Unbounded and Fast-Varying Uncertainties," Automatic, vol 28., no. 2, pp. 265-276, 1992.

30.Colbalugh, R., Seraji, H., Glass, K., "Direct Adaptive Impedance Control Of Robot Manipulator," J. Robotic System, vol. 10, pp. 217-248, 1993.

31.Colbalugh, R., Seraji, H., Glass, K., "A New Class of Adaptive Controllers for Robot Trajectory Tracking," J. Robotic System, vol. 11, pp.761-772, 1994.

32.Liu, C. S., Peng, H., "Road Friction Coefficient Estimation For Vehicle Path Prediction, " !4th IAVSD Symposium on Dynamic of Vehicles on Roads and Tracks, Aug., 1995.

Control of Chaotic Systems: A Review

Christopher Lott
EECS662

December 11, 1995

Abstract

An overview of the recent developments in the control of chaotic systems is presented. Though the most visible of this work is the so-called OGY algorithm, there has been some other work in this area, which is also presented. Both system stabilization and targeting are discussed, and then some experimental work which attempts to confirm the theory is presented. Throughout, questions about originality and value of the work are touched upon. Finally, the lack of adequate simulation results is lamented over, and a long list of possible future work is enumerated.

1 Background and Motivation

1.1 Background

The staid old field of physical dynamics has gone through something of a revolution over the last twenty years. Through most of the twentieth century this established discipline, originally based on Newtonian physics, has been overshadowed by newer and more stimulating developments, such as relativity, quantum mechanics, and particle physics. Work in the area for decades consisted of touching up what had become an imposing, but apparently basically finished, theoretical structure. And this was true even though (or could it be *because*? there are few other cases in human thought where such a

beautiful conceptual and theoretical scientific understanding had been translated so successfully into a useful body of practical design tools. Probably no other area of scientific achievement has been of such benefit to mankind, making possible, for example, the Industrial Revolution.

Hence few were expecting profound new results to arise out of this old paradigm of scientific thinking. But scientists for many decades had also been musing about one of their great non-achievements: their inability to handle even some of the simplest of nonlinear equations analytically. The great Poincaré had attacked the problem head-on, and had ended up developing an extremely useful method for generating qualitative results on how many nonlinear systems develop over time. But he had failed to achieve a *systematic* solution method. Stanislaw Lem had likened the idea of studying nonlinear equations, to some still a great novelty of little scientific interest, to deciding to study "non-human animals". That is, the vast majority of real problems in the world start out nonlinear, and only through vast approximations do we make linear systems out of them. The fact remains: there are some systems in which nonlinearities lead to behaviors wholly unexplainable by *any* linearization technique (though bifurcations and chaos are among the best known today, parasitic oscillation in nonlinear electronic amplifiers is another, and has been known for decades).

It was only when some recent researchers, through a combination of fortunate experimental discoveries and then solid scientific groundwork, and surely under the influence of research environments in which the digital computer was first coming into its own, went back to the simplest of nonlinear systems and looked (or better yet, *computed*) more closely did it become clear how a brand-new science of deterministic dynamics was possible. In short, they then made some fascinating discoveries, the field of Chaotic Dynamics was born, and a plethora of new types of predictable dynamical behaviors came into the light.

A well-known popular retelling of the story behind the origins of chaos theory can be found in [Glei 87]. A good practical overview for engineers of the basic results of the new field can be found in [Moon 92].

Interest in nonlinear equations in many other areas of science and engineering has also been increasing. The linear theories all share the same strengths and weaknesses: they are wonderfully tractable, often allowing for entirely analytic solutions to important problems. For design problems where they are a sufficient approximation, they allow for the simplest and most powerful design tools, sometimes even taking such a straight-forward

algorithmic form that a few commands at a computer screen suffices to produce optimal solutions. But the nagging difficulty remains: there are just too many problems where the nonlinearities produce behavior that can't be captured by linear equations. Hence, attempts to deal analytically with systems of nonlinear equations of all types (not simply chaotic) has been a major focus of numerous researchers over some decades. In the field of Control, the current state of much of this research can be found in such standard textbooks as [Isid 95] and [Vidy 93].

The evidence that chaos might be something control engineers should at least be aware of continues to mount. [Goln 91] describes an experiment where a simple 2nd order system with a 1st order feedback signal showed chaotic behavior under some conditions. [Holm 82] describes a simple case where a ball bouncing on a sinusoidally vibrating table shows chaotic motion, and then goes on to discuss physical mechanisms for which this is a good model. Later authors showed how this theory can be used to improve the design of impact print heads [Tung 88], though this isn't the most pressing engineering need anymore. And somebody was so impressed that he actually built one and controlled it using the OGY algorithm [Vinc 95]. The point is that chaotic phenomena can occur in the simplest of systems, and engineers need to understand the basic mechanism, and how it might be controlled.

1.2 Motivation

A good engineer knows a good theory when she sees it. A good theory has beauty and potential, both. The beauty is often found in the *connections* between different areas of knowledge, and the entirely new perspective on well-known phenomena one gains, leading to the proclamation: *this is truth.* The potential is visualized as new design power: what new behavior does this allow me to model, predict and control, what old problem can I approach anew, in short, what can I *build* with it?

Many agree who study it with care agree: chaos theory has great beauty. The simplest of equations, over easily testable ranges of parameters, behaves in exceedingly complicated ways, yet with the proper application of the theory, even the most random looking outputs can be predicted and understood. So to the engineering mind, the next question is only too clear: what can we do with it? Is this theory actually good for something?

How common is chaos? That is, do the phenomena of chaos occur regularly enough that those interested in controlling real-world dynamic systems

must have an understanding of their mechanisms? Should we try to remove all chaotic effects from any given system? How do we know if some aspects of a system are behaving in a chaotic manner? Could chaos actually be useful if designed *purposefully* into a system?

Many, if not most, of the chaos researchers cited below believe that careful research over the past decade (the first studies where chaotic phenomena are being *looked* for) has shown that chaos is in fact quite common in real physical systems. For example, Moon [Moon 92] describes in some detail a variety of physical systems in which chaos has been observed (e.g. pendulums, rotors, comets, planetary orbits, electrical circuits, biological signals, turbulent phenomena). The practical question for each of these cases is whether or not the chaos in question is objectionable (perhaps it is of quite small magnitude, for example), and if so, whether it is feasibly controllable. We will not attempt to fully answer this question here, but we will give some indication as to the types of practical areas researchers are looking at today where influence of chaotic dynamics is believed (by some) to have a clear benefit, and what kind of success they are having doing so.

What do we mean by "controlling" chaos? We might mean that when chaos is detected in a system, we perform whatever steps is necessary to remove it. Usually, this has meant we drastically change the system itself, if this is possible (analogous to when your high-frequency circuit is oscillating, you move your components around, rather than try to figure out what exactly is going on). Often, this isn't possible or desireable (it could be a planetary orbit, or it could be the print head of a dot-matrix printer, whose dynamics you can't very well change). We might think to try and fully feedback linearize the system, if this is possible, and then see if we can stabilize it to remove the strange chaotic flows. But this might require extreme control effort, and we might also not know the system parameters well enough to make this feasible.

We also might mean not changing the system dynamics in any fundamental way, but instead only applying small perturbations (control) to the system (such as little thrusts to our cruising rocket) which will have the effect of removing the undesired traits of chaotic orbits (e.g. wandering over each point in the attractor, trajectory sensitivity to initial conditions), but still allowing mostly the natural dynamics to flow. This is the challenging problem which most of the results in this paper tackle.

2 Approaches to Control of Chaos

In discussing chaotic control, we must differentiate between *stabilization*, *trajectory generation*, and *targeting*. If our goal is to simply ensure long-term stability, we can use Lyapunov or other techniques, and the chaotic nature of the system doesn't really matter. But as is well-known in nonlinear control, systems with unstable fixed points can sometimes be locally linearized and stabilized, to the point where future dynamics are entirely controlled, so long as the trajectory doesn't deviate too far from the fixed point. This is the type of stabilization we will refer to here.

Trajectory generation, generally a much harder problem, refers to finding time-paths of the system close to a desired path. A related problem is that of *targeting*, where we have a desired destination at some time in the future, but we don't care how we get there. One can imagine that targeting can be used for trajectory generation, where we just simply target at each time step, and hence produce the desired trajectory, but more general targeting allows for arbitrary paths before the target is reached. That is, I can target a point I wish to get to, and then the controller can figure out how long it will take him to move the system there. In general for chaotic systems without very strong control, input trajectory generation is basically an intractable problem, as the natural chaotic dynamics are unlikely to lead in any given desired direction. But targeting, even in the presence of noise, is feasible, as will be shown below.

We start our study of current techniques for chaotic control with the work of a group at the University of Maryland which has gained much notoriety, and in fact is responsible for the current widespread use of the term *chaos control*.

2.1 The OGY Method and its Kin

2.1.1 OGY Stabilization Theory

For better or worse, much of the interest over the past five years in the control of sytems with chaotic dynamics arises from reaction to the original research work of Ott, Grebogi, and Yorke [Ott 90]. The resulting method has thus come to be know as the OGY method. In this short paper the authors spell out results both simple, and yet perhaps also a bit subtle. Their main insight is that once a dynamic system has entered a chaotic state, it now has

an infinite number of embedded unstable fixed points. An example of how this occurs can be imagined by considering the well-known logistic equation:

$$x_{n+1} = \lambda \ x_n(1 - x_n) \tag{1}$$

As λ increases in the range $3 < \lambda < 4$, the system progressively bifurcates, where at each bifurcation the previous stable fixed point becomes unstable (i.e. $\mid slope \mid > 1$), and a new stable fixed point at twice the period comes into being (see the Appendix for a description of bifurcation for equation 1). At the point beyond where the system goes chaotic, there are an infinite number of these unstable fixed points of varying periodicities, and a chaotic dynamic sequence is simply one where the orbit is cycling in the neighborhood of these numerous fixed points. Understanding this process as it occurs in the logistic equation allows us to understand it in other nonlinear systems as well, as the underlying mechanism and behavior are virtually the same in these higher dimensional cases. The main difference is the presence of both stable and unstable directions at fixed points in the problems with higher dimension.

So then the following simple little insight is possible: when even a chaotic dynamic system is near a fixed point, it will tend to spend a bit of time there before flinging off to other portions of the attractive basin (assuming, of course, a reasonably *smooth* nonlinear function), just as a ball will always roll off of a hill, but is slower near the top. Fig. 1 plots Eq. 1, where the initial condition is calculated to be precisely at the period one fixed point, though there is a small error due to finite precision round-off. This small error builds up over time, to the point that by iteration 80 the trajectory has again become chaotic. But note also that at later times there tend to be clumps of points near the fixed point, and that the orbit itelf tends to return to neighborhoods of the fixed point. The OGY control method is based on these latter points.

The ideas can be summarized as:

1. Chaotic orbits are ergodic, in the sense that all points in the basin of the attractor are eventually visited in the unperturbed dynamics.

2. No matter how small a finite control we are willing to make, the orbit will *eventually* come close enough to the fixed point that our control will be able to bring it into the fixed point.

3. Once the orbit is nearly on the fixed point, it takes only minimal control energy to keep it there.

4. Because there are an infinite number of such fixed points, each with different orbits associated with them, it is possible, with very small control effort, to stabilize the system in a wide variety of orbits by merely turning on and off control to stabilize different fixed points.

In a nutshell, that's it. Really. In [Ott 90] they also provide one way to stabilize the fixed point, but it's clear that this method is a bit *ad hoc*, and anyway it's unlikely control engineers need to be taught how to do this. The only really new derivation they perform is a formula for estimating how long we must wait in a given system for the chaotic trajectory to get within a certain distance of our fixed point of interest. Using previous work of their own, they show that the probability distribution of this time has the form:

$$P(\tau) \approx e^{\frac{\tau}{<\tau>}} \tag{2}$$

where the exact formula and ¡τ¿ are functions of a given problem.

The ability to switch from one orbit to another with minimal control effort might be considered the one really important insight in the OGY work, though others before them had similar conceptions (e.g. see [Jackl 91] or [Mohl 73], Ch. 2). Immediately it is intriguing to consider what sort of systems we can think of where we might use the ability to make large changes quickly and with little energy. But the authors go on (and one senses perhaps a trace of that ol' Cold Fusion variation on Pascal's wager):

> Thus, when designing a system intended for multiple uses, purposely building chaotic dynamics into the the system may allow for the desired flexibility. Such multipurpose flexibility is essential to higher life forms, and we, therefore, speculate that chaos may be a necessary ingredient in their regulation by the brain.

The idea of *purposefully* building chaotic dynamics into a system, to take advantage of large potential behavior change with minimal control effort, is a very intriguing one. The engineer's alarm bells go *ring, ring*! But perhaps *bravado* speculation of the more novel and, to be kind, *unproven* sort should be relegated to to the less accessible portions of the document, say, after the list of citations, i.e. once the science is over.

Later work by the same authors, in collaboration with two others, provides the most clarifying description of the method [Rome 92]. One gets the feeling while reading this paper that the authors from two years previous have now gotten together with some control engineers, and together they finally understand what they're doing. Instead of the *ad hoc* stabilization design procedure shown previously, they perform Jacobian linearizations around fixed points, discuss linear controllability and pole placement, and then proceed to stabilize any desired fixed point in this manner. The only difference from what control engineers can presumably do in their sleep is the discussion of the underlying chaotic nature of the dynamics, again allowing only very small controls to be used, as the trajectory is guaranteed to arrive "close" to the fixed point if we just wait long enough. The bottom line on the work is that they have coupled together very well-known results on Jacobian linearization from nonlinear control theory (which works whether a system is chaotic or not) with some of the more recent advances in the understanding of nonlinear dynamical systems, specifically chaos theory. The result is a method of control which uses some facts from chaos theory (ergodicity, multiple stable fixed points) to show how the system evolves over time *before* control is applied, so as to allow the control effort to be applied only when it is most *effective*. That is , you should wait until the trajectory gets near to the desired fixed point, which it is guaranteed to do, eventually. If you can't wait, you can use the targeting ideas, which are spelled out below, but even these can't get you to the target quicker than some pre-specified amount of time.

To get the basic idea of how this control can be done, Fig. 2 plots a MATLAB simulation of a chaotic system, the logistic equation, where the parameter λ is slightly adjusted as the control parameter (this is a convenient way to formulate the problem, and it is equivalent to nudging or shepherding the current x value). The plot alternates between chaotic behavior (as at the beginning) and controlled behavior. In the first controlled strip, the system is linearized around the fixed point for period 1, and a pole is placed at .9 in the digital frequency domain. This control only turns on when the point has come close enough to the fixed point that it can be easily brought in (in this simulation, the point must be within .05 of the fixed point). As can be seen, the system pretty quickly converges to the fixed point, and then is stabilized there. Rather trivial? Yes.

The other two bands are for higher order periods, being periods 2 and 8, respectively. The difference here is that a different linearization point is

chosen (say, one of the two for the period 2 case), and the feedback and capture range are applied to this point. The period 8 case is even more interesting. Note that even when the point is stabilized, we are only providing control inputs when the point is at the stabilized fixed point, i.e. every 8th time point in the map. Hence, this very simple method is extremely sensitive to noise, and was even somewhat troublesome to make work in the noiseless case. In [Rome 92] a different, more robust method to improve the performance of locking onto higher order orbits is given, which essentially consists of breaking up, say, an n-orbit control into n dynamic terms, and then apply this control at each time point, thus reducing the effective noise at each control input.

A major remaining question in all this, though, is how exactly the estimation of the system dynamics is to be performed if they aren't known *a priori*. In the above simulation, the logistic equation was simply known, and the fixed points calculated. If this type of technique is ever to be practical, we must have a way of estimating the fixed points of the attractor just from the measured data. In the original OGY paper [Ott 90] it is pointed out that the well-known (in chaos circles) delay-coordinate embedding method can be used to estimate the local eigenvectors and eigenvalues of the Jacobian linearization of the fixed point. It is an interesting question as to how this relates to nonlinear system identification methods in control theory.

In related work, [Dres 92] modify the OGY method to improve it when used with the time delay-embedding method of experimental practice. This work, often cited, seems to superceded with the summary paper [Rome 92]. [Auer 92] is a later OGY work where the system identification and control algorithms are modified to allow for much higher-dimensional systems. The form of the algorithm is unchanged, however, and the basic idea is to only model those dimensions of the underlying space that are actually chaotic. It turns that many, if not most, chaotic attractors are only of a few dimensions, but they are embedded in a higher dimensional space of more stable dynamics. A more recent paper [Blei 95]

2.1.2 OGY Stabilization Experiment

After the original OGY paper [Ott 90] there began a flurry of experiments to attempt to show experimentally what had been proposed theoretically (though given the simplicity of the theory, it is hard to imagine how the basic ability to stabilize these systems could have been so in doubt). The

biggest question was clearly how well the identification of chaotic phenomena worked in real life, so that the simple feedback algorithm would be sufficient to stablize certain orbits. We will only touch on some of the more important examples of claimed success of controlling chaos in the lab. The review article [Shin 93] gives a nice listing of most of these experiments, though as it is written by the interested parties, it is not unbiased.

Fast on the heels of the original paper was [Ditt 90], which used the OGY technique to control a simple iron sheet coupled to a magnetic coil [Ditt 90]. They claimed to be the *first to control chaos*! Hunt controlled higher period orbits with his resonator circuit made with a nonlinear diode [Hunt 91]. OGY has been used to control an electrochemical cell [Schi 94], and a ball to bounce at a fixed height [Vinc 95] (though see [Holm 82] and [Pust 78] for the basic theory).

But by far the most well-known and, shall we say, *loud* proclamations concerning control of chaos have been heard from biology researchers, who claim to be able to control the regularity of heartbeats [Garf 92], to the "naturally chaotic" signals in the brain [Schi 94]. These experiments have been performed on rabbit hearts and rat brains, respectively, and the idea that if can regulate these types of signals we might be able to control heart attacks and epilepsy has many corners abuzzing. But for a report which questions the very fact that chaos is being controlled at all, see [?], where the algorithm is applied to a simple deterministic plus random noise signal, with very nice results.. And though this paper is not down on the idea of trying to control these signals, and in fact sees the possibilities of such control as being potentially quite useful, we are left staring the matter in the face, wondering: then what exactly is *new* here? Why haven't you done this *before*?

What are we to make of these experiments? First, none of them seem to be anywhere near solving practical problems. Though it can be argued that this is because the field itself is in its infancy, it would be nice if *someone* would come up with some examples of chaotic systems that really *need* to be controlled, besides rat brains (are we really going to allow real-time estimation of fixed points of human brain signals?). Second, it is still unclear which of these signals actually *are* chaotic, and which are just *noisy*. The current criteria for chaos might not be very good at distinguishing noise from chaos. After all, applying nice linear feedback to noise will also stabilize the noise.

2.1.3 OGY Targeting Theory

A more interesting set of ideas to come out of the OGY school has been the idea of targeting future values of the state. The idea is that a very small control now can potentially have a big benefit in the future, given the positive Lyapunov exponent of a chaotic system. So you simulate the sytem running into the future, until you get a range which fully spans the space (i.e. measure 1). You can then pick a local initial condition which will lead to this final results.

Fig. 3 shows how an initial very small difference between points grows over time. We just take where we want to go, and then find the nearest point in a mesh between the two extreme points in a plot like this, and we judge the point locally to achieve the proper starting point. In the presence of noise, we can nudge at each time step.

The major reference works on this topic are [Shin 90], [Shin1 92], [Shin2 92], and [Kost 93].

2.2 The Work of Hübler and Jackson

This is a whole other tradition of control of chaotic systems which does not include any feedback, just sinusoidal input signals. Some major reference works are [Jack 90], [Jack1 91], and [Jack2 91].

2.3 Stochastic Control

This is an interesting counterpart to the other ideas, and again it is open loop. This author [Fahy 92] has found that in certain chaotic systems, if

2.4 Control of Turbulence

Other work that has been going on entirely independently of the OGY school on control of chaotic phenomena has been focussed on the very real engineering problem of turbulent flow at at fluid boundary layers. The idea is that if you can adequately model turbulence as deterministic dynamics, then by proper control (say on the surface of a wing) you might be able to reduce the drag on the wing (a prospect with some amazing potential economic benefit, it seems clear).

It is thought that the major extra drag of turbulent flow occurs due to the *bursting* effect, which is modelled as a jump (aka heteroclinic cycle) from one unstable fixed point to another. With control, these researchers try to slow down these jumps (in some respects similar to the OGY method)

The results they've achieve have been quite promising in simulation when there is no noise, and a bit less promising, though not hopeless, in the presence of noise. And there are major outstanding issues, such as system identification, which need to be solved before anything like this could be practical.

The major references on this very recent work include [Coll1 94], [Coll2 94], and [Coll 95].

To give some perspective on how some other scientists view the OGY work, we will quote one of the main turbulence researchers (also revealing perhaps a bit of youthful ardor):

> The shepherding technique to derive a stabilizing controller is at least several decades old, although many in the dynamics community incorrectly attribute it to the often cited 1990 paper by Ott, Grebogi, and Yorke [Ott 90] who use the technique to stabilize linearly controllable saddle points in two dimensional maps. Nearly twenty years before the original "OGY" paper, Mohler, in his monograph on bilinear systems [Mohl 73], used a similar technique on much more difficult problems. Unlike OGY, who suggest that their work might be the way in which the brain regulates itself . . ., Mohler makes not such dramatic claims but casually presents the technique in a manner which suggests that many others before him had done similar things. [Coll 95]

2.5 harmonic balance

It turns out that harmonic balance methods can be used to detect for chaotic phenomena. See the references [Gene 92] and [Atha 95].

3 Simulation

The only simulation results presented in this paper are in Figs 1-3. These have already been explained, are for the logistic equation 1, and include stabilization and targeting results. I have some other patchy simulation

results, but nothing that is more illuminating than the results presented here.

I really wanted to try and simulate at least a major subset of the following work (using MATLAB):

- Basic OGY stabilization and targeting algorithms for:
  - Logistic equation
  - Lorenz equations
  - Double kicked-rotor equations
  - Ball bouncing on a vibrating plate
- Some quick simulations of the stochastic trajectory tracking of [Fahy 92]
- The periodic control of [Jack 90], at least using the logistic equation
- Compare the targeting ideas of OGY with the cost and accuracy of performing the same work with other methods, most notably:
  - Jacobian linearization control
  - Full-state linearization control
- Try out some techniques for the detection of chaotic systems, and then compare them in detecting systems of different types, including real chaotic systems in noise, and just non-chaotic systems that are very noisy. This work motivated by [Chri 95].
- Perform all of the above simulations with varying noise sources, to try and get a feel for performance robustness.

Sure would be nice to have had more time to simulate these systems properly. Yup, sure would have been nice.

4 Conclusion and Looking Ahead

We have looked at a few different aspects of chaos control, which is in reality a very big field. Chaos control is a work-in-progress, and is sure to become a larger part of control in the future.

My hopes:

I would like to be able to complete all the work in the simulation section at some point in the future.

I would like to look at the relatin of delay coord embedding and nonlinear system identification.

I would like to compare trajectory destination generation comparison of:

- chaotic trajectory vs. feedback lin LQR
- lorenz attract
- double kicked-rotor

Are the methods for detecting chaos in physical systems reliable? It would be interesting to test this.

We need more comparison of what's gone on in the past in control with what's happening now.

I would like to find practical uses of these ideas!!

In what sorts of systems would building in chaos provide a benefit?

Whatever creativity and technical merits one ascribes to the OGY work, it is impossible not to see the service they have performed in bringing the issue of control of chaotic systems to the attention of researchers in many fields. By creating the buzzword *chaos control*, their work has spurred many others on to share the research dollar pie, as prestige and buzzwords are the bread and butter of dollar-distributing bureaucrats. Hence, we have research in scientific journals of the highest-repute reporting experimental results using techniques that *could* have been performed many years ago, if these same researchers had simply spoken more carefully with the control theorists (or vice versa). By bringing up these issues in the traditionally more *scientific* journals, rather than merely the *engineering* ones, OGY has made researchers in these other disciplines (and most notably biology) realize the possibities of control for their own disciplines, which are inherently extremely nonlinear. This is the true value of the OGY work.

It would be interesting for control theorists themselves to become more involved in the problems of these other disciplines, in as they can be modelled as tractable nonlinear systems, and in as control has a useful role to play in solving their problems.

References

[Atha 95] A. Athalye and W. Grantham, "Notch Filter Feedback Control of a Chaotic System", *Proceedings of the American Control Conference*, p.837-841, June 1995

[Auer 92] D. Auerbach, C. Grebogi, E. Ott, J. Yorke, "Controlling Chaos in High Dimensional Systems" *Physical Review Letters*, 69(24):3479-3482, 1990

[Blei 95] M. Bleich, J. Socolar, "Stability of Periodic Orbits Controlled by Time-Delay Feedback", *LANL Nonlinear Science Archive, http://xyz.lanl.gov/list/chao-dyn/9510019*, Oct. 1995, to appear in *Physics Letters A*

[Chri 95] D. Christini and J. Collins, "Controlling Neuronal Noise Using Chaos Control", *LANL Nonlinear Science Archive, http://xyz.lanl.gov/list/chao-dyn/9503*, March 15, 1995

[Coll1 94] B.D. Coller, P. Holmes, J. Lumley, "Control of Noisy Heteroclinic Cycles", *Physica D*, 72:135-160, 1994

[Coll2 94] B.D. Coller, P. Holmes, J. Lumley, "Control of Bursting in Boundary Layer Models", in A.S. Kobayashi, editor, *Mechanics USA 1994, Proceedings of the Twelfth US National Congress of Applied Mechanics*, pp. s139-s143, App. Mech. Rev., 1994

[Coll 95] B.D. Coller, *Suppression of Heteroclinic Bursts in Boundary Layer Models*, Ph.D. thesis, Cornell University, 1995

[Ditt 90] W.L. Ditto, S.N. Rauseo, M.L. Spano, "Experimental Control of Chaos", *Physical Review Letters*, 65(26):3211-3213, 1990

[Dres 92] U. Dressler and G. Nitsche, "Controlling Chaos Using Time Delay Coordinates" *Physical Review Letters*, 68(1):1-4, Jan. 1992

[Fahy 92] S. Fahy and D.R. Hamann, "Transition from Chaotic to Non-chaotic Behavior in Randomly Driven Systems", *Physical Review Letters*, 69(5):761-764, Aug. 1992

[Garf 92] A. Garfinkel, M. Spano, W. Ditto, J. Weiss, "Controlling Cardiac Chaos", *Science*, vol 257:1230-1235, Aug. 1992

[Gene 92] R. Genesio and A. Tesi, "Harmonic Balance Methods for the Analysis of Chaotic Dynamics in Nonlinear Systems", *Automatica*, 28(3):531-548, 1992

[Glei 87] James Gleich, *Chaos: the Making of a New Science* ?????, 1987

[Goln 91] M. Golnaraghi and F.C. Moon, "Experimental Evidence for Chaotic Response in a Feedback System", *Journal of Dynamic Systems, Measurement, and Control*, vol 113:183-187, March 1991

[Holm 82] P.J. Holmes, "The Dynamics of Repeated Impacts with a Sinusoidally Vibrating Table", *Journal of Sound and Vibration*, 84(2),173-189

[Holm 85] P.J. Holmes, "Dynamics of a Nonlinear Oscillator With Feedback Control I: Local Analysis", *Journal of Dynamic Systems, Measurement, and Control*, vol. 107, 159-165, June 1985

[Hunt 91] E. R. Hunt, "Stabilizing High-Period Orbits in a Chaotic System: The Diode Resonator", *Physical Review Letters*, 67(15):1953-1955, Oct. 1991

[Isid 95] Alberto Isidori, *Nonlinear Control Systems*, 3rd. Ed., Springer, 1995

[Jack 90] E.A. Jackson and A. Hübler, "Period Entrainment of Chaotic Logistic Map Dynamics", *Physica D*, 44:407-420, 1990

[Jack1 91] E.A. Jackson, "On the Control of Complex Dynamic Systms", *Physica D*, 50:341-366, 1991

[Jack2 91] E.A. Jackson, "Controls of Dynamic Flows With Attractors", *Physical Review A*, 44(8)4839+, Oct. 1991

[Kost 93] E. Kostelich, C. Grebogi, E. Ott, J. Yorke, "Higher-Dimensional Targeting", *Physical Review E*, 47(1):305-347, Jan. 1993

[Mohl 73] R.R. Mohler, *Bilinear Control Processes: with Applications to Engineering, Ecology, and Medicine*, Academic Press, 1973

[Moon 92] Francis. C. Moon, *Chaotic and Fractal Dynamics*, Wiley Interscience, 1992

[Ott 90] E. Ott, C. Grebogi, J.A. Yorke, "Controlling Chaos", *Physical Review Letters*, 64(11):1196-1199, 1990

[Parm 93] P. Parmananda, P. Sherard, R.W. Rollins, H. Dewald, "Control of Chaos in an Electrochemical Cell", *Physical Review E*, 47(5):R3003-R3006

[Pust 78] L. Pustyl'nikov, "Stable and Oscillating Motions in Nonautonomous Dynamical Systems. II", *Trans. Moscow Math. Soc.*, Issue 2, p. 1+, 1978

[Rome 92] F.J. Romeiras, C. Grebogi, E. Ott, W.P. Dayawansa, "Controlling Chaotic Dynamical Systems", *Physica D*, 58:165-192, 1992

[Schi 94] S. Schiff, K. Jerger, D. Duong, T. Chang, M. Spano, W. Ditto, "Controlling Chaos in the Brain", *Nature*, vol 370:615-620, Aug. 1994

[Shin 90] T. Shinbrot, E. Ott, C. Grebogi, J. Yorke, "Using Chaos to Direct Trajectories to Targets", *Physical Review Letters*, 65(26):3215-3218, Dec. 1990

[Shin1 92] T. Shinbrot, E. Ott, C. Grebogi, J. Yorke, "Using Chaos to Direct Orbits to Targets in Systems Describeable by a One-Dimensional Map", *Physical Review A*, 45(6):4165-4168, March 1992

[Shin2 92] T. Shinbrot, C. Grebogi, E. Ott, J. Yorke, "Using Chaos to Target Stationary States of Flows", *Physics Letters A*, 169:349-354, 1992

[Shin 93] T. Shinbrot, C. Grebogi, E. Ott, J. Yorke, "Using Small Perturbations to Control Chaos", *Nature*, Vol 363, p.411-417, June 1993

[Tung 88] P.C. Tung and S.W. Shaw, "A Method for the Improvement of Impact Printer Performance", *Transactions of the ASME*, Vol. **110**, October 1988

[Vidy 93] M. Vidyasagar, *Nonlinear Systems Analysis*, 2nd edition, Prentice-Hall, 1993

[Vinc 95] T. Vincent, "Controlling a Ball to Bounce at a Fixed Height", *Proceedings of the American Control Conference*, p. 842-846, June 1995

Figure 1

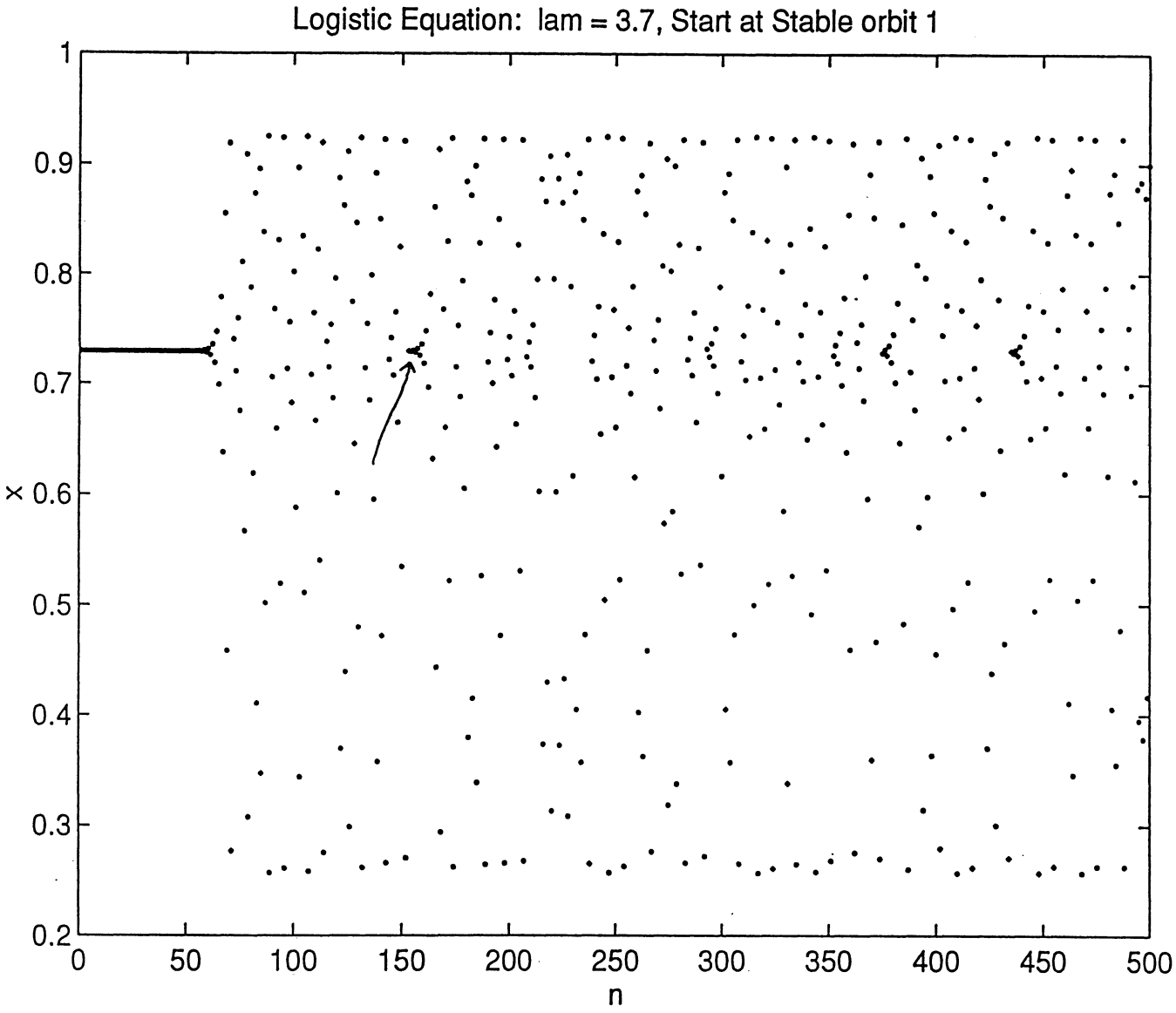

Initial Condition computed as the unstable Fixed point of period 1. $\lambda = 3.7 \Rightarrow$ chaotic region.

Error in the initial state due to Finite resolution $\Rightarrow$ solution eventually becomes chaotic.

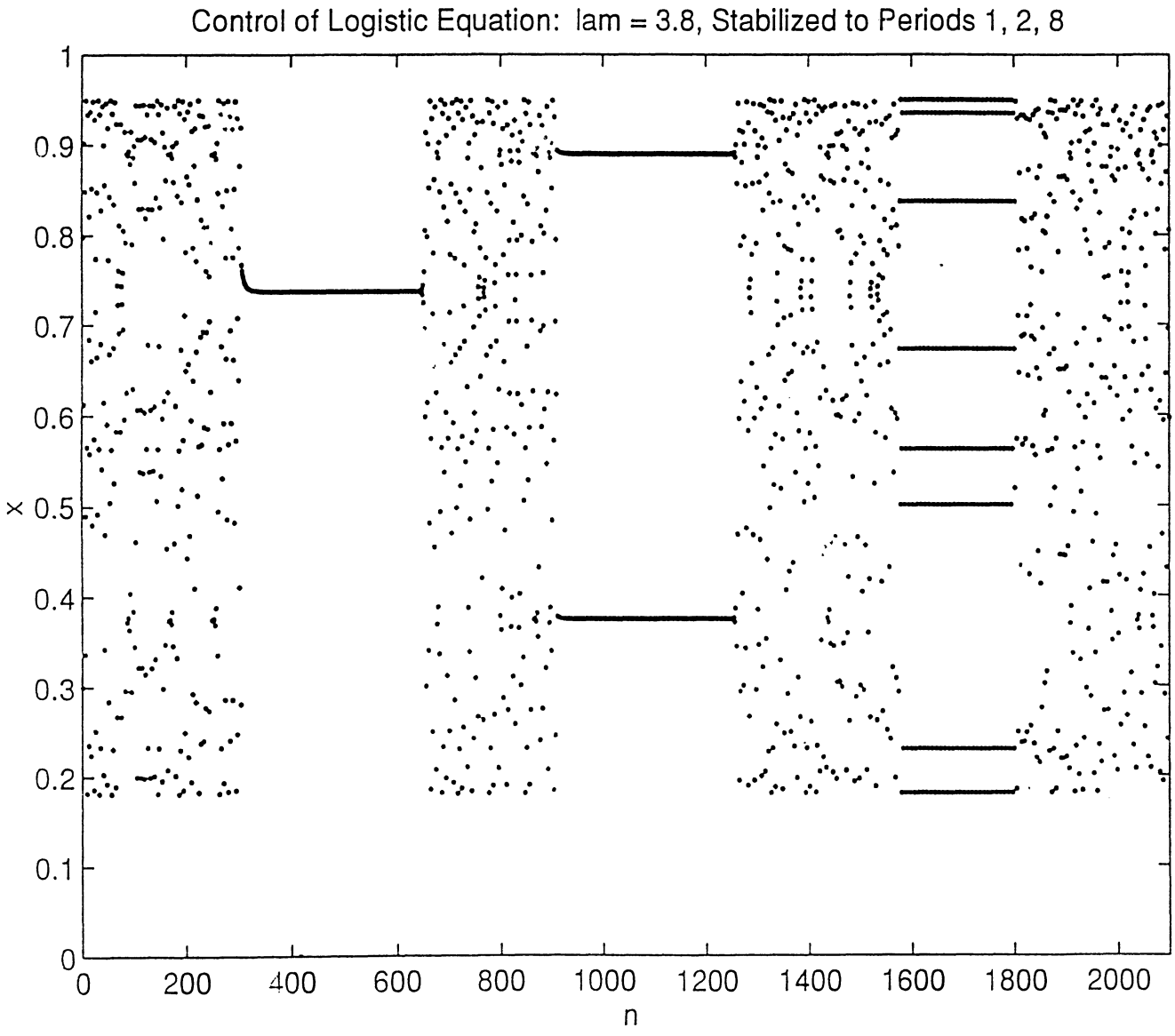
Control of Logistic Equation: lam = 3.8, Stabilized to Periods 1, 2, 8
1
0.9
0.8
0.7
0.6
x 0.5
0.4
0.3
0.2
0.1
0
0
200
400
600
800
1000
1200
1400
1600
1800
2000
n

Figure 2

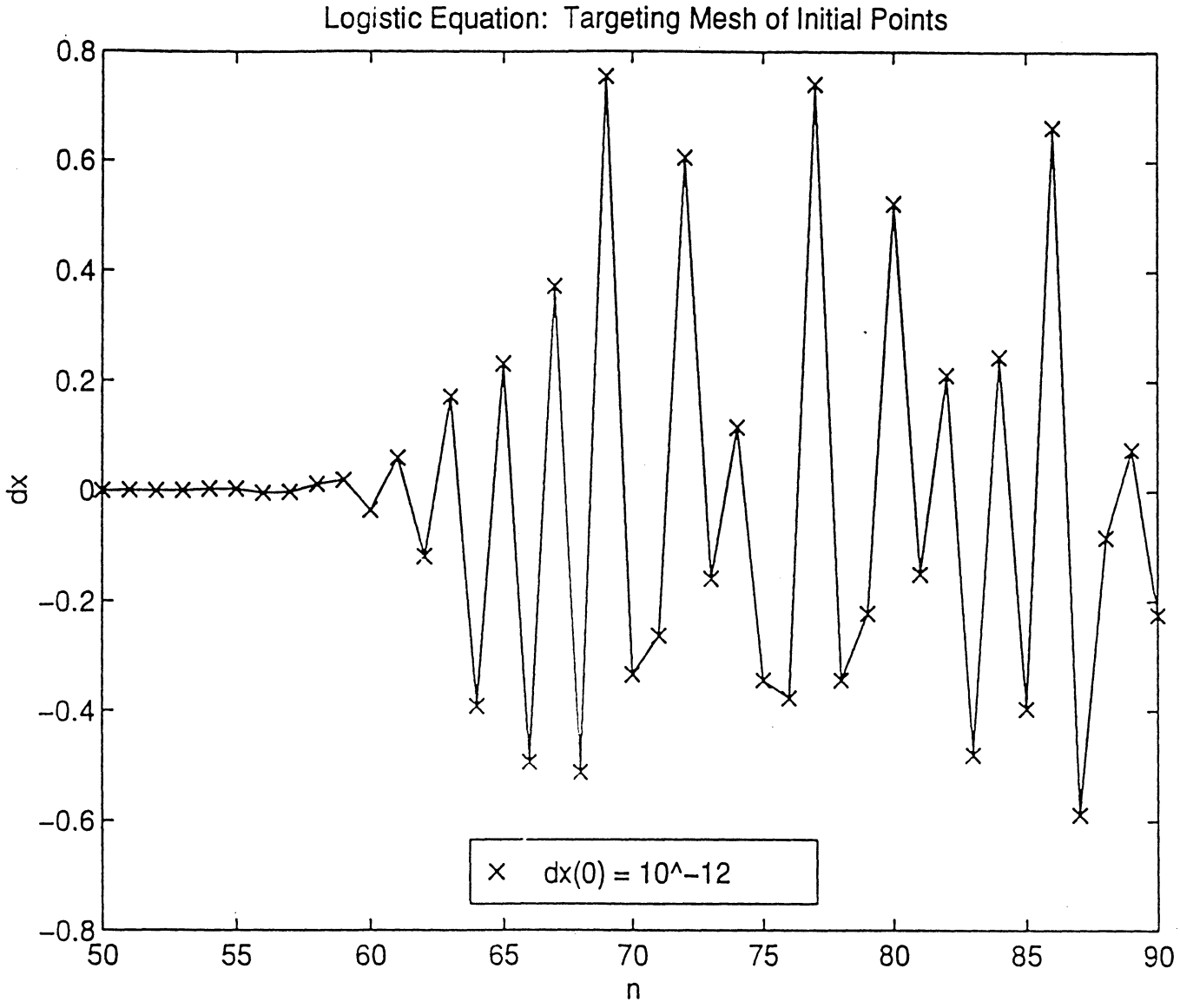
Logistic Equation: Targeting Mesh of Initial Points
0.8
0.6
0.4
0.2
0
−0.2
−0.4
−0.6
−0.8
dx
50
55
60
65
70
75
80
85
90
n
dx(0) = 10^−12

Figure 3

EECS 662 FINAL PROJECT
Advanced Nonlinear Control

A Nonlinear Sliding Observer for Estimating Vehicle Dynamics

ABSTRACT

Longitudinal vehicle speed is estimated given only measured angular wheel speeds and known brake torque inputs using a nonlinear sliding observer. A fourteen degree-of-freedom vehicle dynamics model including compound tire force dynamics is used to simulate true vehicle dynamics. The wheel speed measurements are obtained from the vehicle dynamics model. A reduced order observer model is constructed and simulated in conjunction with the vehicle dynamics model. Simulation demonstrates that vehicle speed can be estimated to within some desired accuracy. Robustness of the observer is analyzed through simulation by introducing steering to the vehicle dynamics model, but not the observer model, adding sensor noise to the wheel speed measurement, and changing vehicle parameters. Concluding remarks present ideas for future research pertaining to the estimation of vehicle dynamics using nonlinear sliding observers.

1.0 INTRODUCTION

Control systems in general require knowledge about the plant dynamics in order to compensate for undesirable behavior. Modern control theories have been developed using state feedback. Compensation designs using state feedback assume that the plant states are available as feedback information. The need for state estimation arises from the fact that, in general, not all of the states can be directly measured. In order to apply compensation to stabilize, to optimize, or to decouple a system, the states of a system must be used as feedback information. If the states cannot be measured directly, then it is necessary to estimate the state dynamics based on a model of the system dynamics. The system dynamics are either represented with a linear or nonlinear model which gives rise to the development of linear and nonlinear state estimation techniques. Several techniques have been developed for estimating states of linear and nonlinear plant models [1-8,10-16]. Sliding observer theory presented in [14] is the technique of interest and thus the motivation behind the following work.

The control of vehicle dynamics for safety and performance enhancement purposes is one such problem where the need for accurate robust state estimation is required. Sensor technology for measuring vehicle state dynamics, such as longitudinal vehicle speed and tire forces, has not met the cost targets required to be production viable. This is not to say that the trend in sensor technology has not been in the right direction, but in order to meet the constraints defined today, sensor technology is not where it needs to be for automotive application. Therefore, vehicle state estimation given a minimal number of measured inputs is the current problem to be investigated. In particular the estimation of longitudinal vehicle speed given only angular wheel speed measurements is the focus.

The following outlines the state estimation problem in terms of the vehicle dynamics model, the reduced order vehicle dynamics model used for state estimation, and the model assumptions. A nonlinear sliding observer for estimating vehicle speed is

proposed. The nonlinear sliding observer along with the vehicle dynamics model are simulated and results analyzed. Finally, concluding remarks are given to summarize and to propose future work.

2.0 PROBLEM DEFINITION

Plant state estimation is an important detail in developing a comprehensive robust control system. State estimators are useful in eliminating the number of required feedback sensors and providing for feedback sensor diagnostic capability. The motivation behind the following is to estimate longitudinal vehicle speed given only angular wheel speed measurements. This may sound simple in concept, but in reality without knowing the nonlinear time-varying compound tire force properties, estimating the true longitudinal vehicle speed is a challenging problem. The estimation of longitudinal vehicle speed enables wheel slip to be regulated to an optimal value so that optimal vehicle acceleration or deceleration is achieved though the modulation of wheel brake pressure or engine drive torque (e.g., anti-lock braking system (ABS) and traction control system (TCS)).

In addition to estimating longitudinal vehicle speed, vehicle dynamics such as lateral vehicle speed and yaw rate can be estimated as more state dynamics are measured. Lateral vehicle dynamics information is necessary for controlling vehicle handling characteristics and yaw stabilization.

2.1 Vehicle Dynamics Model

The fourteen degree-of-freedom vehicle dynamics model used for simulating true vehicle motion contains the conventional longitudinal, lateral, vertical, roll, pitch, and yaw dynamics as well as four wheel speed dynamics and four independent suspension dynamics. The vehicle dynamics model was designed and implemented by the University of Michigan Transportation Institute (UMTRI) using the programming language AUTOSIM. In addition to the nonlinear system dynamics, the vehicle dynamics model also contains a compound tire force model originally developed by Pacejka [9]. The compound tire force model is the nonlinear component of the vehicle dynamics model with the most uncertainty from an estimation standpoint. For simulation purposes, a compound tire force profile is defined, but knowledge of the compound tire force profile is not incorporated into the observer dynamics. The equations of motion for the vehicle dynamics model are:

$$\begin{bmatrix} \dot{v}_x \\ \dot{v}_y \\ \dot{r} \\ \dot{p} \\ \dot{\phi} \\ \dot{\omega}_{fl} \\ \dot{\omega}_{fr} \\ \dot{\omega}_{rl} \\ \dot{\omega}_{rr} \end{bmatrix} = \begin{bmatrix} \frac{1}{m}[-F_{xf} - F_{xr} - m_s hrp] + v_y r \\ \frac{1}{m}[F_{yf} + F_{yr} - m_s h\dot{p}] - v_x r \\ \frac{1}{I_{zz}}[I_{xz}\dot{p} + L_f F_{yf} - L_r F_{yr} + \Gamma + \Lambda + M_z] \\ \frac{1}{I_{xx}}[m_s h(\dot{v}_y + v_x r) + I_{xz}\dot{r} + m_s hg\theta + M_q] \\ p \\ \frac{1}{I_{wf}}[F_{xfl} R_{wf} - T_{bfl}] \\ \frac{1}{I_{wf}}[F_{xfr} R_{wf} - T_{bfr}] \\ \frac{1}{I_{wr}}[F_{xrl} R_{wr} - T_{brl}] \\ \frac{1}{I_{wr}}[F_{xrr} R_{wr} - T_{brr}] \end{bmatrix} \quad (1)$$

where,

$$\Gamma = (F_{xfl}\cos\delta_f - F_{xfr}\cos\delta_f + F_{yfl}\sin\delta_f - F_{yfr}\sin\delta_f) \cdot \frac{t_f}{2} \quad (2)$$

$$\Lambda = (F_{xrf} - F_{xrr}) \cdot \frac{t_r}{2} \quad (3)$$

$$F_{xf} = F_{xfl}\cos\delta_f + F_{xfr}\cos\delta_f + F_{yfl}\sin\delta_f + F_{yfr}\sin\delta_f \quad (4)$$

$$F_{xr} = F_{xrl} + F_{xrr} \quad (5)$$

$$F_{yf} = -F_{xfl}\sin\delta_f - F_{xfr}\sin\delta_f + F_{yfl}\cos\delta_f + F_{yfr}\cos\delta_f \quad (6)$$

$$F_{yf} = F_{yrl} + F_{yrr} \quad (7)$$

m is the total vehicle mass
m_s is the sprung vehicle mass
h is the height of the c.g.
L_f is the distance from the c.g. to the front axle
L_r is the distance from the c.g. to the rear axle
M_z is the aligning torque moment about the z axis
M_q is the aligning torque moment about the roll axis
I_{xx} is the inertia of the entire vehicle about the x axis
I_{zz} is the inertia of the entire vehicle about the z axis
I_{xz} is the product of inertia of the entire vehicle
I_w is the wheel inertial about the wheel axle
R_w is the rolling radius of the wheel
t_f and t_r are the track width of the front and rear of the vehicle, respectively

The remaining six degrees-of-freedom are defined by the following suspension model:

$$\begin{bmatrix} \ddot{z}_s \\ \ddot{z}_{fl} \\ \ddot{z}_{fr} \\ \ddot{z}_{rl} \\ \ddot{z}_{rr} \\ \dot{q} \\ \dot{\theta} \end{bmatrix} = \begin{bmatrix} \frac{1}{m_s}[K_{sf}dz_f + B_{sf}d\dot{z}_f + K_{sf}dz_r + B_{sr}d\dot{z}_r] \\ \frac{1}{m_{fl}}[K_{usf}(z_{0fl} - z_{fl}) + B_{usf}(\dot{z}_{0fl} - \dot{z}_{fl}) - K_{sf}dz_f - B_{sf}d\dot{z}_f] \\ \frac{1}{m_{fr}}[K_{usf}(z_{0fr} - z_{fr}) + B_{usf}(\dot{z}_{0fr} - \dot{z}_{fr}) - K_{sf}dz_f - B_{sf}d\dot{z}_f] \\ \frac{1}{m_{rr}}[K_{usr}(z_{0rl} - z_{rl}) + B_{usr}(\dot{z}_{0rl} - \dot{z}_{rl}) - K_{sr}dz_r - B_{sr}d\dot{z}_r] \\ \frac{1}{m_{rr}}[K_{usr}(z_{0rr} - z_{rr}) + B_{usr}(\dot{z}_{0rr} - \dot{z}_{rr}) - K_{sr}dz_r - B_{sr}d\dot{z}_r] \\ \frac{1}{I_{yy}}[-F_{bf}h_f \cos\delta_f - F_{br}h_r + L_f(K_{sf}dz_f + B_{sf}d\dot{z}_f) - L_r(K_{sr}dz_r + B_{sr}d\dot{z}_r)] \\ q \end{bmatrix} \quad (8)$$

where, for small θ,

$$dz_f = z_f - (z_s + L_f\theta) \quad (9)$$

$$dz_r = z_r - (z_s - L_r\theta) \quad (10)$$

K_s is the sprung mass spring stiffness
B_s is the sprung mass damping coefficient
K_{us} is the unsprung mass spring stiffness
B_{us} is the unsprung mass damping coefficient
I_{yy} is the inertia of the entire vehicle about the y axis
F_{bf} and F_{br} are the transmitted longitudinal forces for the front and rear, respectively
h_f and h_r are the distances from the center of the wheel axle to the horizontal axis of the sprung mass for the front and rear, respectively

The components of $x(t) = [v_x\ v_y\ z_s\ r\ \phi\ \theta\ \omega_{fl}\ \omega_{fr}\ \omega_{rl}\ \omega_{rr}\ z_{fl}\ z_{fr}\ z_{rl}\ z_{rr}]^T$ are longitudinal velocity, lateral velocity, yaw rate, roll angle, pitch angle, front left and right and rear left and right angular wheel velocities and front left and right and rear left and right unsprung mass deflections. The inputs to the vehicle dynamics model are front wheel steering angle, δ_f, (assume steering on left front wheel equals steering on right front wheel) and individual wheel brake torque; $u(t) = [\delta_f\ T_{bfl}\ T_{bfr}\ T_{brl}\ T_{brr}]$. Therefore, only braking and steering maneuvers are analyzed. If additional dynamics are augmented for drive train dynamics, then vehicle acceleration maneuvers can be also considered.

2.2 Vehicle Dynamics Model for State Estimation

Given the defined vehicle dynamics model, if only wheel speeds are measured, then obviously not all of the vehicle states are observable. Since the initial objective is to only estimate longitudinal vehicle speed, v_x, the vehicle dynamics can be reduced from those

defined above. An initial reduction results by assuming a bicycle model, hence the roll dynamics are eliminated. The two front wheel dynamics are lumped into one equation and the two rear wheel dynamics are also lumped into one equation. If relatively small steering inputs are used, then a bicycle model adequately depicts the dynamics desired. Another assumption is to assume quasi-static weight transfer characteristics (i.e., the suspension dynamics will be neglected). The reduced vehicle state equations are formulated as:

$$\begin{bmatrix} \dot{v}_x \\ \dot{v}_y \\ \dot{r} \\ \dot{\omega}_f \\ \dot{\omega}_r \end{bmatrix} = \begin{bmatrix} \frac{1}{m}[-F_{xf}\cos\delta_f - F_{yf}\sin\delta_f - F_{xr}] + v_y r \\ \frac{1}{m}[F_{yf}\cos\delta_f - F_{xf}\sin\delta_f + F_{yr}] - v_x r \\ \frac{1}{I_z}[L_f(F_{yf}\cos\delta_f - F_{xf}\sin\delta_f) - L_r F_{yr}] \\ \frac{1}{I_{wf}}[F_{xf}R_{wf} - T_{bf}] \\ \frac{1}{I_{wr}}[F_{xr}R_{wr} - T_{br}] \end{bmatrix} \tag{11}$$

The components of $x(t) = [v_x\ v_y\ r\ \omega_f\ \omega_r]^T$ are longitudinal velocity, lateral velocity, yaw rate, front and rear angular wheel velocities. The inputs to the reduced order vehicle dynamics model are the front steer angle and the applied brake torque via brake pressure; $u(t) = [\delta_f\ T_{bf}\ T_{br}]^T$. m is the total vehicle mass, I_z is the moment of inertia of the vehicle about its yaw axis, and I_w is the moment of inertia of the wheel about its axle. Components of the force vector, $F(t) = [F_{xf}\ F_{xr}\ F_{yf}\ F_{yr}]$, are the front are rear longitudinal and lateral tire forces. Sign conventions for the forces and motion, and the remaining parameters in (11) are defined in Fig. 1. The analytic tire model of [9] is used to simulate the true tire forces. The model generates a tire force in the longitudinal direction given a wheel slip (λ) and a normal load (F_z) and in the lateral direction given a wheel slip angle (α) and a normal load (F_z). Note that the tire force model is used for simulation of the vehicle dynamics only. The estimation process does not contain information pertaining to the actual tire force profile.

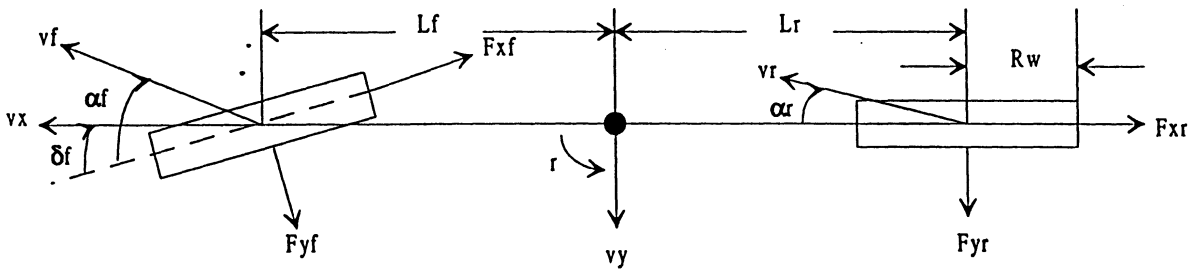

Figure 1: Five degree-of-freedom bicycle model: Schematic and sign convention corresponding to (11)

3.0 OBSERVER DESIGN AND ANALYSIS

Designing an observer for nonlinear systems generally amounts to defining a model of the system dynamics and then applying extended Kalman filter techniques. Extended Kalman filters have been shown to meet the requirements of many nonlinear control systems, but, in general, strict model dependent observers tend to have robustness problems with plant uncertainty.

In order to address the problems with robustness due to plant uncertainty in observer designs, probabilistic techniques have been explored in conjunction with extended Kalman filters [11]. Fuzzy logic based observers have also been studied in [8]. Additional research has explored the notion of sliding surfaces. Sliding surfaces have been predominately researched by Soviet mathematicians, where it has been used to stabilize a class of nonlinear systems. Slotine *et al* studied the concepts of sliding mode control and proposed a dual problem of designing state observers using sliding surfaces [14].

The following three subsections define the basic concepts behind the sliding observer theory presented in [14] and the design of a nonlinear sliding observer for estimating longitudinal vehicle speed.

3.1 Nonlinear Sliding Observer Theory

The basic concepts of the nonlinear sliding observer are developed as the dual of the sliding mode control problem [14]. The following briefly outlines some of the important ideas behind sliding mode control.

Consider the nonlinear system

$$\dot{x}(t) = f(x,t) + g(x,t)u(t) + d(t) \tag{12}$$

where, $u(t)$ is a scalar control input, x is the scalar output, and $x = [x, \dot{x}, \ldots, x^{(n-1)}]^T$ is the state. $f(x,t)$ and $g(x,t)$ are nonlinear functions that are not exactly known except for an upper bound on the parameter variation. $|\Delta f|$ and $|\Delta g|$ denote the parameter variation bounds for $f(x,t)$ and $g(x,t)$, respectively. $d(t)$ is unknown, but bounded in absolute value by a continuous function of time. The control problem is to design a control law, u, such that the state $\boldsymbol{x}$ tracks a desired state $\boldsymbol{x_d} = [x_d, \dot{x}_d, \ldots, x_d^{(n-1)}]^T$. In order to achieve this goal with a finite control, u, the following assumption must be made about the initial condition:

$$\tilde{x}\big|_{t=0} = 0 \tag{13}$$

where, $\tilde{x} \equiv x - x_d = [\tilde{x}, \dot{\tilde{x}}, \ldots, \tilde{x}^{(n-1)}]^T$ is the tracking error vector. A sliding surface is defined on R^n as $\sigma(\tilde{x}, t) = 0$ with

$$\sigma(\tilde{x},t) \equiv \left(\frac{d}{dt}+\lambda\right)^{n-1} \tilde{x}, \lambda > 0 \tag{14}$$

Given initial condition (13), the problem of tracking $x = x_d$ is equivalent to that of remaining of the surface $\sigma(t)$ for all $t > 0$. The sliding condition for initial conditions different from (13) must have control law u designed such that the following holds:

$$\sigma\dot{\sigma} \leq -\eta|\sigma| \tag{15}$$

The idea behind (14) and (15) is to define a well behaved function of the tracking error, σ, according to (14) and then design a control law u such that (14) is satisfied despite the presence of model parameter uncertainty and disturbances. Note that if the initial condition is not as defined in (13), then satisfying (14) still guarantees that $\sigma(t)$ will be reached in finite time. Also, note that control laws that satisfy the defined equations are discontinuous about the sliding surface, thus in practice the control, u, chatters.

Additional topics pertaining to sliding surfaces have been explored such as shearing effects and sliding patches. Shearing generates sliding behavior over a known region called the sliding patch. In order to obtain the shearing effect in the phase plane trajectories, input switching according to a single value of the state, rather than a linear combination, must be applied. In order to increase the region of direct attraction for the sliding surface, σ, damping in terms of the single input must be added to each state equation.

The basic concepts of sliding mode control are used to define an observer structure for nonlinear systems. Slotine *et al* derive the basic concepts of a nonlinear sliding observer using a second order nonlinear system model in companion form and assume only a single measurement. This assumption allows for observability to be assumed. Given a single measurement, the sliding observer structure is as follows:

$$\begin{aligned}\dot{\hat{x}}_1 &= -\alpha_1\tilde{x}_1 + \hat{x}_2 - k_1\,\mathrm{sgn}(\tilde{x}_1)\\ \dot{\hat{x}}_2 &= -\alpha_2\tilde{x}_1 + \hat{f} - k_2\,\mathrm{sgn}(\tilde{x}_1)\end{aligned} \tag{16}$$

where, $\tilde{x}_1 = \hat{x}_1 - x_1$, $\hat{f}$ is the estimated nonlinear dynamics of f, and the constants α_i are chosen as in a Luénberger observer.

The analysis is extended to an n state problem with a single measurement by adding n α terms and n sgn(·) terms; one to each linear differential equation. The general nonlinear observer structure is defined in a similar manner except the system equations are not necessarily in companion form. Given the following general nonlinear system

$$\dot{x} = f(x,t),\ x \in R^n \tag{17}$$

assuming a vector measurement linearly related to the state vector

$$z = Cx,\ z \in R^p, \tag{18}$$

the observer structure is defined as

$$\dot{\hat{x}} = \hat{f}(\hat{x},t) - L\tilde{z} - K\mathbf{1}_s \tag{19}$$

where, $\hat{x} \in R^n$, $\hat{f}$ is a model of f, L and K are $n \times p$ gain matrices to be defined, and $\mathbf{1}_s$ is a $p \times 1$ vector defined as:

$$\mathbf{1}_s = [\mathrm{sgn}(\tilde{z}_1)\ \mathrm{sgn}(\tilde{z}_2) \ldots \mathrm{sgn}(\tilde{z}_p)]^T \tag{20}$$

where,

$$\tilde{z}_i = c_i\hat{x} - z_i \tag{21}$$

and c_i is the ith row of the $p \times n$ C matrix.

Defining the sliding surface to be $\sigma(\tilde{z})$, equations (13), (14) and (15) defined for sliding mode control can help define the matrix gains L and K. The specifics of this analysis are dependent on Δf, the error between the system model, $\hat{f}$, and the actual nonlinear system, f, and therefore, will not be discussed in detail. An example of how to derive the matrix gains L and K is illustrated in [14].

To summarize, the basic concepts involved with designing a nonlinear sliding observer are:

- Define a sliding surface, σ, for a given nonlinear dynamics model
- Define the elements of K associated with the measured states such that σ is attractive
- Derive the reduced order dynamics for when the states are confined in σ
- Define the remaining elements of K such that the reduced dynamics are stable
- Define the elements of L as in a Luenberger observer assuming $K \equiv 0$

A caveat to the nonlinear sliding observer derivation is that in order to design an observer for any system, the system must be observable given the defined measurements. If the system is not observable with the defined measurements, then an observer cannot be defined that is guaranteed to accurately estimate the desired state dynamics.

3.2 Observer Model Definition and Observability Analysis

The nonlinear sliding observer design for the model defined in (11) begins with the determination of nonlinear system observability given ω_f and ω_r as measurements. The

model defined in (11) can be represented in the following form assuming δ_f is sufficiently small (i.e. $\sin\delta_f = \delta_f$ and $\cos\delta_f = 1$)

$$\dot{x} = f(x) + g(x,u) \tag{22}$$

where,

$$f(x) = \begin{pmatrix} v_y r \\ v_x r \\ 0 \\ 0 \\ 0 \end{pmatrix} \text{ and } g(x,u) = \begin{pmatrix} -\frac{F_{xf}}{m} - \frac{F_{xf}}{m}\delta - \frac{F_{xr}}{m} \\ \frac{F_{yf}}{m} - \frac{F_{xf}}{m}\delta + \frac{F_{yr}}{m} \\ \frac{L_f F_{yf}}{I_z} - \frac{L_f F_{xf}}{I_z}\delta - \frac{L_r F_{yr}}{I_z} \\ \frac{F_{xf} R_{wf}}{I_{wf}} - \frac{T_{bf}}{I_{wf}} \\ \frac{F_{xr} R_{wr}}{I_{wr}} - \frac{T_{br}}{I_{wr}} \end{pmatrix}$$

By augmenting dynamics to account for the longitudinal tire forces, the system can be represented as:

$$\dot{x} = f(x) + g(x)u \tag{23}$$

where,

$$f(x) = \begin{pmatrix} -\frac{(x_6 + x_7)}{m} + x_2 x_3 \\ \frac{(x_8 + x_9)}{m} + x_1 x_3 \\ \frac{(L_f x_8 - L_r x_9)}{I_z} \\ \frac{(x_6 R_{wf})}{I_{wf}} \\ \frac{(x_7 R_{wr})}{I_{wr}} \\ K_f (R_{wf} x_4 - x_1) \\ K_r (R_{wr} x_5 - x_1) \\ 0 \\ 0 \end{pmatrix} \text{ and } g(x) = \begin{pmatrix} -\frac{x_8}{m} & 0 & 0 \\ -\frac{x_6}{m} & 0 & 0 \\ -\frac{L_f x_6}{I_z} & 0 & 0 \\ 0 & \frac{-1}{I_{wf}} & 0 \\ 0 & 0 & \frac{-1}{I_{wr}} \\ 0 & 0 & 0 \\ 0 & 0 & 0 \\ C_f & 0 & 0 \\ C_r & 0 & 0 \end{pmatrix}$$

The states $[x_1 \ldots x_9]$ are defined as:

$$\begin{bmatrix} x_1 = v_x \\ x_2 = v_y \\ x_3 = r \\ x_4 = \omega_f \\ x_5 = \omega_r \\ x_6 = F_{xf} \\ x_7 = F_{xr} \\ x_8 = F_{yf} \\ x_9 = F_{yr} \end{bmatrix} \tag{24}$$

The concept of augmenting the force dynamics to the vehicle dynamics model is similar in concept to the notion of a random walk formulation proposed by Ray for a similar problem [10]. The longitudinal tire force dynamics are assumed to be linear with respect to the difference between angular wheel speed and longitudinal vehicle speed, but this model is far from exact and is enormously uncertain. Note that the tire force dynamics are defined given heuristic knowledge of the dynamics, but the model is by no means an accurate depiction of the actual tire profiles. K_f, K_r, C_f, and C_r can be chosen arbitrarily.

Given the basic model assumptions and representation, the observability of the nonlinear system can be analyzed given x_4 and x_5 as measurements. It can be shown that given only x_4 and x_5 as measurements, the nonlinear system defined in (23) is not observable, therefore, either more states must be measured or additional assumptions must be made in order to reduce the observer model. The direction chosen is to reduce the observer model because additional measurements result in the requirement of additional sensor elements in the physical system which is unacceptable.

If the assumption is made that $\delta_f \cong 0 \Rightarrow v_y \cong 0$, $r \cong 0$, $F_{yi} \cong 0$, then the observer model reduces to the following

$$\dot{x} = f(x) + g(x)u \tag{25}$$

where,

$$f(x) = \begin{pmatrix} \dot{} \\ \dot{} \end{pmatrix} \begin{pmatrix} -\dfrac{x_4 + x_5}{m} \\ \dfrac{x_4 R_{wf}}{I_{wf}} \\ \dfrac{x_5 R_{wr}}{I_{wr}} \\ K_f(R_{wf} x_2 - x_1) \\ K_r(R_{wr} x_3 - x_1) \end{pmatrix} \quad \text{and} \quad g(x) = \begin{pmatrix} 0 & 0 \\ \dfrac{-1}{I_{wf}} & 0 \\ 0 & \dfrac{-1}{I_{wr}} \\ 0 & 0 \\ 0 & 0 \end{pmatrix}$$

The state $[x_1 \ldots x_5]$ are defined as

$$\begin{bmatrix} x_1 = v_x \\ x_2 = \omega_f \\ x_3 = \omega_r \\ x_4 = F_{xf} \\ x_6 = F_{xr} \end{bmatrix} \tag{26}$$

The reduced order vehicle dynamics model can be shown to be linearly and nonlinearly observable given x_2 and x_3 as measurements.

Since the lateral dynamics have been eliminated from the model, robustness of the observer to small steering inputs is analyzed. Model parameter variation can exist in the vehicle mass and wheel inertia for obvious reasons. The assumption that R_{wi} is a constant generates uncertainty in the nonlinear system model because the actual tire rolling radius varies as a function of the normal force loading. The dynamics of the change in rolling radius are defined in the suspension model, equation (8).

Given a brief analysis of the uncertainty associated with the observer model, the design of the nonlinear sliding observer can commence because the system is nonlinearly observable. The following subsection defines the observer structure and the means by which the matrix gains L and K are defined.

3.3 Nonlinear Sliding Observer Design

Given the nonlinear model defined in (25), the concepts presented in section 3.1 are employed to design a nonlinear sliding observer. The general structure of the nonlinear sliding observer is

$$\dot{\hat{x}} = \hat{f}(\hat{x}) + \hat{g}(\hat{x})u - \mathrm{L}\tilde{z} - \mathrm{K}\mathbf{1}_s \tag{27}$$

where, L, K, and $\mathbf{1}_s$ are defined above and the sliding surface σ is defined as $\tilde{z}$ where, $\tilde{z}_1 = \hat{x}_2 - x_2$ and $\tilde{z}_2 = \hat{x}_3 - x_3$.

As a means to simplify the notation, let $f(x,u)$ represent $f(x)+g(x)u$. The following briefly defines the design of the matrix gains L and K in order to estimate longitudinal vehicle speed.

Since the observer model is linear, the gain matrix L can be computed as if a linear observer was being designed. From $f(x,u)$ and the fact that x_2 and x_3 are the measured states, the matrix pair (A,C) can be defined. The gain L is chosen such that the matrix (A-LC) has desired linear observer tracking response.

The derivation of K is more complex because it takes into account the uncertainty involved with the system. The elements of K are defined such that $\text{sgn}(\tilde{z}_1)$ only affects the dynamics of ω_f, F_{xf}, and v_x and, similarly, $\text{sgn}(\tilde{z}_2)$ only affects ω_r, F_{xr}, and v_x. Given this assumption, the derivation for one element is illustrated. The remaining elements are derived in a similar manner.

For the sliding surface, $\sigma \equiv \tilde{z}$, to be attractive, the following must be true:

$$\tilde{z}_i \dot{\tilde{z}}_i < 0 \tag{28}$$

Therefore, the following condition results:

$$\tilde{z}_1 (\Delta f_{\omega_f}(x,u) - \alpha_1 \tilde{z}_1 - \alpha_2 \tilde{z}_2 - k_1 \,\text{sgn}(\tilde{z}_1)) < 0 \tag{29}$$

$$\Rightarrow \quad k_1 > \left| \Delta f_{\omega_f}(x,u) + \alpha_1 \tilde{z}_1 + \alpha_2 \tilde{z}_2 \right| \tag{30}$$

When the state dynamics are confined in $\sigma = \tilde{z}_i = 0$, then the following results:

$$\text{sgn}(\tilde{z}_1) = \frac{\Delta f_{\omega_f}(x,u)}{k_1} \tag{31}$$

If we look at the dynamic equation for F_{xf}, then the following holds:

$$\dot{\tilde{F}}_{xf} = -\frac{k_2}{k_1} \Delta f_{\omega_f} + \Delta f_{F_{xf}} \tag{32}$$

The next step is to define $k2$ such that the error dynamics are stable. This process is repeated for each element of K until all of the error dynamics are stable and the parametric uncertainty of the model is considered.

Once L and K are initially defined, it is desirable to simulate the response of the observer with respect to the actual plant. The next section outlines the simulation that is used to analyze the performance of the designed nonlinear sliding observer and analyzes the results obtained.

4.0 SIMULATION RESULTS

Given the defined vehicle dynamics model and observer model, a SIMULINK block diagram is constructed to serve both as an means of illustrating the model and to test the accuracy of the observer design.

Figure 2 illustrates the top level of the simulation model.

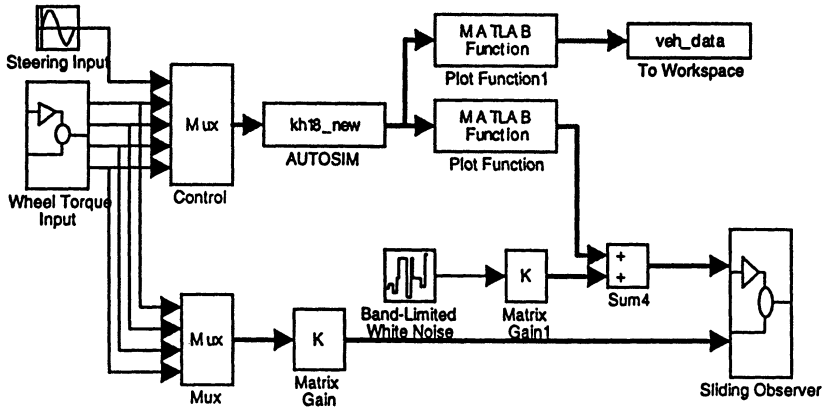

Figure 2: SIMULINK Block Diagram of Top Level Simulation Topology

Note that the sliding observer only receives as input, the brake torque applied to the vehicle dynamics model and the front and rear angular wheel speeds from the vehicle dynamics model. In order to evaluate robustness, three different simulation scenarios are analyzed; (1) apply a steering input to the vehicle dynamics model, (2) add noise to the wheel speed measurement, and (3) modify model parameters such as vehicle mass or wheel inertia. This is by no means an exhaustive list of robustness issues that need to be investigated, but these three scenarios will illustrate important concepts of nonlinear sliding observers.

The first simulation (Figure 3) illustrates the basic performance of the nonlinear sliding observer. Note the chattering of $\tilde{z}_1$ and $\tilde{z}_2$. The chattering is function of the switching feedback used. The chattering is characteristic of the dynamics oscillating about the sliding surface. The absolute percent difference (percent error) is less than 5%. The estimation performance is acceptable given the large uncertainty factor in the observer model versus the actual nonlinear vehicle dynamics model.

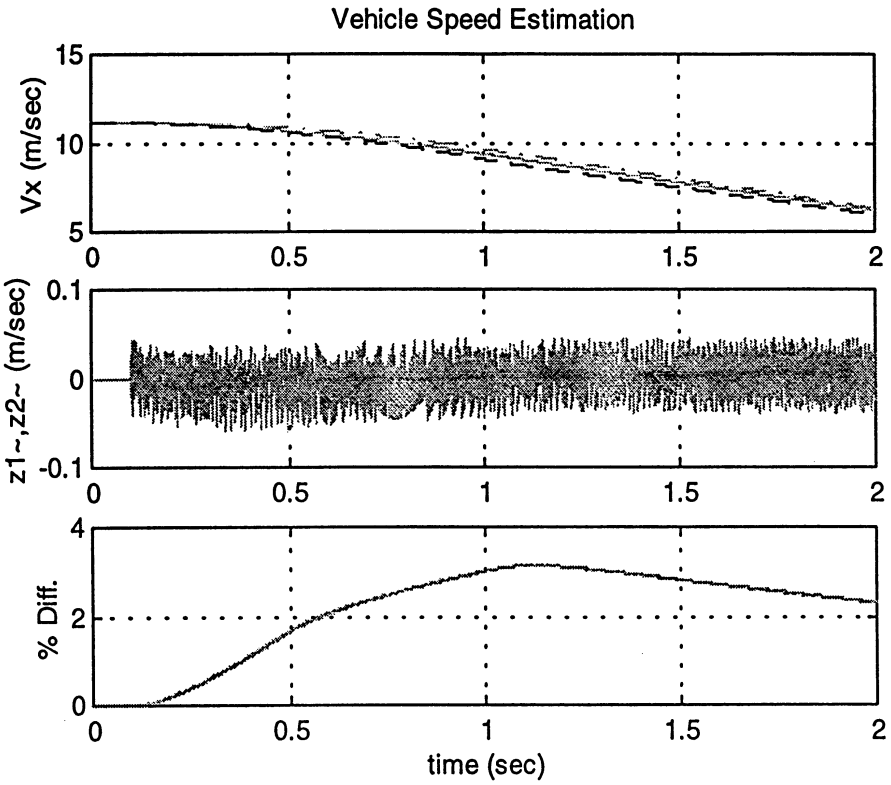

Figure 3: Basic Performance Evaluation Simulation. Plot (a) - Actual Vehicle Speed, -. Estimated Vehicle Speed, -- Wheel Speed (f and r)

The next simulation (Figure 4) exploits the robustness of the observer due to uncertainty in the modeling of the tire force dynamics. The linear model for the tire force dynamics defined in the observer model was chosen so that the system would be observable. The tire force model does not take into account any information pertaining to the actual tire force profile used in the simulation. If enough brake torque is applied to the wheel, then the wheel will lock. During this mode of operation the tire force dynamics will pass through a linear operating region to a nonlinear operating region. The wheel speed dynamics during the locked operation mode are considered *unstable.*

The simulation results tend to match those of the first simulation in terms of absolute percent difference for about the first 1.5 seconds. Once the wheel is locked for a short length of time, the estimation of the wheel dynamics deviates and causes the force dynamics and hence the vehicle speed estimate to deviate to an unacceptable error level. Generally, wheel speed control will keep the wheels from locking, therefore, the erroneous estimation during extended periods of wheel locked may not be a concern. The main point to note is that the robustness due to wheel lock tends to be time dependent.

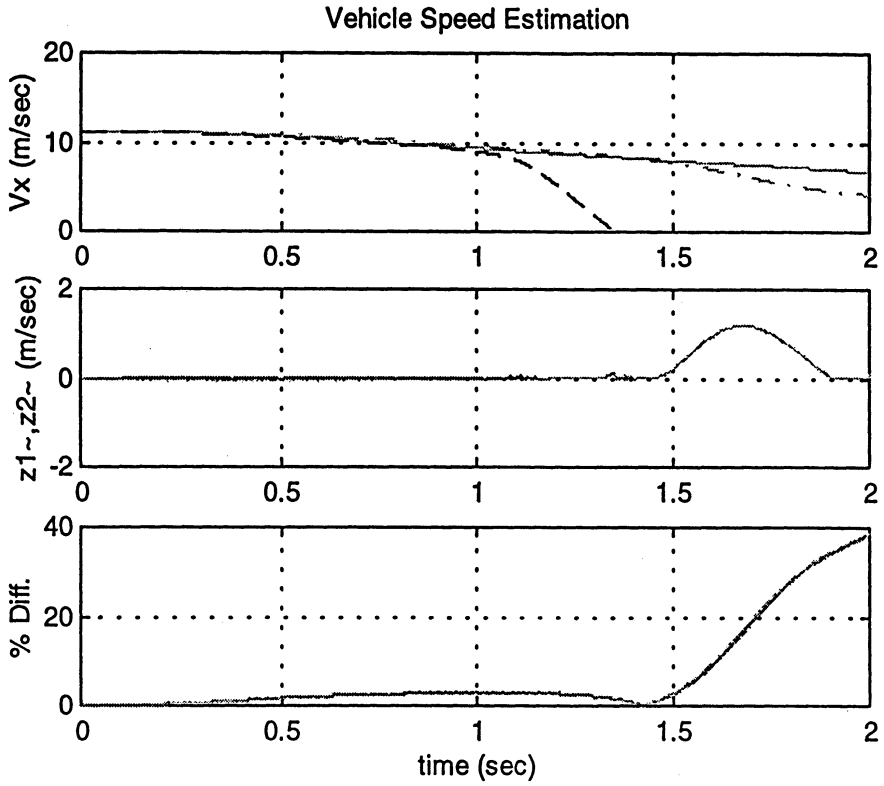

Figure 4: Locked Wheel Mode of Operation. Plot (a) - Actual Vehicle Speed, -. Estimated Vehicle Speed, -- Wheel Speed (f and r)

The remaining four simulations (Figures 5-8) illustrate robustness properties that are of major concern to the problem being studied. The first is that longitudinal vehicle speed is not only a function of longitudinal tire forces, but also a function of lateral speed and yaw rate. The assumptions defined with respect to the steering input were made to reduce the model dynamics, but now it is crucial to investigate what the assumptions have done to the ability to estimate vehicle speed during turning maneuvers. Figure 5 illustrates a simulation response for the same brake torque application as simulated in Figure 3, but now a sinusoidal steering input is applied. The steering input has an amplitude of 2.5 degrees at the road and a frequency of 0.5 Hz. Note from the illustration that the absolute percent difference is relatively close to that without steering. This result depicts the robustness of the observer to steering input and validates the previously made assumptions. Figure 6 illustrates a similar maneuver except the amplitude is increased to 5 degrees at the road. This time the lateral force is operating in a nonlinear region and the estimation error is not as good. Hence, the defined observer structure is valid for small steering inputs where the lateral tire force is linear, but not for nonlinear lateral tire force operation. In order to increase estimation accuracy for the modes when the nonlinear lateral tire dynamics are dominant, additional state measurements are required.

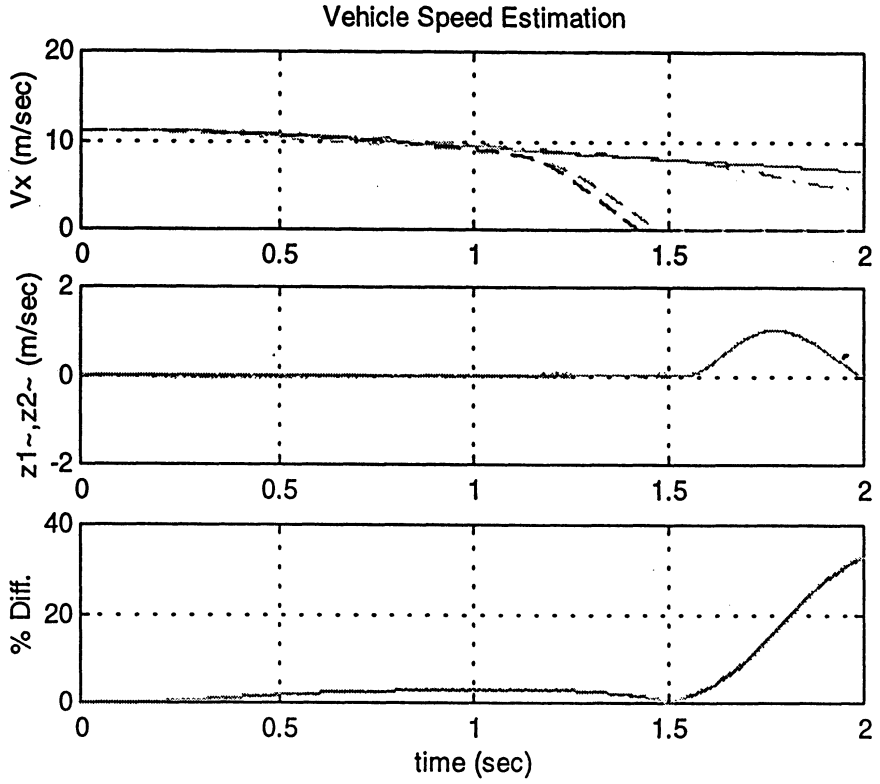

Figure 5: Vehicle Speed Estimation with 2.5 deg. 0.5Hz Sinusoidal Steering Input. Plot (a) - Actual Vehicle Speed, -. Estimated Vehicle Speed, -- Wheel Speed (f and r)

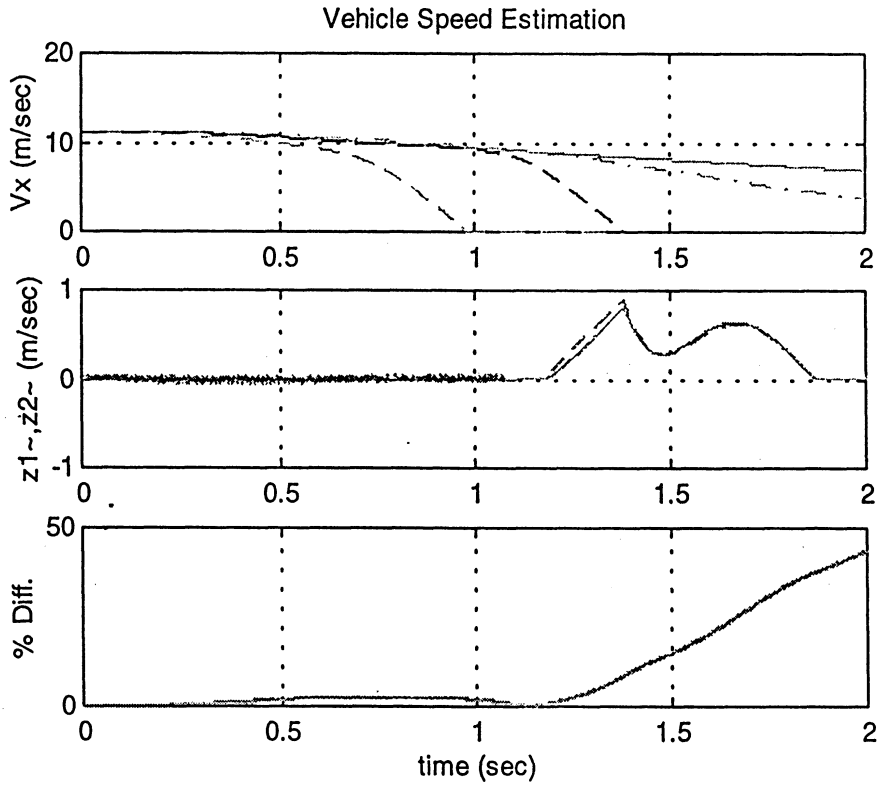

Figure 6: Vehicle Speed Estimation with 5 deg. 0.5Hz Sinusoidal Steering Input. Plot (a) - Actual Vehicle Speed, -. Estimated Vehicle Speed, -- Wheel Speed (f and r)

The next robustness issue to be investigated is the accuracy of the estimation process in the presence of measurement noise. The example simulation shown in Figure 7 is the result of applying the same brake torque input as simulated in Figure 3 with zero-mean Gaussian white noise added to the wheel speed measurement. The maximum amplitude of the noise is 0.5 m/sec. Measurement noise robustness of a sliding observer is mathematically analyzed by Slotine *et al* [14]. The simulation results obtained are similar to those presented by Slotine *et al*. The percent difference is larger than the simulation illustrated in Figure 3. Sliding observers tend to have the same robustness problem with measurement noise as other observer techniques. Hence, sliding observers are not necessarily robust to measurement noise.

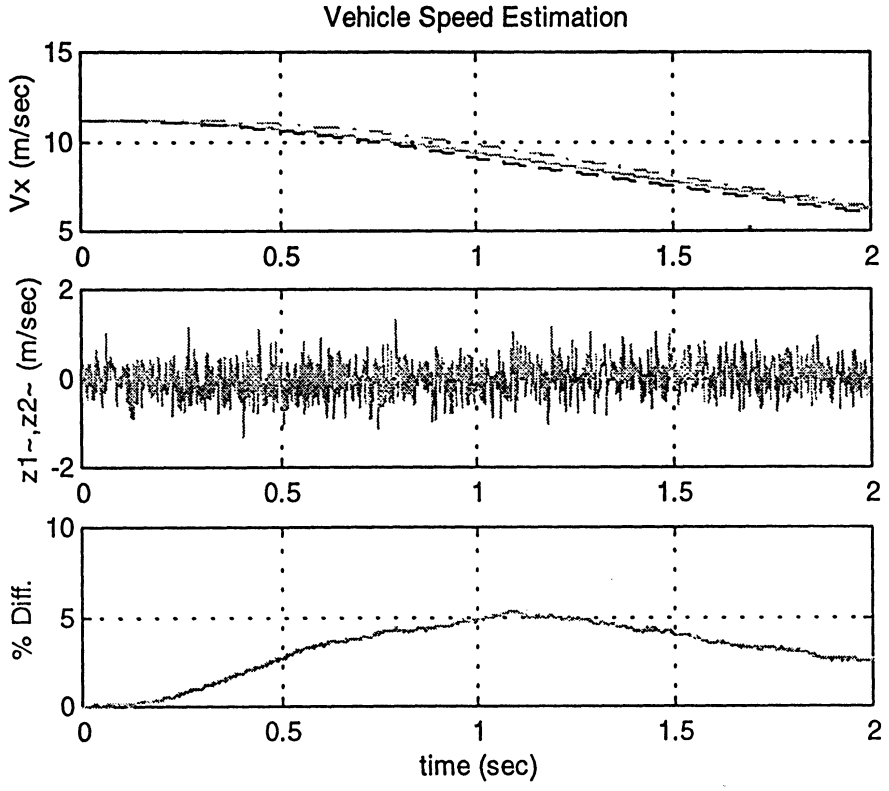

Figure 7: Vehicle Speed Estimation in the Presence of Measurement Noise. Plot (a) - Actual Vehicle Speed, -. Estimated Vehicle Speed, -- Wheel Speed (f and r)

The final robustness issue to be investigated is the robustness of the estimation process given parameter uncertainty. In order to exploit this issue, the mass of the vehicle was changed by 10%. The simulation results illustrated in Figure 8 are for the same brake torque input as simulated in Figure 3 and the vehicle mass modified by 10%.

Sliding observers are characteristically robust to plant uncertainty. Given the simulation results for the observer design defined, the estimation of vehicle speed is acceptable, but not quite as accurate as originally anticipated. However, given the level of uncertainty present in the basic observer model, the result is not unexpected.

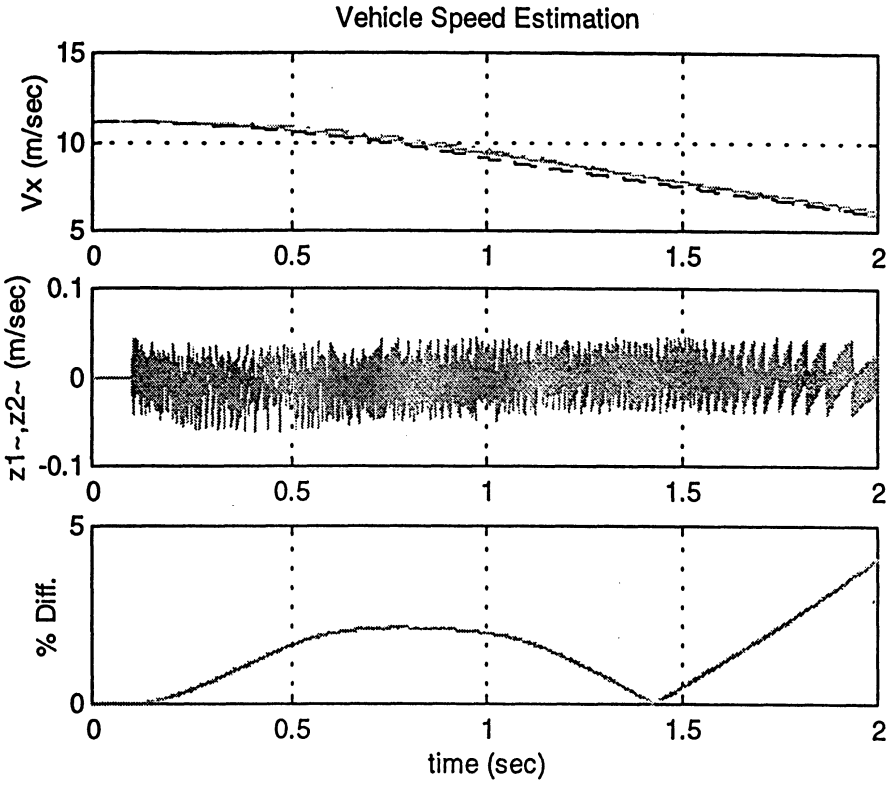

Figure 8: Vehicle Speed Estimation with the Vehicle Mass Different by 10%. Plot (a) - Actual Vehicle Speed, -. Estimated Vehicle Speed, -- Wheel Speed (f and r)

5.0 CONCLUSION

Given a vehicle dynamics model, a state estimation process using sliding mode theory is developed. A fourteen degree-of-freedom nonlinear vehicle dynamics model is used to generate the true vehicle motion. Front wheel steering and brake torque are used as inputs. From the vehicle dynamics model a reduced order vehicle dynamics model is defined. The nonlinear observability of the reduced order model is investigated. Given a dynamics model that is observable, a nonlinear sliding observer is designed. Simulation of the nonlinear sliding observer is used to analyze the basic operation and robustness of the defined observer structure. Simulation results are illustrated with additional comments about the data obtained.

Vehicle state estimation is an important topic for automotive suppliers of active control systems. Sensors tend to drive the cost of most advanced vehicle dynamic control systems. If an estimation process is designed such that a sensor can be eliminated, then the cost of the entire system to the end users is decreased. This study of sliding observer theory for estimating longitudinal vehicle speed is just a small component of what needs to be done. The simulation testing presented is only a minute part of the testing that is required to prove feasibility. Nonlinear sliding observers seem to work well in the presence of large model uncertainty. Given the nature of the vehicle dynamics model, uncertainty is major concern. Future research will be focused on the addition of more complex dynamics to the basic observer structure so that additional states can be

estimated given a minimal number of sensors. Additional work will also be done to analyze how the longitudinal vehicle speed estimation can enhance wheel speed control for systems such as ABS or TCS.

REFERENCES

[1] Danyang, L. and Xaunhaung, L. (1994). Optimal state estimation without the requirement of a priori statistics information of the initial state. *IEEE Trans. Automatic Control, 39:10*, 2087-2091.

[2] Doyle, J. C. and Stein, G. (1979). Robustness with Observers. *IEEE Trans. Automatic Control, AC-24:4*, 607-611.

[3] Grizzle, J. W. and Moraal, P. E. (1995). Observer Design for Nonlinear Systems with Discrete-Time Measurements. *IEEE Trans. Automatic Control, 40:3*, 395-404.

[4] Grizzle, J. W. and Song, Y. (1992). The Extended Kalman Filter as a Local Asymptotic Observer for Nonlinear Discrete-Time Systems. In Proc. 1992 ACC, Chicago, 3365-3369.

[5] Hedrick, J. K. and Rajamani, R. (1995). Adaptive Observers for Active Automobile Suspensions: Theory and Experiment. *IEEE Trans. Control System Technology, 3:1*, 86-93.

[6] Jin, Y., Jiang, J., and Zhu, J. (1994). State Estimation and Adaptive Control of Multivariable Systems via Neural Networks and Fuzzy Logic. *Advances in Modeling and Analysis C: Systems Analysis, Control and Design, 43:2*, 15-22.

[7] Marino, R. and Tomei, P. (1995). Adaptive Observers with Arbitrary Exponential Rate of Convergence for Nonlinear Systems. *IEEE Trans. Automatic Control, 40:7*, 1300-1304.

[8] Milot, D. Design and Analysis of a Fuzzy Observer Structure for Nonlinear Systems. Technical Research Paper, Summer 1995. Shaout, A., University of Michigan.

[9] Pacejka, H. B. and Bakker, E. (1993). The Magic Formula Tyre Model. *Vehicle System Dynamics, 21*, 16.23-16.32.

[10] Ray, L. R. (1995). Nonlinear State and Tire Force Estimation and Advanced Vehicle Control. *IEEE Trans. Control Systems Technology, 3:1*, 117-124.

[11] Ray, L. R. (1995). Real-Time Determination of Road Coefficient of Friction for IVHS and Advanced Vehicle Control. *Proceedings of the American Control Conference*, 2133-2137.

[12] Shiao, Y. and Moskwa, J. J. (1995). Cylinder Pressure and Combustion Heat Release Estimation for SI Engine Diagnostics Using Nonlinear Sliding Observers. *IEEE Trans. Control System Technology, 3:1*, 70-78.

[13] Shouse, K. R. and Taylor, D. G. (1995). Discrete-time Observers for Singularly Perturbed Continuous-time Systems. *IEEE Trans. Automatic Control, 40:2*, 224-235.

[14] Slotine, J. J., Hedrick, J. K., and Misawa, E. A. (1987). On Sliding Observers for Nonlinear Systems. *Journal of Dynamics Systems, Measurement and Control, 109*, 245-252.

[15] Wang, L. X. (1995). Design and Analysis of Fuzzy Identifiers of Nonlinear Dynamics Systems. *IEEE Trans. Automatic Control, 40:1*, 11-23.

[16] Xie, L. and de Souza, C. E. (1993). H_∞ State Estimation for Linear Periodic Systems. *IEEE Trans. Automatic Control, 38:11*, 1704-1707.

Final Project for 662

Optimistic Title: Control of 6Dof Car

Realistic Title: Control of a Brick In Space Given Ideal Force Inputs

Justin Shriver
Charanjit Brahma

Summary

This project is an investigation of what can be gained by using more complex models in the study of the dynamic effects of four wheel steering (4WS). In order to correctly ascertain what effects are important to study, a literature survey was done. After that a non-linear six degree of freedom dynamic model was formulated. The model was transferred into Simulink for verification and simulation, and both linear and non-linear control techniques were applied.

Introduction

The cornering behavior of a motor vehicle is an important performance mode often equated with handling. The equations that govern high-speed turning and low-speed turning are different. At high speeds, lateral accelerations will be present. To counteract the lateral acceleration, the tires must develop lateral forces, which they do by deforming and undergoing a change in slip angle. Slip angle is the angle between the direction the tire is oriented and the direction the car is traveling. [1]

> In conventional two wheel steering cars it is obvious that only the front two tires are used in a controlled way to generate lateral accelerations. Indeed the rear tires generate cornering force only by the sideslip angle resulting from vehicle motion [rotation around the cg]. The rear tires are not directly involved in controlling the course of the vehicle. This observation has led to the concept that if the rear wheels were directly steered as well to control the sideslip angle, vehicle lateral movement could be changed more quickly. The idea, theoretical, in a sense, of steering the rear wheels simultaneously with the front ones as a means of improving the vehicle performance in lateral motion marks a great, innovative step forward in this technological area based on a drastically different concept. Steering the rear wheels could help not only reduce a delay in the generation of cornering force but also permit the vehicle path and attitude (a body sideslip angle) to be controlled independently of each other. Making the most of this characteristic would therefore decrease the required motion of the vehicle body around the z-axis and offer better responsiveness during a change in vehicle course. Another favorable result would be a reduction in off-tracking between front and rear tires at low speed which has been annoying to inexperienced drivers. [2]

Literature Review

Basics of Steering Dynamics

---

[1] Gillespie, Thomas D., Fundamentals of Vehicle Dynamics, SAE ,1992, 195-196pp.

[2] Furukawa, Yoshimi, "A Review of Four-Wheel Steering Studies from the Viewpoint of Vehicle Dynamics and Control," Vehicle System Dynamics, Volume 18, No.1-3, 1989, 198p.

Turning dynamics can be categorized as low and high speed. In low-speed steering, it is assumed that the wheels are aligned with the vehicle velocity. Low-speed turning happens with the wheels pointed in the direction the vehicle is traveling. This does not generate side slip angles. At high speeds, the velocity direction of the vehicle at the wheel is not equal to the velocity direction of the wheel. The difference between these two directions is defined as the side slip angle.

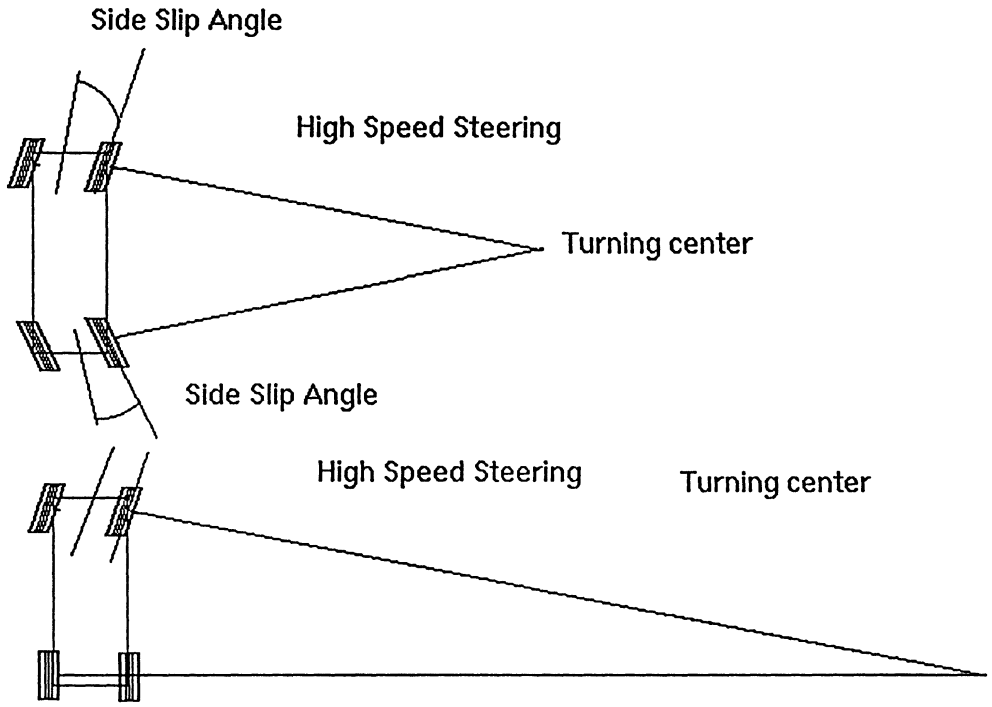

From the above diagram[the lower plot of which should be labeled low speed steering], we see the need for the wheels to be steered differently at low speeds. We are interested in handling which is a dynamic effect present only in high speed steering. Having limited ourselves to high speed analysis we still must determine what performance measures we might be able to affect and what tests we would want to perform. At high speeds the turning radius is assumed to be much larger than the wheelbase of the vehicle, and thus the difference in angles between the front wheels is unimportant. This leads to the use of bicycle models for much of the performance analysis. However, the simple bicycle model does not handle roll. There is an augmented version of the bicycle model that adds a "fake" torsional spring to allow the calculation of roll in cornering. For control, most work is performed on the basic bicycle model.

Basic Bicycle Augmented Bicycle

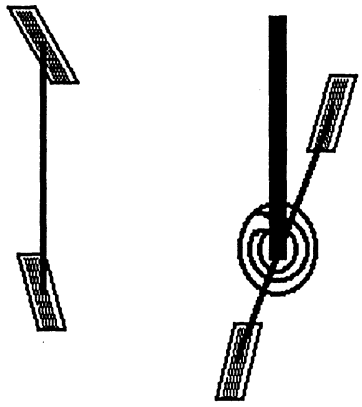

Starting from the simple two degree of freedom bicycle model and making the usual small angle approximations yields the following set of equations:[3]

Linearized Equations

$$\begin{bmatrix} R \\ S^2Y \end{bmatrix} = \begin{bmatrix} G_r(0)\dfrac{1+T_r s}{1+2\dfrac{\zeta}{\omega_n}s+\dfrac{1}{\omega^2{}_n}s^2} & -G_r(0)\dfrac{1+T'_r s}{1+2\dfrac{\zeta}{\omega_n}s+\dfrac{1}{\omega^2{}_n}s^2} \\ G_{\ddot{y}}(0)\dfrac{1+T_1 s+T_2 s^2}{1+2\dfrac{\zeta}{\omega_n}s+\dfrac{1}{\omega^2{}_n}s^2} & G_{\ddot{y}}(0)\dfrac{-1+T'_1 s+T'_2 s^2}{1+2\dfrac{\zeta}{\omega_n}s+\dfrac{1}{\omega^2{}_n}s^2} \end{bmatrix} \begin{bmatrix} \Delta_f \\ \Delta_r \end{bmatrix}$$

Assuming that the steering response characters of the vehicle are close to neutral [the same for front and rear], the primed and unprimed variables will be equal. This allows us to reduce the equations to the following:[4]

$$\begin{bmatrix} R \\ S^2Y \end{bmatrix} = \begin{bmatrix} \dfrac{1-k}{n}G_r(0)\dfrac{1+T_r s}{1+2\dfrac{\zeta}{\omega_n}s+\dfrac{1}{\omega^2{}_n}s^2} \\ \dfrac{1-k}{n}G_{\ddot{y}}(0)\dfrac{1+(1+\lambda)T_1 s+(1+\lambda)T_2 s^2}{1+2\dfrac{\zeta}{\omega_n}s+\dfrac{1}{\omega^2{}_n}s^2} \end{bmatrix} * \Delta_f ; \lambda = \frac{2k}{1-k}$$

From this it is clear that as k is increased so is lambda. This will increase the gain at low frequencies as well as the phase since we are moving a zero toward lower frequencies.[5] Another view of the equations can be arrived at by describing what they mean in words. The motion of a turning vehicle is complex but can be reduced to a set of elemental steps. When front wheel steering is applied, the following steps occur:

Driver Inputs Desired Steering Angle

---

[3] Sano et al., "The Effect of Improved Vehicle Dynamics on Driver Control Performance," 7th International Technical Conference on Experimental Safety Vehicles, 1979, 10p.

[4] Furukawa, p153-153.

[5] Ibid.

Slip Angle at Front Tires
Lateral Force on Front Tires
Start of Turning Around Vehicle C.G.
Vehicle Slide-Slip Angle
Slip Angle at Rear Tires
Lateral Force on Rear Tires
Centripetal Force by Front and Rear Tires Resulting in Vehicle Turn[6]

Steering Performance Measures

There are two measures of performance that appeared in virtually every paper. First, there is phase lag between steering input and lateral acceleration. In "Improvement of Vehicle Dynamics by Vehicle-Speed-Sensing Four-Wheel Steering System" by Yasuda and Furutani, summaries of several physical tests on a Mazda SS 4WS are provided. These results should be useful for verifying performance of full mathematical models. In "Four Wheel Steering: Maneuverability and High Speed Steering,"[7] by Whitehead, an analysis is presented that allows one to bound steering wheel input frequencies. He concludes that human drivers cannot produce steering frequencies in excess of 10rad/s. Further, he derives a formula for maximum frequency before tire adhesion limits are exceeded at 3rad/s. In most of the literature, the double lane change is a standard maneuver and its is approximated by a sin wave for simulation. It is argued that the delay between phase lag and steering is important from an ergonomic perspective. Reducing the yaw is thought to improve both ergonomics and dynamics. The dynamic argument is that it leads to more balanced use of the tires. This is clearly illustrated in reference 8[8]. All reference mentioned so far uses mechanical linkages to steer the wheels.

Given how ubiquitous the bicycle model is, a natural question to ask is would a more complex model be of interest? In Mathematical Formulation of Wheeled Vehicle Dynamics by Peter Jurkat, an analytical model for the full car model is derived. Unfortunately, as is the case for most existing models, it was designed for simulation but not control work. As such, all motions are described in the car's coordinate system. However, for the problem we want to explore, we would like to track trajectories described in the inertial frame. However, analysis of these equations did turn out to be useful. We noted that the transformation between car coordinates was defined differently from that defined by Sastry. As it turned out, Sastry's equation was incorrect.

Finally, we wanted to see what controller strategies had already been implemented. In general two strategies are proposed. Feed forward where the rear wheels are steered in proportion to the front wheels. This scheme is easy

---

[6] Sano et al., "Four Wheel Steering System with Rear Wheel Steer Angle Controlled as a Function of Steering Wheel Angle," SAE #860625, 1989.

[7] Whitehead J., "Four Wheel Steering: Maneuverability and High Speed Stabilization," SAE# 880642, 1989, 4.674p.

[8] Takiguchi et al., "Improvement of Vehicle Dynamics by Vehicle-Speed-Sensing Four-Wheel Steering System," AE#860624, 1987, 3.878p.

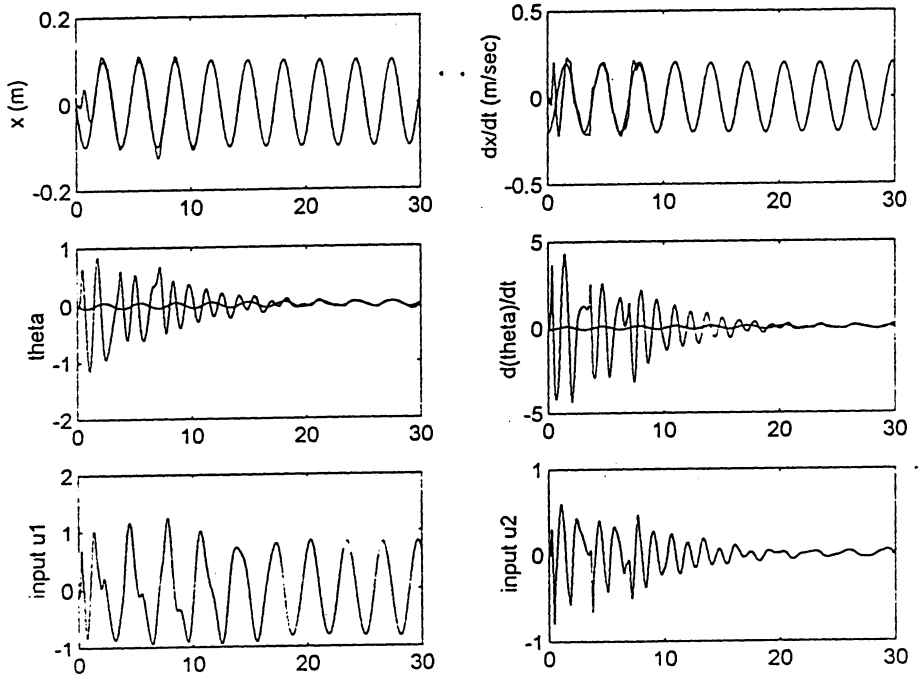

Figure 24a

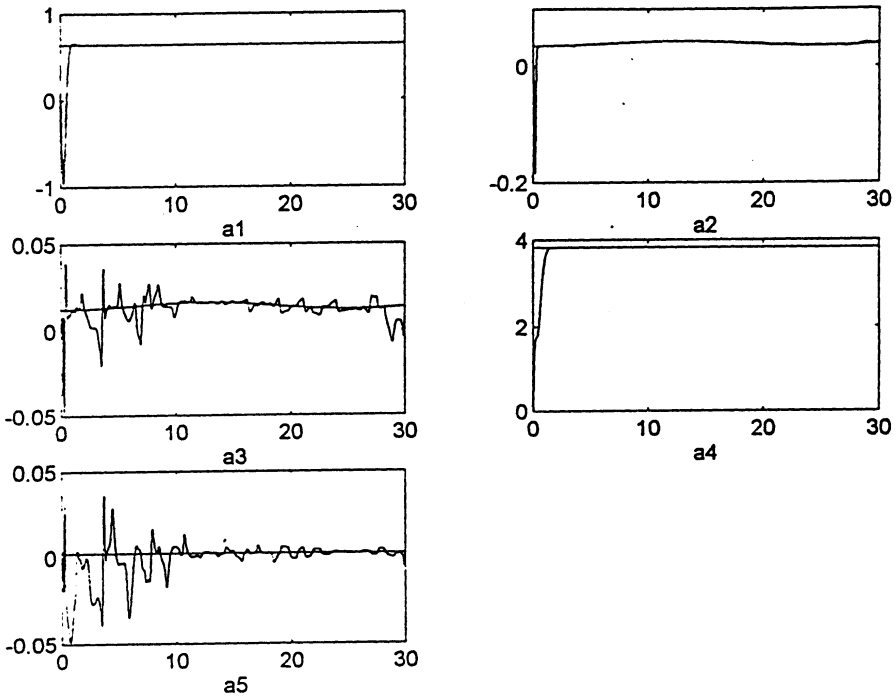

Figure 24b

to implement and has the advantage that it provides a built in predictability from the drivers view point.

Feed Forward

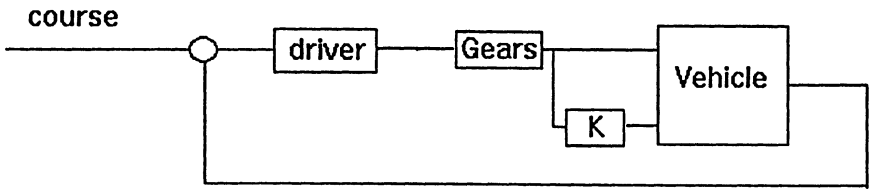

Active control of the rear wheel has been proposed in several papers but we were unable to find any physical implementations. The biggest concern with active 4WS is that an improperly designed controller could make the car unpredictable.

Rear wheel control

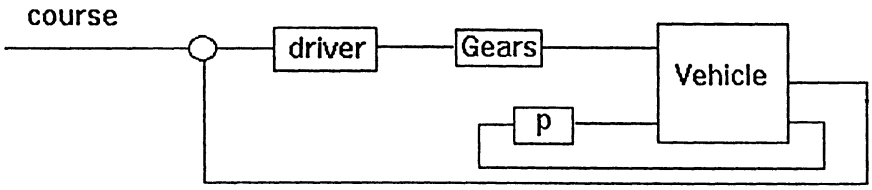

Research

Derivation of Equations of Motion

Since most papers use the bicycle model for development, an obvious question is would a higher order model provide some useful information? In order to answer this question a new model needed to be developed. Currently, it is assumed that the steering angle and DC motor driving torque for each wheel will be controlled. The model developed must relate the earth-fixed frame position and velocity of the vehicle to input torques and steering angles so that a given vehicle trajectory can be tracked. In addition, the model must calculate the roll, pitch and yaw velocities and corresponding Euler angles of the vehicle from these inputs so that ride comfort constraints can be placed on the control action.

Since the development of an inertial frame model for the vehicle is necessarily nonlinear from a theoretical and practical standpoint, the model will be built as a combination of simpler blocks representing different systems within the vehicle. This construction allows future use of integrator-backstepping control methods to deal with the nonlinearities of the system. Although it is uncertain what level of model complexity is adequate for simulation of an actual vehicle like the one described above, performance simulations using this model and varying its parameters should determine whether a controller is robust enough to deal with inevitable modeling inaccuracies.

Car Body Block:

The **car body block** inputs forces and torques (expressed in terms of the inertial frame) applied to the center of gravity of the car. Its states are the x, y, and z, positions and linear velocities and roll (f), pitch (q) and yaw (y) angles and angular velocities of the vehicle in the inertial frame.

We know that

$$M\ddot{x}_{l,c} = C(x)\dot{x}_{l,c} + F_{l,c}$$
$$H\ddot{x}_{r,c} = P(x)\dot{x}_{r,c} + T_{r,c}$$

and

$$\dot{x}_{l,o} = R\dot{x}_{l,c},$$
$$\dot{x}_{r,o} = J\dot{x}_{r,c}$$
$$\ddot{x}_{l,o} = R\ddot{x}_{l,c} + \dot{R}\dot{x}_{l,c}$$
$$\ddot{x}_{o} = J\ddot{x}_{c} + \dot{J}\dot{x}_{c}$$

where $\dot{x}_c = \left[\dot{x}\ \dot{y}\ \dot{z}\ \dot{\phi}\ \dot{\theta}\ \dot{\psi}\right]^T = \left[\dot{x}_{l,c}\ \dot{x}_{r,c}\right]^T$ and $\ddot{x}_c = \left[\ddot{x}\ \ddot{y}\ \ddot{z}\ \ddot{\phi}\ \ddot{\theta}\ \ddot{\psi}\right]^T$ are the velocity and acceleration vectors, respectively, in the non-inertial car frame, and $\dot{x}_o = \left[\dot{x}_o\ \dot{y}_o\ \dot{z}_o\ \dot{\phi}_o\ \dot{\theta}_o\ \dot{\psi}_o\right]^T = \left[\dot{x}_{l,o}\ \dot{x}_{r,o}\right]^T$ and $\ddot{x}_o = \left[\ddot{x}_o\ \ddot{y}_o\ \ddot{z}_o\ \ddot{\phi}_o\ \ddot{\theta}_o\ \ddot{\psi}_o\right]^T$ are the velocity and acceleration state vectors in the inertial frame. It should be noted that for the center of gravity, many of the terms in $\dot{R}$, namely those dependent on $x_{l,c}$ states can be disregarded since the center of gravity is always at the origin of the non-inertial frame. The state-dependent matrices P_r, the skew-symmetric equivalent of the angular momentum vector, P_l, a similar matrix representing Coriolus' forces, and R and J, the correlation matrices between the inertial translational and Euler angular velocities and the car frame translational and angular velocities, can be expressed as :

$$P_r = \begin{bmatrix} 0 & 0 \\ 0 & H[\dot{x}_{r,c}^*] \end{bmatrix}$$
$$P_l = \begin{bmatrix} 0 & 0 \\ 0 & \dfrac{\partial R}{\partial \gamma}[\dot{\gamma}^*] \end{bmatrix}$$

where each of the elements represents a 3x3 matrix and the star symbol represents the skew-symmetric equivalent matrix of a vector cross product. Also,

$$J = \begin{bmatrix} 1 & \sin\phi\tan\theta & \cos\phi\tan\theta \\ 0 & \cos\phi & -\sin\phi \\ 0 & \sin\phi\sec\theta & \cos\phi\sec\theta \end{bmatrix}$$

$$R = \begin{bmatrix} \cos\psi\cos\theta & \cos\psi\sin\theta\sin\phi - \sin\psi\cos\phi & \cos\psi\sin\theta\cos\phi + \sin\psi\sin\phi \\ \sin\psi\cos\theta & \sin\psi\sin\theta\sin\phi + \cos\psi\cos\phi & \sin\psi\sin\theta\cos\phi - \cos\psi\sin\phi \\ -\sin\psi & \cos\theta\sin\phi & \cos\psi\cos\theta \end{bmatrix} = R^{-T}$$

P_r and P_I can therefore be rewritten as

$$P_r = \begin{bmatrix} 0 & 0 \\ 0 & HJ[\dot{x}_{r,I}*] \end{bmatrix}$$

$$P_I = \begin{bmatrix} 0 & 0 \\ 0 & MJ^{-1}[\dot{\gamma}*] \end{bmatrix}$$

The vector F represents force and torque inputs to the system from the four wheel/suspensions and is of the form $F_c = \begin{bmatrix} F_{x,c} & F_{y,c} & F_{z,c} & \tau_{x,c} & \tau_{y,c} & \tau_{z,c} \end{bmatrix}^T$. In this case, since we assume four wheel are present, F is a 12x1 vector. For this model $M = diag[m \; m \; m \; I_{x,c} \; I_{y,c} \; I_{z,c}]$. Lastly, we can also say that

$$F_I = \begin{bmatrix} F_{x,I} & F_{y,I} & F_{z,I} & \tau_{x,I} & \tau_{y,I} & \tau_{z,I} \end{bmatrix}^T = \begin{bmatrix} R & 0 \\ 0 & J^T \end{bmatrix} F_c$$

Using these equations, it is possible to derive a set of equations relating inertial frame force and torque inputs to inertial frame linear and angular positions and velocities. It can be expressed as

$$\begin{bmatrix} \dot{x}_I \\ \ddot{x}_I \end{bmatrix} = A \begin{bmatrix} x_I \\ \dot{x}_I \end{bmatrix} + BF_I$$

where $A_r = [x_{r,I}*]J^{-1}$, $A_I = R^T([J^{-1}g*]-R)R$
$B_r = JH^{-1}J^T$, $B_I = R^TM^{-1}R = 1/m\ I$

Suspension block:

The **suspension block** is constructed in order to calculate z forces from inertial state information and to correlate suspension forces in the car frame x and y coordinates to forces in the inertial x and y coordinates. For the z-direction, the suspensions are assumed to be simple sets of sprung masses and linear springs and dampers, as shown in Figure 1. The unsprung (tire) mass and tire stiffness (K_t) are neglected for the time being. The z forces are thus calculated according to the equation

$$F_{z,i} = -k_i z_i - b_i \dot{z}_i$$

where z_i can be expressed as a function of the z position of the center of gravity, the roll angle and the pitch angle, which are all inputs to the block from the car body block. Similarly, the vertical velocity at each of these suspension points can be expressed as a function of the equivalent velocity states.

The x and y forces at the suspension points (inputs from the road-tire block) are projected onto the inertial frame axes. These forces are then summed in order to get the total forces in the inertial x and y directions. The inertially-expressed forces at the suspension points are also multiplied by their moment arms from the center of gravity in order to calculate torques in the inertial frame. This process is reflected in the equation

$$F_I = RF_c$$

Road-Tire Contact Block:

The **road-tire contact block** uses steering wheel angle (in the car frame), and the car frame suspension point vertical forces calculated in the suspension block as well as the inertial states of the car body block to calculate the x and y (car frame) forces exerted by the road on the tire. It is assumed that the force in the y direction is directly proportional to the tire slip angle (a) i.e.

$$F_{y,i} = C_{a,i}a$$

where $C_{a,i}$ is the cornering stiffness associated with the i^{th} tire. As seen in Figure 2, the cornering stiffness can be assumed constant over the small range of slip angles normally encountered in driving. The tire slip angle is calculated as the angle between the velocity of the car body suspension point related to the tire and the car frame. Therefore,

$$\alpha_1 = \delta - \arctan\left(\frac{\dot{y}_c + \omega_z b}{\dot{x}_c - w_z d/2}\right)$$

$$\alpha_2 = \delta - \arctan\left(\frac{\dot{y}_c + \omega_z b}{\dot{x}_c - w_z d/2}\right)$$

$$\alpha_3 = \delta - \arctan\left(\frac{\dot{y}_c + \omega_z b}{\dot{x}_c - w_z d/2}\right)$$

$$\alpha_4 = \delta - \arctan\left(\frac{\dot{y}_c + \omega_z b}{\dot{x}_c - w_z d/2}\right)$$

In the above equation, the car frame velocities $\dot{x}_c$ and $\dot{y}_c$ can be obtained from the inertial velocity states using the transformation matrix R and its Jacobian

with respect to g.

The force in the x direction is modeled as having a maximum possible value of

$$F_{x,i} = m(l)F_{z,i}$$

where m is the friction coefficient between the tire and the road and lambda is forward slip, defined as

$$\lambda = \frac{\dot{x}_c - \omega r}{\dot{x}_c}$$

where r is the radius of the tire and w is the rotational velocity of the tire. the longitudinal friction force traction force is, therefore, modeled as saturating at this boundary value, which is a highly nonlinear function. It is evident from Figure 3 that the correlation between m and l is nonlinear but that it can be parametrically expressed as an exponential function. Since it is not possible to measure these parameters as they change during vehicle operation, any applied control system must be robust over the range of possible m parameter values.

Mechanical Tire Block:

The **mechanical tire block** performs a torque balance on each wheel. Torques applied by the DC wheel motor, road forces in the x direction, brakes and kinetic friction are added together to determine the rotational speed of the wheels (the only states in this block). The general equation used is

$$I_w\dot{\omega}_i = -b_w\omega_n + \tau_i - \tau_{b,i} - r_w F_{x,i}$$

I_w is the rotational inertial of the wheel, b_w is the frictional damping associated with the wheel, $t_{b,i}$ is the braking torque and t_i is the motor torque.

Motor Block:

Finally, the **motor block** is a linear, dynamic electrical model of the DC motors on each of the wheels. Assuming that a voltage e is input to a motor with internal resistance R, inductance L and motor constant K_t the general state equation used (according to Kirchoff's Law)

$$\dot{i}_i = \frac{-R_i}{L_i} i_i - \frac{K_{t,i}}{L_i}\omega_i + \frac{1}{L} e_i$$

The output of the block is actually motor torque, which is directly proportional to

current.

Implementation of Equations of Motion

In order to be able to verify control design and test that the dynamic equations performed reasonably, they needed to be placed in a simulation environment. The first equation of motion we tried to implement was the car body block. This seemed like both the most important and most difficult block to implement. All equations were originally derived in Mathematica. Originally, they were fully expanded in Mathematica and transferred to C MEX files for speed. This method turned out to be impossible since it required entering hundreds of expressions by hand, and verifying the correctness of the equations was nearly impossible.

In parallel we also developed a model in Autosim. Autosim has the advantage that it produced C code optimized for speed that was easy to port to Simulink. Early testing was highly encouraging, Appendix one contains the code used for testing, the Simulink diagram and one out of 4 plots from a set of 120. The first set of 120 was just inputting forces into the four corners of the car that would produce pure moments and pure translations. Since this appeared to be going better than the manual derivation of the equations we tried to use Mathematica on the raw equations to derive the equations in a symbolic form. This produced equations that were no doubt valid but were not analytically useful, as they were 7-8 pages long in Mathematica. We wrote a program to run Simplify on a matrix term by term saving each simplified term. Unfortunately, one day latter the equations were still not of reasonable length.

However, it did look like we could use the equations in Simulink and at least perform the Matlab command linmod to generate a linearized model. The non-linear nature of the system was clear in attempting to linearize the system. Depending on the chosen point, to linearize around the system was either controllable or uncontrollable. Specifically, attempting to linearize around 0 velocity led to an uncontrollable system, whereas any non-zero velocity made the system controllable. This block was used to design the suspension block. Unfortunately, the code turned out to be unstable and calls to Mathworks revealed that the C MEX interface for windows is not yet "stable."

In the meantime, the analytical equations were being implemented as Matlab MEX files. This allowed the equations to be represented as matrices and made debugging possible. However, these equations are extremely slow -- over two orders of magnitude slower than the C MEX equations. The speed decrease is to be expected as Matlab MEX files are slower than C MEX files. More significantly, the C MEX files were already multiplied out whereas the Matlab files performed the matrix multiplications at each step. The Matlab MEX files were tested with the same procedure used on the Autosim model. However, since these equations take in forces at the center of gravity the testing set was much smaller.

Control Work

As a first attempt at control work we decided to attempt the method of Slotine and Li.[9] Starting with the dynamic equations which were in the proper form.

$$1.\ M\ddot{x} + C\dot{x} = F$$

The tracking error, e is defined by the equation

$$2.\ e = x - x_d$$

where x_d is the desired trajectory. We can also define a intermediate variable r such that

$$3.\ r = \alpha e + \dot{e}$$

From these equations, we, can calculate the following derivatives

$$4.\ \dot{e} = \dot{x} - \dot{x}_d$$
$$5.\ \ddot{e} = \ddot{x} - \ddot{x}_d$$
$$6.\ \dot{r} = \alpha\dot{e} + \ddot{e}$$

Substituting these derivatives into the dynamic equation, we get

$$7.\ M(\dot{r} - \ddot{x}_d - \alpha\dot{e}) + C(r - \alpha e - \dot{x}_d) = F$$

and thus

$$8.\ M\dot{r} = M(\ddot{x}_d + \alpha\dot{e}) + C(\dot{x}_d + \alpha e) - Cr + F$$

We propose a Lyapunov function of the form

$$9.\ v = \frac{1}{2} r^T M r$$

The matrix M is a positive definite matrix which is the equivalent of the car frame mass and inertia matrices represented in the inertial frame. We can prove that v is also positive definite by the following

H which is the inertia in the car frame is full rank, positive, and diagonal.

$x^T Hx > 0$

Create the synthetic vector

$\bar{x} = J^{-1}x$

Then

[9] Slotine et Li, Applied Nonlinear Control,Prentice Hall,1991.

$\bar{x}^T H\bar{x} > 0$

$x^T J^{-T} H J^{-1} x > 0$

by definition

$M = J^{-T} H J^{-1}$

QED M will always be positive definite.

10. $\dot{v} = \frac{1}{2} r^T \dot{M} r + r^T M \dot{r}$

Substituting from the dynamics in terms of r

11. $\dot{v} = \frac{1}{2} r^T \dot{M} r + r^T \left(M(\ddot{x}_d + \alpha \dot{e}) + C(\dot{x}_d + \alpha e) - Cr + F \right)$

12. $F = -\left(M(\ddot{x}_d + \alpha \dot{e}) + C(\dot{x}_d + \alpha e) + Kr \right)$

13. $\dot{v} = \frac{1}{2} r^T \dot{M} r + r^T (-Cr) - r^T Kr$

From physics of the system this matrix will be skew symmetric. Note that this applies to the torque transformation matrix and NOT to the linear transformation matrix. Slotine and Li do not develop the equations for linear translation.

14. $r^T \left[\frac{1}{2} \dot{M} - C \right] r = 0$

15. $\dot{v} = -r^T Kr$

Therefore since K is a free design parameter, we can make it positive definite and thus v dot is negative definite and we have a valid Lyapunov function.

We would also like to have some information about the stability or rate of convergence of this system. Following the method present by Dawson et al.[10] We will propose canceling the terms in 13 with a bounding function rather than exact cancellation. Assume 16

16. $-\left(M(\ddot{x}_d + \alpha \dot{e}) + C(\dot{x}_d + \alpha e) \right)$

Is bounded by 17

17. $\rho(x, \dot{x}, t)$

Then we can propose to cancel the terms with

18. $vr = \frac{r\rho^2}{\|r\|\rho + \varepsilon}$

Rather than attempting exact cancellation.

With this formulation we get the general bound on error refer to Dawson for details.

19. $e(t) < e^{-\alpha t} \|e(0)\| + \frac{a}{\alpha}\left(1 - e^{-\alpha t}\right) + \frac{b}{\alpha - k}\left(e^{-kt} - e^{-\alpha t}\right)$

20. $a = \sqrt{|A|}$ 21. $A = \frac{\varepsilon}{M1 * k}$

---

[10] Dawson et al, Nonlinear Control of Robotic Systems for Environmental Waste and Restoration,Prentice Hall,1995.

22. $b = \sqrt{|B|}$ 23. $B = \frac{M2}{M1} * \|r(0)\|^2 - \frac{\varepsilon}{M1 * k}$

If we attempt the deterministic case first then the following will be true

1. M1=M2=M
2. $\rho = -\left(M(\ddot{x}_d + \alpha\dot{e}) + C(\dot{x}_d + \alpha e)\right)$
3. $\varepsilon = 0$

Then the bound on the error will reduce to

24. $e(t) < e^{-\alpha t}\|e(0)\| + \frac{\|r(0)\|^2}{\alpha - k}\left(e^{-kt} - e^{-\alpha t}\right)$

25. $r^T\left(\Delta M(\ddot{x}_d + \alpha\dot{e}) + C(\dot{x}_d + \alpha e)\right)$

26. $-r^T Kr$

As long as the term 26 dominates the term 25 our stability properties will be preserved.

Controller Performance

Early on we achieved a standard exponential response to a step input. This seemed quite encouraging and we turned to the tracking problem. Since we knew a we wished to track a sinusoid that was the next logical input. At his point we discovered that we did NOT have the correct controller. Sinusoids should have been tracked within a decaying exponential, however they were simply tracked in a lagging fashion with constant error. After examining the system we discovered that we had assumed that a translational terms has a similar cancellation property to equation 14. This is not the case and we turned to trying to control an angle.

Control of the angles in the car is not of particular use. However, we wished to verify the control design technique so we turned to this simpler problem. Note that the equations for the plant and the Simulink diagram are presented in Appendix II. Init_Par was used to hold car parameters it also calculates the "precomputed" values needed in AutoSim. Carmex implements the basic equations for the car. Latcont is the Lypanov controller. Cal_r calculates matrices used in both carmex and latcont. While reducing speed this assures that the controller and the plant are being calculated from equations of the same form.

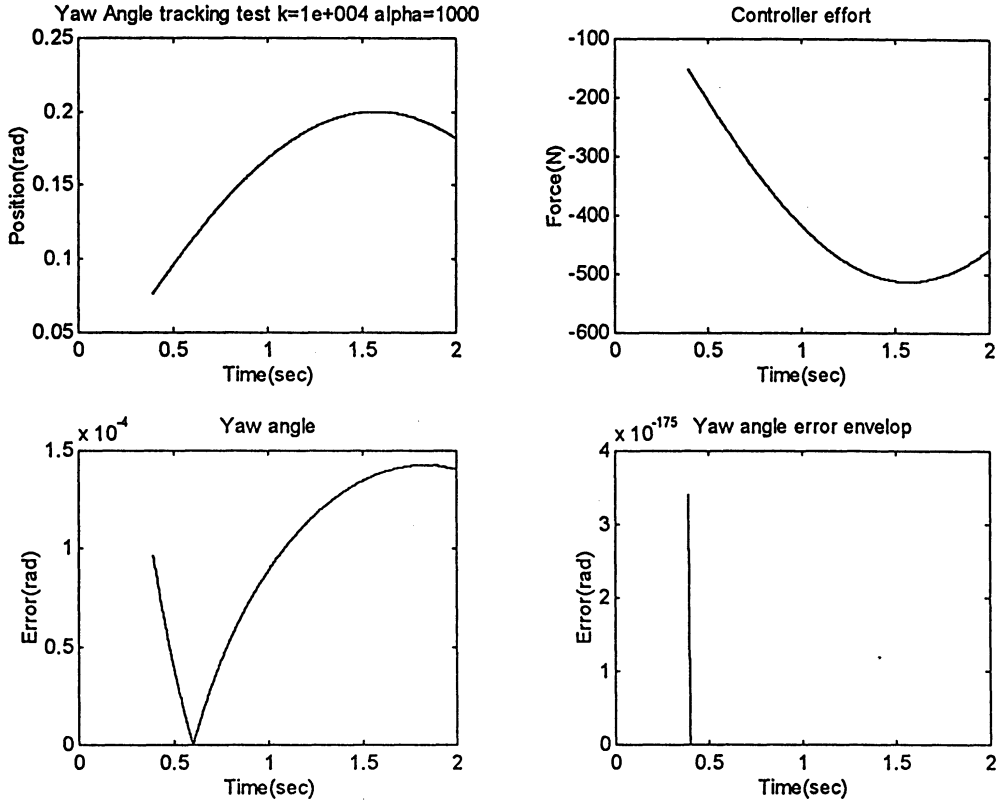

High gains yield a quick response. The error is lower here at two seconds than it is for gains that are a factor of 10 lower. Interestingly, this one has one of the better controller effort curves. This only helps to reinforce that tuning these controllers is exceptionally difficult. As a matter of fact we are aware of no methodology for doing tuning of these controllers, except for controlling error envelop size.

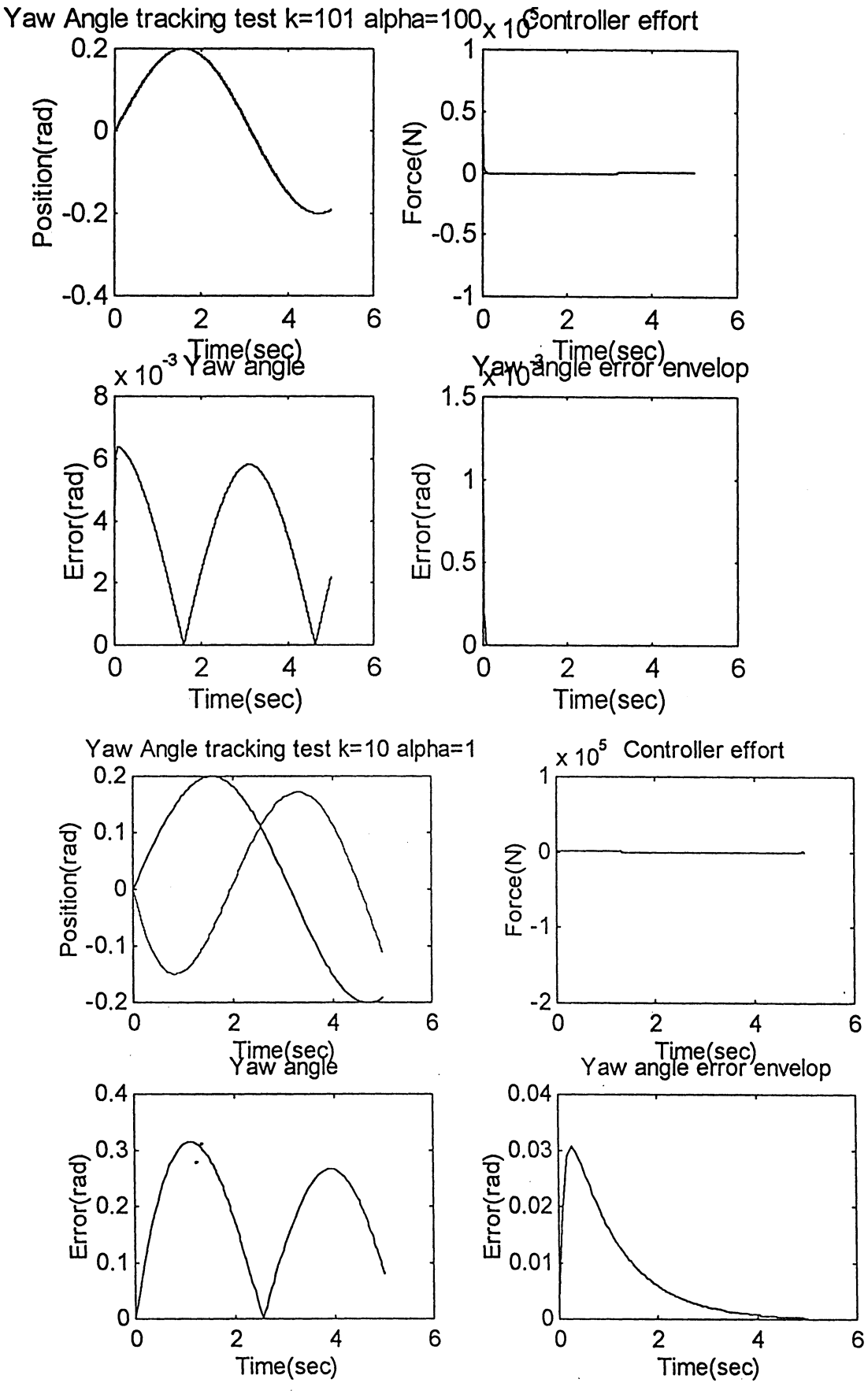

Lower gains leading to slower response times and more persistent error. Note that this case also perturbs the inertia matrix by 20%. The unperturbed case has

an identical shape the only difference is that the maximum error goes down to 6e-3. Note there is still a problem in the system. The error is clearly not within the theoretical error envelop. Since the controller is successfully tracking a sinusoid we believe it is an error in our transformation of the error bounding equations rather than a controller problem.

Conclusions

Difficulty does NOT increase linearly with increasing complexity. This is undoubtedly why almost all vehicle controls work is done on simple models. We originally we trying to see how we could improve on the simple linear models. The answer is that we never got close to controlling real car dynamics. In implementing large systems you need either an automatic program writer like Autosim, or you must express the equations in an inefficient but debuggable format. The full model might be useful in that it would allow one to examine if steering the wheels to different angles based on the load at each tire would improve turning performance. The Lyapnov controller turned out to be quite simple to implement. However, it would be much more difficult in the context of the entire model, which would include suspension and tire dynamics. For the full model we envision the use of integrator backstepping to glue the various subsystems together.

Sorry, about the last few paragraphs they were written on very little sleep.

But we Got results some something is not quite correct but the controller tracks. Now I will sleep until my 560 Exam.

Control of Underactuated Robot Manipulators

Yung-Chang Tan

ME 662 Final Project Report

Instructor : Prof. Tilbury

December, 1995

University of Michigan

1. Introduction

The underactuated system refers to the fact that the system has more joints than control actuators. A common design for the underactuated system is realize the manipulator with kinematically redundancy but using only a minimum number of actuators. A manipulator is said to be kinematically redundant if the dimension of the task space is less than the number of the degrees of freedom (DOF). The kinematically redundant manipulators are able to change the internal structure of configuration of the mechanisms without changing the end effector or of the object. Therefore, they have the advantages of avoiding obstacles, geometrical singularities, and joint limits, and optimizing various performance criteria.

Redundant manipulators using only a minimum number of actuators, equal to the dimension of the task space, are important from the viewpoint of energy saving, lightweight design and compactness.

In the case of rigid manipulators the inverse dynamics control and the feedback linearizing control are the same. This inverse dynamics control technique guarantees that the fully actuated n-link manipulator is always exactly linearizable. Because it can always decouple this nonlinear system into n linear second order system without considering the friction and flexibility at the joints. That gives us the intuition that we can decouple the underactuated system into the linearizable subsystem and the internal dynamics.

Assume that the Jacobian of the task equations has full rank, i.e., the manipulator is not at a geometrically singular configuration. The singularity occurs if the control forces cannot effect the end-effector accelerations instantaneously in some directions. This project deals with the singularities by using the modified equations to approximately get the solutions. However, without trajectory planning to avoid the singular points, the manipulator still undergoes some unexpected movements and needs extremely large control torque to go through them.

2. Feedback Linearization and Riemannian curvature

For a manipulator with n degree of freedom, if we write the kinetic and potential energies as

$$T = \frac{1}{2}\sum_{i,j}^{n} d_{ij}(q)\dot{q}_i\dot{q}_j \tag{2.1}$$

$$U = U(q_1,\ldots,q_n) \tag{2.2}$$

The traditional Lagrange's equations of motion can be written as

$$\sum_{j=1}^{n} d_{kj}(q)\ddot{q}_j + \sum_{i,j=1}^{n} \Gamma_{ijk}(q)\dot{q}_i\dot{q}_j + \phi_k(q) = \tau_k \tag{2.3}$$

where $\Gamma_{ijk} = \frac{1}{2}\left\{\frac{\partial d_{kj}}{\partial q_i} + \frac{\partial d_{ki}}{\partial q_j} + \frac{\partial d_{ij}}{\partial q_k}\right\}$ are known as Christoffel symbols of the first kind, and

$$\phi_k = \frac{\partial U}{\partial q_k} \tag{2.4}$$

It is common to write Eq.2.3 in matrix form as

$$M(q)\ddot{q} + C(q,\dot{q})\dot{q} + \phi(q) = \tau \tag{2.5}$$

This equation will be in later use to derive the equations of the under-actuated system. Although this equation is extremely complicated , there are a number of dynamic effects that are not included in it. For example, friction at the joints and flexibility of the robot arms.

Hamiltionian is defined as the sum of the kinetic and potential energy

$$H = p^T\dot{q} - L = P^T\dot{Q} - L \tag{2.6}$$

which implies the canonical transform

$$\begin{aligned} P &= P(p,q) \\ Q &= Q(p,q) \end{aligned} \tag{2.7}$$

such that $p^T\dot{q} = P^T\dot{Q}$

If the inertia matrix $M(q)$of an n-link robot manipulator can be factored as $N^T(q)N(q)$ where $N(q)$is integrable,i.e.,the Jocobian of a function $Q(q)$

$$dQ = \frac{\partial Q}{\partial q}dq = N(q)dq \tag{2.8}$$

then Q and $P = N(q)\dot{q}$ define a canonical transformation relative to which the robot dynamic equations are particularly simple.

Theorem 1. Hamilton's equations in the canonical variables Q,P are given by

$$\begin{aligned} \dot{Q} &= P \\ \dot{P} &= N^{-T}\tau \end{aligned} \tag{2.9}$$

Hence $\ddot{Q} = N^{-T}\tau = a_Q$ results in the double integrator, definitely a linear system. The mass matrix is the identity matrix, and there are no Coriolis forces. But the condition is that the factorization $M(\dot{q}) = N^T(q)N(q)$ exists. It is known that the mass matrix M defines a metric tensor on the configuration manifold. M can be diagonalized if and only if the metric tensor is a Eucliidean metric tensor. Thus we have the following theorem.

Theorem 2 . Let M be the Riemannian manifold defined by the robot inertia matrix $D(q)$. Then M is locally flat, i.e., there exists an isometry $Q(q)$ such that

$$\sum_{i,j} d_{ij}dq_i dq_j = \sum_i dQ_i^2 \tag{2.10}$$

if and only if the Riemann symbols vanish identically.

The Riemannian curvature is defined in local coordinates by constructing a covariant tensor of order 4

$$R_{ijkl} = \sum_{h=1}^{n} d_{ih} R_{ikl}^{h} \tag{2.11}$$

where

$$R_{ikl}^{j} = \frac{\partial \Gamma_{ik}^{j}}{\partial q_l} - \frac{\partial \Gamma_{il}^{j}}{\partial q_k} - \sum_{h=1}^{n} \left[\Gamma_{ik}^{h} \Gamma_{hl}^{j} - \Gamma_{il}^{h} \Gamma_{hk}^{j} \right] \tag{2.12}$$

$$\Gamma_{ij}^{k} = \sum_{h=1}^{n} d^{kh} \Gamma_{ijh} \tag{2.13}$$

For example, the inertia matrix of following two-link manipulator is

$$M(\theta) = \begin{bmatrix} m_1 l_{c1}^2 + m_2 l_1^2 + I_1 & m_2 l_1 l_{c2} \cos(\theta_2) \\ m_2 l_1 l_{c2} \cos(\theta_2) & m_2 l_{c2}^2 + I_2 \end{bmatrix} \tag{2.14}$$

the curvature tensor for this case is not zero

$$R_{1212} = -\frac{c_0 l_{c2} \cos(\theta_2)}{\det[D(\theta)]} \tag{2.15}$$

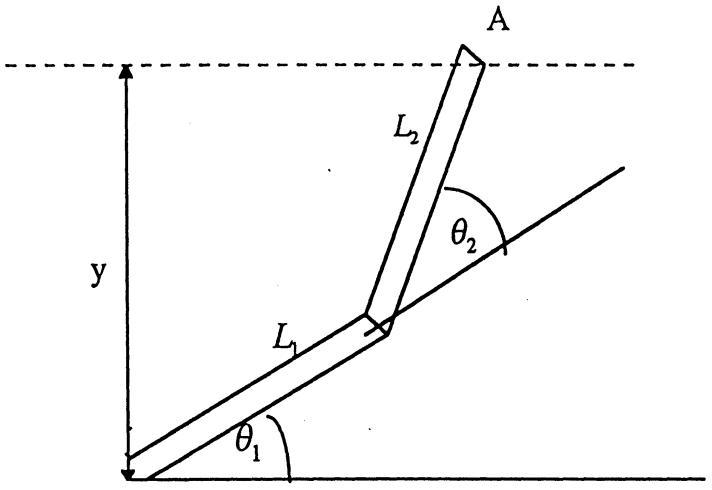

Figure 1. Two-link manipulator

Thus the factorization does not exist. A. Jain and G.Rodriquez[1] argued that the conditions in the theorem are very restrictive and are rarely satisfied by practical multibody system. They proposed an alternative approach to diagonalize the equation of motion that is broadly applicable to complex multibody systems. They do not require N(q) be a Jacobian

matrix. They finally led to a simpler equation $\dot{v} + C(\theta, v) = \varepsilon$ but Coriolis force term is no longer zero.

Because the zero curvature condition can not be satisfied in some cases, the imaginary robot concept is presented as an alternative robust design methodology [Gu and Loh 1990]. The methodology starts out by decomposing M(q) as follows:

$$M(q) = J^T(q)J(q) + \tilde{M}(q) \tag{2.16}$$

where J is the Jacobian between output and joint variables $\dot{y} = J\dot{q}$. and $\tilde{M}(q)$ is small in some appropriate sense.

3. Feedback Linearization for the under-actuated system

Consider a manipulator with n DOF whose joint variables are denoted $q_i(t), i = 1,...,n$. The prescribed end-effector Cartesian variables $r_i(t), i = 1,...,m (m \le n)$ represent tasks of the manipulator. The relations between the joint variables due to the prescribed motions, $f_i(q_1,...,q_n) = r_i$, can be written at velocity level as

$$J_{ij}\dot{q}_j = \dot{r}_i \qquad i = 1,...,m, \quad j = 1,...,n \tag{3.1}$$

where J is an $m \times n$ Jacobian matrix and J_{ij} are, in general, functions of q_i. Differentiation of Eq.3.1 yields the task equations expressed at the acceleration level

$$J_{ij}\ddot{q}_j = \ddot{r}_i - \dot{J}_{ij}\dot{q}_j = I_i \tag{3.2}$$

The equation of motion of the manipulator can be expressed as

$$M(q)\ddot{q} + h(q,\dot{q}) = \tau \tag{3.3}$$

$$\text{where } h(q,\dot{q}) = C(q,\dot{q})\dot{q} + \phi(q).$$

Let there be m actuators for performing the m prescribed motions. Then τ is

$$\tau = A^T u \tag{3.4}$$

where A is an $m \times n$ full rank control force direction matrix being functions of q_i, and u is an $m \times 1$ vector of control force magnitudes. Each row of A represents the direction of one actuator force in the generalized space. Depending on the locations of the actuators, the control forces may have arbitrary directions in relation to the task surfaces. Substitution of Eq.3.4 into Eq.3.3 yields

$$M\ddot{q} - A^T u = -h(q,\dot{q}) \tag{3.5}$$

Let B be an $n \times (n-m)$ matrix that is an orthogonal complement to A. There are several methods to obtain B. These include row equivalence transformation, zero eigenvalue

method, and singular value decomposition. Premultiplying Eq.3.5 by B^T yields reduced equations

$$B^T M\ddot{q} = -B^T h \tag{3.6}$$

These $n-m$ equations constitute the internal dynamics.

Rewrite Eq.3.5 as

$$J\ddot{q} - JM^{-1}A^T u = -JM^{-1}h \tag{3.7}$$

In order to linearize the under-actuated system by using input-output linearization procedure, let us define a new input $v = \ddot{r} = J\ddot{q} + \dot{J}\dot{q}$. Substituting $J\ddot{q} = v - \dot{J}\dot{q}$ into Eq.3.7, we obtain

$$v = \dot{J}\dot{q} - JM^{-1}h + JM^{-1}A^T u \tag{3.8}$$

$$\text{or} \quad u = (JM^{-1}A^T)^{-1}(JM^{-1}h - \dot{J}\dot{q}) + (JM^{-1}A^T)^{-1}v \tag{3.9}$$

Then we have the linearized subsystem, with the change of coordinates

$$\begin{aligned} z_1 &= r \\ z_2 &= \dot{r} = J\dot{q} \end{aligned} \tag{3.10}$$

and the input v such that

$$\begin{aligned} \dot{z}_1 &= z_2 \\ \dot{z}_2 &= v \end{aligned} \tag{3.11}$$

Thus this subsystem turns out to be a double integrator, and we can determine v by the feedback control law $v = -Kz$

4. Singularity problem

From Eq.3.9 we can solve for control force u only if the matrix $JM^{-1}A^T$ is invertible, i.e., it is nonsingular. Let's assume that the Jacobian matrix J has full rank, i.e.,the system is not at a geometrically singular configuration. Then the control force direction matrix A determines if we can always obtain the solutions of u. How to arrange the limited amount of actuators among the joints becomes an significant issue. But this design problem is not going to be investigated in this project.

According to S.K.Ider [3], Eq.3.2 and Eq.3.6 can be reformulated as

$$\begin{bmatrix} H \\ J \end{bmatrix} \ddot{q} = \begin{bmatrix} R \\ I \end{bmatrix} \tag{4.1}$$

where $H = B^T M$, $R = -B^T h$, $I = v - \dot{J}\dot{q}$ and let $\overline{\mathbf{H}} = \begin{bmatrix} H \\ J \end{bmatrix}$

these n differential equations can be integrated to get $q, \dot{q}, \ddot{q}$, and u can be expressed as

$$u = (AA^T)^{-1} A(h + M\ddot{q}) \tag{4.2}$$

In a redundant manipulator, if **A** is chosen such that $\overline{\mathbf{H}}$ is singular then it cannot be inverted, hence a solution cannot be obtained from the dynamical equations written at the acceleration level. However, the realization of the prescribed motions with the control forces is usually still possible due to the effects of the right-hand side term h. Then, to obtain the solution one should consider higher order information by further differentiation of the related equations. To this end, let the singularity be detected during the inversion of $\overline{\mathbf{H}}$ by comparing the pivot elements with a specified small number ε . the linearly dependent rows in $\overline{\mathbf{H}}$ can be identified, and the linear combination constants can be determined from the Gaussian form as obtained by elementary row operations.

Ider used the following modified equation to replace Eq.4.1 in the neighborhood of the singular configurations

$$\begin{bmatrix} H \\ D \end{bmatrix} \ddot{q} = \begin{bmatrix} R \\ d \end{bmatrix} \tag{4.3}$$

$$\text{where } D_{qp} = \begin{cases} J_{qp} & q = a_k, k = 1,\ldots,n-r \\ G_{qp} - \alpha_{ki} G_{b_i p} - \beta_{kj} K_{jp} & q = b_i, i = 1,\ldots,m-n+r \end{cases}$$

$$d_q = \begin{cases} I_q & q = a_k, k = 1,\ldots,n-r \\ E_q - \alpha_{ki} E_{b_i} - \beta_{kj} F_j & q = b_i, i = 1,\ldots,m-n+r \end{cases}$$

$$\text{where} \quad \begin{aligned} \dot{J}_{kp}\ddot{q}_p - \dot{I}_k &= G_{kp}\ddot{q}_p + E_k \\ \dot{H}_{jp}\ddot{q}_p - \dot{R}_j &= K_{jp}\ddot{q}_p + F_j \end{aligned}$$

5. Simulation results

The dynamic and kinematic equations of the 2 and 3 link manipulator are listed in the Appendix A. However, the equation set that is really used in the simulation is Eq.4.3. New control input v can be directly used in Eq.4.3 to solve for $\ddot{\theta}, \dot{\theta}, \theta$, and then u can be constructed by Eq.4.2.

(a). In the two-link planar manipulator the generalized coordinates are θ_1 and θ_2 (n=2). The end point A is prescribed to move along the horizontal line shown as Figure 1.,i.e., y_A=1 (m=1). The task is required to be performed by only one actuator, which is

located at the lower joint of the first link. Let $I_1 = \frac{1}{12} m_1 l_1^2, I_2 = \frac{1}{12} m_2 l_2^2$ and choosing numerical values $l_1 = l_2 = 1, m_1 = m_2 = 6$, different initial conditions can be tested. Figure 3. shows that the end point A is stabilized around the set points y=1 by carefully choosing the initial condition. Figure 4. presents the similar scenario as Figure 3., but as time proceeds the manipulator will approach the singular configuration. We can identify that by the outraging control torque.

Given the numerical values, because the left hand side matrix of Eq.4.1 has the following determinant

$$-2\cos\theta_1 + 3\cos\theta_2 \cos(\theta_1 + \theta_2)$$

which will be zero at $\theta_1, \theta_2 = \pm 90^\circ$ and some other configurations.

Figure 5 shows that the modified equations can help us construct the control torque in the reasonable range when system goes through "minor" singularities. But Figure 6 tell us even the modified equation does not work at some "major" singularities.

(b). Let's consider now a 3-DOF planar manipulator (Figure 2.) with generalized coordinates θ_1, θ_2 and θ_3. This case will have richer results because the end point A can get to any point on the plane as long as the kinematical constraints are not violated. We have to place two actuators to the manipulator to complete the task because the dimension of the task space is two.

Figure 7. shows that the control scheme presented here can stabilize the set point at the velocity level, thus the end point of the manipulator can trace a trajectory, which is a straight line. As can be seen from Figure 8., end A is also capable of getting to the desired point (1,1). The singularity problem still become serious sometimes. Figure 9. shows that when the end A approaching the desired point the singular configuration is encountered. The link 1 spins around its lower joint several times before it settles down. Note that the singular configurations for this case are $\theta_2 = 0$ or $\pm\pi$.

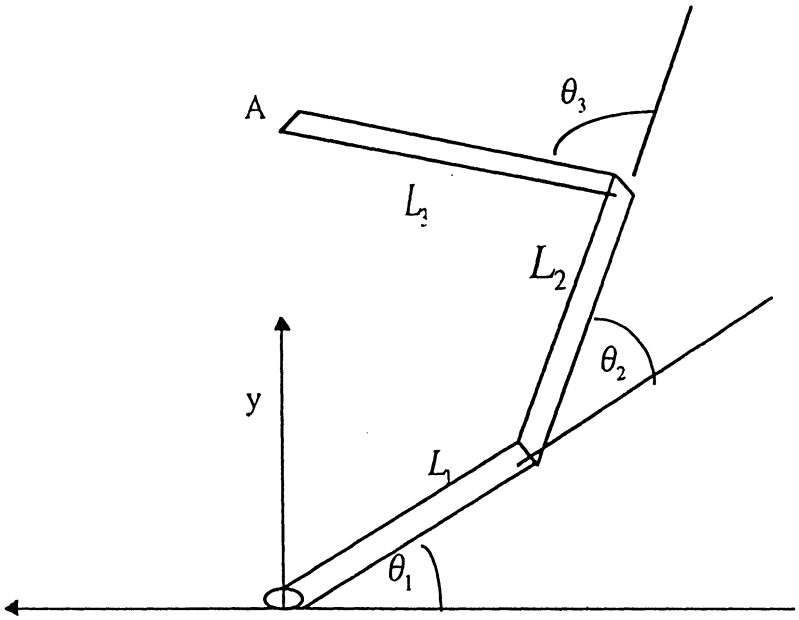

Figure 2. Three-link manipulator

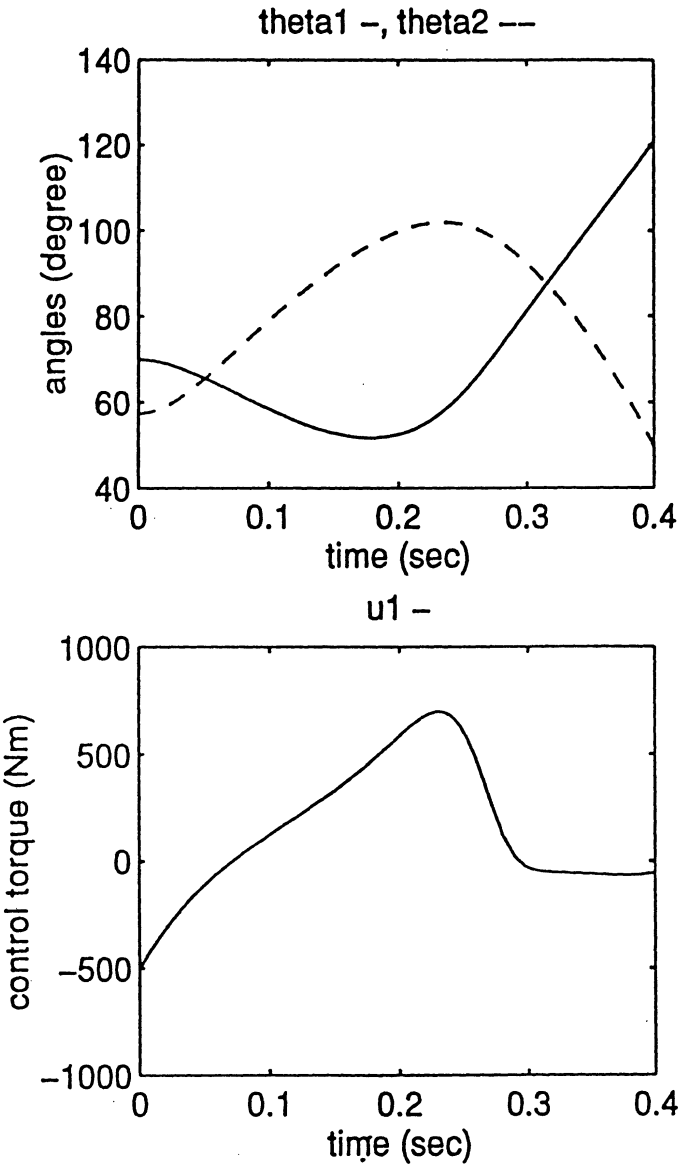

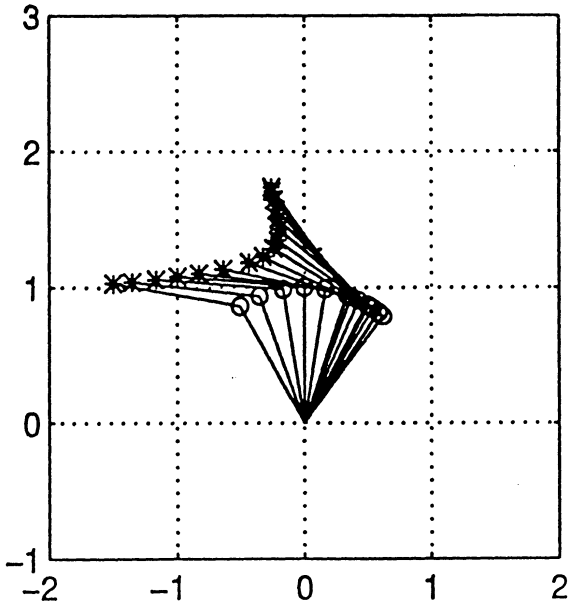

Initial Conditions : theta1=70 deg

theta1=57.2958 deg

th1_dot=0

th2_dot=0

prescibed motion : Y=1 m

Figure.3

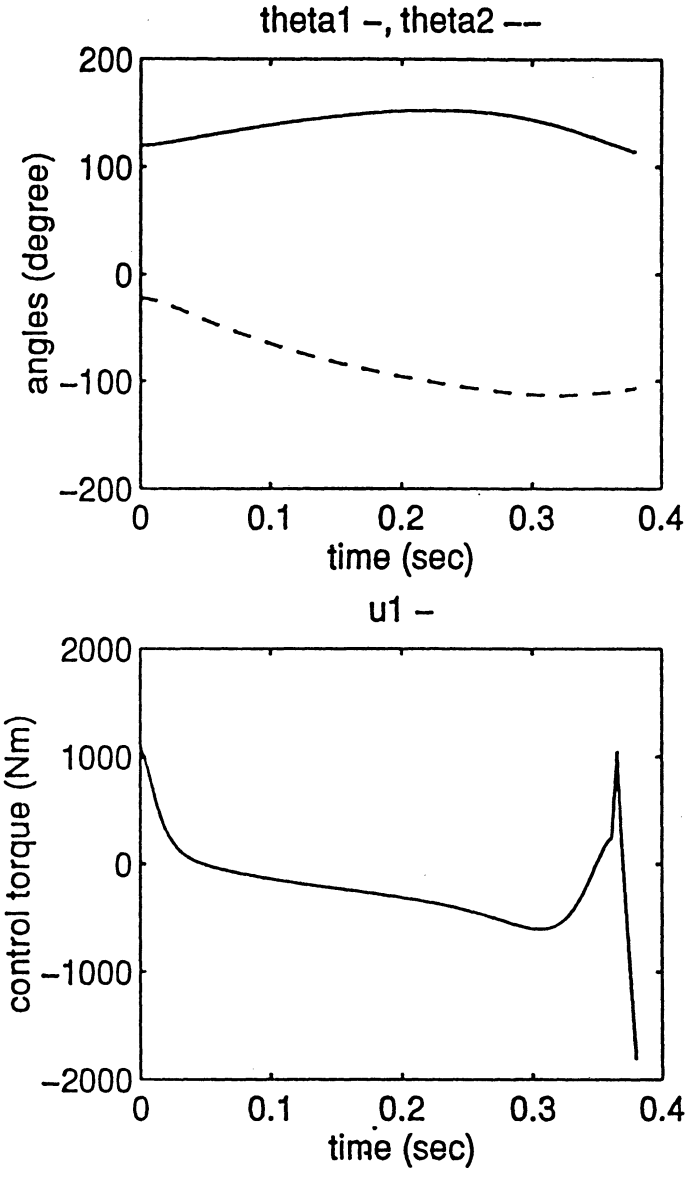

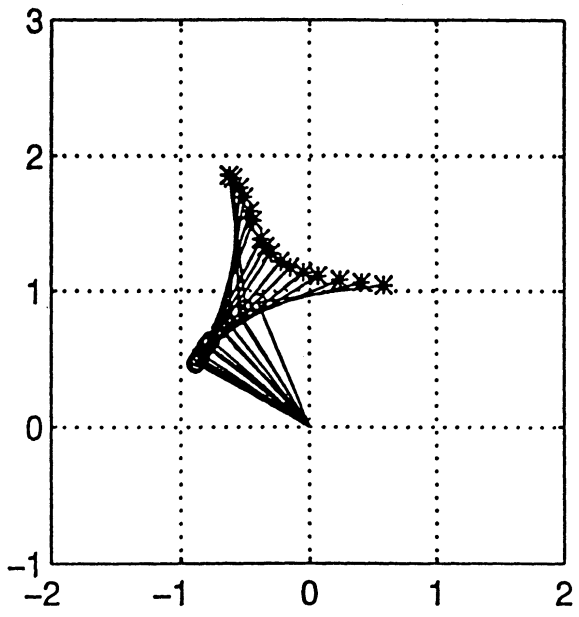

Initial Conditions : theta1=120.000 deg

theta2=-22.500 deg

theta1_dot=0.000

theta2_dot=0.000

prescribed motion : Y=1 m

Figure.4

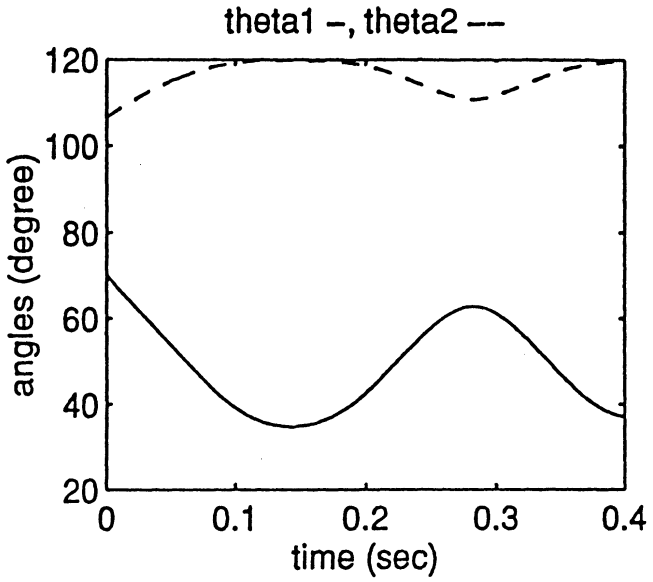

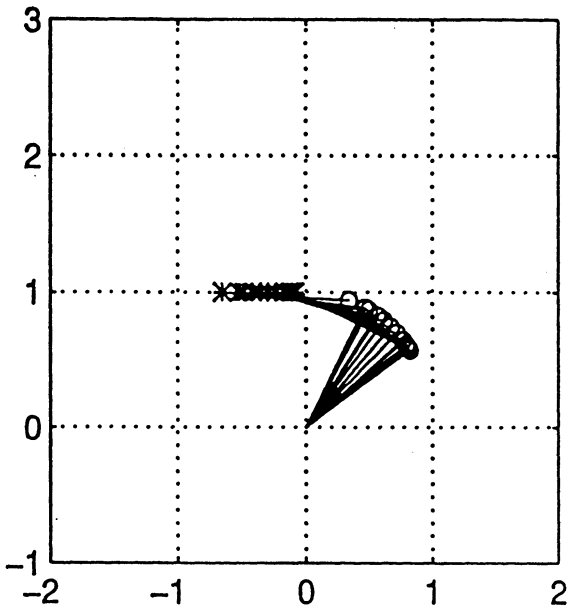

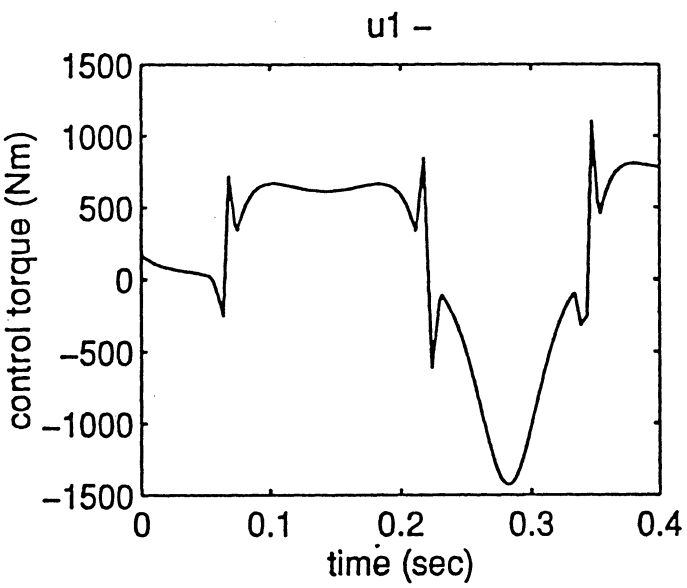

Initial Conditions : theta1=70.000 deg
theta2=106.543 deg
theta1_dot=–5.727
theta2_dot=3.765

prescribed motion : Y=1 m

Figure.5

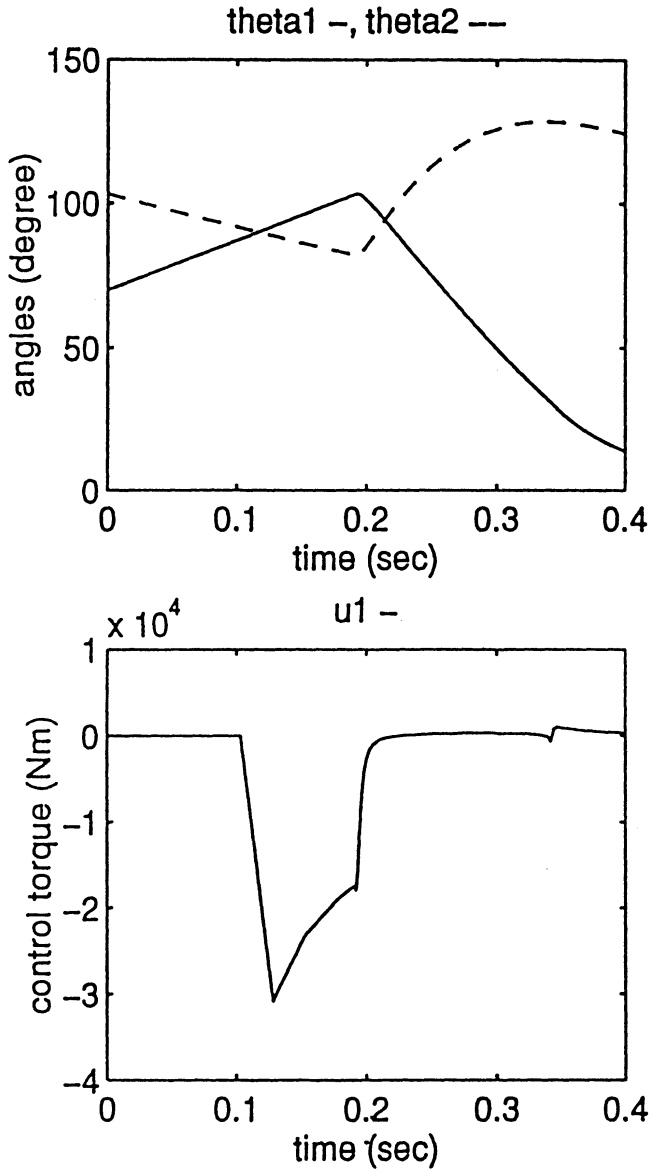

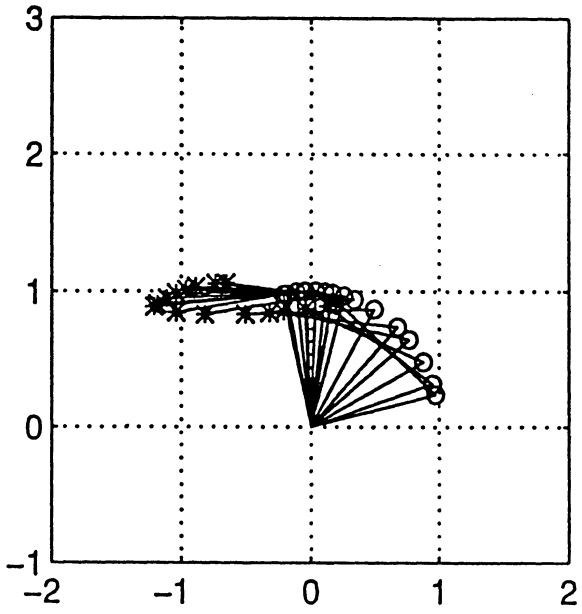

Initial Conditions : theta1=70.000 deg

theta2=103.132 deg

theta1_dot= 3

theta2_dot= −2

prescribed motion : Y=1 m

Figure.6

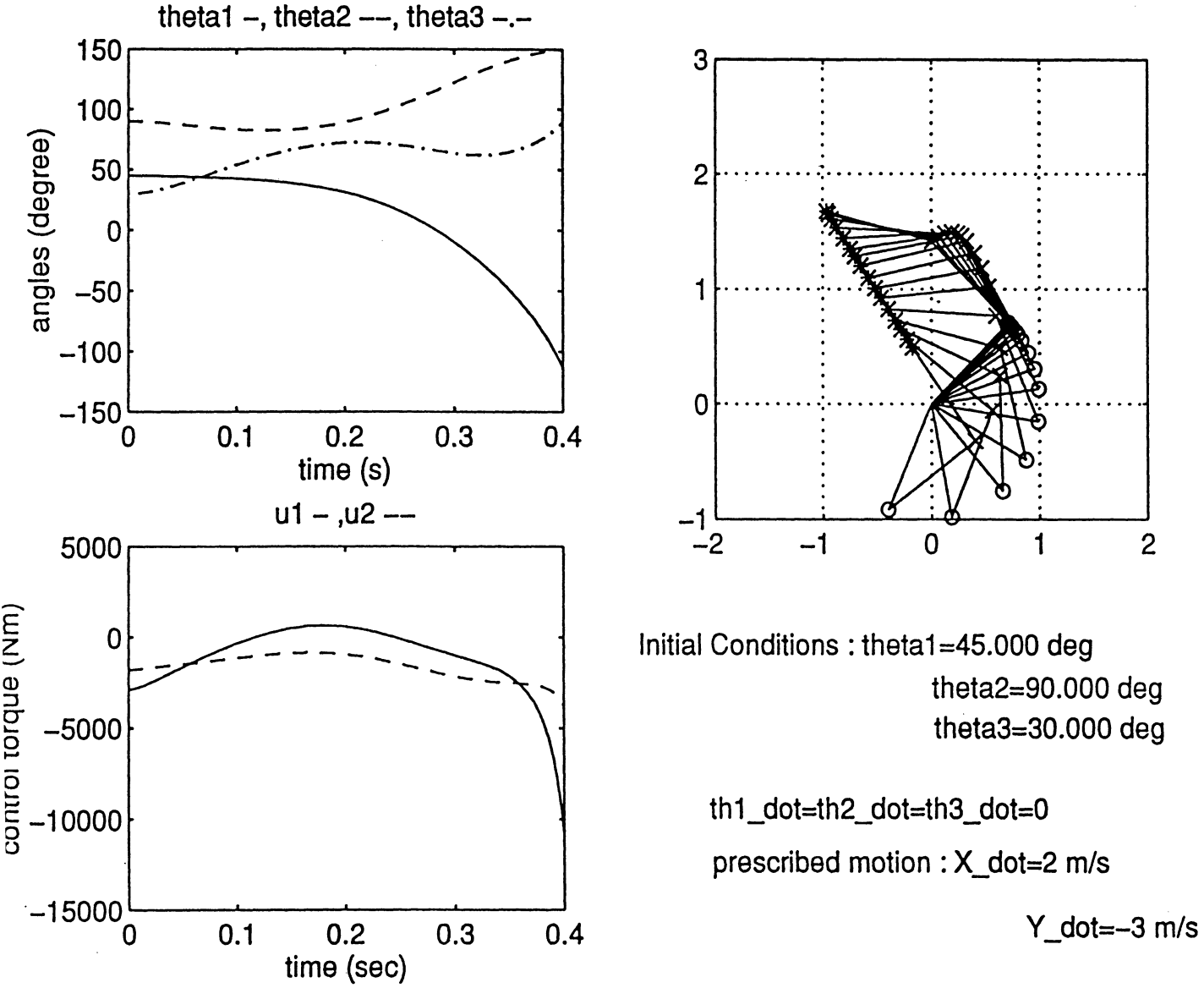
theta1 –, theta2 ––, theta3 –.–
angles (degree)
time (s)
u1 – ,u2 ––
control torque (Nm)
time (sec)
Initial Conditions : theta1=45.000 deg
theta2=90.000 deg
theta3=30.000 deg
th1_dot=th2_dot=th3_dot=0
prescribed motion : X_dot=2 m/s
Y_dot=–3 m/s

Figure.7

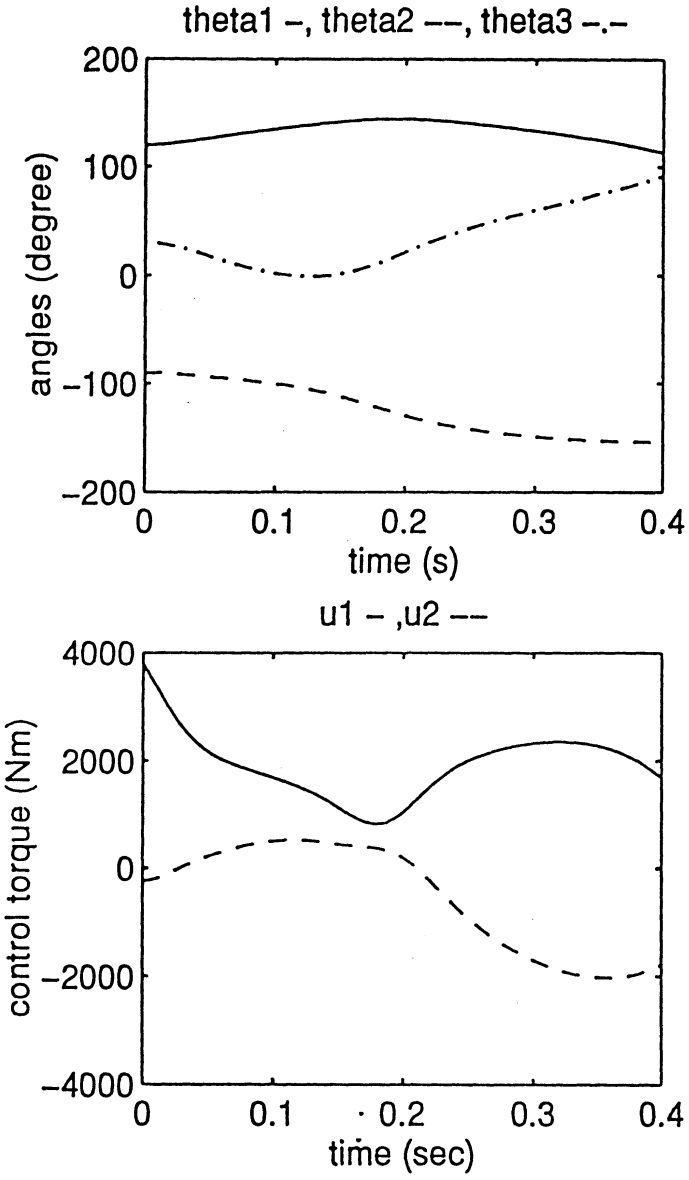

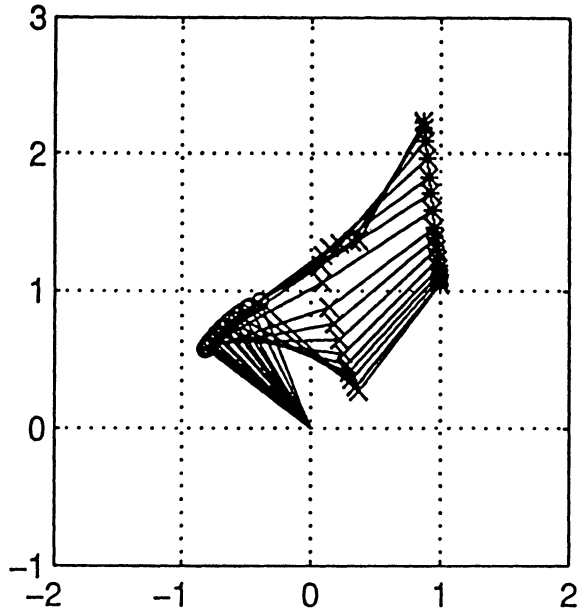

Initial Conditions : theta1=120.000 deg

theta2=–90.000 deg

theta3=30.000 deg

th1_dot=th2_dot=th3_dot=0

prescribed motion :

X=1.00 m Y=1.00 m

X_dot=0.00 m/s Y_dot=0.00 m/s

Figure.8

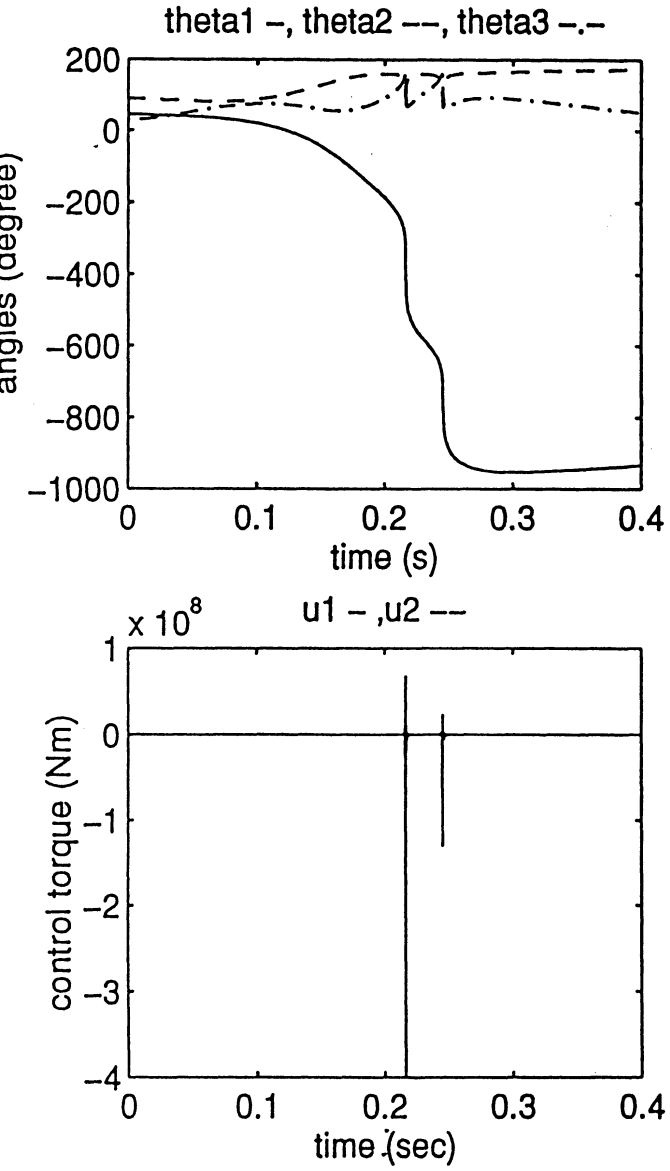

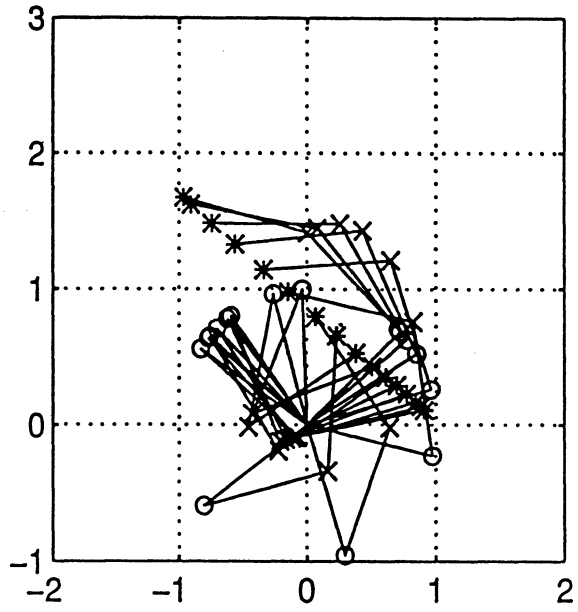

Initial Conditions : theta1=45.000 deg
theta2=90.000 deg
theta3=30.000 deg

th1_dot=th2_dot=th3_dot=0

prescribed motion :

X=1.00 m Y=0.00 m

X_dot=0.00 m/s Y_dot=0.00 m/s

Figure.9

6. Conclusion

There has been recent interest in finding a canonical transformation that can linearize the robot dynamics except for gravity terms. The existence of such a transformation is that the inertia matrix $M(q)$ of an n-link robot can be factored as $N^T(q)N(q)$ with $N(q)$ integrable. And that requires the Riemannian curvature of $M(q)$ vanish identically. These conditions are well-established in the theory of Hamiltonian mechanics and Riemannian geometry [2]. However, such a transformation can not be found for a planar two-link arm. Therefore, we have to turn to another approach to solve the problem.

Because the traditional inverse dynamics or computed torque method works for the fully actuated n-link robot manipulators, this technique and the feedback linearization are used in this article to control the underactuated system. Considering deriving the control algorithm directly in the Cartesian task space, kinematic equations and internal dynamics are solved for the joint variables and their higher order derivatives simultaneously. Then control torques are derived from these information.

The control scheme is verified by the simulation. When singularities happens, the dynamical equations are modified by utilizing higher-order derivative information. However, simulations showed that this method can not be realized very well and sometimes it fail to give reasonable control input. Therefore, the trajectory planning should be further investigated to avoid the singular configurations.

Reference

1. A.Jain and G.Rodriguez,"Diagonalized Lagrangian robot dynamics," IEEE Trans. Rob. Autom., vol. 11, pp.571-584, Aug. 1995

2. N.S.Bedrossian and M.W.Spong, "Feedback linearization of robot manipulators and Riemannian curvature," J. Robotic Systems 12(8), 541-552 (1995)

3. S.K.Ider, "Inverse dynamics of redundant manipulators using a minimum number of control forces," J. Robotic Systems 12(8), 569-579 (1995)

4. M.Bergerman,C.Lee and Y.Xu, "A dynamic coupling index for underactuated manipulators," J. Robotic Systems 12(10), 693-707 (1995)

5. M.W. Spong and M.Vidyasagar, "Robot dynamis and control," John Wiley, New York, 1989

6. F.L.Lewis, C.T.Abdallah and D.M.Dawson, "Control of robot manipulators," Macmillan, 1993

ME 662 Advanced Nonlinear Control

Final Project

Adaptive Nonlinear Control:

Inverted Pendulum-Cart System Case

Fuu-Ren Tsai

12/05/95

Abstract :

The purpose of this project is to study the application of adaptive nonlinear control. A simple nonlinear inverted pendulum-cart system is chosen as the candidate to understand these control methods. By investigating its derived flag, this is system can not be full state linearized. Also, the zero dynamics of this system is either stable or unbounded depend on the input we give. A modified inverted pendulum system which is a MIMO system is used in this project. We can design adaptive trajectory tracking control for this system. Performance of computed torque controller and Lyapunov controller with gradient estimator and weight least squares estimator are shown. Results of time-varying systems and system with friction force are also shown.

Background

Adaptive nonlinear control

In recent years adaptive control of nonlinear system has become as an interesting area. Many papers relative to this research area have been published. Lots of efforts have been made to push this area further. One of the pioneers of this area is Professor Petar V. Kokotovic. His early work focus on the adaptive control method of feedback linearizable systems [1]. A systematic design procedure called adaptive bcakstepping is developed by him and co-workers. He and co-workers further extend adaptive control area to the output-feedback problems [2,3,4]. In their recent paper[5], Kokotovic and co-worker propose three new control schemes to remove the drawbacks of Marino-Tomei controller. In 1995 Professor Kokotovic published a book [6] to introduce the resent development of adaptive nonlinear control.

The ability of parameter convergence of adaptive output-feedback nonlinear control is studied by Kanellakopoulos and co-worker [7]. They show that parameter convergence is guaranteed if an appropriately defined matrixes persistently exciting.

Other control methods are studied by many researchers. Miyasato investigated model reference adaptive control for nonlinear systems with unknown degrees [8]. Robust adaptive nonlinear control is studied by Yao and co-worker [9].

There are still lots of the papers relative to adaptive nonlinear control. Thus the first work for this project is to do literature survey of adaptive nonlinear control.

Inverted pendulum-cart system

Inverted pendulum mounted on a motor-driven cart is shown in the following figure.

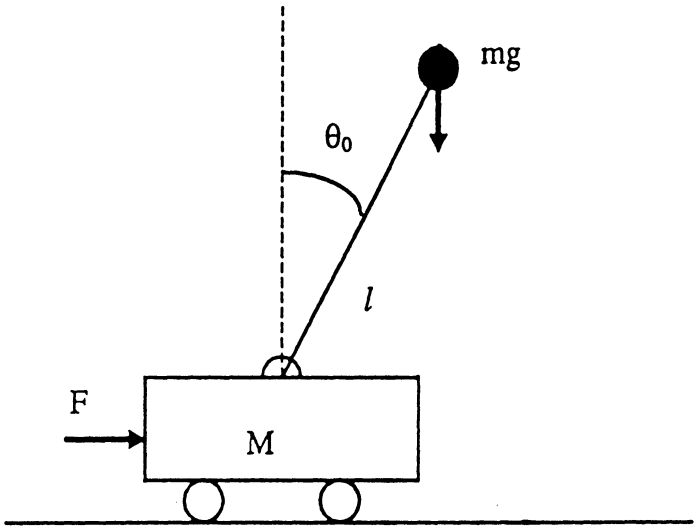

The purpose of this model is used as the attitude control of a space booster on takeoff. The attitude control problem is to take space booster in a vertical position. The difference between actual space booster and inverted pendulum system in this problem is that it is unstable and fall over any time in any direction unless a suitable control force is applied. While the inverted pendulum system is assumed to be a two-dimensional problem so that the pendulum moves only in the plane of the page.

The system dynamics of inverted pendulum can be found in many books relative to control system design. By considering the cart moving in the x direction, we have

$$(M+m)\ddot{r} + ml\cos\theta\ddot{\theta} = ml\cos\theta\dot{\theta}^2 + F$$

For the rotational motion of the inverted pendulum about pivot, we have

$$ml\cos\theta\ddot{r} + (J + ml^2)\ddot{\theta} = mlg\sin\theta$$

where

r : cart position

θ : pendulum angle

F : force input

M : cart mass

m : pendulum mass

l : pendulum length

J : moment of inertia

Re-arrange equation 1 and 2, we have

$$\ddot{r} = \frac{(J+ml^2)ml\sin\theta\dot{\theta}^2 - m^2l^2g\sin\theta\cos\theta}{(M+m)(J+ml^2) - m^2l^2\cos\theta^2} + \frac{(J+ml^2)}{(M+m)(J+ml^2) - m^2l^2\cos\theta^2}F$$

$$\ddot{\theta} = \frac{(M+m)mlg\sin\theta - m^2l^2\cos\theta\sin\theta\dot{\theta}^2}{(M+m)(J+ml^2) - m^2l^2\cos\theta^2} - \frac{ml\cos\theta}{(M+m)(J+ml^2) - m^2l^2\cos\theta^2}F$$

By choosing

$$x1 = r, x2 = \dot{r}, x3 = \theta, x4 = \dot{\theta}, u = F$$

We can express this nonlinear system as

$$\dot{x} = f(x,\dot{x}) + g(x,\dot{x})u \qquad (3)$$

where

$$f(x,\dot{x}) = \begin{bmatrix} x2 \\ \dfrac{(J+ml^2)ml\sin x3x4^2 - m^2l^2g\sin x3\cos x3}{(M+m)(J+ml^2) - m^2l^2\cos x3^2} \\ x4 \\ \dfrac{(M+m)mlg\sin x3 - m^2l^2\cos x3\sin x3x4^2}{(M+m)(J+ml^2) - m^2l^2\cos x3^2} \end{bmatrix}$$

$$g(x,\dot{x}) = \begin{bmatrix} 0 \\ \dfrac{(J+ml^2)}{(M+m)(J+ml^2)-m^2l^2\cos x3^2} \\ 0 \\ \dfrac{-ml\cos x3}{(M+m)(J+ml^2)-m^2l^2\cos x3^2} \end{bmatrix}$$

Relative Degree of inverted pendulum-cart system

Since our interest is to control position of inverted pendulum, we may choose x3, θ, as output. Thus

$$y = x3$$

take derivative of y twice, u shows up.

$$\dot{y} = \dot{x}3 = x4$$

$$\dot{y} = \dot{x}4 = \frac{(M+m)ml\,g\sin x3 - m^2l^2\cos x3\sin x3x4^2}{(M+m)(J+ml^2)-m^2l^2\cos x3^2} - \frac{-ml\cos x3}{(M+m)(J+ml^2)-m^2l^2\cos x3^2}u$$

Therefore, relative degree of this system is 2. This means in this two degree of freedom system, we always has a second degree zero dynamics if we choose x3 as output. To investigate the stability of zero dynamics, we may choose $\zeta 1 = x3, \zeta 2 = x4$. Let $\eta 1 = x1$ and $L_g\eta 1 = 0$. To choose $\eta 2$, assume $\eta 2 = \eta 2(x2, x3, x4)$. We have

$$L_g\eta 2 = \frac{\partial \eta 2}{\partial x2}\frac{(J+ml^2)}{(M+m)(J+ml^2)-m^2l^2\cos x3^2} + \frac{\partial \eta 2}{\partial x4}\frac{ml\cos x3}{(M+m)(J+ml^2)-m^2l^2\cos x3^2}$$

We can find

$$\eta 2 = ml\cos x3x2 - (J+ml^2)x4$$

or

$$x2 = \frac{\eta 2 + (J+ml^2)\varsigma 1}{ml\cos\varsigma 1}$$

Substitute $\varsigma 1, \varsigma 2, \eta 1, \eta 2$ into equation 3, we get

$$\dot{\varsigma}1 = \varsigma 2$$

$$\dot{\varsigma}2 = \frac{(M+m)ml\,g\sin\varsigma 1 - m^2l^2\sin\varsigma 1\cos\varsigma 1\varsigma 2^2}{(M+m)(J+ml^2)-m^2l^2\cos\varsigma 1^2} - \frac{ml\cos\varsigma 1}{(M+m)(J+ml^2)-m^2l^2\cos\varsigma 1^2}$$

and

$$\dot{\eta}1 = \frac{\eta 2 + (J + ml^2)\varsigma 1}{ml\cos\varsigma 1}$$

$$\dot{\eta}2 = -ml\sin\varsigma 1\varsigma 2 + \frac{(J + ml^2)m^2l^2 g\sin\varsigma 1\cos\varsigma 1\varsigma 2^2 - m^3l^3\sin\varsigma 1\cos\varsigma 1}{(M+m)(J+ml^2) - m^2l^2\cos\varsigma 1^2}$$
$$+ \frac{(J + ml^2)m^2l^2\sin\varsigma 1\cos\varsigma 1\varsigma 2^2 - (J+ml^2)m\,lg\sin\varsigma 1}{(M+m)(J+ml^2) - m^2l^2\cos\varsigma 1^2}$$

If $\varsigma 1 = \varsigma 2 = 0$, $\dot{\eta}1$ and $\dot{\eta}2$ become

$$\dot{\eta}1 = \eta 2$$

$$\dot{\eta}2 = 0$$

So, $\dot{\eta}1 = \text{constant}$ and $\eta 1$ is unbounded or zero. We can understand that if the inverted pendulum is regulated to the origin, 0 degree, the cart will move in constant velocity or stop moving depends on the given input.

In Lewis's books [18], several examples with pole placement method or LQR method by using Jacobian linearization of this model are demonstrated. Many papers deal with this inverted pendulum cart system either to regulate or to stabilize the pendulum to the origin position. Mori and co-workers [10] designed an observer-regulator type dynamic stabilizer to keep pendulum from falling down. Wang [11] use linear robust control theory and H_∞ control theory to solve this problem. Linden and co-worker [12] consider dry friction effect for this system and used H_∞ control theory to stabilize the pendulum. Double or triple inverted pendulum systems are also studied by many researchers [13;14,15,16,17]. We can design a linear controller to regulate pendulum to the vertical position. Its performance is shown in figure 1.

Modified inverted pendulum-cart system

Since the original system has a second degree zero dynamics and its stability depends on the given input. This means that there will be two uncontrollable and unobservable states. If we try to control the degree of pendulum, the position of cart might become unbounded.

The inverted pendulum-cart system has two degree of freedom. Our goal is to track the positions of pendulum and cart for a sinusoid reference input. Also, our interest is to apply adaptive control method to this system. To make thing easy, we may add an extra input which is the torque applied on the pivot of pendulum. The original SISO system will become MIMO system. Thus with these two inputs, we can trace two outputs which we choose as the positions of pendulum and cart. We may think this modified system as a one arm robot moving back and forth in one direction and trying to lift its arm. Application of this model may be control of the position of the lifting ladder of a moving firefighter car.

By applying a pivot torque input, the equation of motion becomes

$$(M+m)\ddot{r} + ml\cos\theta\ddot{\theta} = ml\cos\theta\dot{\theta}^2 + F$$

$$ml\cos\theta\ddot{r} + (J+ml^2)\ddot{\theta} = mlg\sin\theta + T$$

where T is the applied torque.

Thus we have state space equation as

$$\dot{x} = f(x,\dot{x}) + g_1(x,\dot{x})u1 + g_2(x,\dot{x})u2$$

and

$$f(x,\dot{x}) = \begin{bmatrix} x2 \\ \dfrac{(J+ml^2)ml\sin x3x4^2 - m^2l^2g\sin x3\cos x3}{(M+m)(J+ml^2) - m^2l^2\cos x3^2} \\ x4 \\ \dfrac{(M+m)mlg\sin x3 - m^2l^2\cos x3\sin x3x4^2}{(M+m)(J+ml^2) - m^2l^2\cos x3^2} \end{bmatrix}$$

$$g_1(x,\dot{x}) = \begin{bmatrix} 0 \\ \dfrac{(J+ml^2)}{(M+m)(J+ml^2) - m^2l^2\cos x3^2} \\ 0 \\ \dfrac{-ml\cos x3}{(M+m)(J+ml^2) - m^2l^2\cos x3^2} \end{bmatrix}$$

$$g_2(x,\dot{x}) = \begin{bmatrix} 0 \\ \dfrac{-ml\cos x3}{(M+m)(J+ml^2) - m^2l^2\cos x3^2} \\ 0 \\ \dfrac{M+m}{(M+m)(J+ml^2) - m^2l^2\cos x3^2} \end{bmatrix}$$

Full state feedback linearization condition

We try to test full state linearization condition. We have

$$g_3 = [f, g_1] = \begin{bmatrix} \dfrac{-(J+ml^2)}{(M+m)(J+ml^2)-m^2l^2\cos x3^2} \\ 0 \\ \dfrac{ml\cos x3}{(M+m)(J+ml^2)-m^2l^2\cos x3^2} \\ \dfrac{ml\sin x3x4}{(M+m)(J+ml^2)-m^2l^2\cos x3^2} \end{bmatrix}$$

$$g_4 = [f, g_2] = \begin{bmatrix} \dfrac{ml\cos x3}{(M+m)(J+ml^2)-m^2l^2\cos x3^2} \\ \dfrac{-ml\sin x3x4}{(M+m)(J+ml^2)-m^2l^2\cos x3^2} \\ \dfrac{-(M+m)}{(M+m)(J+ml^2)-m^2l^2\cos x3^2} \\ 0 \end{bmatrix}$$

and $[g_1, g_2] = 0$ indicates G_0 is involutive. Also, g1, g2, g3 and g4 are all independent. Therefore, G_1 has dimension as 4. Thus we can full state feedback linearize this system.

By defining $\varsigma_1^1 = x1$, $\varsigma_2^1 = x2$, $\varsigma_1^2 = x3$, $\varsigma_2^2 = x4$, we transform the system as

$$\dot{\varsigma}_1^1 = \varsigma_2^1$$

$$\dot{\varsigma}_2^1 = a1(\varsigma_1^1, \varsigma_2^1, \varsigma_1^2, \varsigma_2^2) + b1(\varsigma_1^1, \varsigma_2^1, \varsigma_1^2, \varsigma_2^2)u$$

$$\dot{\varsigma}_1^2 = \varsigma_2^2$$

$$\dot{\varsigma}_2^2 = a2(\varsigma_1^1, \varsigma_2^1, \varsigma_1^2, \varsigma_2^2) + b2(\varsigma_1^1, \varsigma_2^1, \varsigma_1^2, \varsigma_2^2)u$$

where $u = [u1 \;\; u2]^T$

We may define

$$v1 = a1(\varsigma_1^1, \varsigma_2^1, \varsigma_1^2, \varsigma_2^2) + b1(\varsigma_1^1, \varsigma_2^1, \varsigma_1^2, \varsigma_2^2)u$$

$$v2 = a2(\varsigma_1^1, \varsigma_2^1, \varsigma_1^2, \varsigma_2^2) + b2(\varsigma_1^1, \varsigma_2^1, \varsigma_1^2, \varsigma_2^2)u$$

We have

$$\dot{\varsigma}_1^1 = \varsigma_2^1$$

$$\dot{\varsigma}_2^1 = v1$$

$$\dot{\varsigma}_1^2 = \varsigma_2^2$$

$$\dot{\varsigma}_2^2 = v2$$

We can use pole placement method to design a linear controller to stabilize this system. Fig. 2 shows its performance. We can see that all the states are driven to zero after lots of vibration. The other case indicates that this vibration can be elliminated if appropriate control gain is chosen as shown in fig. 3.

Trajectory Control

Computed torque method

We can view this system as the following equation

$$H(q)\ddot{q} + C(q,\dot{q})\dot{q} + Q(q) = \tau$$

Assume determinant of H(q) is always not zero at any position along trajectory.

We can replace τ as

$$\tau = H(q)v + C(q,\dot{q})\dot{q} + Q(q)$$

where v is the new control input. The above equation is called as the "computed torque".

If we let $v = \ddot{q}$, the computed torque equation and system equation are identical.

Now, we may defined the tracking error as $\tilde{q} = q - q_d$

and let

$$v = \ddot{q}_d - 2\lambda\dot{\tilde{q}} - \lambda^2\tilde{q}$$

where $\lambda > 0$

The closed-loop system becomes

$$\ddot{\tilde{q}} + 2\lambda\dot{\tilde{q}} + \lambda^2\tilde{q} = 0$$

Thus the closed-loop system is exponentially stable.

Fig. 4a illustrates the system follow the desired sinusoid reference inputs by using computed torque method. Fig. 4b shows tracking error of each state.

Lyapunov function method [19]

Given $q_d(t)$ as desired trajectory. We want output *q(t)* to track this desired trajectory. We may define a position error term as $\tilde{q} = q - q_d$, and a velocity error term as

$$s = \dot{\tilde{q}} + \Lambda\tilde{q} = \dot{q} - \dot{q}_r$$

where $\dot{q}_r = \dot{q}_d - \Lambda\tilde{q}$ and Λ is a symmetric positive definite matrix.

Also we may define a parameter estimation error as $\tilde{a} = \hat{a} - a$,

where a is the system's unknown parameter vector.

$$a = \begin{bmatrix} M+m \\ ml \\ J+ml^2 \end{bmatrix}$$

and $\hat{a}$ is its estimation value.

$$\hat{a} = \begin{bmatrix} M+m \\ ml \\ J+ml^2 \end{bmatrix}_{estimated}$$

Thus we can choose Lyapunov function candidate as

$$V(t) = \tfrac{1}{2}s^T Hs + \tfrac{1}{2}\tilde{a}^T\Gamma^{-1}\tilde{a}$$

Differentiating the above equation

$$\dot{V}(t) = s^T(H\ddot{q} - H\ddot{q}_r) + \frac{1}{2}s^T\dot{H}s + \dot{\tilde{a}}\Gamma^{-1}\tilde{a}$$

Substitute $H\ddot{q} = \tau - C\dot{q} - Q = \tau - C(s + \dot{q}_r) - Q$ into above equation, yields

$$\dot{V}(t) = s^T(\tau - H\ddot{q}_r - C\dot{q}_r - Q) + \frac{1}{2}s^T(\dot{H} - 2C)s + \dot{\tilde{a}}\Gamma^{-1}\tilde{a}$$

where

$\dot{H} - 2C$ is a skew-symmetric matrix and $\frac{1}{2}s^T(\dot{H} - 2C)s = 0$.

Thus,

$$\dot{V}(t) = s^T(\tau - H\ddot{q}_r - C\dot{q}_r - Q) + \dot{\tilde{a}}\Gamma^{-1}\tilde{a} \quad (4)$$

We can rearrange the system equation as function of the unknown parameter vector a as :

$$H(q)\ddot{q}_r + C(q,\dot{q})\dot{q}_r + Q(q) = Y(q,\dot{q},\dot{q}_r,\ddot{q}_r)a \quad (5) \text{ [Appendix 1]}$$

and use control law as

$$\tau = Y\hat{a} - K_d \ s \qquad (6)$$

substitute (5) (6) into (4) leads to

$$\dot{V}(t) = s^T Y\tilde{a} - s^T K_d \ s + \dot{\tilde{a}}\Gamma^{-1}\tilde{a}$$

If we choose $\dot{\tilde{a}}$ which leads to $(s^T Y + \dot{\tilde{a}}\Gamma^{-1}) = 0$, then we get

$$\dot{V}(t) = -s^T K_d \ s$$

This indicates that $\tilde{q}$ and $\dot{\tilde{q}}$ will converge to 0 as t goes to infinity.

Adaptive Control [19]

We can combine the above control laws with gradient estimator or weighted least-squares estimator to form the adaptive control of this modified inverted pendulum - cart system.

Design of control law

We can use control laws derived from computed torque method or Lyapunov function method. We have

$\tau = H(q,\hat{a})(\ddot{q}_d - 2\lambda\dot{\tilde{q}} - \lambda^2\tilde{q}) + C(q,\dot{q},\hat{a})\dot{q} + Q(q,\hat{a})$ (Computed torque method)

and

$\tau = Y\hat{a} - K_d \ s$ (Lyapunov function method)

Parameter estimation

We can represent output y as function of system parameters

$$y(t) = W(t)a$$

where

$y(t)$ is output vector, a is system's unknown parameter vector.

$W(t)$ is a known signal matrix.

We can define prediction error as

$$e1(t) = \hat{y}(t) - y(t) = W\hat{a} - Wa = W\tilde{a}$$

Gradient estimator

The basic idea is that we can update estimated parameter vector in the opposite direction of the gradient of the squared prediction error with respective to the system parameter vector. thus we have

$$\dot{\hat{a}} = -P_0 \frac{\partial[e1^T e1]}{\partial \hat{a}} = -P_0 W^T e1$$

where P_0 is positive definite matrix.

Weighted Least-Squares estimator

The basic idea is that we want to minimize the total estimation error function, J,

$$J = \int_0^t \exp[-\int_s^t \lambda(r)dr] \| y(s) - W(s)\hat{a}(t) \|^2 ds$$

We can have the parameter update law is still of the same form

$$\dot{\hat{a}} = -P(t)W^T e1$$

but the gain update law is

$$\frac{d}{dt}[P^{-1}] = -\lambda(t)P^{-1} + W^T(t)W(t)$$

or

$$\frac{d}{dt}P = \lambda(t)P - PW^T(t)W(t)P$$

where $P(t)$ is the positive definite matrix for all time.

Simulation results

for frictionless inverted pendulum system

Adaptive control

We design different adaptive control law with different parameter estimators. In order to let the estimated parameters approach to the real values, we use a sinusoid reference input to excite the system. Adaptive controller can track this sinusoid reference input.

In fig. 5 we use Lypunov controller with gradient estimator. Fig. 5a shows its performance. After 10 second, the system will approach the desired trajectory. Fig. 5b shows the performance of parameter convergence. The convergence speed is slow. After 150 seconds, the system reaches its real parameter value.

In fig. 6, we use the same Lyapunov controller with WLS estimator. The tracking performance of x1 and x2 are not as good as x3 and x4 shown in fig. 6a. However, the WLS estimator performs very good, parameters will reach its real values. after 2.5 seconds shown in fig. 6b.

In fig. 7, the computed torque controller with WLS estimator is used. The tracking performance shown in fig 7.a is not as good as the other cases. But estimated parameters will reach to real values after 1.5 seconds shown in fig. 7.b.

Trajectory tracking

In this section, we want to track the system outputs to the different desired reference inputs. We may define sinusoid reference inputs as $x1_r = -mag_1 \sin(\varpi_1 t)$ and $x3_r = -mag_2 \sin(\varpi_2 t)$.

Table 1 shows the trajectory variables for fig. 8, 9, 10 and 11. The performances of trajectory tracking are good as shown in fig. 8a, 9a, 10a and 11a. From fig. 8b, 9b and 10b we can see the parameter convergence speed is related to the frequency of reference inputs. If we give a fast frequency inputs, the parameters will converge to the real values faster than the slow frequency reference inputs did.

If we don't give enough excited reference input, the estimated parameters will converge to the wrong values. In fig. 11b, we maintain the pendulum to the vertical position when the cart is moving. The estimated $\hat{a}_3$ stay at its initial value, 0, instead of converging to the real value. The reason is that persistent excitation guarantees parameter estimator

converges to desired value. For a constant reference input, the parameter may not reach to the correct value. The adaptive controller just deal with trajectory tracking. So, when system follows its desired trajectory, the output error, s, will be zero. This leads to estimator may approach to the wrong parameter value.

Time-varying parameter estimation

Now we assume the system's parameters might vary according to time. We want to see the performance of adaptive controller to track desired trajectory and performance of estimator to adjust estimated parameters to the correct values.

In fig 12 the mass of cart is varying according to the following relation $M = 0.48(1 - 0.5\cos(t))$. Fig. 12a shows system outputs will follow the desired trajectory after 30 seconds. The estimated parameters will not approach to desired value smoothly shown in fig. 12b.

Next we assume pendulum mass is time-varying according to $m = 0.16(1 - 0.1\cos(t))$ .Fig. 13a shows this case yields worst trajectory tracking. The outputs are totally lost to follow trajectory. And results of parameter convergence is very bad. In fig. 13b it shows that $\hat{a}_3$ is too much sensitive to the small change of pendulum mass.

In the third case we change length of pendulum by $l = 0.25(1 - 0.1\cos(0.25t))$. Fig. 14a shows that outputs will need a long time, 30 seconds, to track the desired trajectory. Again $\hat{a}_3$ is sensitive to variation of pendulum length.

Modified frictional inverted pendulum system

Consider now the inverted pendulum - cart system consists of friction. The equation of motion becomes :

$$(M + m)\ddot{r} + ml\cos\theta\ddot{\theta} = -f\dot{r} + ml\cos\theta\dot{\theta}^2 + F$$

$$ml\cos\theta\ddot{r} + (J + ml^2)\ddot{\theta} = -c\dot{\theta} + mlg\sin\theta + T$$

where

f: friction coefficient

c: angular friction coefficient

The state equation becomes

$$\dot{x} = f(x,\dot{x}) + g_1(x,\dot{x})u1 + g_2(x,\dot{x})u2$$

$$f(x,\dot{x}) = \begin{bmatrix} x2 \\ \dfrac{(J+ml^2)(-fx2+ml\sin x3x4^2)-(ml\cos x3)(-cx4+mlg\sin x3)}{(M+m)(J+ml^2)-m^2l^2\cos x3^2} \\ x4 \\ \dfrac{(M+m)(-cx4+mlg\sin x3)-(ml\cos x3)(-fx2+ml\sin x3x4^2)}{(M+m)(J+ml^2)-m^2l^2\cos x3^2} \end{bmatrix}$$

$$g_1(x,\dot{x}) = \begin{bmatrix} 0 \\ \dfrac{(J+ml^2)}{(M+m)(J+ml^2)-m^2l^2\cos x3^2} \\ 0 \\ \dfrac{-ml\cos x3}{(M+m)(J+ml^2)-m^2l^2\cos x3^2} \end{bmatrix}$$

$$g_2(x,\dot{x}) = \begin{bmatrix} 0 \\ \dfrac{-ml\cos x3}{(M+m)(J+ml^2)-m^2l^2\cos x3^2} \\ 0 \\ \dfrac{M+m}{(M+m)(J+ml^2)-m^2l^2\cos x3^2} \end{bmatrix}$$

Then the estimated parameter vector is

$$\hat{a} = \begin{bmatrix} M+m \\ ml \\ J+ml^2 \\ f \\ c \end{bmatrix}_{estimated}$$

The simulation conditions are shown in table 2. Fig. 15 to fig. 24 are their results. We can compare the frictionless cases and friction cases to see their performance. Intuitively, friction in the inverted pendulum system likes a damper which will absorb energy. Thus we expect the time need to follow trajectory in friction cases will be faster

than that of ideal cases because mechanical energy will dissipate during vibration or moving due to existence of damper. We can find this phenomena in fig. 16, 17, 18,19, 20 and 21 which are friction cases and use the same initial conditions, controller law and estimation law as ideal cases in fig. 6, 7, 8, 9, 10 and 11 respectively. Especially, in fig. 21 we find the angle and angular velocity of pendulum will soon reach to desired zero value in about 2 seconds compared to those of the ideal case shown in fig. 11, which will oscillate quit a long time before pendulum stay at vertical position. Again, in fig. 21, the third estimated parameter will not converge to correct value because lack of enough excitation. But surprisingly, the fifth estimated parameter which is angular friction coefficient will illustrate the same situation.

Fig. 22, 23 and 24 are the time-varying parameter cases for frictional system. In fig. 22, the cart mass is time-varying . We can see that it takes a long time to follow the desired trajectory. In this case, the situation of parameter convergence is good.

In fig. 23, the pendulum mass is varying. Again, we see the system is lost in tracking the trajectory and convergence of third and fifth estimated parameters are bad. We can make sure that the pendulum's mass is the most sensitive parameter in this system.
In fig. 24, the time varying pendulum length will yield slow trajectory tracking. The third and fifth estimated parameters have bad convergence.

Conclusion

The original inverted pendulum system can not use full state feedback linearization. The input-output linearization shows that this system has a zero dynamics which is either unbounded or stable depends on the given input. Most of the previous work try to stabilize this system with various methods. Actually, the original system is suitable for optimal control instead of adaptive control because the positions of pendulum and cart can not be trace at the same time by one input with presence of zero dynamics.

In order to apply the adaptive nonlinear control, we modify the original system by adding another input, the pivot torque, to make the system controllable and full state feedback linearizable. So, the equation of motion of this system has the same form as that of two-link robot. Therefore, we can use computed torque method and Lyapunov function to design control laws. We can use gradient estimator or weighted least-squares estimator incorporated with control laws to design adaptive nonlinear control system. It shows that the gradient estimator is slower than WLS estimator to drive estimated parameters to correct values. However, the performance of both control laws with same estimator are quit the same.

Simulations for the system without friction and with friction for different sinusoid reference input are presented. The results illustrate that the trajectory tracking and parameter convergence are very good. To investigate the parameter convergence, we use a constant reference input. One of three estimated parameters will not converge to correct value due to lack of excitation. The estimation of time-varying parameters also present in this project. The results show that the pendulum mass is the most sensitive parameter in this system. A slight variation in pendulum mass will cause estimation law failed and system will become unstable. We also investigate inverted pendulum system with friction force. The simulation results show that the time need to follow the desired trajectory is less than that of the frictionless system. We may consider the friction coefficient as parametric uncertainty. Thus a robust adaptive nonlinear controller [20] can be applied in this case. Because we have run out of time, we have no choice but to give up.

We spend lots of time in finding linearization method for the original system. Approximation linearization and Riemannian manifold decoupling method are investigated. But with presence of zero dynamics, it is very difficult to find a trajectory-tracking controller. This give us an idea to investigate adaptive nonlinear control method for tracking multi-outputs system with single input in the future.

Table 1 Simulation conditions for frictionless inverted pendulum system

figure *	initial condition	reference inputs (time-varying parameter)	control law **	estimator ***
1	[0.05, 0, -0.1, 0]	xr1 = 0, xr3 = 0	PD	None
2	[1,0,0,0]	xr1 = 0, xr3 = 0	Place	None
3	[0.05, 0, -0.1, 0]	xr1 = 0, xr3 = 0	CT	None
4	[0,0,0,0]	xr1 = -0.1sin(t), xr3 = 0.05sin(t)	CT	None
5	[0,0,0,0]	xr1 = -0.1sin(2t), xr3 = 0.05sin(2t)	LY	Grad
6	[0,0,0,0]	xr1 = -0.1sin(2t), xr3 = 0.05sin(2t)	LY	WLS
7	[0,0,0,0]	xr1 = -0.1sin(2t), xr3 = 0.05sin(2t)	CT	WLS
8	[0,0,0,0]	xr1 = -0.1sin(2t), xr3 = -0.05sin(2t)	LY	WLS
9	[0,0,0,0]	xr1 = -0.1sin(2t), xr3 = -0.05sin(4t)	LY	WLS
10	[0,0,0,0]	xr1 = -0.1sin(4t), xr3 = -0.05sin(2t)	LY	WLS
11	[0,0,0,0]	xr1 = -0.1sin(2t), xr3 = 0	LY	WLS
12	[0,0,0,0]	xr1 = -0.1sin(2t), xr3 = -0.05sin(2t) M = 0.48(1-0.1cos(t))	CT	WLS
13	[0,0,0,0]	xr1 = -0.1sin(2t), xr3 = -0.05sin(2t) m = 0.16(1-0.1cos(t))	CT	WLS
14	[0,0,0,0]	xr1 = -0.1sin(2t), xr3 = -0.05sin(2t) l = 0.25(1-0.1cos(0.25t))	CT	WLS

* Fig. 1 is ideal inverted pendulum system, fig 2 to 14 are modified inverted pendulum case. All initial estimated parameters are set to zero.

** PD : PD controller

$$u1 = 10\tilde{q}_1 + 40\tilde{q}_2 + 100\tilde{q}_3 + 20\tilde{q}_4$$

$$u2 = 0$$

Place : pole-placement method. place closed poles to Butterworth position

CT : controller designed by computed torque method

$$u = \hat{H}(\ddot{q}_d - s) + \hat{C}\dot{q}_d + \hat{Q} \quad \text{where } s = 0.4\dot{\tilde{q}} + 20\tilde{q}$$

LY : controller designed by Lyapunov function method

$$u = \hat{H}\ddot{q}_d + \hat{C}\dot{q}_d + \hat{Q} - s \quad \text{where } s = 0.4\dot{\tilde{q}} + 20\tilde{q}$$

*** WLS : weighted least-squares estimator

Grad : gradient estimator

Table 2 Simulation conditions for frictional inverted pendulum system

figure	initial condition	reference inputs (time-varying parameter)	control law **	estimator ***
15	[0,0,0,0]	xr1 = -0.1sin(t), xr3 = 0.05sin(t)	CT	None
16	[0,0,0,0]	xr1 = -0.1sin(2t), xr3 = 0.05sin(2t)	LY	WLS
17	[0,0,0,0]	xr1 = -0.1sin(2t), xr3 = 0.05sin(2t)	CT	WLS
18	[0,0,0,0]	xr1 = -0.1sin(2t), xr3 = -0.05sin(2t)	LY	WLS
19	[0,0,0,0]	xr1 = -0.1sin(4t), xr3 = -0.05sin(2t)	LY	WLS
20	[0,0,0,0]	xr1 = -0.1sin(2t), xr3 = -0.05sin(4t)	LY	WLS
21	[0,0,0,0]	xr1 = -0.1sin(2t), xr3 = 0.0	LY	WLS
22	[0,0,0,0]	xr1 = -0.1sin(2t), xr3 = -0.05sin(2t) M = 0.48(1-0.1cos(t))	CT	WLS
23	[0,0,0,0]	xr1 = -0.1sin(2t), xr3 = -0.05sin(2t) m = 0.16(1-0.1cos(t))	CT	WLS
24	[0,0,0,0]	xr1 = -0.1sin(2t), xr3 = -0.05sin(2t) l = 0.25(1-0.1cos(0.25t))	CT	WLS

* All initial condition and all initial estimated parameters are set to zero.

** CT : controller designed by computed torque method

$$u = \hat{H}(\ddot{q}_d - s) + \hat{C}\dot{q}_d + \hat{Q} \quad \text{where } s = 0.4\dot{\tilde{q}} + 20\tilde{q}$$

LY : controller designed by Lyapunov function method

$$u = \hat{H}\ddot{q}_d + \hat{C}\dot{q}_d + \hat{Q} - s \quad \text{where } s = 0.4\dot{\tilde{q}} + 20\tilde{q}$$

*** WLS : weighted least-squares estimator

Grad : gradient estimator

Appendix 1

Derive $H(q)\ddot{q}_r + C(q,\dot{q})\dot{q}_r + Q(q) = Y(q,\dot{q},\dot{q}_r,\ddot{q}_r)a$

Frictionless system:

We have

$$(M+m)\ddot{q}_{1r} + ml\cos q_2\ddot{q}_{2r} - ml\cos q_2\dot{q}_2\dot{q}_{2r} = \ddot{q}_{1r}(M+m) + (\cos q_2\ddot{q}_{2r} - \cos q_2\dot{q}_2\dot{q}_{2r})ml$$

$$ml\cos q_2\ddot{q}_{1r} + (J+ml^2)\ddot{q}_{2r} - mlg\sin q_2 = (\cos q_2\ddot{q}_{1r} - g\sin q_2)ml + \ddot{q}_{2r}(J+ml^2)$$

where

$$q_1 = r,\ \ q_2 = \theta,\ \ q_{1r} = r_r,\ \ q_{2r} = \theta_r$$

which yields

$$H(q)\ddot{q}_r + C(q,\dot{q})\dot{q}_r + Q(q) = Y(q,\dot{q},\dot{q}_r,\ddot{q}_r)a$$

where

$$Y(q,\dot{q},\dot{q}_r,\ddot{q}_r) = \begin{bmatrix} \ddot{q}_{1r} & (\cos q_2\ddot{q}_{2r} - \cos q_2\dot{q}_2\dot{q}_{2r}) & 0 \\ 0 & (\cos q_2\ddot{q}_{1r} - g\sin q_2) & \ddot{q}_{2r} \end{bmatrix}$$

$$a = \begin{bmatrix} a1 \\ a2 \\ a3 \end{bmatrix} = \begin{bmatrix} M+m \\ ml \\ J+ml^2 \end{bmatrix}$$

Frictional system :

We have

$$(M+m)\ddot{q}_{1r} + ml\cos q_2\ddot{q}_{2r} + f\dot{q}_{1r} - ml\cos q_2\dot{q}_2\dot{q}_{2r} = \ddot{q}_{1r}(M+m) + (\cos q_2\ddot{q}_{2r} - \cos q_2\dot{q}_2\dot{q}_{2r})ml + \dot{q}_{1r}f$$

and

$$ml\cos q_2\ddot{q}_{1r} + (J+mi^2)\ddot{q}_{2r} + c\dot{q}_{2r} - mlg\sin q_2 = (\cos q_2\ddot{q}_{1r} - g\sin q_2)ml + \ddot{q}_{2r}(J+ml^2) + \dot{q}_{2r}\,c$$

where

$$q_1 = r,\ \ q_2 = \theta,\ \ q_{1r} = r_r,\ \ q_{2r} = \theta_r$$

which yields

$$H(q)\ddot{q}_r + C(q,\dot{q})\dot{q}_r + Q(q) = Y(q,\dot{q},\dot{q}_r,\ddot{q}_r)a$$

where

$$Y(q,\dot{q},\dot{q}_r,\ddot{q}_r)=\begin{bmatrix}\ddot{q}_{1r} & (\cos q_2\ddot{q}_{2r}-\cos q_2\dot{q}_2\dot{q}_{2r}) & 0 & \dot{q}_{1r} & 0\\ 0 & (\cos q_2\ddot{q}_{1r}-g\sin q_2) & \ddot{q}_{2r} & 0 & \dot{q}_{2r}\end{bmatrix}$$

$$a=\begin{bmatrix}a1\\a2\\a3\\a4\\a5\end{bmatrix}=\begin{bmatrix}M+m\\ml\\J+ml^2\\f\\c\end{bmatrix}$$

Reference

[1] Kanellakopoulos, I., Kokotovic, P. V. 1991, "Systematic design of adaptive controllers for feedback linearizable system," IEEE Transaction on Automatic Control, vol. 36, pp. 1241-1253.

[2] Kanellakopoulos, I., Kokotovic, P. V. and Middleton, R. H. 1990 "Observer-based adaptive control of nonlinear systems under matching conditions," Proceedings of the 1990 American Control Conference, pp. 549-555, San Diego, CA.

[3] Kanellakopoulos, I., Kokotovic, P. V. and Middleton, R. H. 1990 "Indirect adaptive output-feedback control of a class of nonlinear systems," Proceedings of the 29th IEEE Conference on Decision and Control, pp. 2714-2719, Honolulu, HI.

[4] Kanellakopoulos, I., Kokotovic, P. V. and Morse, A. S. 1992 "Adaptive output-feedback control of systems with output nonlinearities," IEEE Transaction on Automatic Control, vol. 37, pp. 1266-1282.

[5] Krstic, M, Kokotovic, P. V. 1994, "Adaptive nonlinear output-feedback schemes with Marino-Tomei controller," Proceedings of the 1994 American Control Conference, pp. 861-866.

[6] Kanellakopoulos, I., Krstic, M. and Kokotovic, P. V. 1995, Nonlinear and adaptive control design.

[7] Kanellakopoulos, I., Lin, J. S. 1995, "Adaptive output-feedback nonlinear control with parameter convergence," Proceedings of the 1995 American Control Conference, pp. 3029-3033.

[8] Miyasato, Y., 1995, "Model reference adaptive control for nonlinear systems with unknown degrees (minimal number of tuning parameters)," Proceedings of the 1995 American Control Conference, pp. 2505-2509.

[9] Yao, B. and Tomizuka, M., 1995, "Robust adaptive nonlinear control with guaranteed transient performance," Proceedings of the 1995 American Control Conference, pp. 2500-2504.

[10] Mori, S., Nishihara, H. and Furuta, K., 1976, "Control of unstable mechanical system,", International Journal of Control, vol., 23, No. 5, 673-692.

[11] Wang, J., 1989, "Optimal robust output feedback control for SISO nonlinear systems," IEEE conference on Decision and Control., vol. ??, pp. 2376-2381.

[12] Linden, G. and Lambrechts, P. F., 1993, "H_∞ control of an experimental inverted pendulum with dry friction," IEEE Control System., August 1993.

[13] Yamakita, M., Iwashiro, M., Sugahara. Y. and Furuta, K., 1995, "Robust swing up control of double pendulum," Proceedings of the 1995 American Control Conference, pp. 290-295.

[14] Schaefer, J. F., Cannon, R. H., Jr. 1966 "Continuous linear systems on the control of unstable mechanical systems," Proceedings of third congress of the IFAC, Paper 6C1.

[15] Furuta, K., Kajiwara, H. and Kosuge, K. 1980 "Digital control of a double inverted pendulum on a inclined rail," International Journal of Control, vol., 32, No. 5, 907-924.

[16] Furuta, K., Ochiai, T. and Ono, N. 1984 "Attitude control of a triple inverted pendulum," International Journal of Control, vol., 39, No. 6, 1351-1366.

[17] Meier, H., Farwig, Z. and Unbehaue, H. 1990 "Discrete computer control of a Triple-inverted pendulum," Optimal Control Applications and Methods, vol. 11, pp. 157-172.

[18] Lewis, Frank L. 1992 Applied Optimal Control and Estimation, Prentice Hall, Inc., pp.224-229,

[19] Slotine, Jean-Jacques E. and Li, Weiping, 1991 Applied Nonlinear Control, Prentice Hall, Inc., Chaper 9.

[20] Polycarpou, M. M. and Ioannou, P. A., 1991 "A robust Adaptive Nonlinear Control Design," Proceedings of the 1993 American Control Conference, pp. 1365-1369.

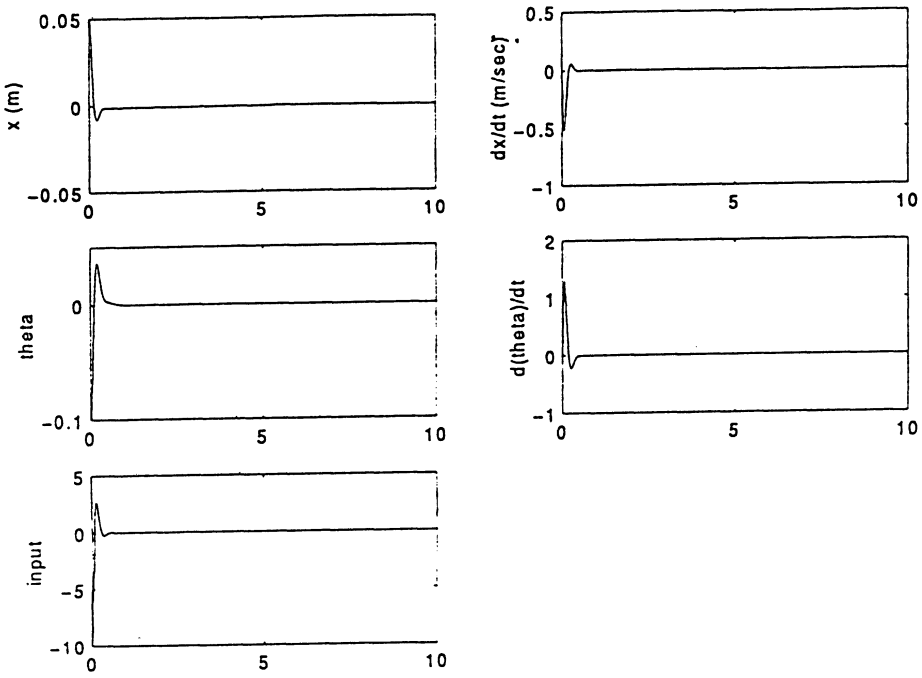

Figure 1a

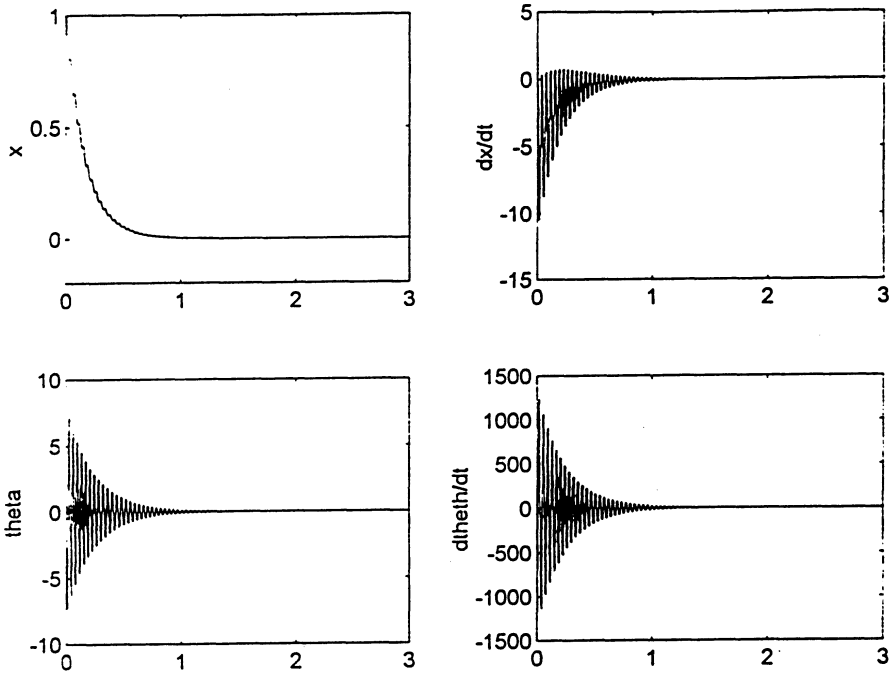

Figure 2a

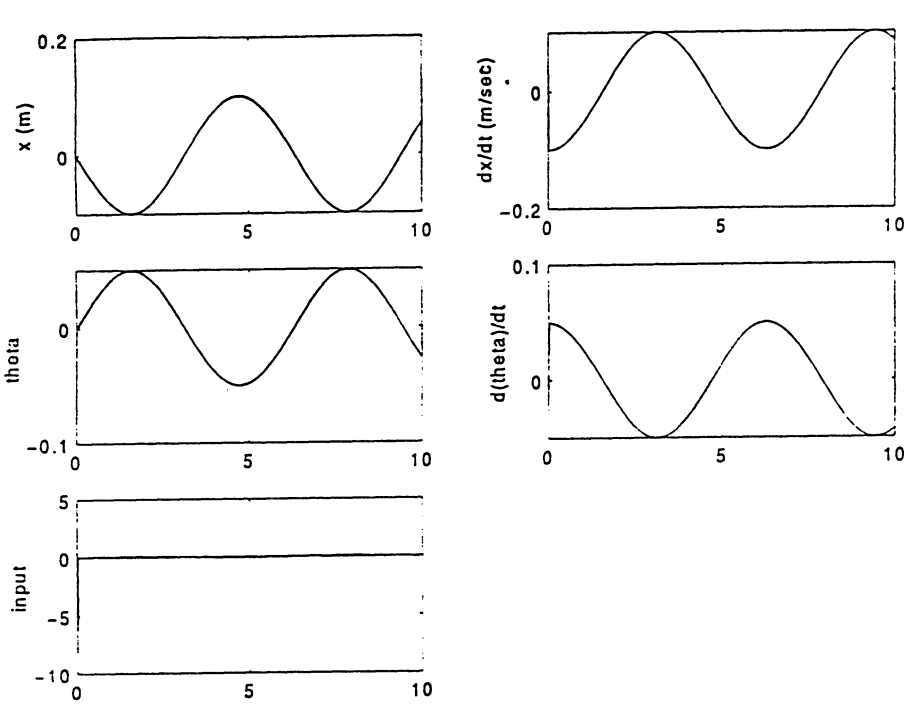

Figure 4a

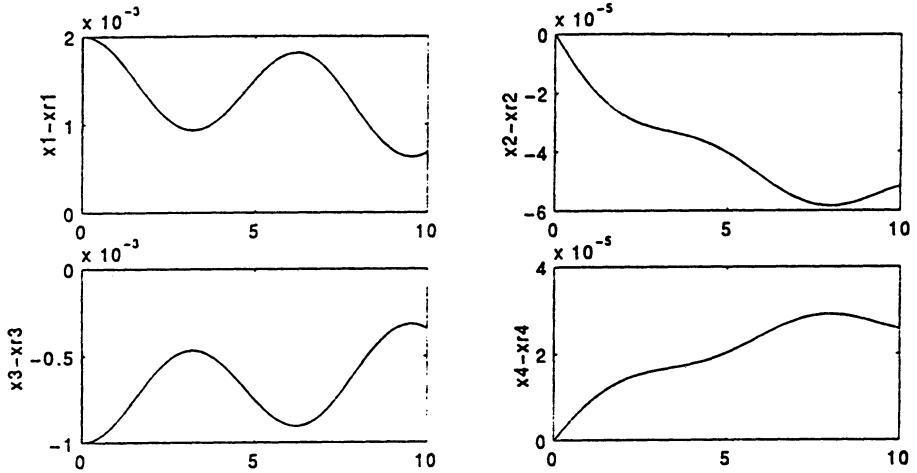

Figure 4b

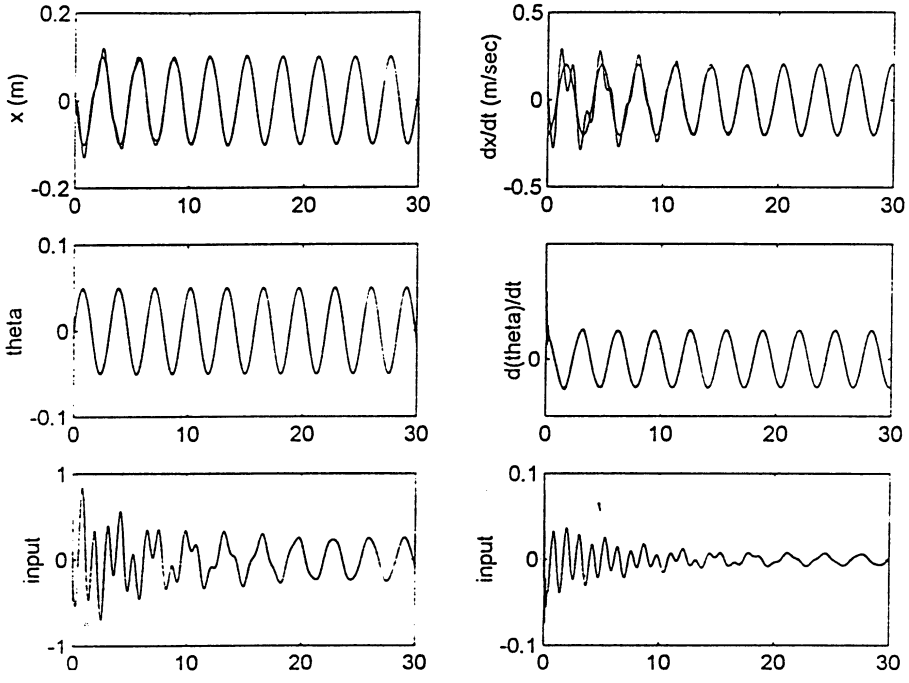

Figure 5a

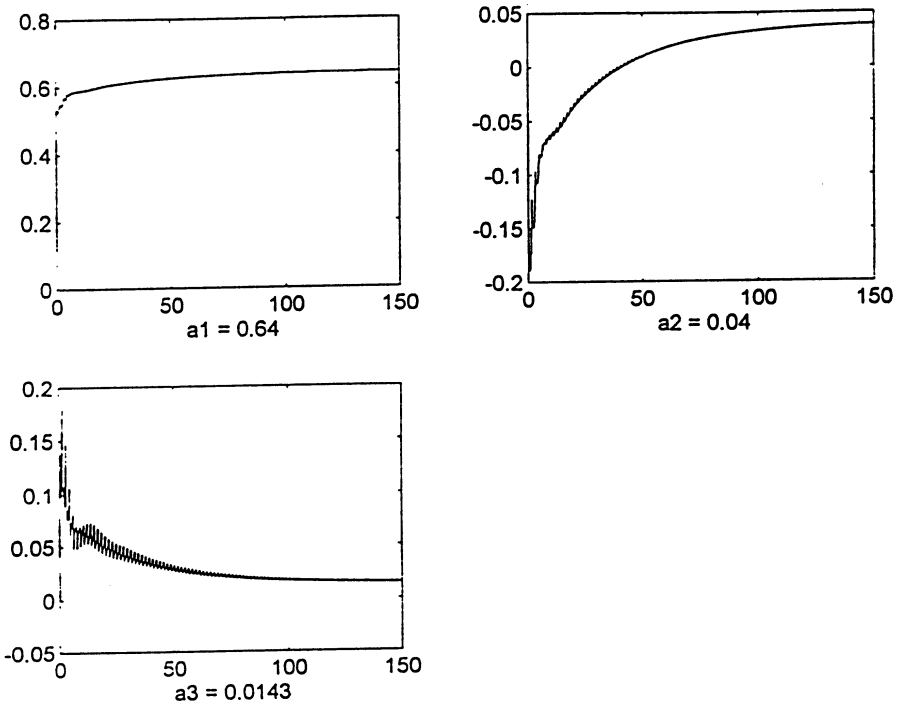

Figure 5b

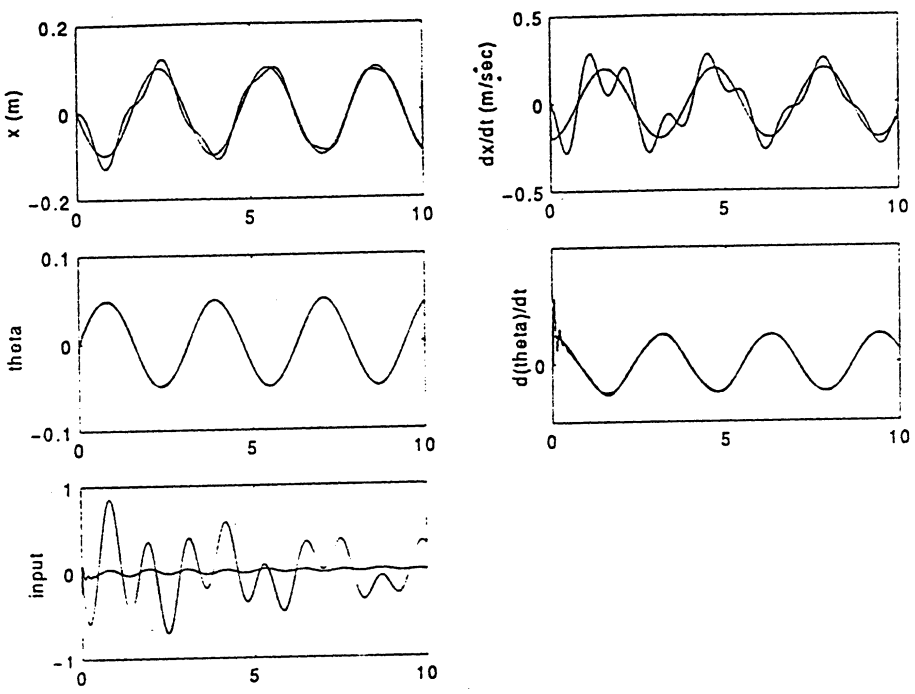

Figure 6a

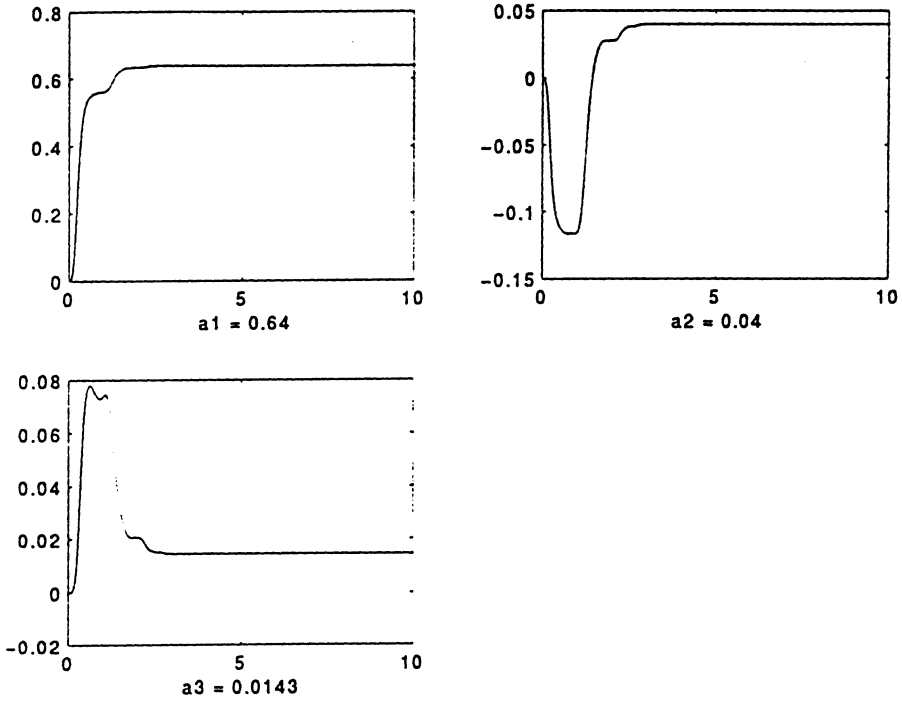

Figure 6b

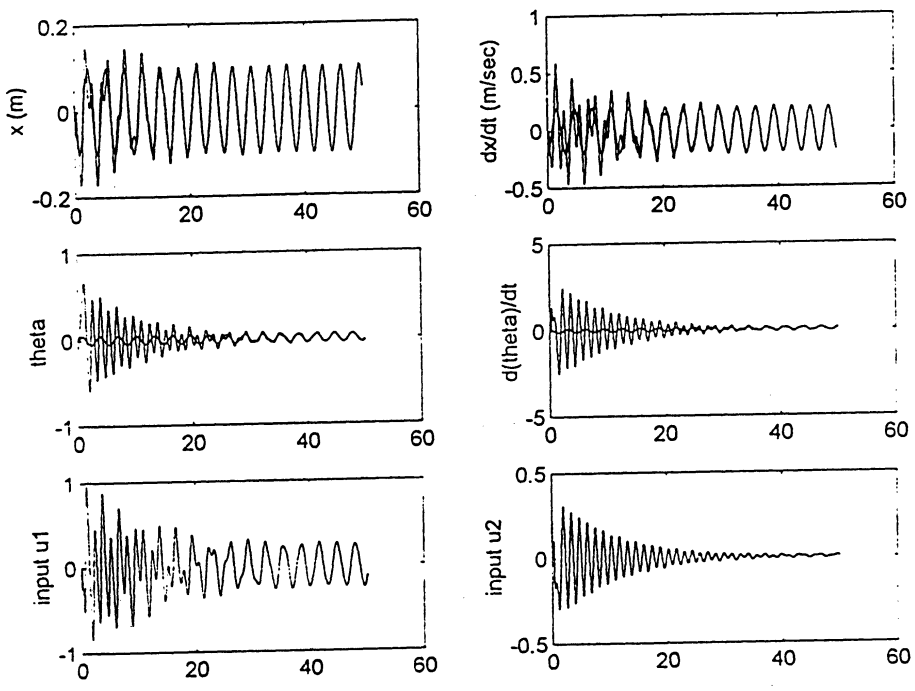

Figure 7a

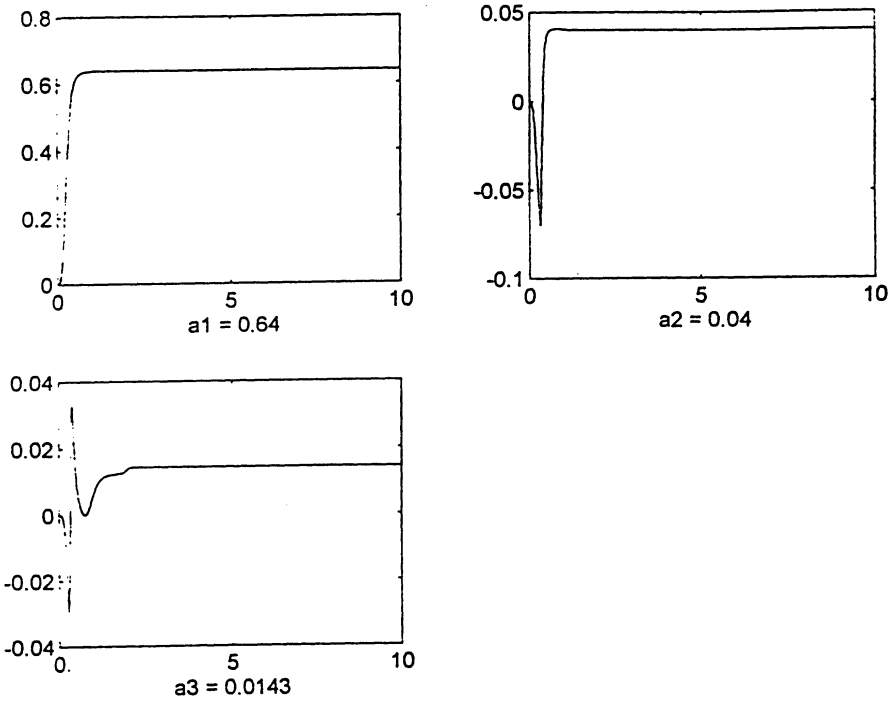

Figure 7b

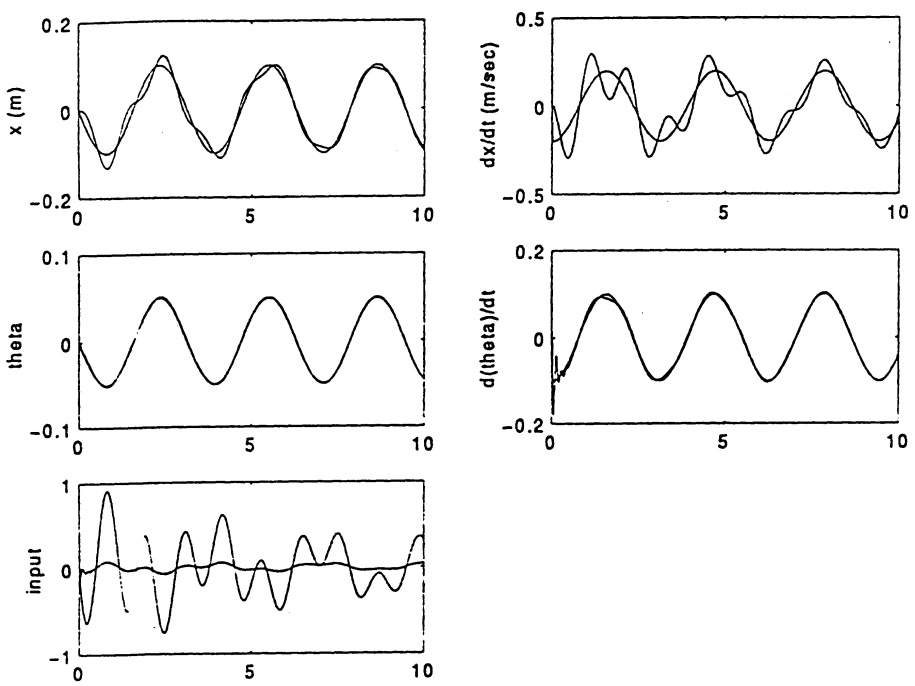

Figure 8a

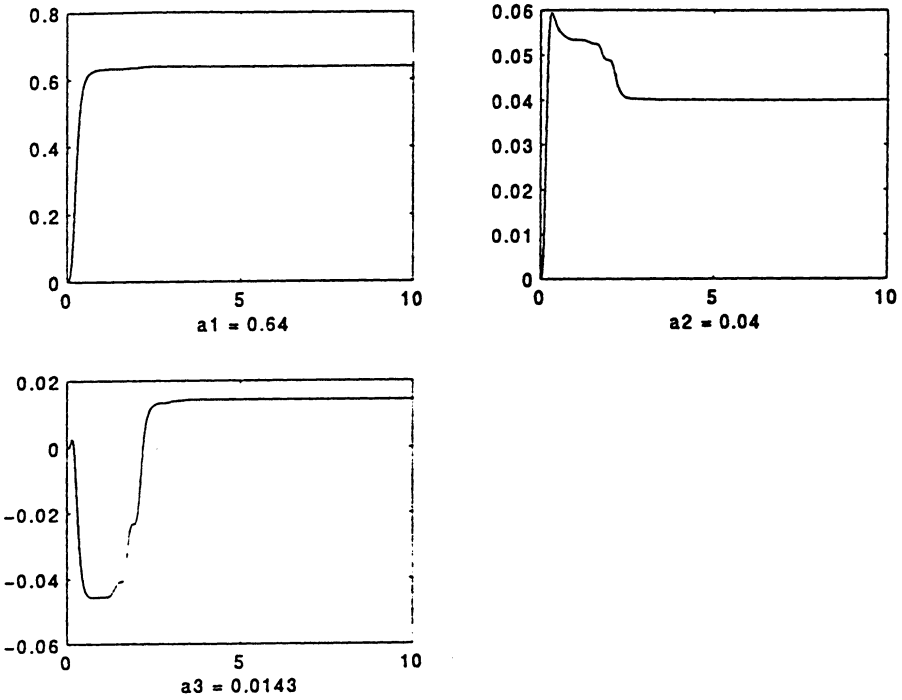

Figure 8b

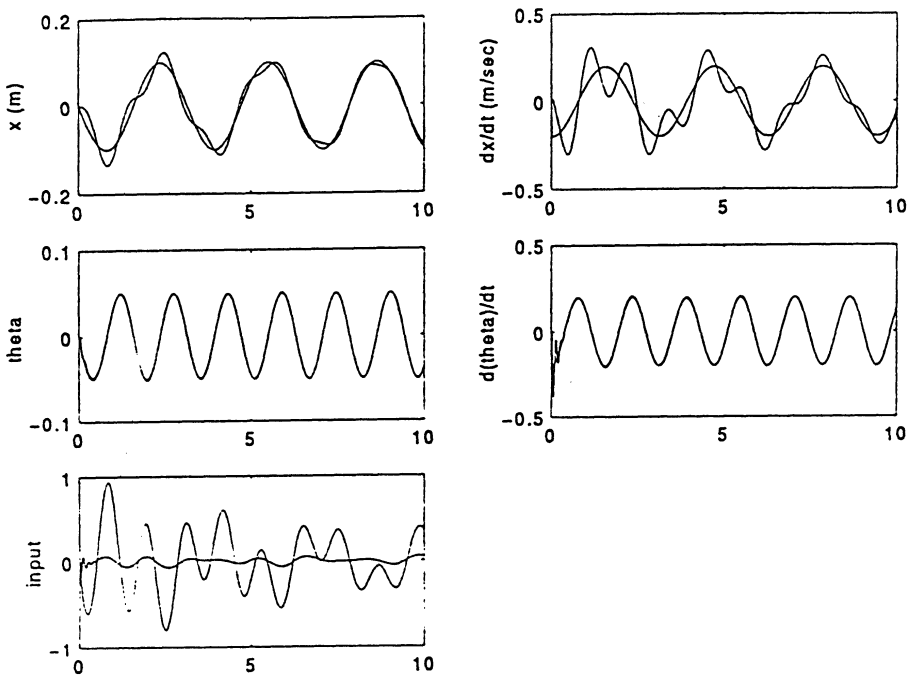

Figure 9a

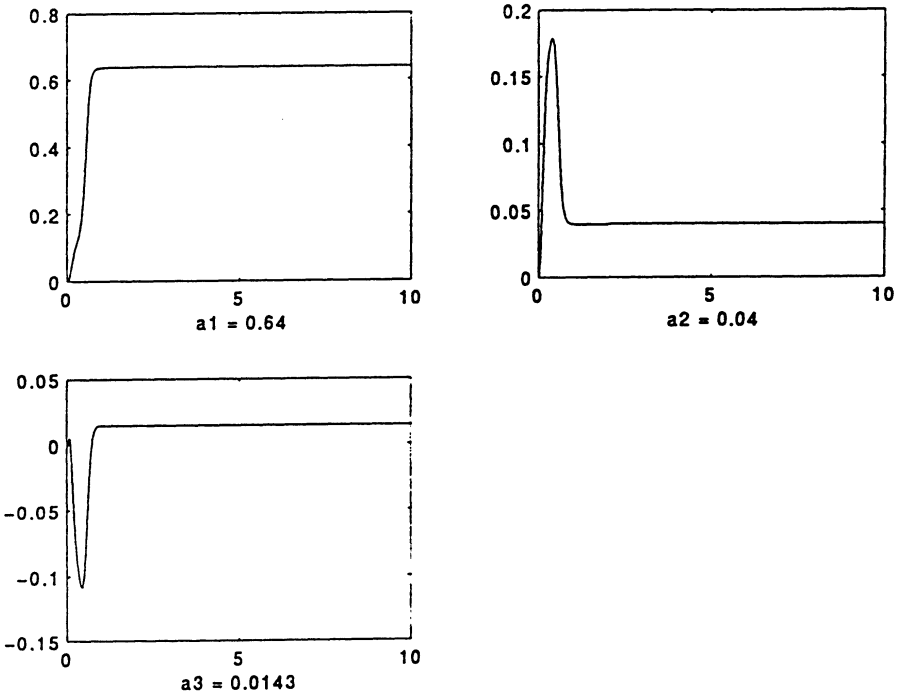

Figure 9b

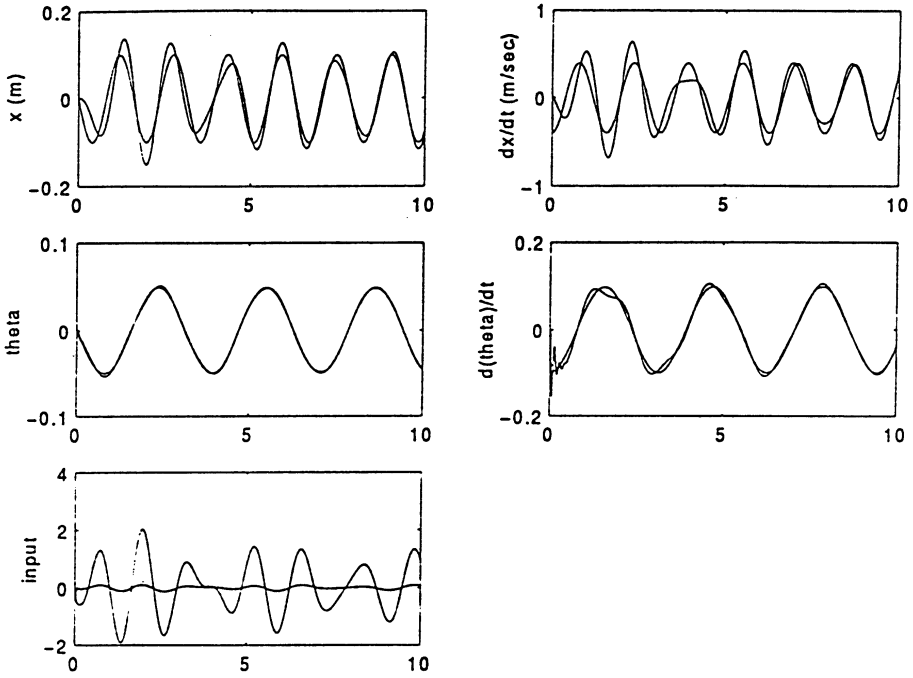

Figure 10a

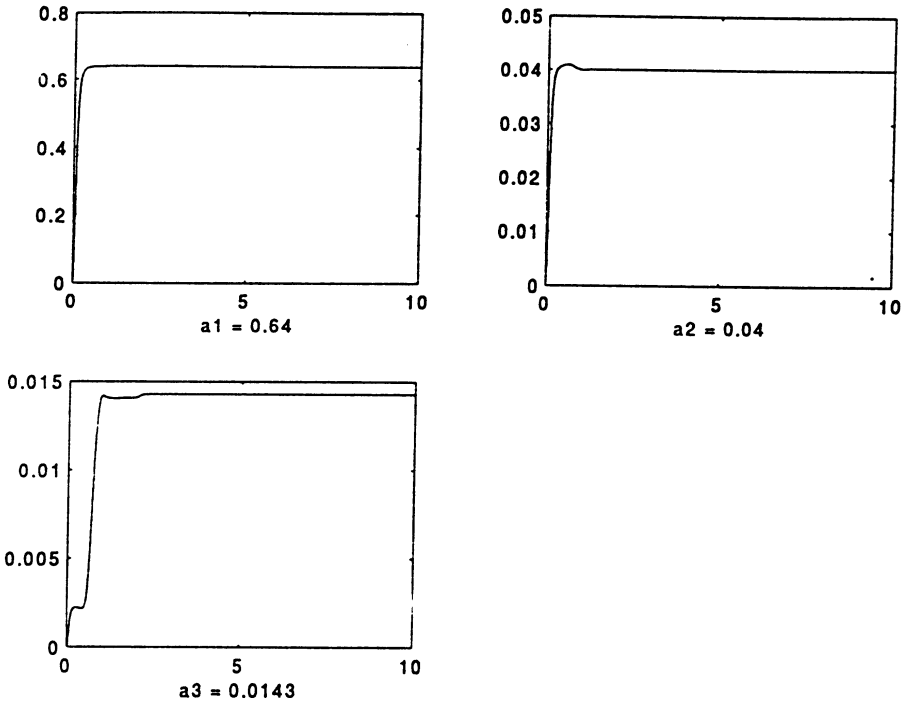

Figure 10b

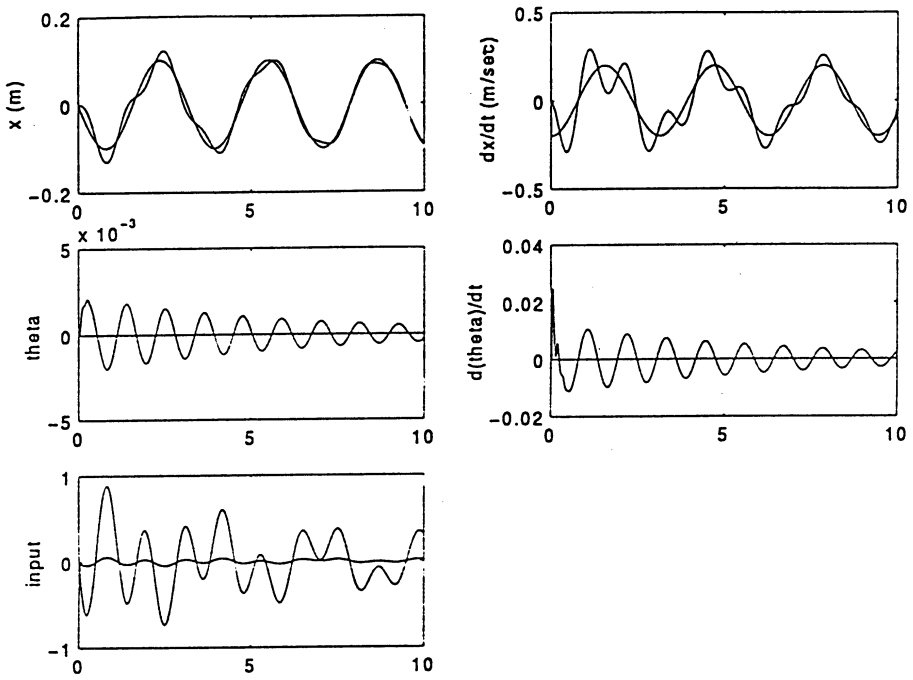

Figure 11a

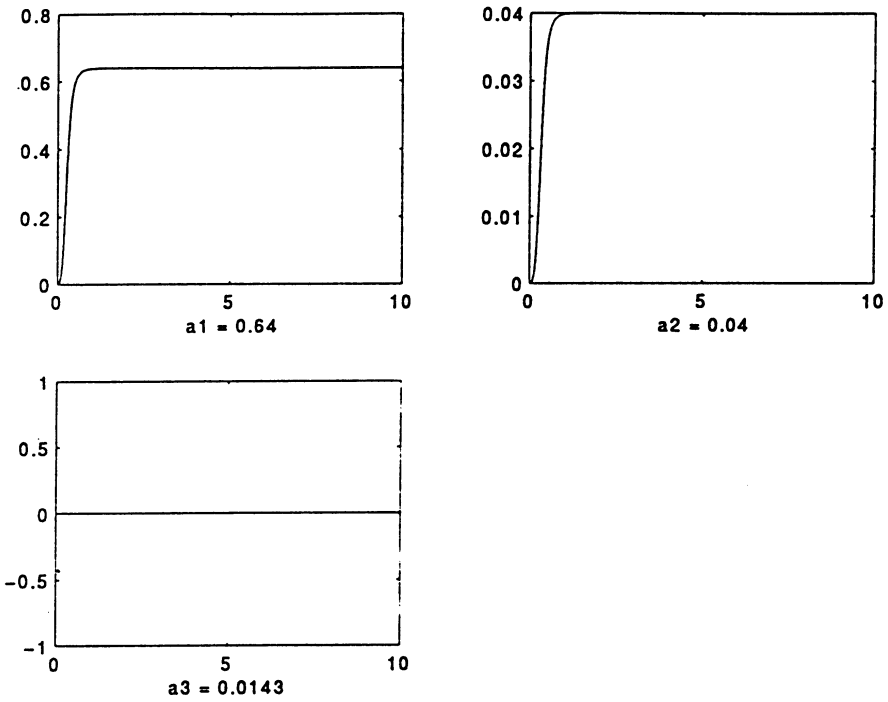

Figure 11b

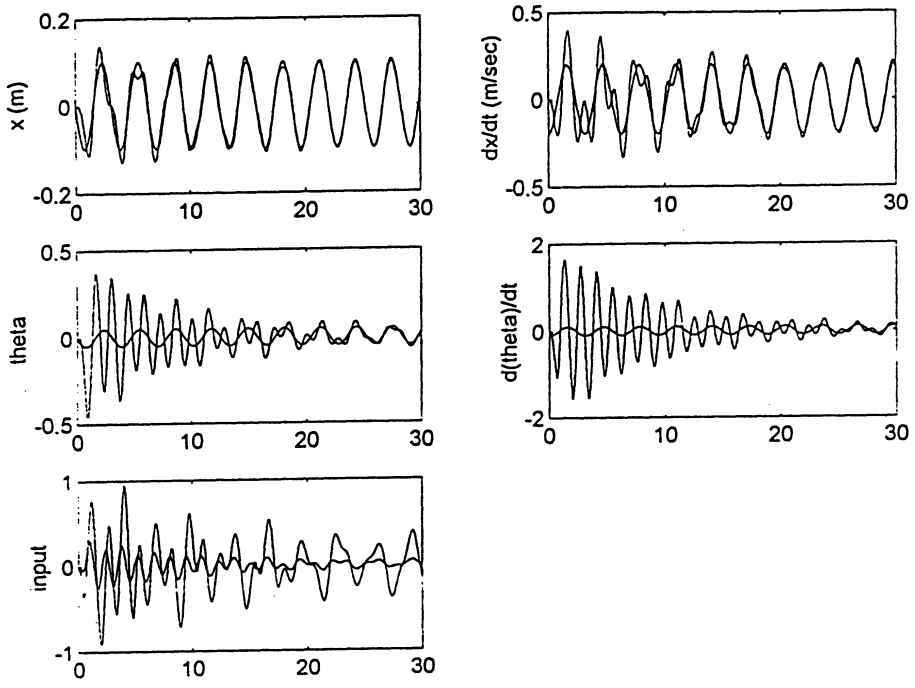

Figure 12a

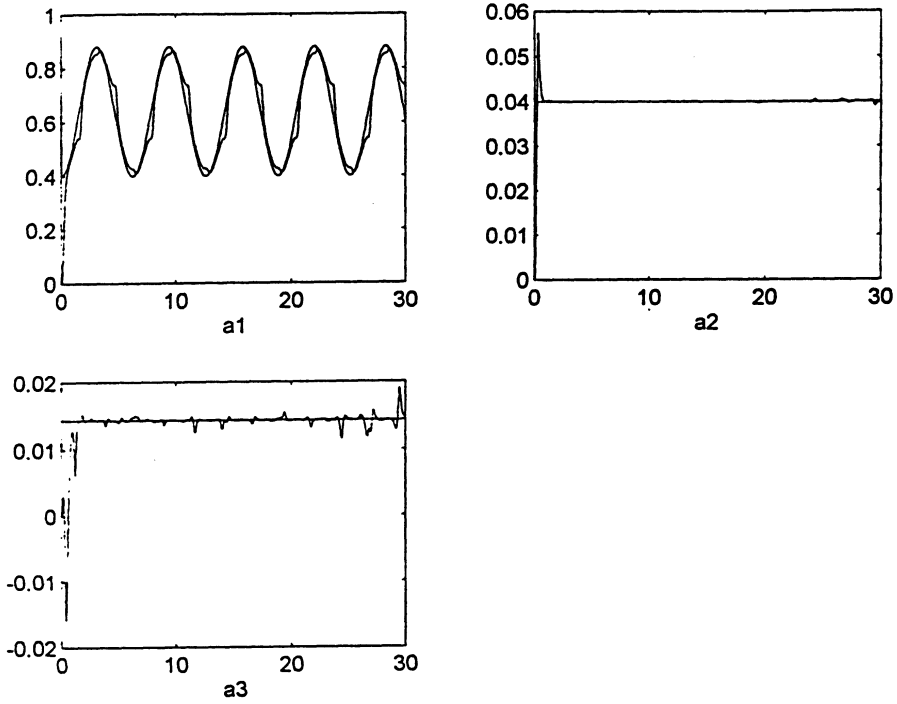

Figure 12b

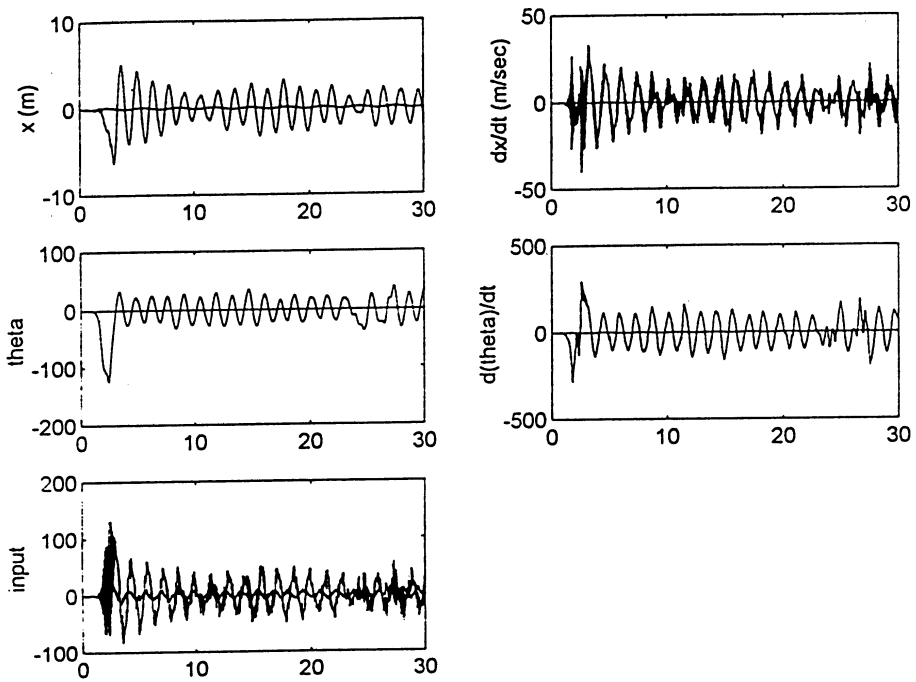

Figure 13a

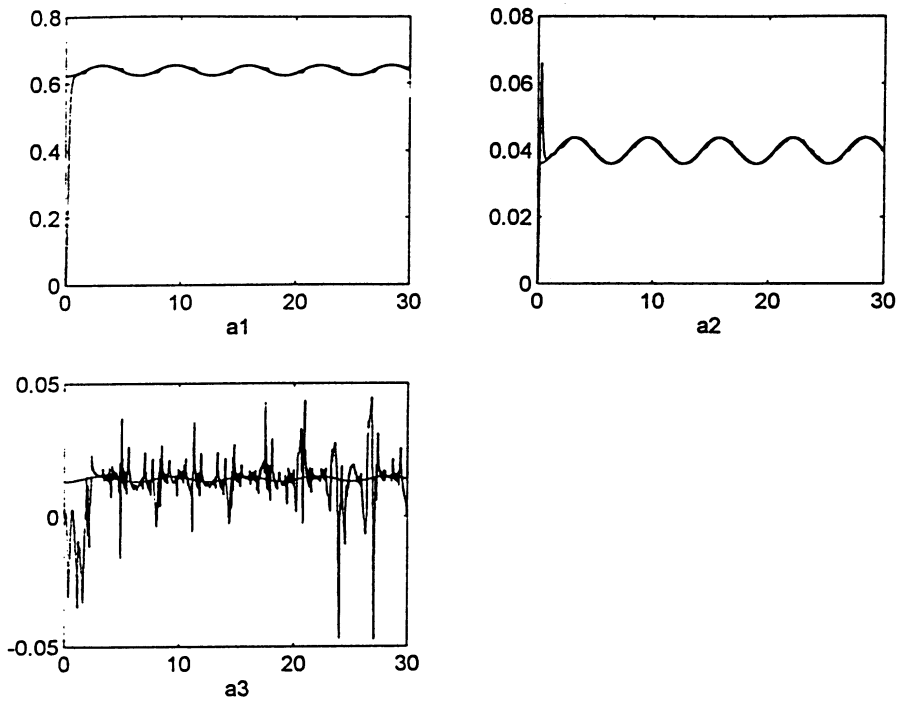

Figure 13b

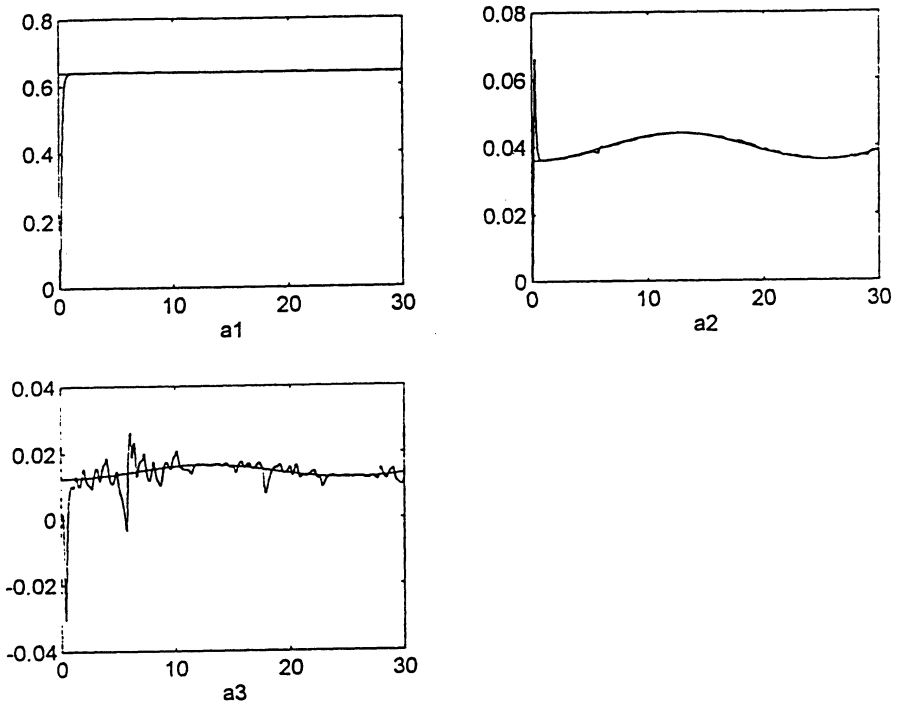

Figure 14b

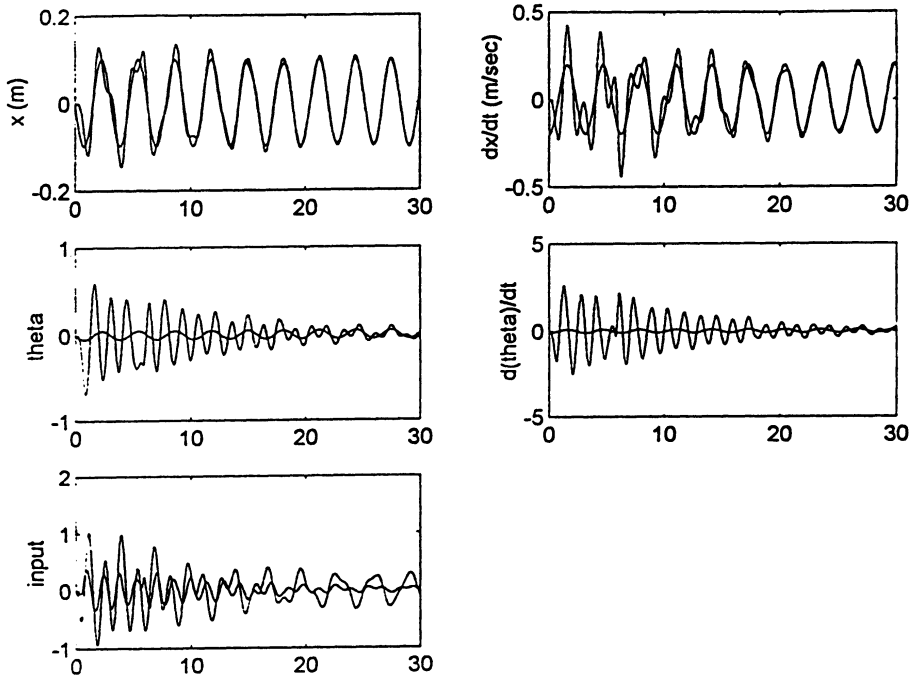

Figure 14a

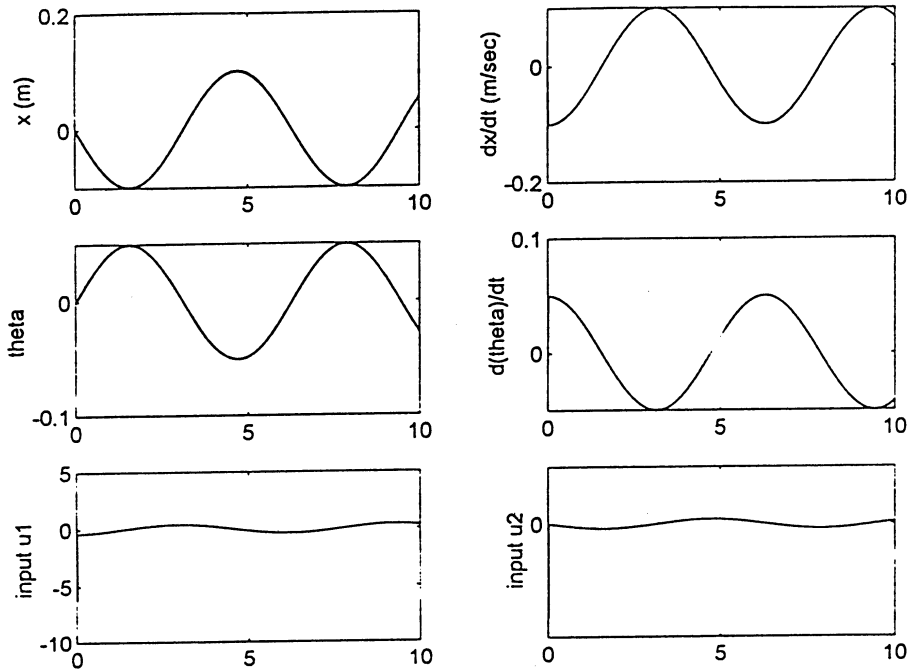

Figure 15a

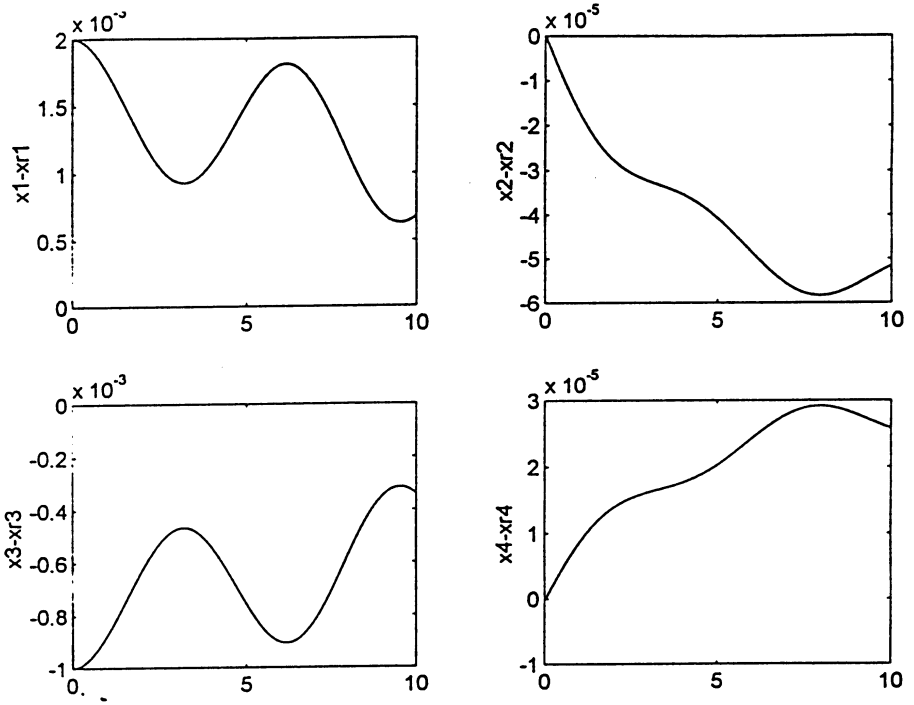

Figure 15b

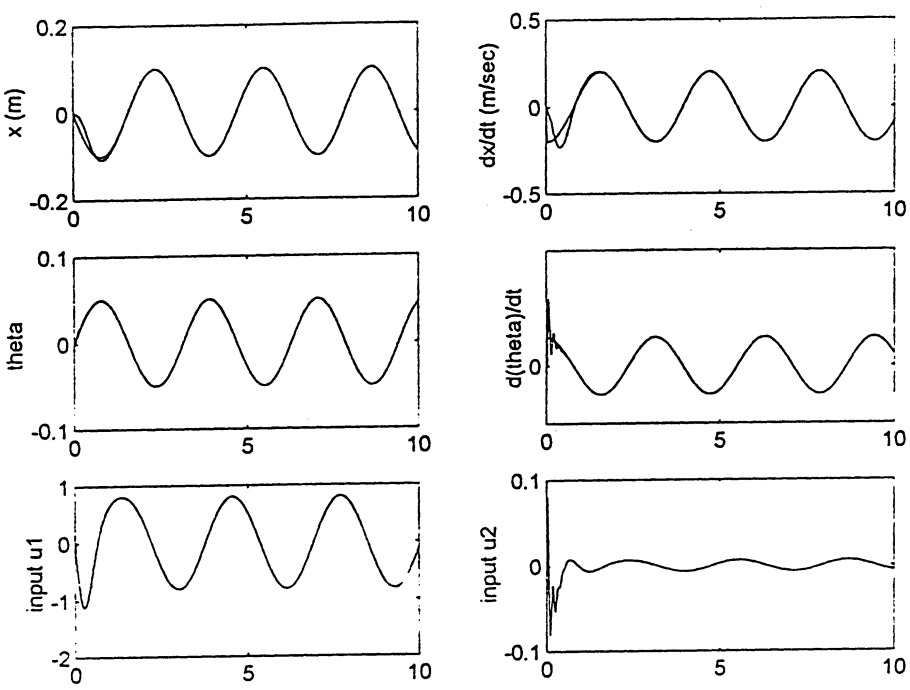

Figure 16a

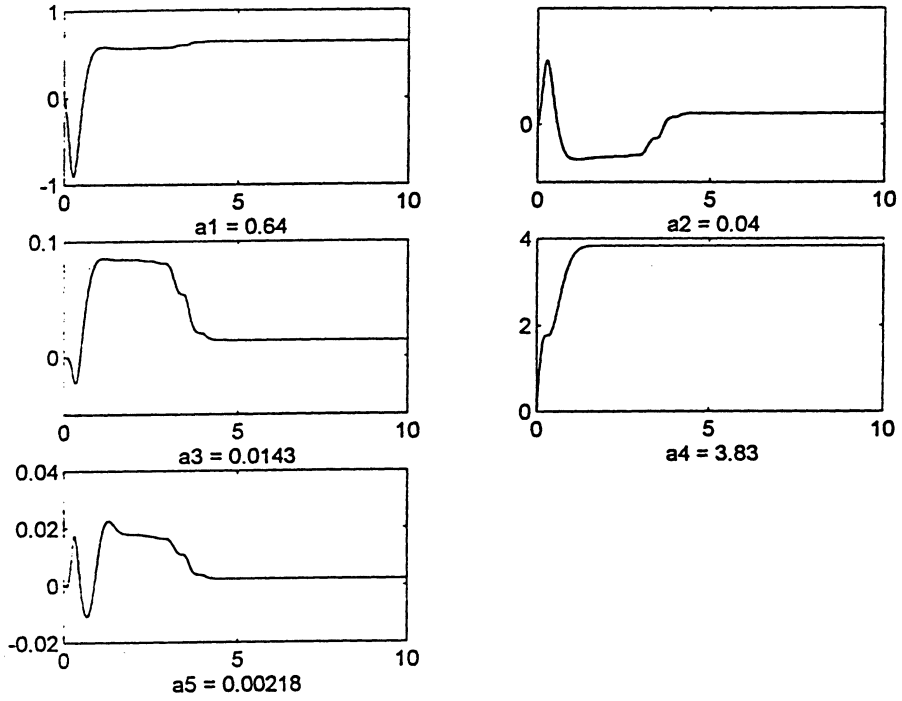

Figure 16b

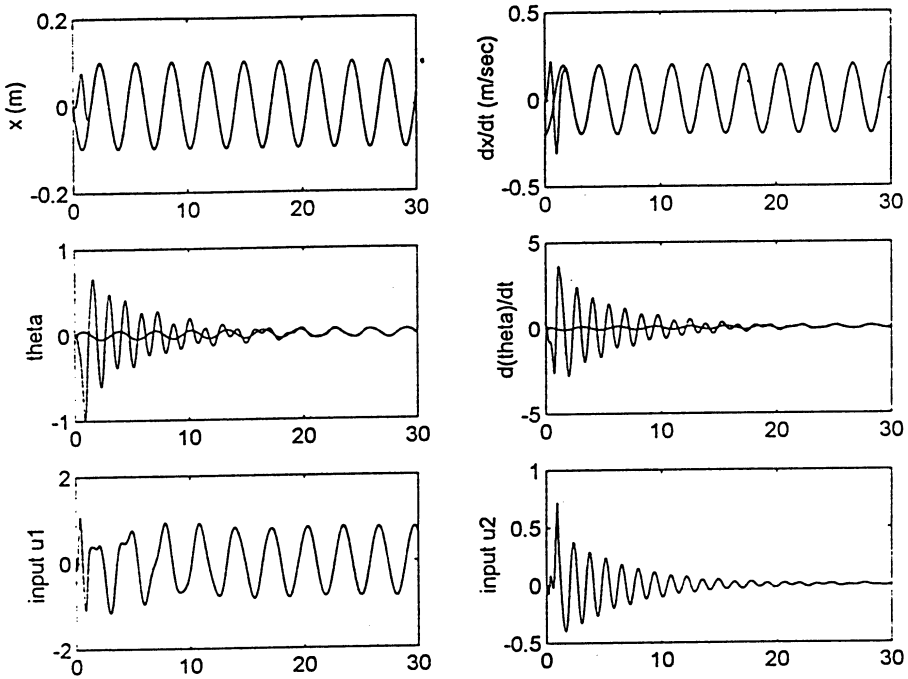

Figure 17a

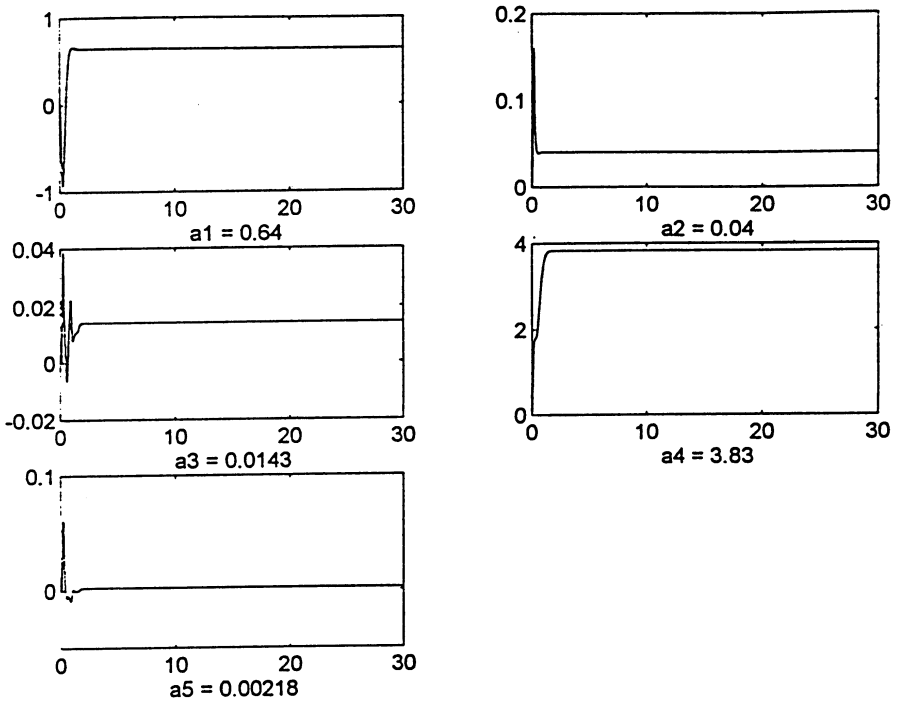

Figure 17b

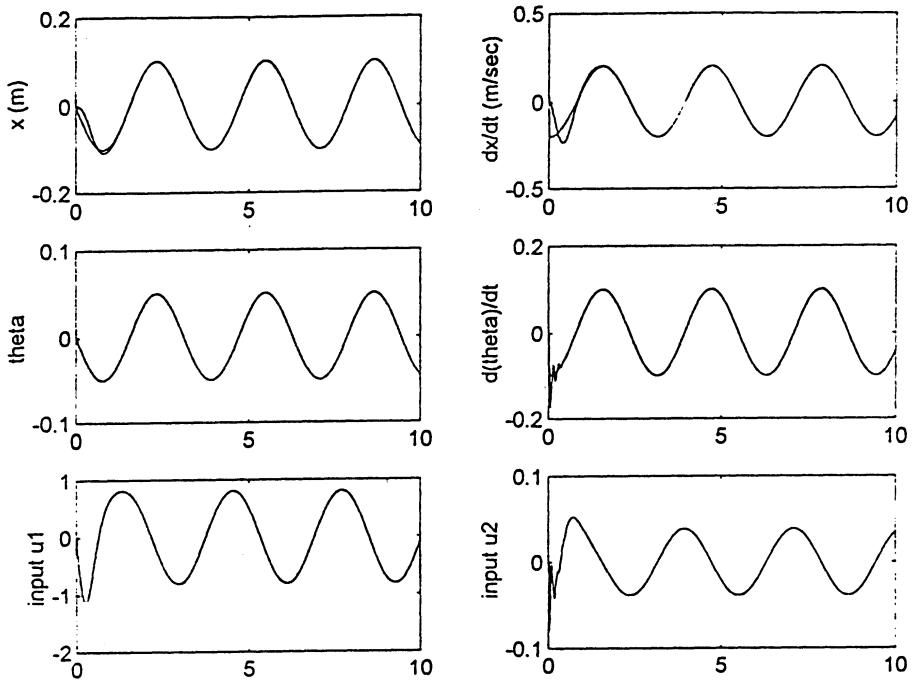

Figure 18a

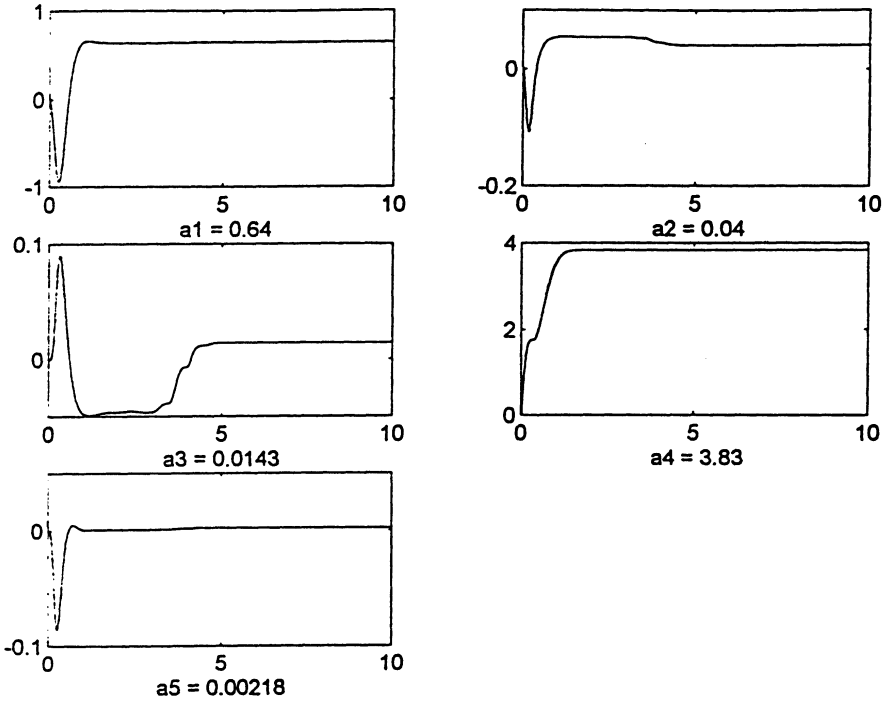

Figure 18b

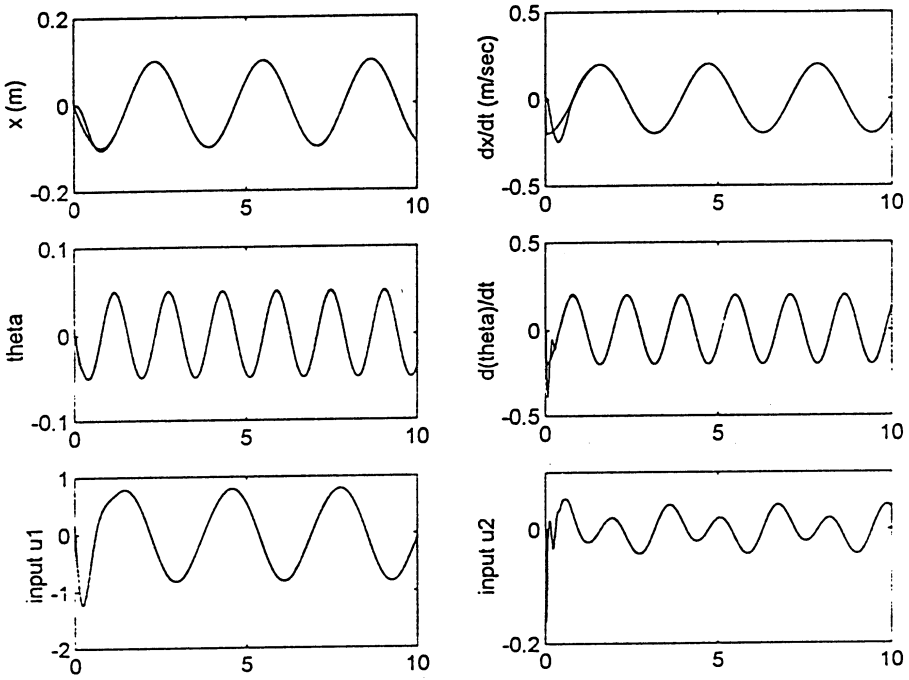

Figure 19a

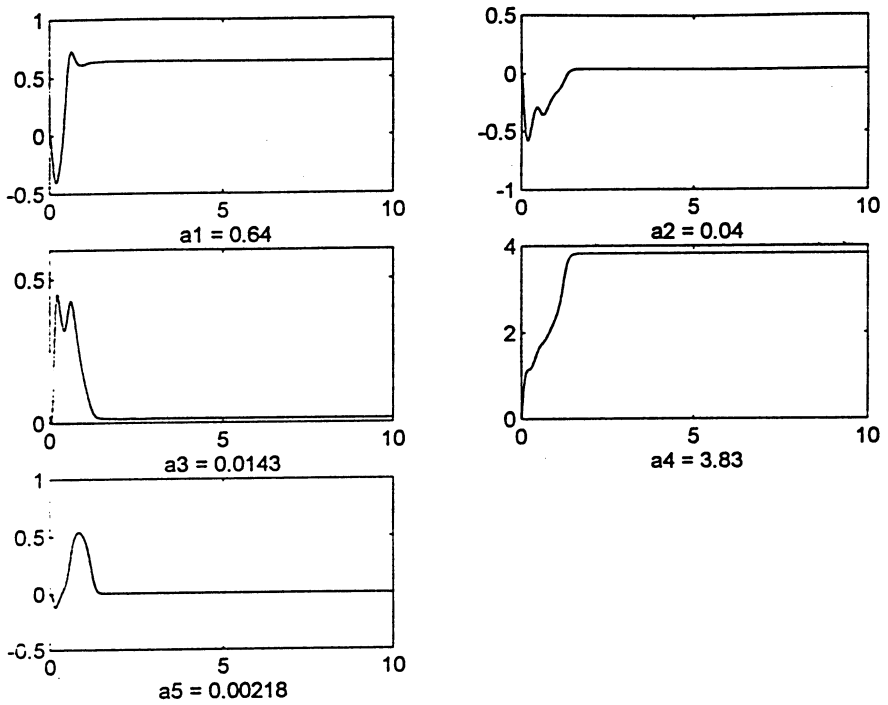

Figure 19b

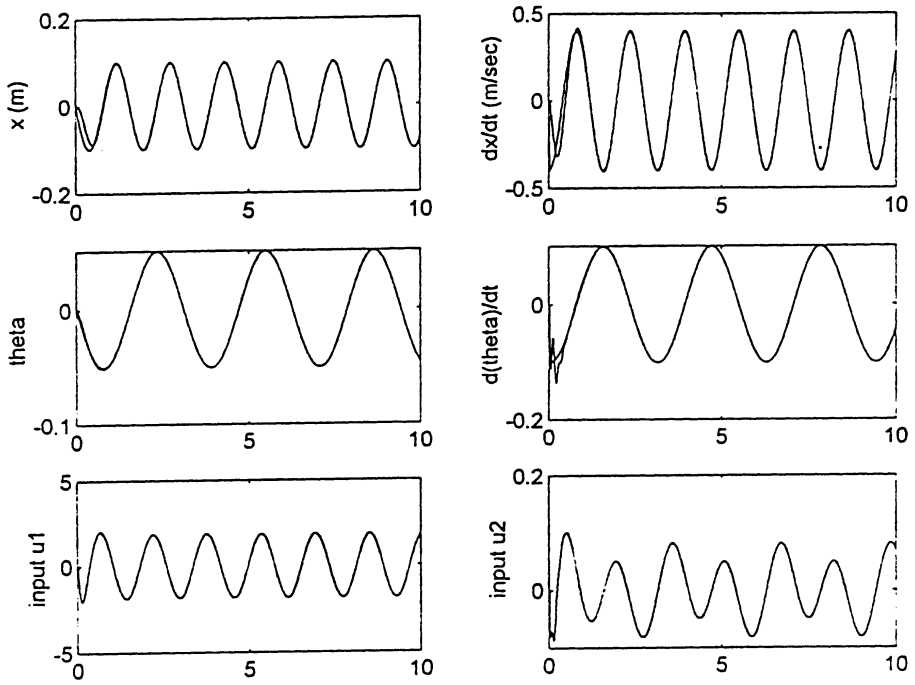

Figure 20a

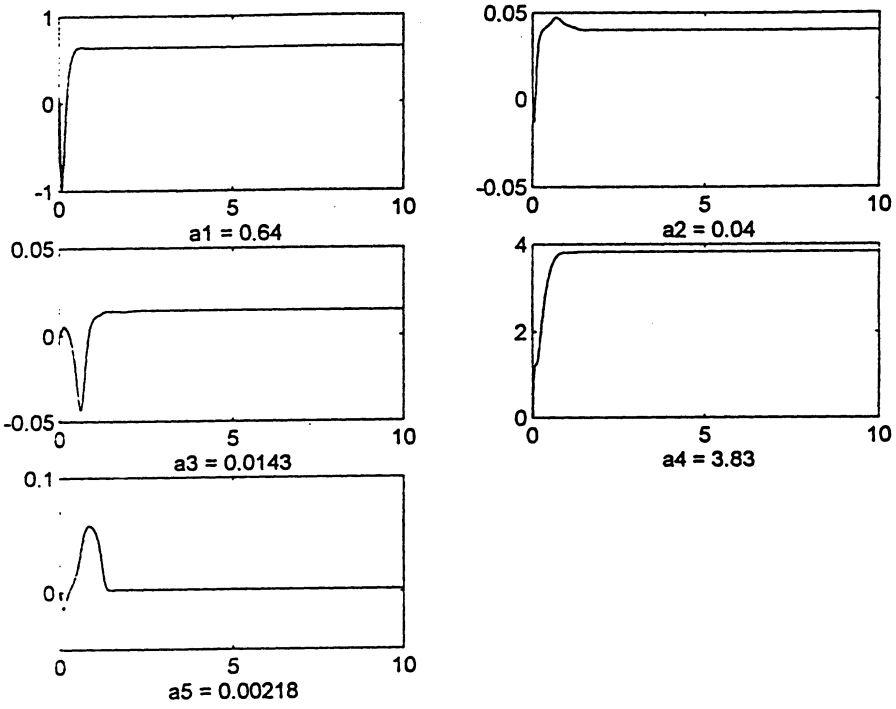

Figure 20b

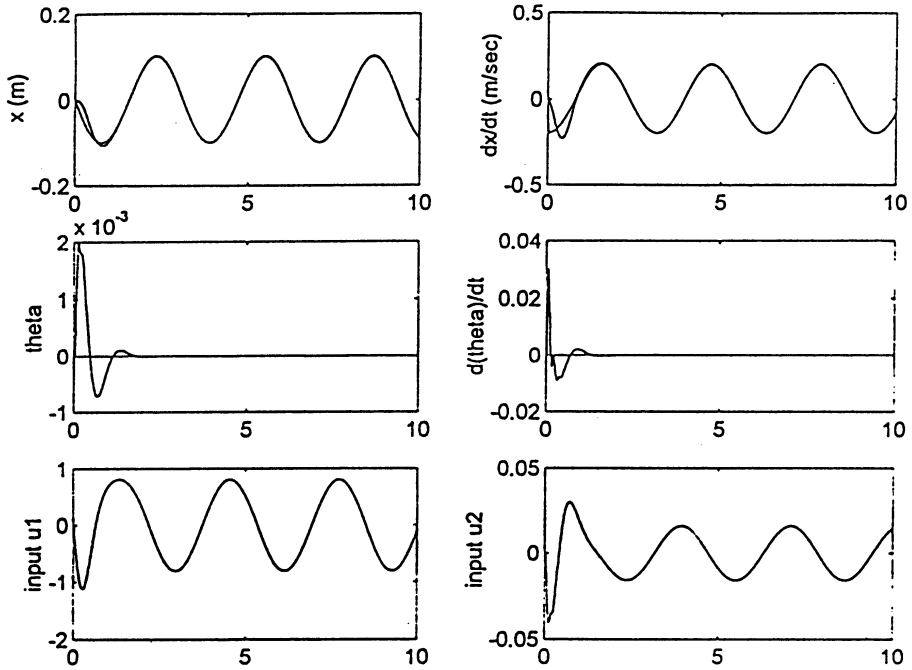

Figure 21a

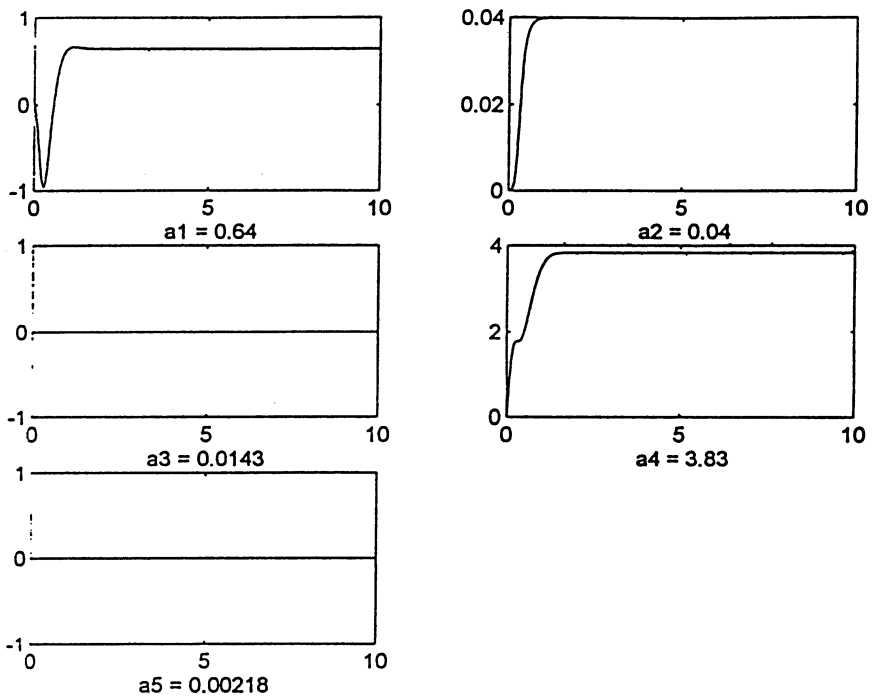

Figure 21b

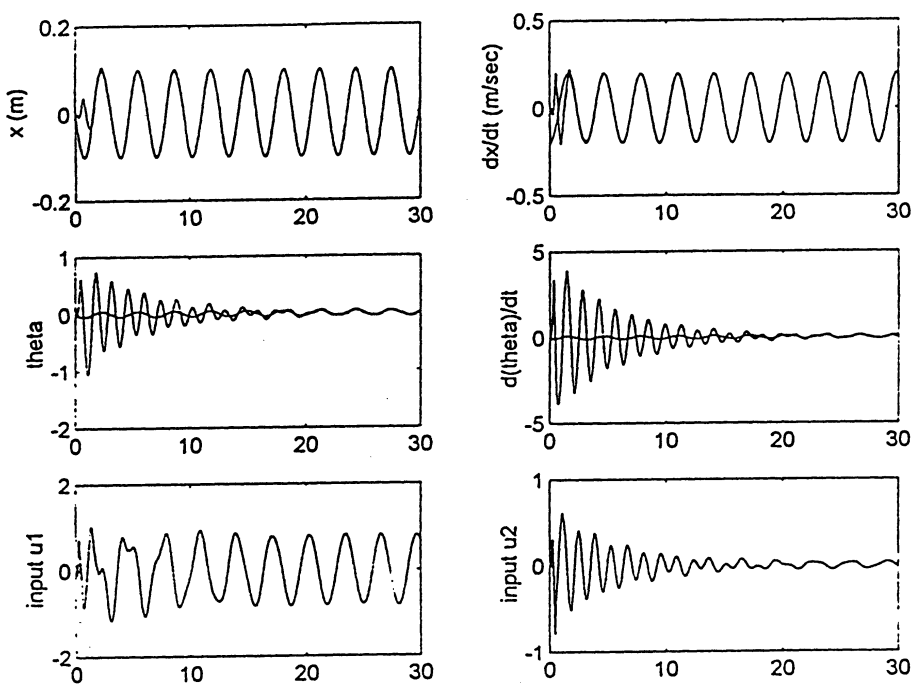

Figure 22a

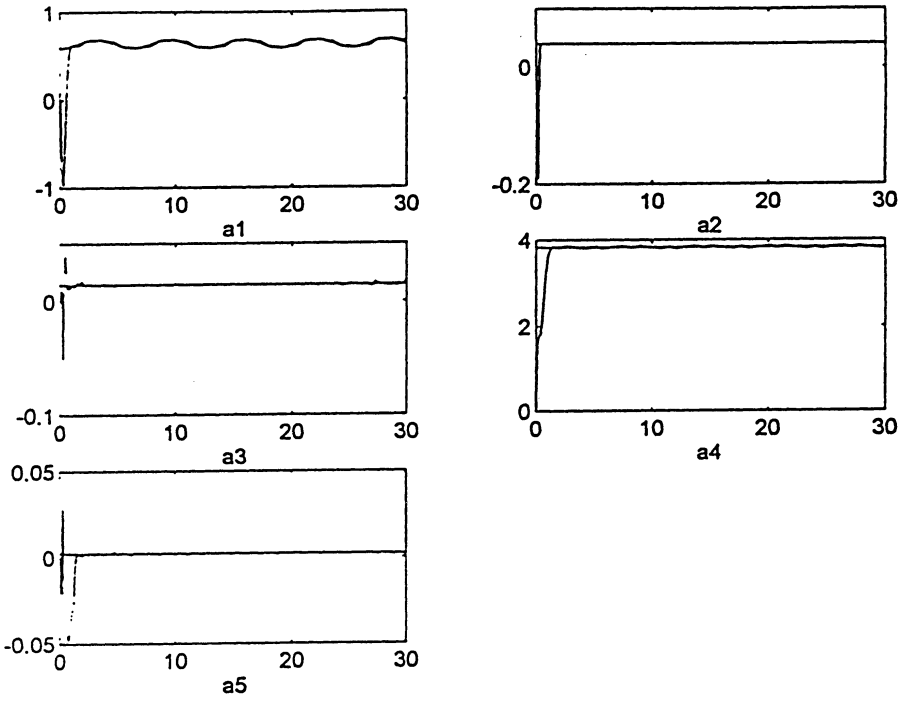

Figure 22b

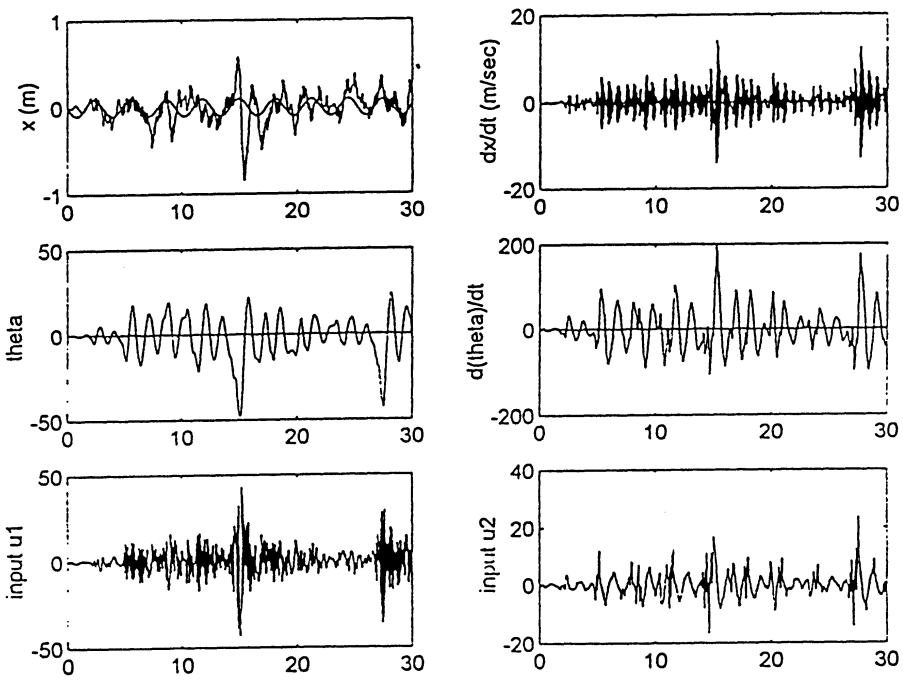

Figure 23a

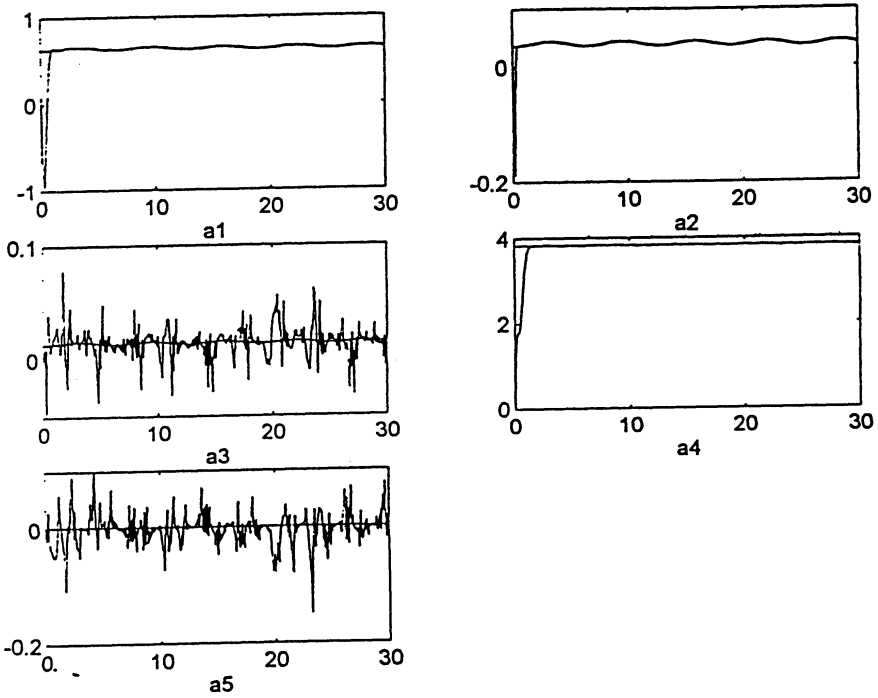

Figure 23b